Feasibility Study of In-situ Heat Generation for Oil Reservoirs Underlying the Permafrost

By

Mohammad Ali Kargarpour

A Thesis Submitted in Partial Fulfillment of the Requirements

for the Degree of

Master of Science

in

Petroleum Engineering

University of Alaska Fairbanks

May 2017

APPROVED:

Mohabbat Ahmadi, Committee Chair

Obadare Awoleke, Committee Co-Chair

Catherine Hanks, Committee Member

Abhijit Dandekar, Chair

Department of Petroleum Engineering

Doug Goering, Dean

College of Engineering and Mines

Michael Castellini, *Dean of the Graduate School*

Abstract

Development of a heavy oil reservoir is a challenging issue in the oil industry. One of the major issues in heavy oil recovery is its high viscosity; so, using heating methods for producing oil have been developed and employed from the early 1950s. The existing relatively thick permafrost layer which overlays the heavy oil reservoirs of the North Slope of Alaska creates additional complexities for development of these heavy oil reservoirs. Applying any heating oil recovery process in regular way to these heavy oil Alaskan reservoirs would potentially jeopardize the permafrost layer. A down-hole heat generation system has been developed that uses a chemical and a special catalyst to generate heat. The effluent of this system would be steam and nitrogen. The system can be installed in a well string and at the bottom of the injector well. This thesis investigates the feasibility of employing this system for development of the heavy oil reservoirs that underlie the permafrost. The results of this study can be used for any steam injection process which uses any device for down-hole steam generation.

The STARS module of the CMG reservoir simulation package is used for this study. In the model, live oil with a viscosity of about 30,000 cp is used. By examining several models with vertical and horizontal wells, a 3-D model with two horizontal injector and producer wells is ultimately constructed for final runs. Different sensitivities are run to find out the optimum operational parameters. Based on the results, a lateral well length of 800 ft in the middle of a reservoir with length of a 1250 ft is selected as a base case. Areal grid block size of 10 ft × 10 ft with the layer thickness of 10 ft in a reservoir with thickness of 50 ft is employed. To minimize the down-hole well bore temperature of the producer, just the last 50 ft (out of 800 ft of lateral length) at the toe of the well is opened to flow.

Three different steam injection processes are examined: Steam Assisted Gravity Drainage (SAGD), Cyclic SAGD (CSAGD) and Cyclic Steam Stimulation (CSS). Simulation results reveal that the producer well bore temperature in optimum cases for SAGD, CSAGD and CSS is more than 140 °F, 110 °F and 100 °F, respectively. Also, the 10-year simulation period oil recoveries for optimum cases of SAGD, CSAGD and CSS are about 35%, 18% and 12%, respectively. On the other hand, results show applying any steam injection recovery method (SAGD, CSAGD or CSS) can only be recommended when the thickness of the overlying

Sagavanirktok sand formation (which separates the permafrost from the heavy oil reservoir) is equal or more than 300 ft. The results also show that the addition of nitrogen has negative effect on the oil recovery.

Based on the results, it is recommended to employ SAGD or CSAGD, but employ a system to cool the producer well-string to avoid melting the permafrost. A simple system of cooling the producer well-string is suggested.

Table of Contents

Page

List of Figures

List of Tables

Acknowledgment

First of all, I would like to express my appreciation to the chair of my advisory committee, Dr. Mohabbat Ahmadi for his constant support, encouragement, and invaluable guidance during my graduate studies, especially in this thesis. I would also like to thank my advisory committee members Dr. Obadare Awoleke and Dr. Catherine Hanks for their valuable suggestions and commitment to this thesis.

I would also like to appreciate all other professors of the Petroleum Engineering Department who support me during my studies in UAF: Dr. Shirish Patil, Dr. Abhijit Dandekar and Dr. Yin Zhang I would also like to thank all the other faculties, staff, and fellow students of the Petroleum Engineering Department. Special thanks to Leanne Isaacson (office manager), who constantly supports and helps all persons without considering his/her formal official level or ethics.

Chapter 1: Introduction

The demand for oil is increasing. At the same time, conventional oil resources are decreasing. With this situation, developers have turned toward heavy oil. In comparison to conventional oil, heavy oil is more difficult to produce and transport and thus has had less attention paid to it. But over the last decades, investments have been directed toward heavy oil production, even in the Middle East oil-exporting countries, whose resources hold the largest amount of conventional oil. Table 1-1 lists the estimated heavy oil and bitumen resources of the world.

Table 1-1: The estimated heavy oil and bitumen resources of the world (Meyer et al., 2007).

Classification	Discovered Oil In Place (Bbbl)	Density (°API)	Viscosity at 100 °F (cP)	Average Depth (ft)
Heavy Oil	3366	13.5-19.2	137-2318	558-6472
Natural Bitumen	4512	4.4-9.5	1322-500659	20-8751

One of the major challenges to recovering heavy oil is its high viscosity. To address this issue, heating methods for producing oil were developed and have been employed since the early 1950s (Offeringa et al., 1981). Of course, the idea of injecting hot fluids is quite old, but the serious interest in this class of oil recovery processes is recent (Ramey, Jr., 1967). One of the first thermal recovery projects, based on research by Burns (1969), was implemented by Shell Oil Company, who began steam soak operations on a pilot basis in the Yorba Linda field in California. Over the past decades, different methods of heating formations have been invented and executed.

Current estimates of the magnitude of identified 'viscous oil' and 'heavy oil' in Alaska's North Slope are 12 billion barrels of oil-in-place and 12–18 billion barrels of oil-in-place, respectively (Pospisil, 2011; Attanasi and Freeman, 2015; Patil et al., 2008; Targac et al., 2005); the definitions of 'heavy and viscous' oils are presented in the following sections. Figure 1-1 is a map of heavy oil accumulations on Alaska's North Slope (Chmielowski, 2013). The Ugnu sands, with 12 to 18 billion bbl original oil-in-place, account for about one half of the heavy-oil resource (Hulm et al., 2013). The other important Alaska heavy oil pools are West Sak, Schrader Bluff, Orion Polaris, and Nikaitchuq-Schrader Bluff (Figure 1-2). Their oil density ranges from 14 to 24 API with depth ranges from 3500 ft to 5000 ft (Attanasi and Freeman, 2015).

Recovery of these viscous and heavy oils in the arctic climate is challenging for oil companies, especially in permafrost lands. Permafrost is a permanently frozen layer below the earth's surface. It consists of soil, gravel, and sand, usually bound together by ice. Permafrost usually remains at or below 0°C. The permafrost thickness can range from 1 meter (3 feet) to more than 1,000 meters (National Geography website, 2016). The Ugnu resource occurs at depths between 610 and 1524 m (2000 and 5000 ft) true vertical depth subsea, with API gravities that range from 8 to 14 API (Hulm et al., 2013).

It is in the interest of the State of Alaska to identify conditions that would lead to commercial production of these enormous oil resources (Attanasi and Freeman, 2015). Thermal recovery methods proven efficient and practicable in other regions are considered dangerous for permafrost layers. Attanasi and Freeman (2015) emphasized that steam-based thermal recovery methods are not practical in the North Slope because of the costs and risks associated with the transport of steam through injector wells in contact with the thick permafrost.

Several other oil recovery methods have been attempted. The use of vertical wells and water flooding did not result in an attainable production rate. Multilateral horizontal wells with water flood configurations were able to produce viscous oils at commercial rates, but the recovery of in-place oil was no more than 22 % (McGuire et al. 2005) and often considerably less (Attanasi and Freeman 2015).

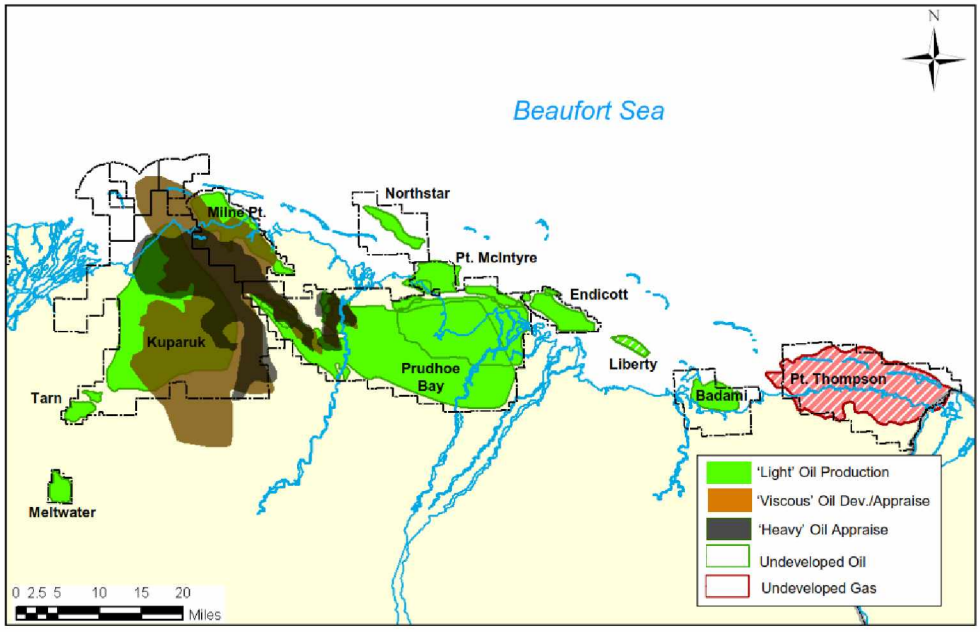

Figure 1-1: Alaska light, viscous and heavy oil (Chmielowski, 2013).

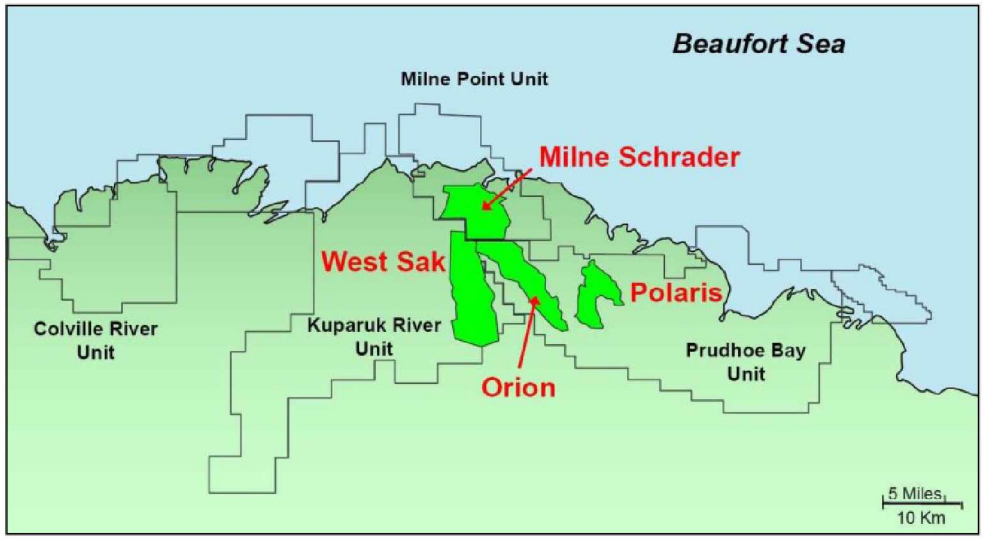

Figure 1-2: Alaska's Viscous Oil Reserves (Source: BP Exploration Alaska Inc. presentation to Alaska Department of Revenue, February 18, 2005).

Operators of North Slope immiscible gas EOR projects have found that injection of viscosity reducing agents (lean gas or carbon dioxide (CO2)) into light oil reservoirs increases recovery of the oil-in-place beyond water flood by 6 to 9% (Ning and McGuire, 2004; McGuire et al., 2005; Attanasi and Freeman, 2015). The laboratory experiments and reservoir simulations predict an additional recovery of 3% of the original oil-in-place beyond water flood recovery if a viscosity-reducing agent is introduced into a viscous oil reservoir as part of an immiscible-water

alternating gas (IWAG) EOR process (Attanasi and Freeman, 2015). Also, laboratory experiments and reservoir simulations predict that, beyond water flood, CO2 IWAG flood yields an additional 11% recovery and CO2 IWAG enriched with NGLs yields an additional 12% recovery of the original oil-in-place (Ning et al., 2011; Attanasi and Freeman, 2015).

Since research (including laboratory activities or pilot plan implementation) shows that non-thermal methods are not optimal for sustaining economical production from Alaska's heavy oil reservoirs, modified thermal recovery systems are now being contemplated in this project. The goal of the project detailed in this thesis is to investigate the feasibility of using a new industrial-scale method of in-situ down-hole heat generation to optimize reservoir heating while minimizing or even eliminating heat transfer to the overlying permafrost. The available information on this technology is extremely limited: the fuel is a "monopropellant," and the products of this fuel are steam and nitrogen. No other data have been released.

In this project, the following activities were considered:

1. Trying to understand the concepts of new technologies without elaborating the details of them. For this project, the effluents of the down-hole heat generation system are what are important.
2. Review of similar down-hole heat generation methods.
3. Review of some thermal recovery performed projects or studies.
4. Compilation of the best PVT and geological data of heavy oil reservoirs, with emphasis on Alaskan reservoirs.
5. Review and compilation of the best data corresponding to thermal properties of rocks.
6. Construction of a simple-base case simulation model with CMG STARS module. In this model, just two wells (one injector and one producer) will be considered.
7. Running different scenarios to find optimum parameters.
8. Analysis and discussion of the simulation results.

Chapter 2: Literature Survey

2.1. Heavy Oil Definition

Heavy oil and natural bitumen are important energy sources, currently contributing significantly to the overall energy supply of the United States and Canada. These two terms, especially the term *heavy oil,* constitute a broad range of definitions. The definition of heavy oil is not crystal clear. Each country – even each company – might have its own definition of heavy oil. In the oil trading industry, one can even encounter the term 'heavy oil' for oil with gravity of more than 30°API. In the following paragraphs, a few heavy crude oil definitions are presented.

The crudes are divided into several groups by their density and viscosity. The generally accepted definition for crude density is the one provided by the American Petroleum Institute (API). This institute (API) has recommended the use of API gravity for crude oil, defined as simple function of the ratio of density of oil to the density of pure water, both taken at 60°F and 1 atmosphere pressure (Chopra et al., 2010). By definition, API gravity is calculated as follows:

$$API = \frac{141.5}{Specific\ Gravity\ at\ 60\ ^{\circ}F} - 131.5 \quad \text{..... (2-1)}$$

Density is a necessary parameter for categorizing crude oil; however, it is not the only one. Viscosity is another crude oil specification used to define heavy oil. The definition of viscosity is adopted from Bansal (2005).

Viscosity is defined as the property of a fluid which offers resistance to the movement of one layer of fluid over another adjacent layer of the fluid. When two layers of a fluid, a distance '*dy*' apart, move one over the other at different velocities, say *u* and *u*+ *du* as shown in the following sketch, the viscosity together with relative velocity causes a shear stress acting between the fluid layers: the top layer causes a shear stress on the adjacent lower layer while the lower layer causes a shear stress on the adjacent top layer.

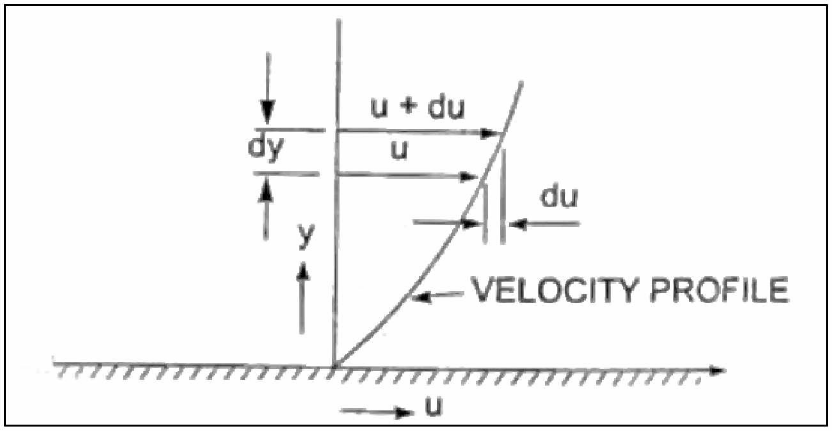

Figure 2-1: Schematic definition of viscosity (Bansal, 2005).

This shear stress is proportional to the rate of change of velocity with respect to *y;* it is denoted by the symbol τ called Tau.

Mathematically:

$$\tau \propto \frac{du}{dy} \text{ or } \tau = \mu \frac{du}{dy} \qquad \text{(2-2)}$$

Where μ (called *mu)* is the constant of proportionality and is known as the co-efficient of dynamic viscosity or only viscosity. $'\left(\frac{du}{dy}\right)'$ represents the rate of shear strain or rate of shear deformation or velocity gradient.

Thus viscosity is also defined as the shear stress required to produce a unit rate of shear strain.

The unit of viscosity is obtained by putting the dimensions of the quantities into equation (2-2).

$$\mu = \frac{shear\ stress}{\frac{change\ of\ velocity}{change\ of\ distance}} = \frac{force\ /area}{\left(\frac{length}{time}\right)\times\frac{1}{length}} = \frac{force\ /(length)^2}{\frac{1}{time}} = \frac{force\ \times time}{(length)^2} \qquad \text{(2-3)}$$

In MKS system, force is represented by kgf and length by meter (M), in CGS system, force is represented by dyne and length by cm and in SI system force is represented by Newton (N) and length by meter (m).

Therefore:

MKS unit of viscosity: $= \frac{Kgf - sec}{m^2}$

CGS unit of viscosity: $= \frac{dyne - sec}{cm^2}$

SI unit of viscosity: $= \frac{N - sec}{m^2}$

In the above expression, N/m^2 is also known as Pascal (Pa); thus,

SI unit of viscosity: $= Pa.s$

The unit of viscosity in CGS is also called Poise which is equal to dyne-sec/cm^2.

The relationships between these units are as follow:

$$1\frac{Kgf-sec}{m^2} = 98.1\ poise \quad \ldots\ldots (2\text{-}4)$$

$$1Pa.s = 10\ poise \quad \ldots\ldots (2\text{-}5)$$

Kinematic Viscosity is defined as the ratio between the dynamic-viscosity and density of fluid. It is denoted by the Greek symbol (ν) called 'nu'. Thus, mathematically:

$$\nu = \frac{viscosity}{density} = \frac{\mu}{\rho} \quad \ldots\ldots (2\text{-}6)$$

In MKS and SI, the unit of kinematic viscosity is metre^2/sec or m^2/sec while in CGS units it is written as cm^2/s. In CGS units, kinematic viscosity is also known as stoke.

$$1stoke = 10^{-4}\ m^2/s \quad \ldots\ldots (2\text{-}7)$$

Figure 2-2 shows the world-wide relation of API gravity with crude oil viscosity (Law, 2011).

In the 1982 UNITAR conference in Venezuela, certain definitions were agreed upon, summarized in Table 2-1 (Farouq Ali et al., 1997).

Table 2-1: The 1982 UNITAR conference of heavy oil definition (Farouq Ali et al., 1997)

Classification	Viscosity at res. temp. (cP)	Density at 15.6 °C (Kg/m^3)	API Gravity
Heavy oil	100-10000	943-1000	20-10
Tar Sand Crude	>10000	1000	<10

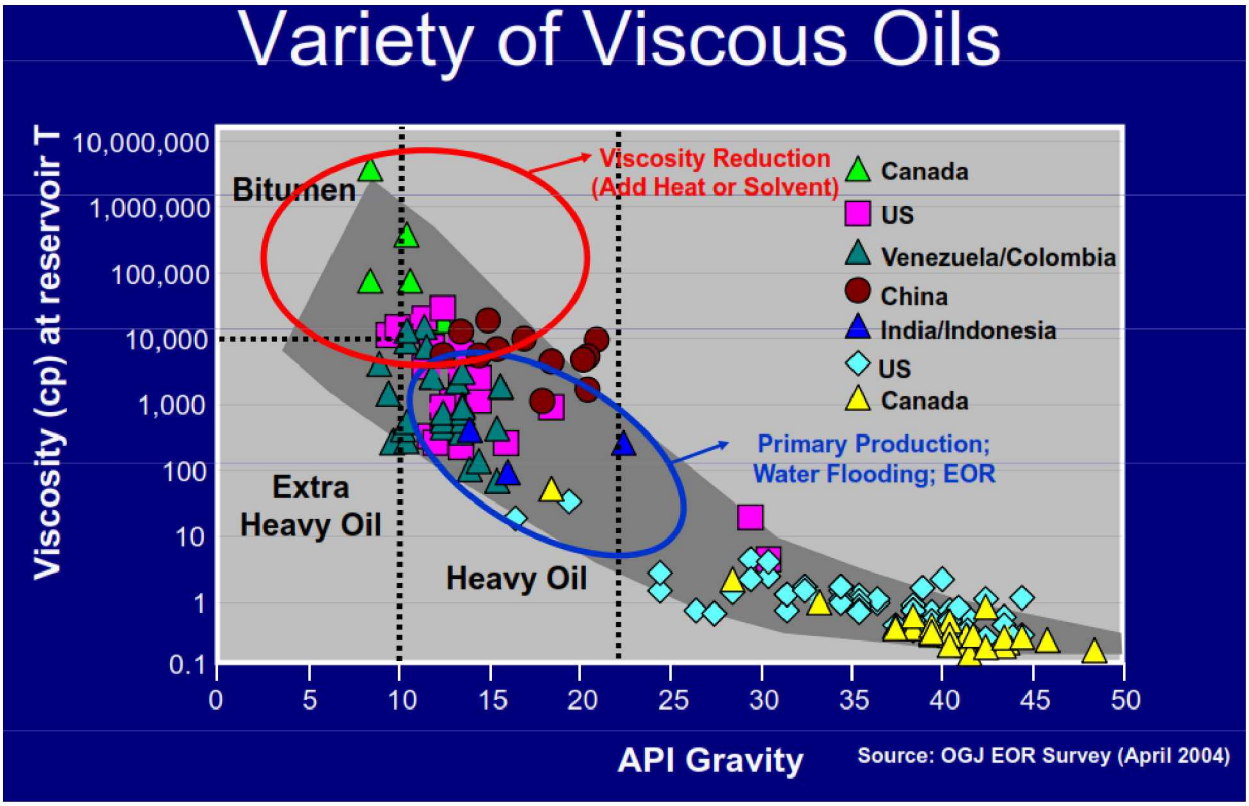

Figure 2-2: World-wide API Gravity and Viscosity of crude oil relationship (Law, 2011).

The US Geological Survey (US Department of the Interior) has the following definitions (Meyer et al., 2007):

- Conventional (light) Oil: oil with API gravity greater than 25°.
- Medium Oil: oil with API gravity greater than 20°API but less than or equal to 25°API.
- Heavy Oil: oil with API gravity from 10°API to 20°API and viscosity greater than 100 cP.
- Natural Bitumen: oil with API gravity less than 10° and with viscosity commonly greater than 10,000 cP.

The U.S. DOE definition of heavy crude oil is oil with API gravity between 10°API and 20°API inclusive at 60°F, or having a gas free viscosity >100 cP and less than 10,000 cP inclusive at reservoir temperature (Ried, 1996).

On the basis of its API gravity, crude oil is graded light (>31.1°), medium (22.3°–31.1°), heavy (<22.3°), or extra heavy (bitumen) (<10°). This grading, recommended by the U. S. Department

of Energy, is followed as a standard (Chopra et al., 2010). Oil that does not flow at all or cannot be pumped without some form of stimulation is called "bitumen" (Chopra et al., 2010).

Total (2006) classifies heavy oil by its viscosity. Heavy oils (Class A) are those with viscosity ranging from 10 to 100 centipoises (cP). Extra-heavy oils (Class B) have a viscosity range from 100 to 10,000 cP. These two classifications, which range from 25° to 7° API gravity, include mobile oils that can be recovered by cold production. The classification of hydrocarbons with viscosity above 10,000 cP (Class C) comprises bitumens of less than 7° API gravity, immobile in reservoir conditions and therefore requiring thermal recovery methods (such as steam injection) or mining techniques. The fourth classification (Class D) comprises bituminous shales, considered as source rock. These resources are extracted using mining or in-situ (i.e., via wells) techniques.

The API gravities of some standard crudes are presented in Table 2-2 (BP, 2010).The World Petroleum Congress (WPC) in 1987 agreed to the definitions of Table 2-3 (Law, 2011).

Table 2-2: API gravities of some standard crude (BP, 2010).

Crude	API Gravity	API Definition
West Texas Intermediate	40	Light
Canadian Syn-crude	33	
Arab Light	32	
Alaska NS Crude	29	Medium
Arab Heavy	27	
Alaska Viscous	16–24	Heavy
Alaska Heavy (Ugnu)	8–14	
water	10	Extra Heavy
Venezuela (Orinoco)	10	
Canadian Lloydminster	9–18	
Canadian Athabasca	6–10	

Table 2-3: Heavy oil World Petroleum Congress (WPC), 1987 definitions (Law, 2011).

	API Gravity	Viscosity (cp)
Heavy Oil	10° – 22.3°	100 – 10,000
Extra Heavy Oil	< 10°	100 – 10,000
Extra Heavy Oil	< 10°	>10,000

Attanasi and Freeman (2015) classified the low API gravity oil of Alaska's North Slope as 'viscous oil' and 'heavy oil'. The North Slope's known viscous oils have gravity values that range from 15 to 22 °API and are primarily contained in the (informally named) West Sak/Schrader Bluff sands (Werner 1987). The 'heavy oil' is more properly classified as bitumen, having gravity values that range from 8 to 12 °API, with most of the resource having viscosity values greater than 10,000 centipoise. The North Slope's 'heavy oil' is contained in the (informally named) Lower and Upper Ugnu sands (Attanasi and Freeman, 2015).

British Petroleum tried to correlate viscosity with depth for Alaska's crudes. The results are presented in Figure 2-3 (BP 2010).

Figure 2-4 shows the variation of Ugnu's API crude (Chmielowski, 2013).

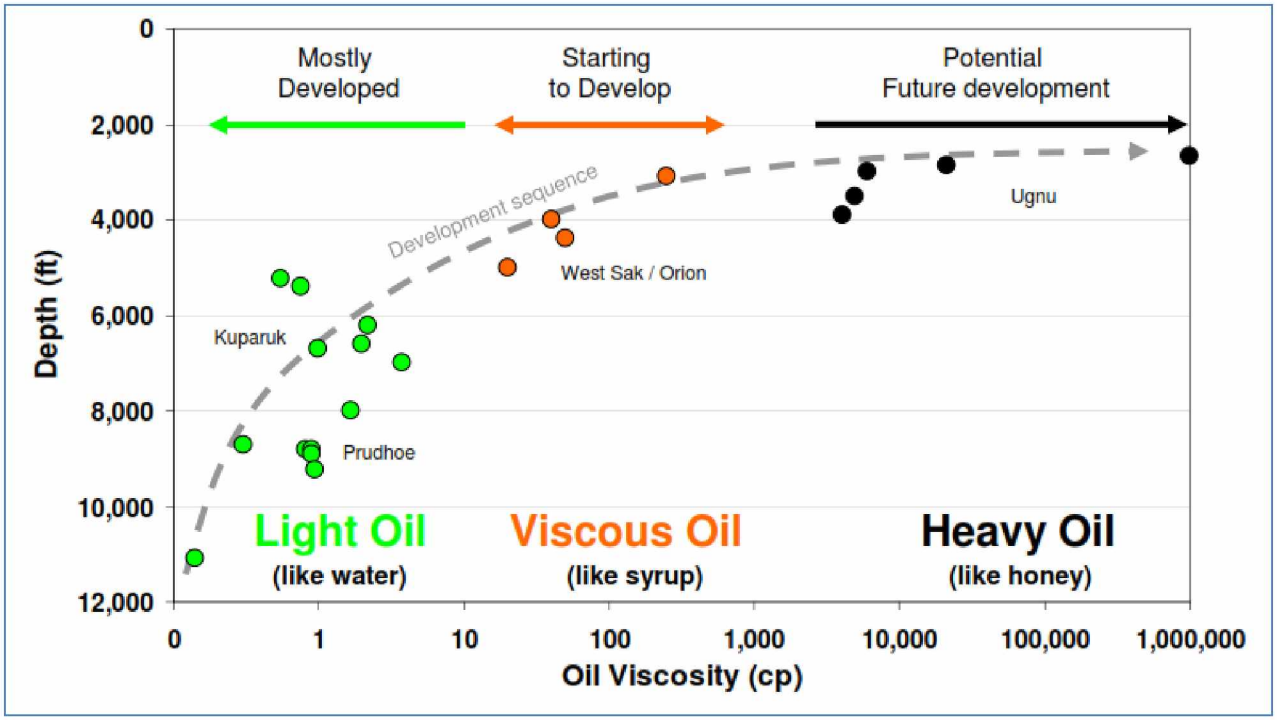

Figure 2-3: North Slope oil fields oil viscosity versus depth (BP 2010).

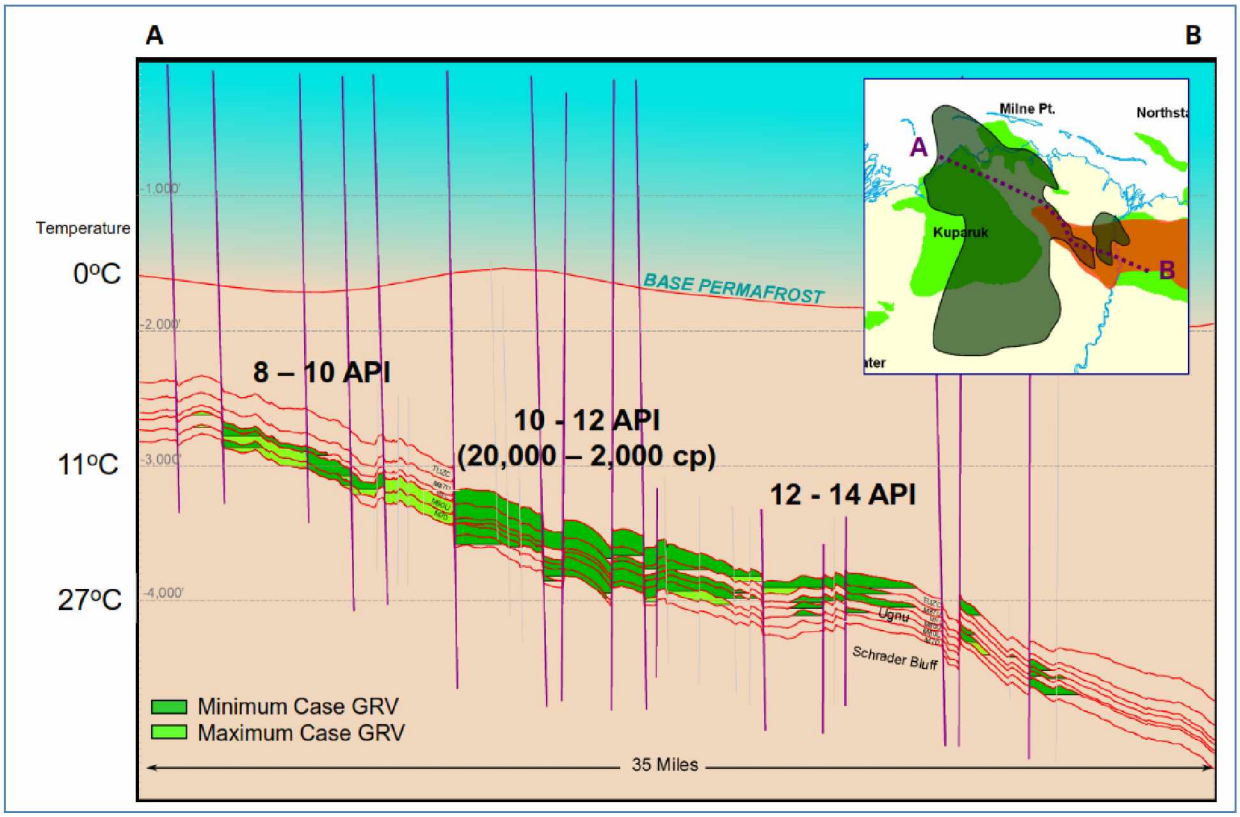

Figure 2-4: The variation of Ugnu API crude (Chmielowski, 2013).

2.2. Monopropellant Potential Reactions and Products

Thermal energy is the most common energy found in nature, and it can readily be converted to other types of energy (e.g., mechanical energy). For producing heat, two material sources are necessary: oxidation material and fuel. The simplest oxidation material is the oxygen in air. As for fuel, certain materials during decomposition produce some heat; their decomposition reaction is exothermic. This type of fuel is usually employed for propelling rockets, and for this reason these fuels are called monopropellant. The difficulty with monopropellant fuel is 'low rate of reaction.' To increase the rate of reaction and consequently increase rate of heat generation, an appropriate catalyst or catalysts are employed. There are different monopropellants; however, two of the more common ones are hydrogen peroxide (H_2O_2) and hydrazine (N_2H_4).

2.2.1. Hydrogen Peroxide

Hydrogen peroxide (H_2O_2) is a strong oxidizing agent. High concentration H_2O_2 or High Test Peroxide (HTP) has been used extensively in the past in propulsion applications as mono- and bipropellant. At low temperature, HTP can be catalytically decomposed to water and oxygen. The decomposition of the monopropellant HTP is accompanied by the production of an enormous amount of heat (85% HTP releases 586 cal/gm at 25˚C) (Sengupta et al., 2004).
Thermochemical study of hydrogen peroxide decomposition allows us to determine the adiabatic decomposition temperature and such other thermochemical parameters as molar mass, specific heat ratio (γ), and the decomposition products as a function of H_2O_2 concentration. The catalytic decomposition of liquid H_2O_2 at any concentration "n" of liquid water is given by Amri et al. (2012):

$$2(H_2O_2)_{Liquid} + n(H_2O)_{Liquid} \rightarrow (n+2)(H_2O)_{Gas} + (O_2)_{Gas} - 108.48\, KiloJoule \quad \ldots\ldots (2\text{-}8)$$

Characteristics of hydrogen peroxide are summarized in Table 2-4 (Ventura and Wernimont, 2001).

Table 2-4: Characteristics summary of hydrogen peroxide (Ventura and Wernimont, 2001).

		Weight % of H2O2	
Property		90	98
Density	(lbm/gal.)	11.57	11.95
Boiling point, 1 atm	(deg. F)	286.2	299.2
Freezing point, 1atm	(deg. F)	11.3	27.5
Vapor pressure, 77 deg. F	mm Hg	3.8	2.2
Viscosity, 77 deg. F	centipoise	1.153	1.155
Surface tension, 68 deg. F	dynes/cm	79.3	80.2
Heat of Vaporization, 77 deg. F	Btu/lb	700.3	662.0

Figure 2-5 shows Adiabatic Decomposition Temperature of H_2O_2 (Ventura and Wernimont, 2001).

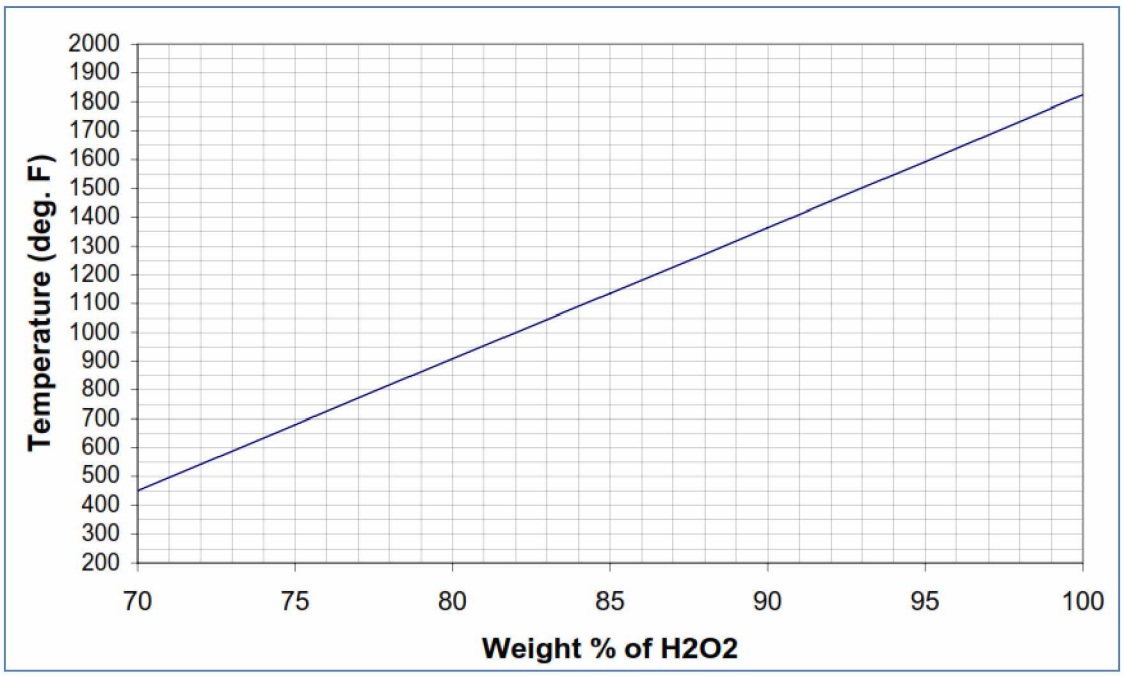

Figure 2-5: Adiabatic decomposition temperature of H_2O_2 (Ventura and Wernimont, 2001)

The weak point of heat generation by hydrogen peroxide is that oxygen is one of its decomposition products. Oxygen can react with hydrocarbon to produce further heat; however, using this material means having an in-situ combustion process in the reservoir. The work of Bayless and Williams (1989), who patented hydrogen peroxide decomposition for heating viscous oil, was based on this concept. They claimed:

'Hydrogen peroxide decomposes into water and oxygen with the liberation of a considerable amount of heat,

$H_2O_2 \rightarrow H_2O+(1/2)\ O_2 \quad \Delta H \sim 23$ Kcal/gm-mole H_2O_2 ..... (2-9)

The oxygen liberated during the decomposition of the peroxide can react with hydrocarbons (assume carbon/hydrogen ratio 1.1) to generate additional amounts of heat.

$$2CH + (5/2)\,O_2 \rightarrow 2CO_2 + H_2O \quad \Delta H \sim 81 \text{ Kcal/gm-mole } O_2 \quad \ldots\ldots\ldots\ldots\ldots\ldots\ldots\ldots \quad (2\text{-}10)$$

The hydrocarbon-oxygen reaction generates considerable quantities of CO_2 gas, which is able to dissolve in adjacent oil and reduce its viscosity, thereby enhancing its recovery. Both above reactions produce heat and water as direct products. This water together with water in the hydrogen peroxide solution will generate steam and/ or hot water zone (depending on the concentration of peroxide solution used) which will reduce the viscosity of the oil to be recovered. The hot, lower viscosity oil can more easily and rapidly be produced than the cooler more viscous oil originally present.'

2.2.2. Hydrazine

Much work was done on hydrazine in the 1950s and 1960s in an attempt to find a better and higher-energy monopropellant (Makled and Belal, 2009); and some researchers tried to use hydrazine for recovery of precious metals (Paul Chen and Lim, 2002). In general, hydrazine (N_2H_4) is considered a powerful reductant widely used in various chemical operations.

Hydrazine is more favorable monopropellant as it is chemically and thermally stable; however, it easily decomposes. Because of stability of this chemical, using a catalyst is essential to obtain the best performance (Makled and Belal, 2009). Sketch of a typical monopropellant engine is shown in Figure 2-6.

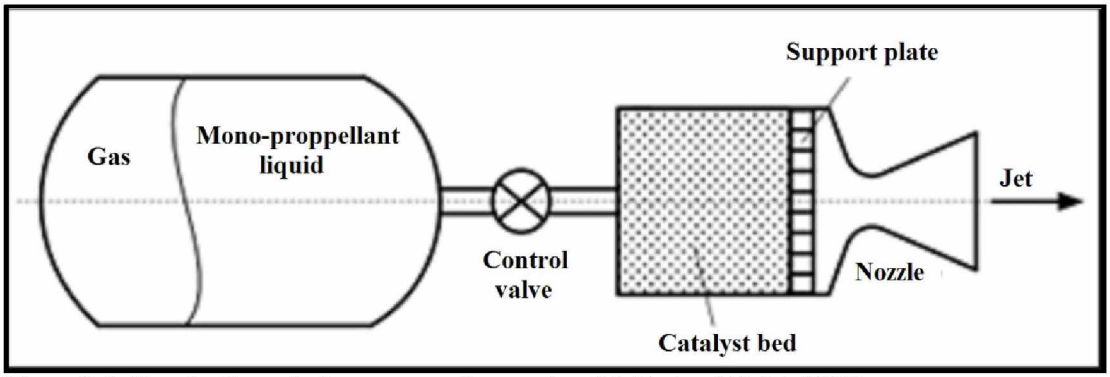

Figure 2-6: Sketch of a typical monopropellant engine (Makled and Belal, 2009)

The first spontaneous hydrazine decomposition catalyst, based on the work of Makled and Belal (2009), were introduced by Shell Development Company in 1963. It was a ruthenium-iridium catalyst with 2.1–28% active metal on activated charcoal: one example consisted of 3.7% Ru and 4.3% Ir on activated charcoal. The most active catalysts described are those containing iridium or a mixture of iridium and ruthenium as active metals.

Also, Makled and Belal (2009) mentioned the following steps for the decomposition mechanism of hydrazine:

a. When the propellant control valve is in the open condition, the pressurized N_2H_4 monopropellant liquid is injected into the catalyst bed at certain flow rate,
b. Once in touch with the catalyst, the N_2H_4 propellant decomposes according to the chemical reaction formula,

$$3\ N_2H_4 \rightarrow 4\ NH_3 + N_2 \qquad \Delta H_r = -36360.71\ cal \quad \text{..... (2-11)}$$

c. A part of the ammonia, NH_3 is further decomposed via the chemical reaction

$$4\ NH_3 \rightarrow 2\ N_2 + 6\ H_2 \qquad \Delta H_r = +19956.81\ cal \quad \text{..... (2-12)}$$

Unfortunately, if the reaction is allowed to continue, the ammonia decomposes in an endothermic reaction. Therefore, the art of N_2H_4 catalyst bed design is aimed at minimizing the effect of this second reaction which lowers operating temperature, reducing overall thruster performance.

The freezing and boiling points colorless liquid hydrazine are 2 ˚C and 113.5 ˚C, respectively. By looking at its relatively high boiling point, it can be judged that a hydrogen bonding should occur among the hydrazine molecules (Zumdahl and Zumdahl, 2007).

Hydrazine is a powerful reducing agent that has been used widely as a rocket propellant. For example, its reaction with oxygen is highly exothermic:

$$N_2H_4(l) + O_2(g) \longrightarrow N_2(g) + 2H_2O(g) \qquad \Delta H^\circ = -622\ \text{kJ} \quad \text{..... (2-13)}$$

Since hydrazine also reacts vigorously with the halogens, fluorine is often used instead of oxygen as the oxidizer in rocket engines. Substituted hydrazines, where one or more of the hydrogen atoms are replaced by other groups, are also useful rocket fuels. For example, mono-methyl-hydrazine, $CH_3N_2H_3$, is used with the oxidizer dinitrogen tetroxide (N_2O_4) to power the U.S. space shuttle orbiter. The reaction is follows:

$$5N_2O_4(l) + 4N_2H_3(CH_3)(l) \longrightarrow 12H_2O(g) + 9N_2(g) + 4CO_2(g) \quad \text{..... (2-14)}$$

As mentioned before, little information is available about the claimed 'new down-hole heat generation technology.' What is known is that this new technology is based on the use of a monopropellant material and that the exhaust products are steam and nitrogen. Since one of the products of hydrogen peroxide decomposition is oxygen, it is very suitable for in-situ combustion (Bayless and Williams, 1989). In this thesis, it is assumed that the monopropellant would be hydrazine and its final products water (steam) and nitrogen. Also, it is assumed that the new technology can produce any amount of heat and products (steam and nitrogen) necessary for reservoir stimulation.

2.3. Other Methods of Down-Hole Heat Generation

An appreciable amount of heat loss occurs in the transportation of fluid (steam or hot water) from the generation site to the down-hole of injection wells, and from early on in the execution of thermal stimulation methods, down-hole heat generation has been an important issue for researchers. Their investigations can be categorized as follows:

- Down-hole steam generation,
- Down-hole electrical heating systems,
- Down-hole methanation.

There are other methods of chemically changing the heavy molecules of crude in situ by applying heat to heavy oil reservoirs. This process is called 'aquathermolysis,' and it involves the application of specific temperature and pressure conditions to break chemical bonds (like C-S bond) in heavy oils molecules and improve the concentration of saturated hydrocarbons and lighter aromatics. Nowadays scientists realize that application of a catalyst improves the extent

of bond breakage and viscosity reduction, and with 'catalytic aquathermolysis' the appropriate catalyst or catalysts are used to efficiently achieve viscosity reduction (Muraza and Galadima, 2015). In the 'open literature', one finds some documents that claim they have conducted experiments and have pilot tested this method in heavy oil reservoirs (Wen et al., 2007). For further detailed data about this method, the reader is referred to a good review on this subject written by Muraza and Galadima (2015).

2.3.1. Down-Hole Steam Generation

A steam generator, a surface piping network, and an appropriate well completion string are essential for application of any steam stimulation method. In transmission from steam generator down to sand face, a lot of energy in thermal form is lost. It is claimed that steam generated in an above-ground boiler will lose 50% of its heat energy in transit (R.I.I. North America, 2016). Lost energy means lost money; so, down-hole steam generation with zero heat lost sounds very attractive. Surface steam-generation methods are usually considered suitable for shallow oil bearing formations of about 1000 ft (Fox and Stosur, 1981).
Fox and Stosur (1981) reported that the U. S. Department of Energy initiated development of tools for the down-hole production of steam 1978: field testing of a high-pressure combustion generator was carried out in a shallow reservoir (275 meters). Later field tests examined the performance of the device for down-hole operations in reservoirs below 700 meters.

It seems that the down-hole steam generation method has become a matured technology; so, several companies claim that they can manufacture the required devices (R.I.I. North America, 2016 and eSteam™, 2016). In addition to these conventional down-hole steam generation systems, a few companies claim to have used the catalytic system for down-hole steam generation (Precision Combustion, Inc., 2015).

2.3.2. Down-Hole Electrical Heating System

Using electricity for down-hole heating of heavy oil-bearing formations was first proposed by Ritchey (1956); (Bera and Babadagli, 2015). This method was claimed suitable for heating thin

heavy oil-bearing formations or for preventing paraffin breakout, clay swelling, or fluid blockage (Isaev and Tsigankova, 2011; Davison, 1995; Jamaluddin et al., 1998). Researchers (Mohsin Rehman and Meribout, 2012) considered this method, called Electrical-based EOR (EEOR), as an alternative/complementary technique to conventional EOR techniques. Any method that uses some electrical means (e.g., sound waves, RF waves, inductive heating, DC heating) falls into the category of EEOR thermal recovery method. The basic function of an EEOR process is to increase the mobility of the oil by reducing its viscosity, which in turn helps the oil easily move toward the production well, because the electrical energy supplied to the reservoir will either raise the temperature of the oil or create vibrations in the hydrocarbon molecules.

Using the frequency of electrical current, electric heating methods were divided into two classes by Carrizales et al. (2008) and into three main categories by Mohsin Rehman and Meribout (2012). Here, it is mainly referred to categories division made by Mohsin Rehman and Meribout (2012). Low-frequency electric current is best suited for Ohmic or Resistive heating, while high-frequency electric current can be used for microwave heating methods. For inductive heating, a range of low- and medium-frequency electric currents can be used depending on the energy availability (Hascakir et al., 2008).

Low frequency currents are used in electrical resistive heating (ERH), and their levels are less than 60 Hz so that resistance heating dominates the process (Carrizales et al., 2008). In this method, the electric current passes through the formation and, due to power dissipation, heat is produced, which in turn heats the reservoir. This method can be employed using two oil wells: one as anode and the other as cathode. A potential difference is provided between these two electrodes, and a current is allowed to pass through the formation. Since formation water is commonly saline, the formation conducts electricity fairly well (Sierra et al., 2001). A sketch view of the low-frequency heating procedure is shown in Figure 2-7 (Mohsin Rehman and Meribout, 2012).

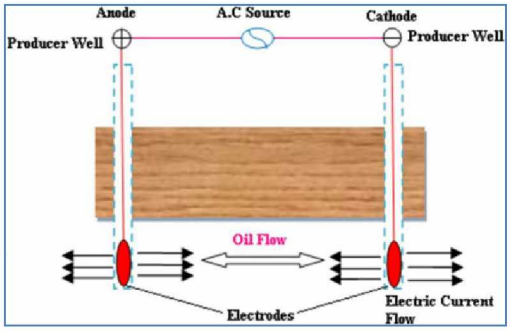

Figure 2-7: A sketch view of the low-frequency heating procedure (Mohsin Rehman and Meribout, 2012).

High frequency currents are used in microwave heating (MW) or radio frequency (RF) heating (Carrizales et al., 2008). These frequencies may vary from KHz to MHz level, and in this mode dielectric heating dominates the process (Kim, 1987; Sahni et al., 2000; Sierra et al., 2001). Normally microwaves are either transmitted by a material, absorbed, or reflected. In most cases microwaves interact with water molecules, as they are polar in nature. Hence, when microwaves are applied, these polar water molecules are set into circulatory motion, and they collide speedily with other molecules with the frequency of these collisions equal to the frequency of applied microwaves. In result much heat is produced (Okassa et al., 2010). This rise in temperature reduces the viscosity of oil and hence causes it to flow toward the production well from which it can be extracted (Mohsin Rehman and Meribout, 2012).

Electromagnetic (EM) induction heating is a technique where electrically conductive materials are placed in a variable magnetic field generated by an exciting winding which is called inductor. Exciting winding produces electromotive force (emf) to set up the flux in an electric machine or other apparatus. The current produced in this process is also called Eddy current. Due to the Joule effect ($P_{dissipiated} = I^2R$, where P is the power in Watt, and I is the current in amp, and R is the resistance in ohm), this current dissipates heat in the material in which it is placed. The governing factors of the heating process are the specific heat of the material, the frequency of induced current, the permeability of the material, and the resistance of the material to flow current through it (Bera and Babadagli, 2015). In the case of induction heating, a number of inductors are normally installed at the bottom of production tubing facing the production zone. Production tubing acts as an inductively heated source to radiate heat inside the production zone as shown in Figure 2-8 (Vermeulen and McGee, 2000; Mohsin Rehman and Meribout, 2012).

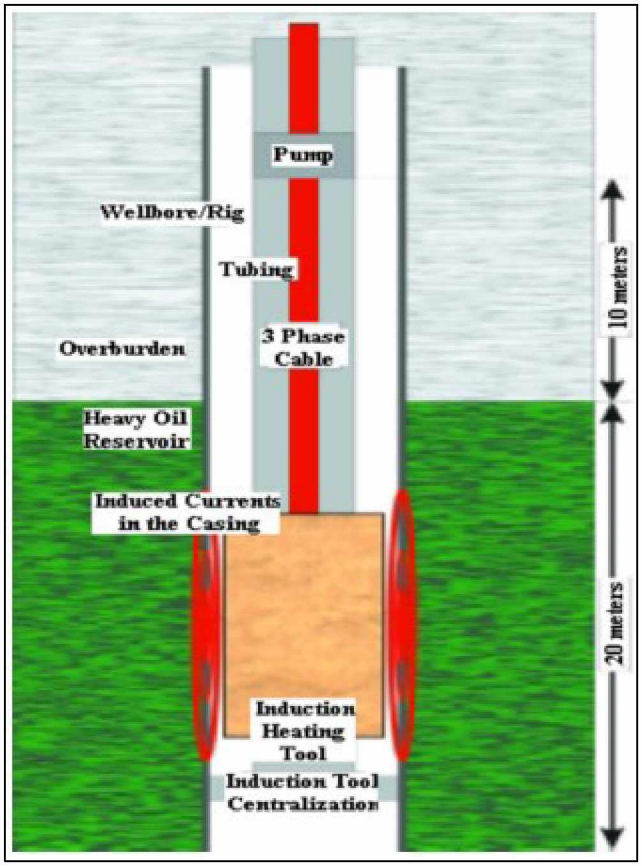

Figure 2-8: Sketch of EM heating (Vermeulen and McGee, 2000; Mohsin Rehman and Meribout, 2012).

Mostly inductive heating is employed for near-well bore heating in vertical wells. The inductive tool can be installed near the heavy formation and results in increased oil recovery because of the reduction in the viscosity of the formation oil (Mohsin Rehman and Meribout, 2012).

The advantages of these Electric Bottom Hole Heating Systems are summarized by Isaev and Tsigankova (2011):

(1) Economical advantage – lowest cost of any thermal recovery method.

(2) Non-contaminating – no foreign or corrosive materials

(3) Safety – no damage to well bore or production formation; temperatures are maintained well below cooking point.

(4) Efficiency – essentially all heat generated is delivered to the producing zone.

(5) Simplicity – no special well completions required and no need for complex support equipment.

(6) Continuous operation – no downtime; well is pumped at all times during heater operation, unlike with cyclic stimulation methods.

In the open literature, one can find several examples of electrical down-hole heating system field applications. For example, Islam et al. (1991) investigated fluid injection along with electromagnetic heating in the tar sand reservoir of Ugnu, Alaska. They claimed numerical results indicated that by using horizontal wells in conjunction with electromagnetic heating, a significant amount of oil in place could be recovered. This recovery could be substantially improved by injecting gravity stable gas. Also, a vertical injector with electrically heated horizontal wells in both Upper and Lower Ugnu formations recovered over 40% of the oil in place.

Davison (1995) presented the field results of electromagnetic stimulation of Lloydminster heavy oil reservoirs. He claimed that through the application of electromagnetic (EM) heating, the production can be improved by factor 2 just for a capital investment of 25 - 30% over normal well costs.

2.3.3. Methanation

For generating down-hole steam for heavy oil recovery, a process based on methanation was patented by Rhoades and Meeks (1983). Methanation is the catalytic conversion of CO and/or CO_2 to methane and is also known as a Sabatier reaction (Wang and Gong, 2011). This type of reaction was discovered by Sabatier and Senderens in 1902 (Er-rbib and Bouallou, 2013). The following reactions take place in this type of process (Wang and Gong, 2011; Er-rbib and Bouallou, 2013; Bridger and Woodward, 1975):

$CO_2 + 4H_2 \leftrightarrow CH_4 + 2H_2O \quad \Delta H_{298k} = -252.9\ kcal/mole$ ..... (2-15)

$CO + 3H_2 \leftrightarrow CH_4 + H_2O \quad \Delta H = -206.28\ kcal/mole$ ..... (2-16)

$CO + H_2O \leftrightarrow CO_2 + H_2 \quad \Delta H = -41.16\ kcal/mole$ ..... (2-17)

$CO + 3H_2 = CH_4 + H_2O \quad \Delta H_{573k} = -51.8\ kcal/mole$ ..... (2-18)

$CO_2 + 4H_2 = CH_4 + 2H_2O \quad \Delta H_{573k} = -41.9\ kcal/mole$ ..... (2-19)

Notice: 1 cal. = 4.184 Joule

2.4. Enhanced Oil Recovery (EOR)

Conventional oil recovery methods that rely on natural depletion drives cannot drain all oil in place. To increase oil recovery, additional artificial drives should be added to hydrocarbon

reservoirs. Of course, this is true only for relatively low viscosity crude reservoirs from which oil can naturally flow under reservoir conditions. But the ability of oil to flow under reservoir conditions decreases as oil viscosity increases, and application of some sort of EOR method becomes essential. In the past, EOR methods were applied near the end of the natural depletion life of a reservoir. But in the last decades, in big international development oil companies, a development whereby EOR methods are applied early in the life of the reservoir has been contemplated.

Babadagli (2012) defined EOR as oil recovery by the injection of materials not normally present in the reservoir. In other words, EOR is applying methods to recover more oil than is producible by natural mechanisms or primary recovery. Carcoana (1992) considered the producing hydrocarbons as the 'primary reserve' when they are produced by primary recovery methods using natural energy inherent in the reservoir. The driving energy may be derived from liberation and expansion of dissolved gas, from the expansion of the gas cap or an aquifer, from gravity drainage, or from a combination of these effects. He differentiated between improved and enhanced oil recovery; 'improved recovery reserves' are produced by improved recovery methods, in addition to the primary reserves, using additional energy. Improved recovery methods are subdivided into conventional methods (secondary methods), which involve injection of gas and/or water into the reservoir, and enhanced oil recovery methods (tertiary methods), of which thermal, chemical, and miscible methods are generally recognized as most promising. However, Donaldson et al. (1989) divided oil recovery methods into three major categories: primary, secondary and enhanced oil recovery. Madaoui (2005) did not include gas injection as a secondary recovery method (see Figure 2-9). Carcoana (1992) divided the oil reservoirs depletion methods to primary and improved recovery schemes.

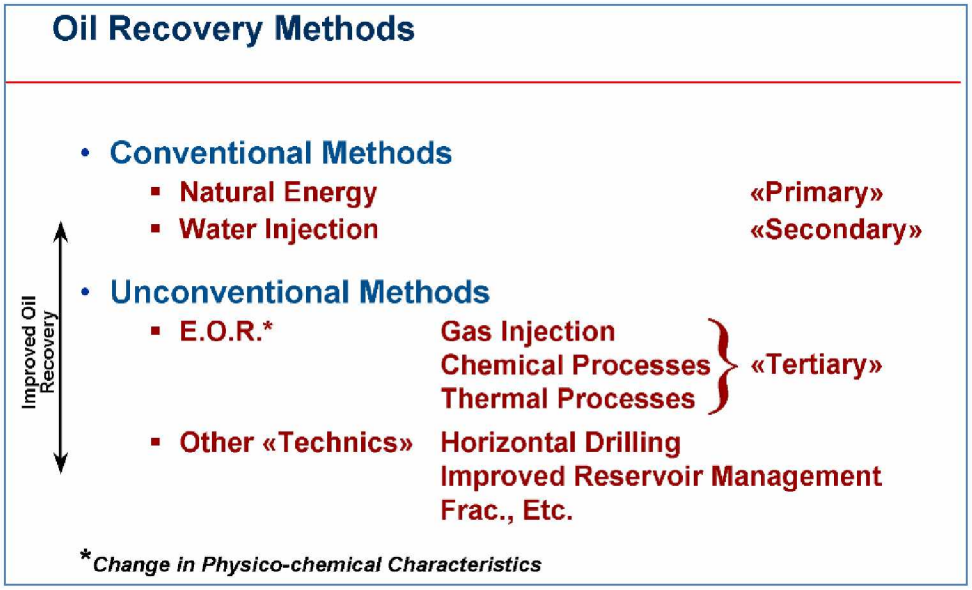

Figure 2-9: Oil recovery methods (Madaoui, 2005).

Taber et al. (1997a) stated that the *Tertiary* recovery method should not be used as a synonym for EOR because some EOR methods work quite well as either secondary or tertiary projects (e.g., CO_2 flooding), while others, such as steam- or polymer flooding, are most effective as enhanced secondary operations. To them, EOR simply means that something other than plain water or brine is being injected into the reservoir.

As is obvious from the above paragraphs, different researchers categorized oil recovery methods in different ways. Three of these oil recovery process subdivisions are presented in the following tables. Table 2-5 presents a good review of current and past EOR methods. For detail of each of these methods, reader is referred to Taber et al. (1997a). In Table 2-6, the EOR processes are divided to three main categories: chemical processes, thermal processes, and miscible displacement process. However, in Figure 2-10 EOR methods are categorized according to their basic concepts: gas based EOR, water based EOR, and thermal methods.

Table 2-5: Categorized EOR methods (Taber et al., 1997a)

CURRENT AND PAST EOR METHODS	
Method	Table Number (ref.: Taber et al., 1997b)
Gas (and Hydrocarbon Solvent) Methods	
"Inert" gas injection	
Nitrogen injection	1
Flue-gas injection	1
Hydrocarbon-gas (and liquid) injection	2
High-pressure gasdrive	
Enriched-gasdrive	
Miscible solvent (LPG or propane) flooding	
CO_2 flooding	3
Improved Waterflooding Methods	
Alcohol-miscible solvent flooding	
Micellar/polymer (surfactant) flooding	4
Low IFT waterflooding	
Alkaline flooding	4
ASP flooding	4
Polymer flooding	5
Gels for water shutoff	
Microbial injection	
Thermal Methods	
In-situ combustion	6
Standard forward combustion	
Wet combustion	
O_2-enriched combustion	
Reverse combustion	
Steam and hot-water injection	7
Hot-waterflooding	
Steam stimulation	
Steamflooding	
Surface mining and extraction	—

Table 2-6: Various EOR processes (Donaldson et al., 1989).

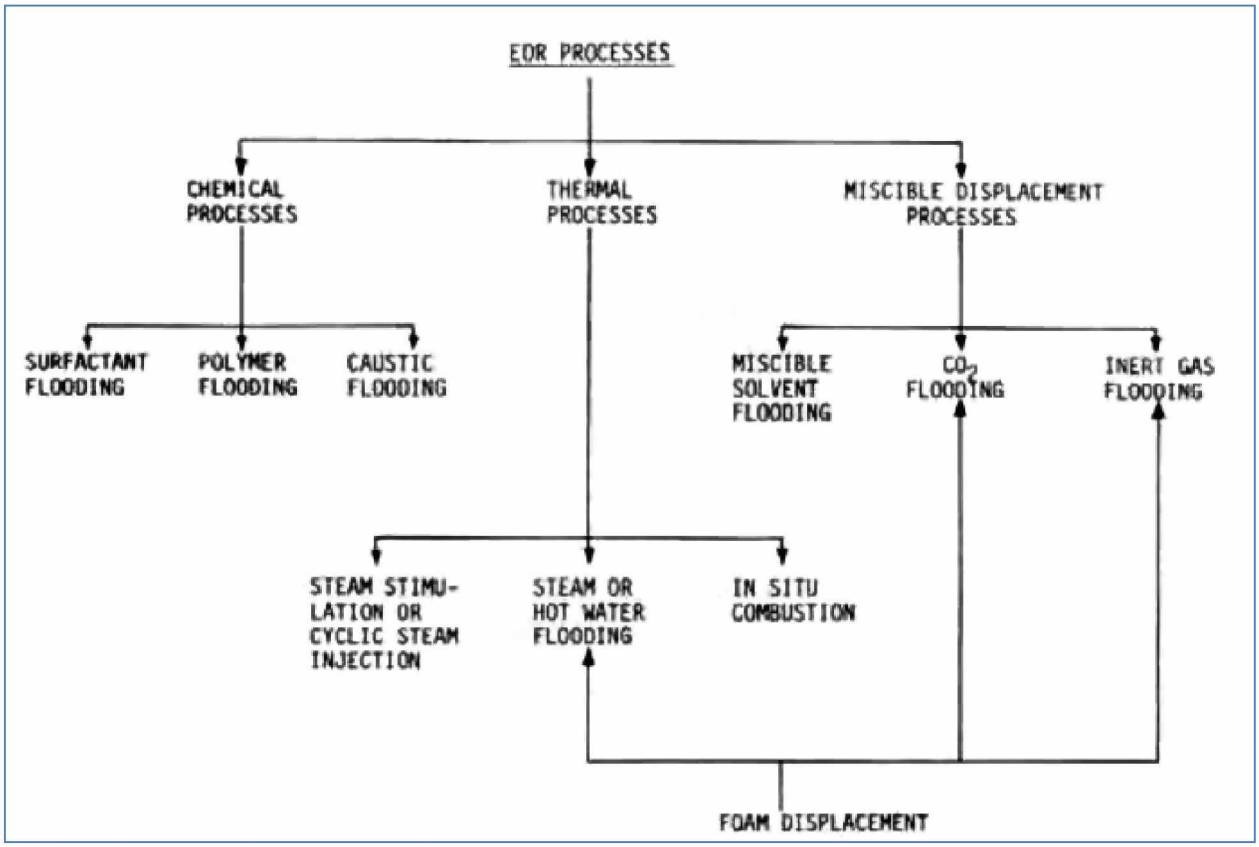

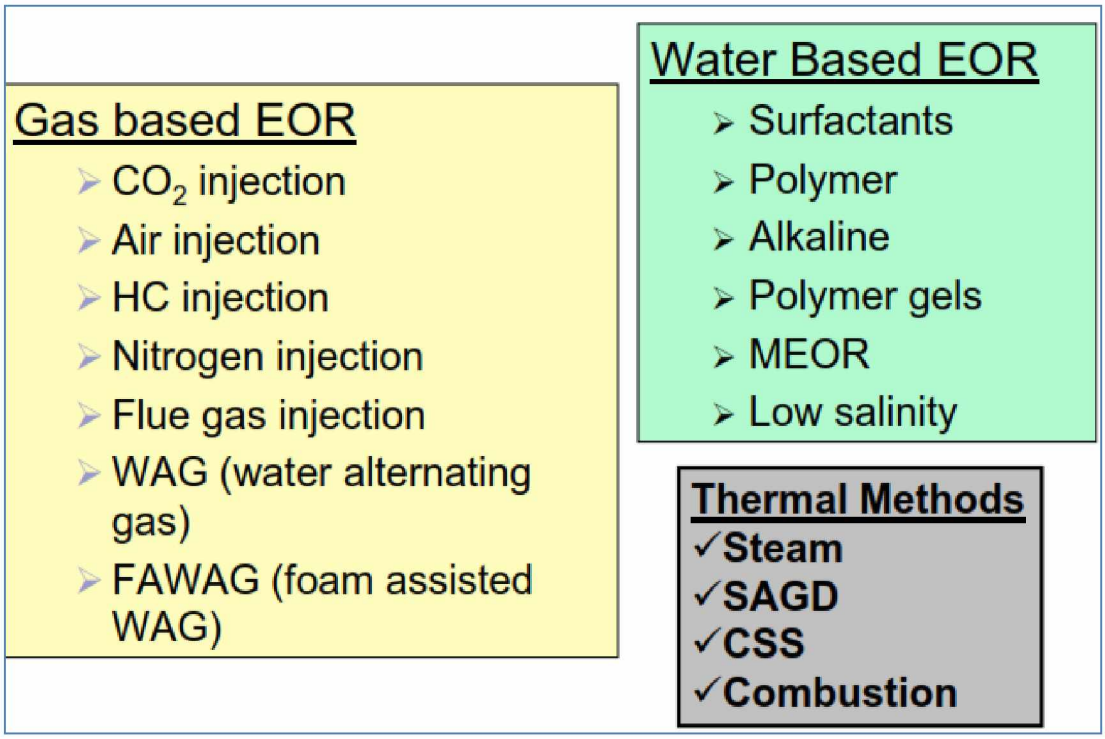

Figure 2-10: EOR methods (Delshad, 2011).

Table 2-7: Recovery mechanisms (Delshad, 2011).

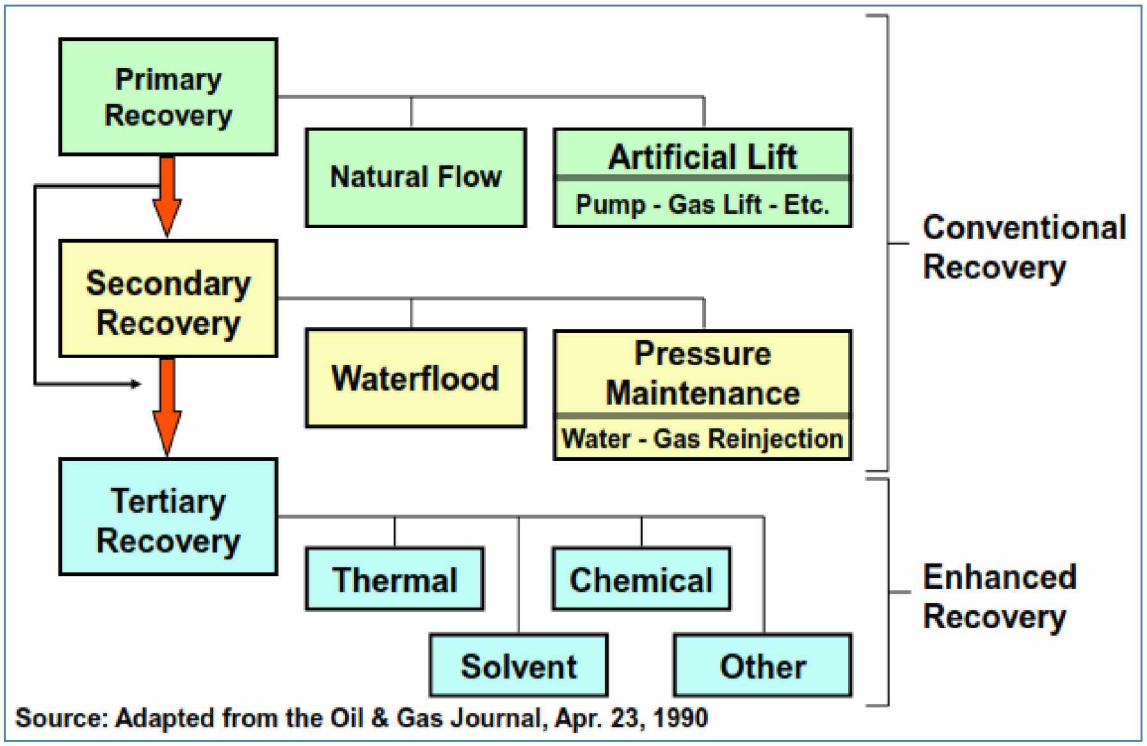

Although, recovery methods for both conventional and heavy oil are more or less the same, there are also specialized recovery processes for heavy oil production. Law (2011) divided the heavy oil recovery system into four classes: surface mining, primary recovery, thermal and non-thermal methods (see Figure 2-11). The thermal methods are divided to steam-based and combustion methods. The steam-based heavy oil recovery method is related to subject of this thesis.

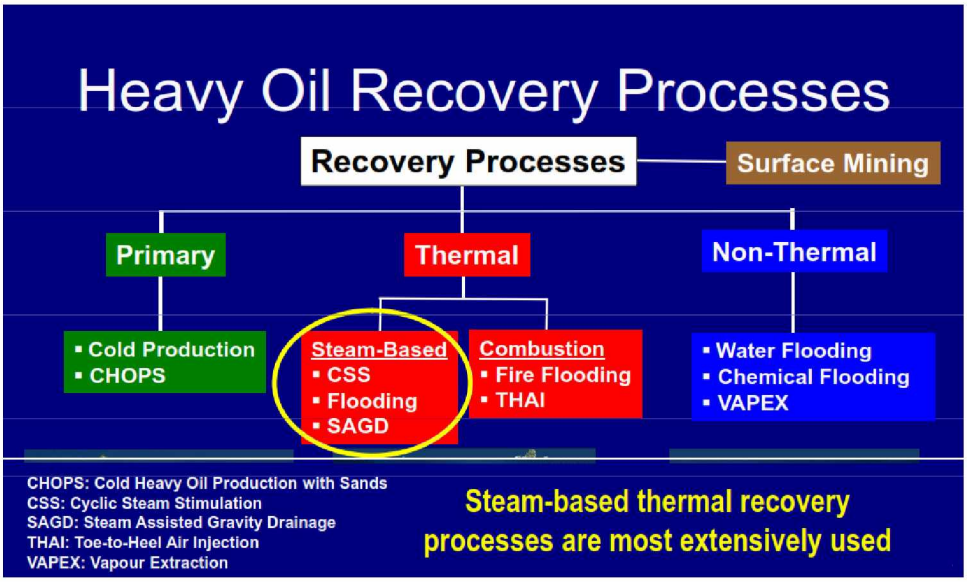

Figure 2-11: Heavy oil recovery process (Law, 2011).

Dickson et al. (2010) presented an extensive methodology for screening hydrocarbon recovery methods. Screening criteria for thermal methods are shown in Table 2-8.

Table 2-8: Screening criteria for EOR thermal methods (Dickson et al, 2010).

SCREENING CRITERIA FOR THERMAL METHODS				
Property	CSS	Steamflooding	SAGD	Hot Water Inj.
Oil Gravity (API)	8–35	8–20	7–12	10–35
In-situ Oil Viscosity (cP)	10^3–10^6	10^3–10^4	4,000–10^6	10^3–10^4
Reservoir Depth (ft)	400–3,000	400–4,500	250–3,000	<3,000
Pay Thickness(ft)	>20–150	15–150	50–100	>20
Average Horz. Perm. (mD)	>250	>250	>5,000	>35
Reservoir Pressure (psia)	400–1,500	<1,500	High	>2,000
Oil Saturation (%)	>50	>40	>50	>50

Based on the work of Dickson et al. (2010), the following table for general EOR was prepared by Delshad (2011).

Table 2-9: EOR screening (Delshad, 2011).

Property	HC gas	CO2	N2/Flue	CSS	Steam	SAGD	Hot water	Polymer	ASP
Oil API	>30-40	>22	>40	8-35	8-20	7-12	10-35	>15	>20
Oil viscosity, cp	<3	<10	<0.4	10^3 - 10^6	10^3 - 10^4	4000 - 10^6	10^3 - 10^4	10-1000	<35
Reservoir Depth, ft	4000-16000	>2500	>10,000	400-3000	400-4500	250-3000	<3000	800-9000	500-9000
Permeability, md	--	--	--	>250	>250	>5000	>35	>100	>100
Pressure, psia	>MMP	>MMP	<MMP	400-1500	<1500	High	>2000	--	--
Oil saturation, %	>30	>20	>40	>50	>40	>50	>50	>30	>45
Thickness, ft	Thin	Thin	Thin	>20-150	15-150	50-100	>20	--	--
Salinity, ppm	--	--	--	--	--	--	--	<3000	< 200,000
Temperature, F	Affect MMP	Affect MMP	--	--	--	--	--	< 170	<200

Delshad (2011) also provided the range of viscosity for potential heavy oil recovery processes as shown in the following figure (Figure 2-12).

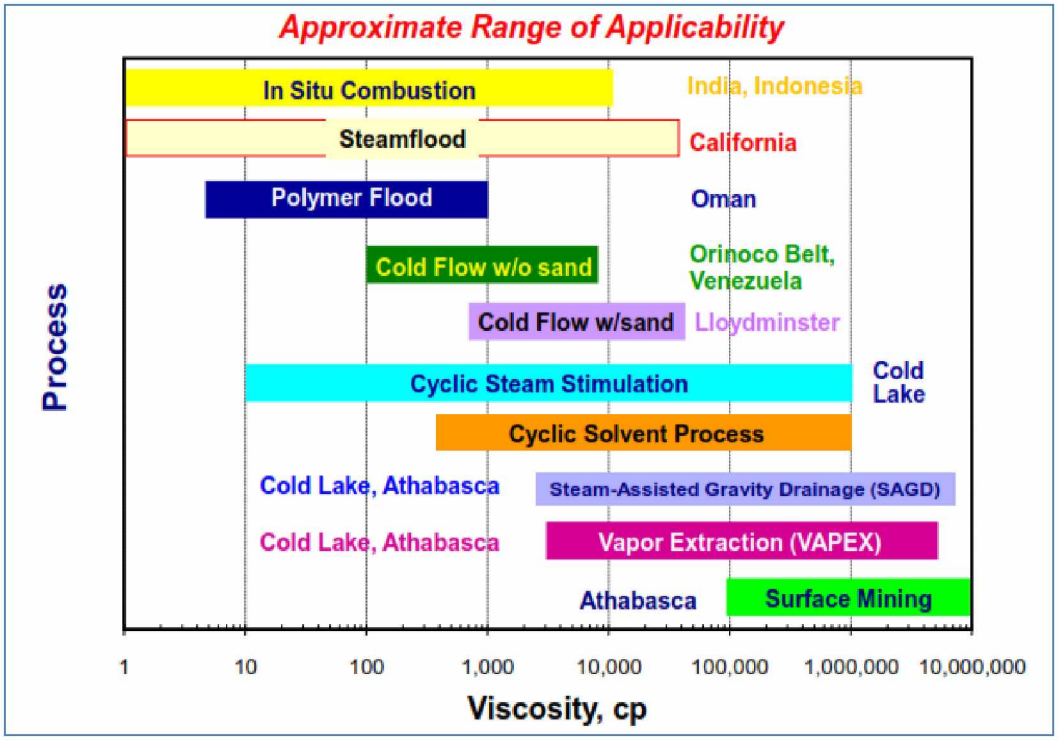

Figure 2-12: Approximate range of applicability for heavy oil recovery methods (Delshad, 2011).

This thesis investigated the feasibility of using down-hole heat generated by some sort of catalytic chemical decomposition (e.g., hydrazine); however, as mentioned before, the final product of reaction/decomposition of the injected chemical was assumed to be nitrogen and water in gaseous phase. Therefore, this thesis can be considered as a feasibility study of application of one special type of thermal, steam injection, EOR method in heavy oil reservoirs of the North Slope of Alaska. Thus in the following sections, main focus will be on a type of steam injection process. So, the theoretical basics of steam injection methods are reviewed next.

2.4.1. Steam Injection

Steam injection is one thermal EOR method that uses hot water vapor injection into the formation to reduce the viscosity of oil. Delshad (2011) prepared the following guide for screening a reservoir for steam injection EOR (Table 2-10).

Table 2-10: Technical screening guide for steam injection methods.

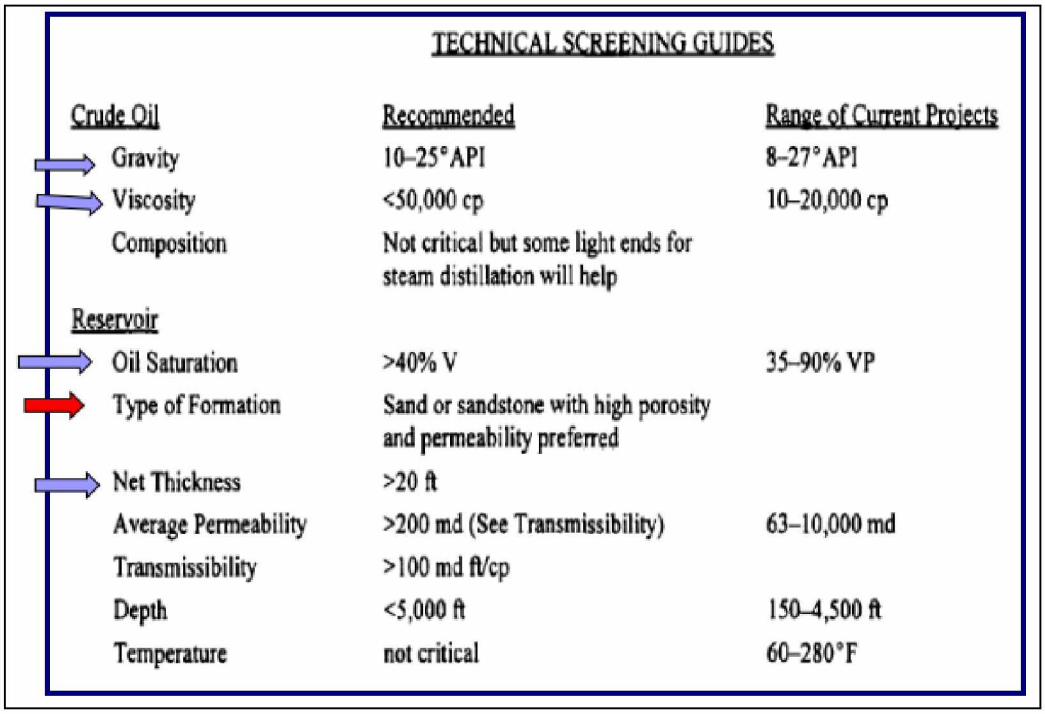

TECHNICAL SCREENING GUIDES

Crude Oil	Recommended	Range of Current Projects
Gravity	10–25°API	8–27°API
Viscosity	<50,000 cp	10–20,000 cp
Composition	Not critical but some light ends for steam distillation will help	
Reservoir		
Oil Saturation	>40% V	35–90% VP
Type of Formation	Sand or sandstone with high porosity and permeability preferred	
Net Thickness	>20 ft	
Average Permeability	>200 md (See Transmissibility)	63–10,000 md
Transmissibility	>100 md ft/cp	
Depth	<5,000 ft	150–4,500 ft
Temperature	not critical	60–280°F

Steam injection methods are divided into three main categories: Steam Simulation or Cyclic Steam Stimulation (CSS), steam flooding, and Steam Assisted Gravity Drainage (SAGD). In cyclic steam stimulation ('huff and puff' or CSS), the following stages are considered for well/reservoir stimulation (see Figures 2-13 and 2-14) (Delshad, 2011):

- Steam injection: 2–30 days,
- Soak period: 5–30 days,
- Production: 1–6 months

In steam flood, steam is injected into one or more wells. Oil is produced from adjacent wells.

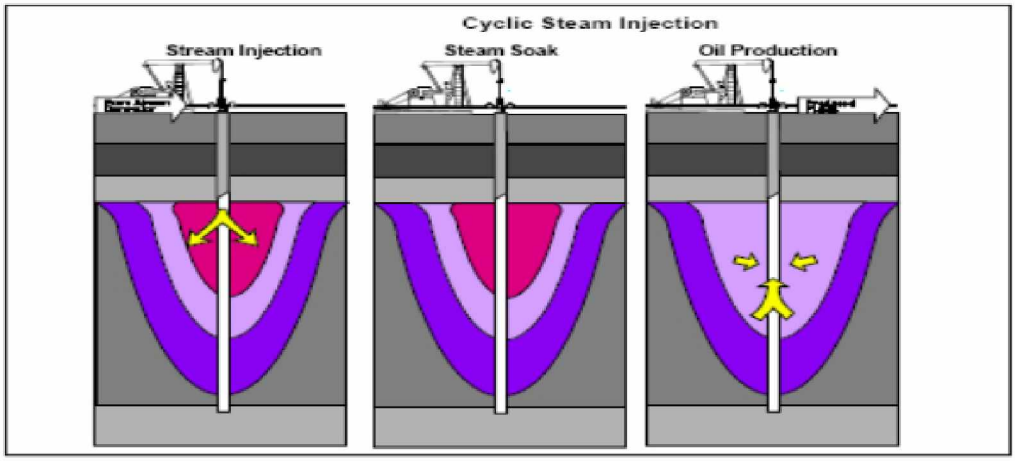

Figure 2-13: Operation stages in CSS method (Delshad, 2011).

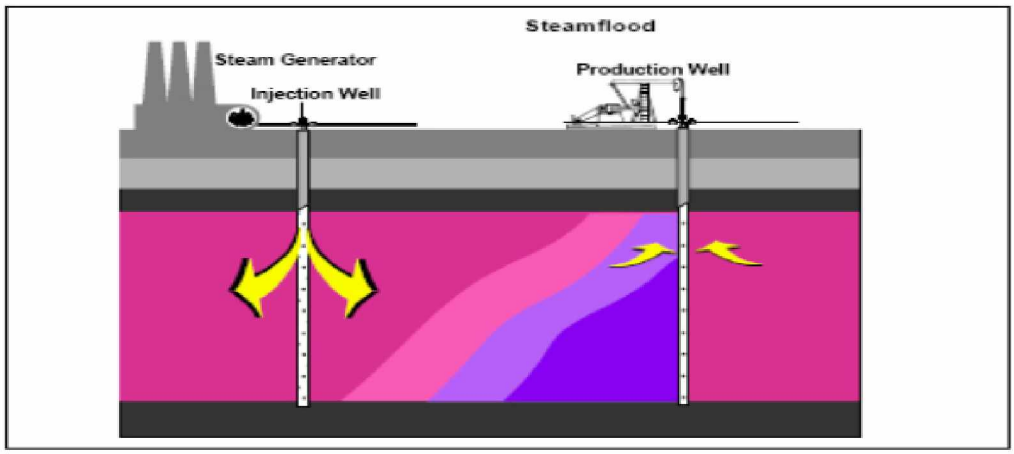

Figure 2-14: Schematic steam flood method (Delshad, 2011).

The stimulation of heavy oil reservoirs with steam injection can be well distinguished from a steam drive displacing heavy oil. With steam stimulation (or steam soak) a small amount of steam will heat a small fraction of the reservoir. With steam drive, a large amount of steam is injected and a large part of the reservoir is heated (Van Lookeren, 1982). Another way to distinguish steam stimulation from steam drive is that the first process will not lead to oil production if there are no oil producing mechanisms present or put to work. Steam drive on the other hand is essentially a powerful gas drive with some of the effect of a water drive from the condensed steam, and with usually effective gravity drainage.

Delshad (2011) considered the following zones during operation of steam flood: unheated zone, hot condensate zone and steam zone (see Figure 2-15). In unheated zone which is adjacent to producer well, neither heat propagated and nor hot fluid reached to the formation and the oil saturation is about at initial value. In the steam zone, close to injector well, steam sweeps the oil

and the oil saturation is its minimum value. Between these two zones, there is a zone that a mixture of oil, condensed water and even some condensate co-exist. The condensate in this zone is produced from vaporization of light components of crude oil and then condensed back to liquid.

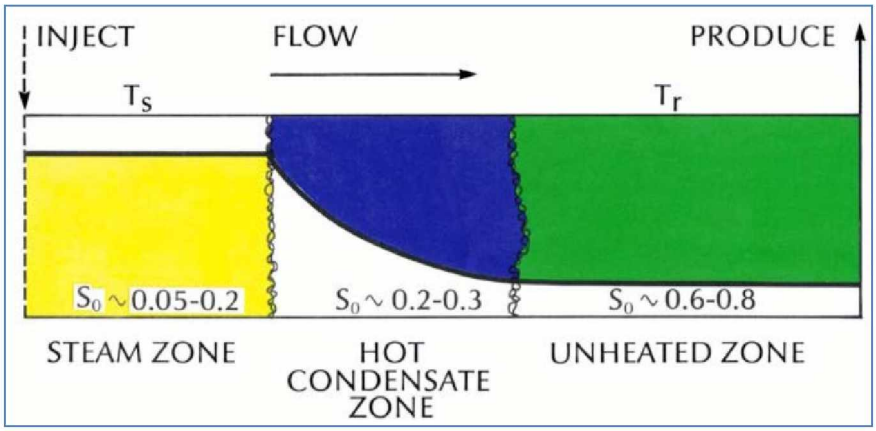

Figure 2-15: Fluid zones in steam drive (Delshad, 2011).

The Steam Assisted Gravity Drainage (SAGD) method can be considered an improvement to steam flooding. In this method two horizontal wells are drilled in a reservoir with thick, heavy oil usually near the bottom of the pay zone (Law, 2011). Steam is injected in the upper well, and the lower well is used for oil production. A schematic view of this method is shown in Figure 2-16 (Madaoui, 2005).

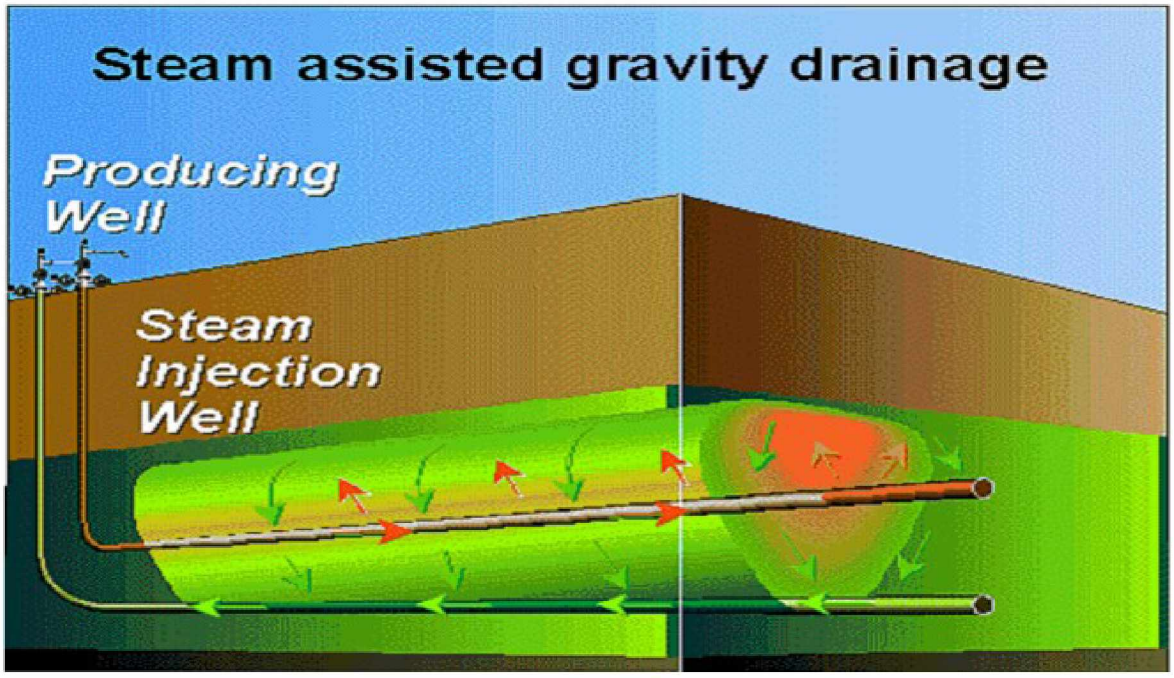

Figure 2-16: Steam Assisted Gravity Drainage (Madaoui, 2005).

In the SAGD method, the steam chamber rises then spreads sideways, and oil drains down to the oil producer. Law (2011) mentioned that the oil recovery in this method can be greater than 50 percent of Original Oil In Place (OOIP). A schematic presentation of oil drainage in SAGD method is presented in Figure 2-17 (Madaoui, 2005).

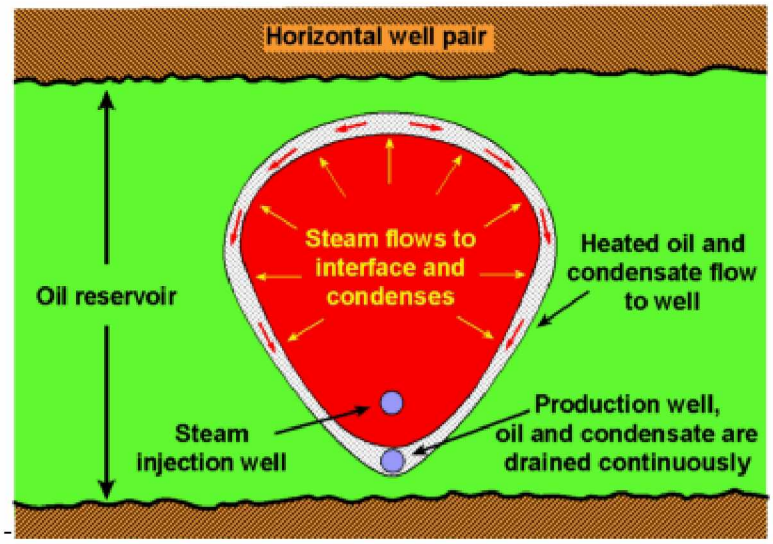

Figure 2-17: Schematic presentation of oil drainage in SAGD method (Madaoui, 2005).

2.4.1.1. Properties of Steam

Steam injection is similar to the other hot fluid injection. Hot water and gas injection into the formation heat up the rock and fluid of the reservoir. As water has higher heat capacity than gas, water is more favorable reservoir's heating agent. By injecting hot water into the formation, sensible heat of the water is transferred to the reservoir. Steam, in addition of sensible heat, contains latent heat that its amount is much more than the sensible heat. By steam injection, entire latent heat plus some of sensible heat is transferred to the reservoir. For example, latent heat of steam at 350 °F is about 970 Btu/lbm; however, sensible heat of water from 350 °F to 130 °F is just about 224 Btu/lbm. Also, steam has more benefits in regard to other favorable effects such as vaporization and condensation (Carcoana, 1992). An example of a Cartesian plot of amount of sensible and latent heat of water/steam system as a function of pressure is shown in Figure 2-18 (Carcoana, 1992).

In steam injection process, a mixture of water and steam is usually injected in the formation. To show the amount of steam to total injected fluid, the term quality is used. Steam quality is defined as

$$f_s = \frac{m_v}{m_v + m_l} \quad \text{.....} \quad (2\text{-}20)$$

Heat capacity is expressed in units of Btu/(lbm-°F). A "Btu" is defined as the amount of heat required to raise the temperature of 1 lbm of water from 60 to 61°F. Notice that petroleum has a specific heat of 0.5 (half that of water) and sandstone is only 20% of water on a mass basis. No other liquid or gas carries as much heat per pound as water (Jones, 2007). Here, it is worthwhile to mention the general definition of specific heat units. Somerton (1992) described the units this way: specific heat is derived from the amount of heat required to raise the temperature of a unit mass of pure water one degree at standard conditions (15°C, atmospheric pressure). This value is 1.00 cal/g-°C, 1.00 Btu/lb-°F or 4.184 kJ/kg-K.

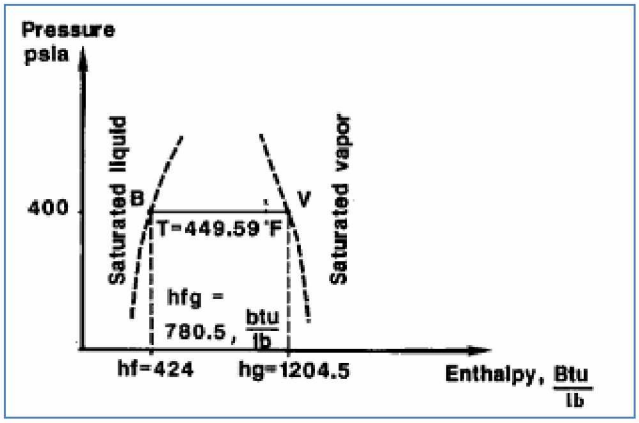

Figure 2-18: Water-steam enthalpy curve at P=400 psia and T=449.59°F (Carcoana, 1992).

The volume occupied by 1 lbm of steam at any pressure is its specific volume in ft^3/lbm and is represented by v_s. The values for these thermal properties of water are published widely (Jones, 2007). The properties of steam are tabulated (Keenan and Keyes, 1967; GPSA, 2004) for wide range of saturation temperatures and corresponding pressures in step increments of 1°F between 32°F and 200°F, 2°F between 200°F and 400°F, and 5°F between 400°F and 700°F, There are also tables with saturation pressures and corresponding temperatures for different step increments. For instance, between 350 psia and 500 psia, the step increment is 10 psia; and between 500 psia and 1000 psia, the step increment is 20 psia. For oilfield steam operations, the properties of interest are:

- Enthalpy of saturated vapor (total heat), h_g or h_v
- Change in enthalpy (latent heat), $h_{fg} = h_g - h_f$ or $h_{fv} = h_v - h_f$
- Specific volume of saturated liquid, V_f, ft^3/lbm
- Specific volume of saturated vapor, V_g, ft^3/lbm

The following tables show enthalpy and specific volume values of water and steam at saturation temperatures from 425 to 445°F and at saturation pressures between 400 and 440 psia (Carcoana, 1992).

Table 2-11: Steam properties based on temperature (Carcoana, 1992).

Temp., °F T	Abs. Press., psia p	Specific Volume (ft^3/lb_m) of Saturated Liq. v_f	Specific Volume (ft^3/lb_m) of Saturated Vap. v_g	Enthalpy, Btu/lb_m Saturated Liquid h_f	Enthalpy, Btu/lb_m Change in Enthalpy h_{fg}	Enthalpy, Btu/lb_m Saturated Vapor h_g
425	325.92	0.01902	1.4226	402.77	801.2	1203.5
430	343.72	0.01910	1.3499	407.79	796.0	1203.8
435	362.27	0.01918	1.2815	413.34	790.8	1204.1
440	381.59	0.01926	1.2171	418.90	785.4	1204.3
445	401.608	0.01935	1.1565	424.49	780.0	1204.5

Table 2-12: Steam properties based on pressure (Carcoana, 1992).

Abs. Press., psia p	Temp., °F T					
400	444.59	0.0193	1.1613	424.0	780.5	1204.5
410	447.01	0.0194	1.1330	426.8	777.7	1204.5
420	449.39	0.0194	1.1061	429.4	775.2	1204.6
430	451.73	0.0194	1.0803	432.1	772.5	1204.6
440	454.02	0.0195	1.0556	434.6	770.0	1204.6

The enthalpies and specific volumes of saturated water and saturated steam at different pressures and temperatures can also be found from charts especially prepared. The following figure is a pressure-enthalpy chart for steam.

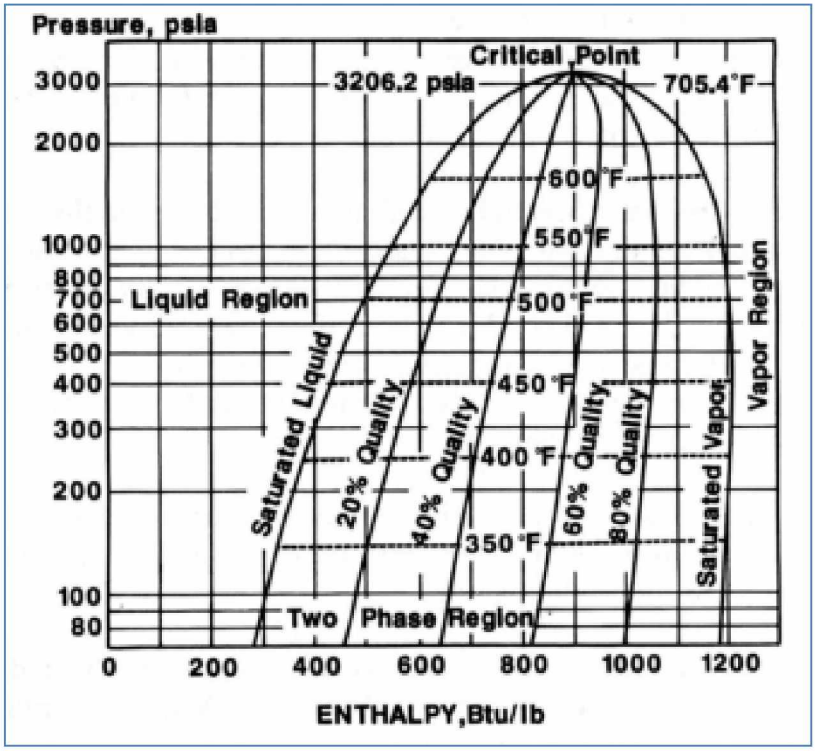

Figure 2-19: Pressure-enthalpy chart for steam (Carcoana, 1992; Bleakley, 1965).

Figure 2-20 represents the variation of sensible (h_v), latent (h_{fg}), and total heat of steam (h_g) with pressure. Of interest is that starting at approximately 470 psia, the total heat of steam decreases with an increase in pressure. The reason for this can be understood by observing how the two-phase area (latent heat) is reduced when the saturated vapor line and saturated liquid line converge at the critical point. The decrease in the latent heat content of steam becomes larger than the increase of the sensible heat with pressure. In other words, if the steam's injection pressure is just enough to displace the reservoir fluids, it will have more heat content than at higher pressures (Carcoana, 1992).

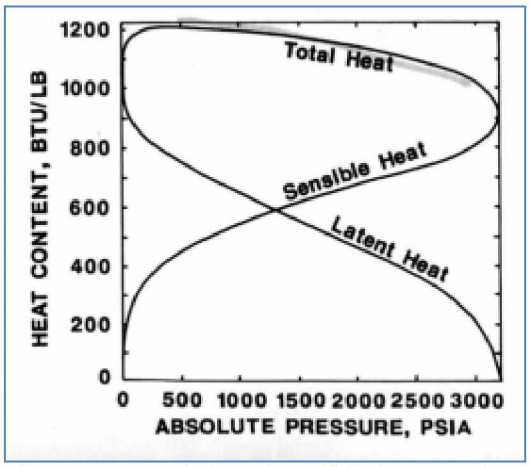

Figure 2-20: Variation of sensible, latent, and total heat of steam with pressure (Carcoana, 1992; Farouq Ali, 1970).

2.4.1.2. Heat Losses

Carcoana (1992) stated that the steam generated by a steam generator is the heat carrier agent injected into the reservoir. It raises the temperature of the rock and fluids it contains and displaces the oil. Not all the heat carried by the steam reaches the reservoir fluid and stays in the reservoir. Some of the heat is lost at the surface, some is lost into the wellbore, and some is lost to the adjacent formations. Heat can be transmitted away by conduction, convection, radiation, or combinations of all three means. Also, part of the heat reaching the reservoir is lost through produced fluids. Detailed information regarding heat loss calculations and heat transmission was presented by Ramey (1962), Pacheco and Farouq Ali (1972), Prats (1982), White and Moss (1983), and Jones (2007) among others.

The amount of formation heated depends on the amount of heat lost:

- in the steam generator,
- on the surface transmission lines,

- from the wellbore,
- to adjacent formations.

Details of heat losses in the steam generator, surface injection lines, and in the well bore was presented by Carcoana (1992). In the following section, a brief of heat lost to the adjacent strata is presented which adopted from Carcoana (1992).

2.4.1.2.1. Heat Amount to the Formation

Steam injection's beneficial effect on oil displacement and recovery depends on the amount of heat transferred to the formation itself and on the porous volume swept by the hot fluids. To evaluate this effect, the amount of heat loss to adjacent strata must be known. Some of the first results from mathematical heat models of heat transfer and heat loss in the formation were published by Lauwerier (1955), Marx and Langenheim (1959), Rubinstein (1959), and Willman et al. (1961). Gates and Ramey (1964) and Ramey (1965) made a graphical comparison of these results by plotting on a Cartesian scale the fraction of total injected heat lost to adjacent strata, W_a^*; versus the logarithm of the dimensionless time function, t_D (see Figure 2-21).

The dimensionless time is defined as:

$$t_D = \frac{4D \times t}{h^2} \qquad \text{(2-21)}$$

Where:

t = time, days

D = thermal diffusivity of the cap rock, ft^2/day

h = formation thickness, ft.

The amount of heat lost to adjacent strata varies directly with time of injection and inversely with formation thickness. So the heat lost can be a high percentage of the cumulative heat injected in a steam-drive process's lifetime. To reduce the amount of heat lost to adjacent strata, a process of heat scavenging is accomplished by displacing the hot fluid "slug" with cold water injection. The process is also useful for saving energy when the formation is heated and the steam breaks through into the producers.

Notice: thermal diffusivity is also denoted by 'α' and defined as the ratio of thermal conductivity to volumetric heat capacity. This will be discussed in more detail in the following sections.

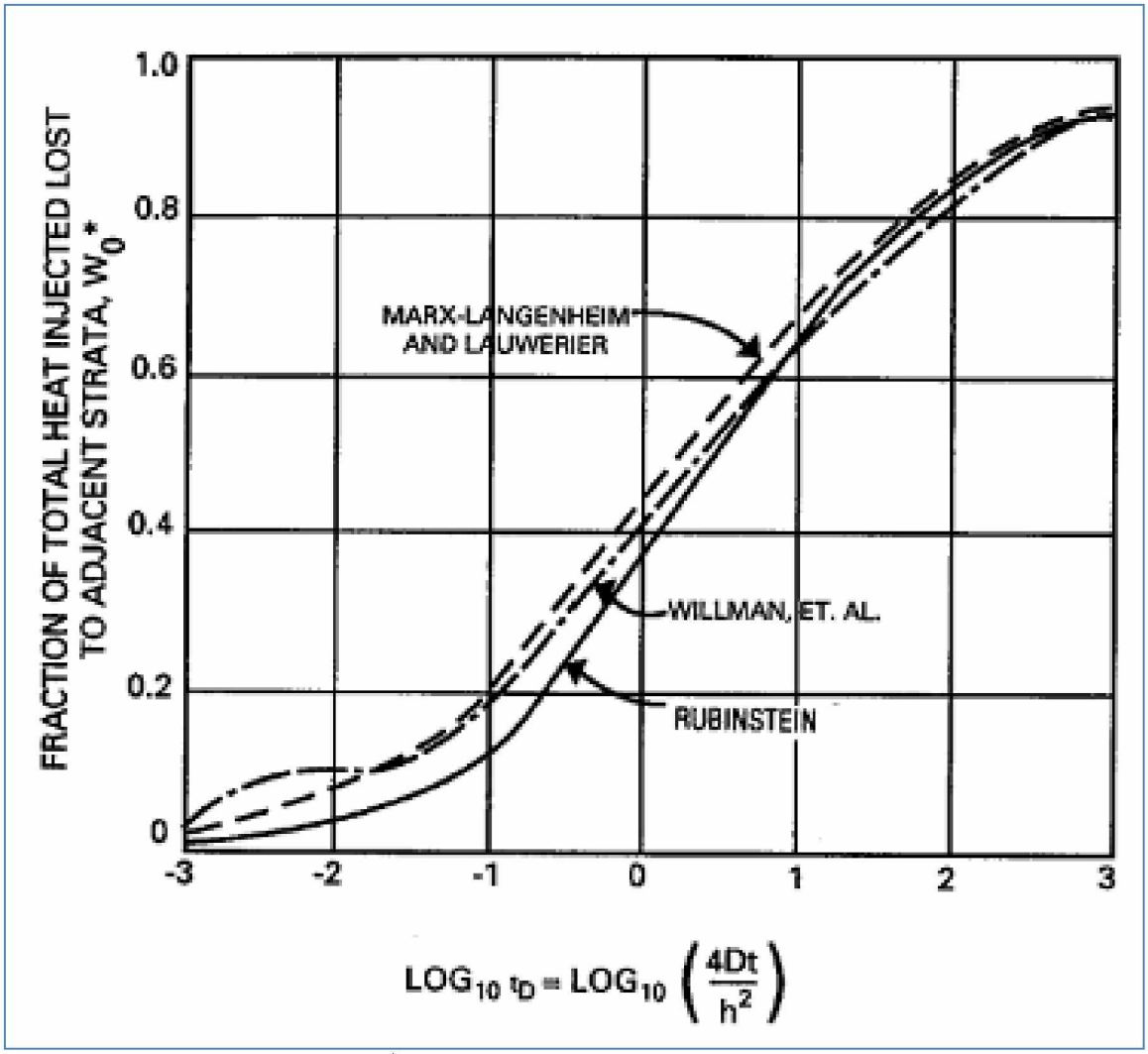

Figure 2-21: Vertical heat loss, W_a^*; versus the logarithm of the dimensionless time function, t_D (Ramey, 1965; Carcoana, 1992).

Carcoana (1992) presented good materials for calculating the heated radius, oil displacement rate, oil recovery, and cyclic steam injection.

2.5. History of Thermal Recovery Methods

In this section, summary of some papers that reviewed different aspects of thermal recovery methods is presented. Ramey (1967) presented a good history of the steam injection method. A brief of this history is presented in the following paragraphs.

Interest in hot fluid injection to recover oil has been apparent since the early 1930s. It is likely that an early publication concerning hot water injection by Schaller and Bjornsson in 1923 was a

stimulus. In 1934, Stovall described both laboratory and field trials of steam injection. The work was described as initiated in 1926, leading to a field trial in 1931. Injection of hot, non-condensable gas was described by Lindsly in 1928. In regard to hot gas injection, it was discovered early that the low sensible heat of non-condensable gases (flue gas, natural gas) made these fluids poor heat exchange mediums. Lapuk published an excellent review of early work in thermal recovery in 1939. During the 1940s, several interesting articles reported hot air injection field tests by E. W. Hartman near Bartlesville, Oklahoma. It appears Hartman was successful in transporting heat to the formation and may have ignited the oil and moved a combustion front. On the other hand, a hot (450°F) natural gas injection project conducted in the early 1950s resulted in no detectable temperature increase at a depth of 300 feet after more than one year of injection (for references mentioned, refer to Ramey, 1967).

There were several different ideas involving hot fluid injection described during the 1950s. Breston and Pearman described injection of hot water to increase injectivity of water into tight sands. Injection of warm water in Pembina field, Canada, was proposed to guarantee that water would enter the formation at formation temperature.

Modern hot fluid injection interest initially concerned continuous injection in a normal flooding pattern. Hot water injection in the Schoonebeek Field, Holland, was started in the mid-1950s, and operations in Venezuela and California started in the late 1950s. But interest shifted to a cyclic injection-production process in the early 1960s.

Burns (1969), by summarizing the active steam stimulation projects in the State of California in period of 1958 until June 1968, described some of the more important steam soak operation were being conducted in 29 oil fields of California through June 1967. He mentioned that Shell Oil Co. began steam soak operations on a pilot basis in the Yorba Linda field in 1958.

Hammershaimb et al. (1983) reviewed the 117 reported field tests to find out the recovery efficiency of six major EOR techniques:

- Steam Drive
- In-Situ Combustion
- Carbon Dioxide Flooding
- Surfactant Flooding

- Polymer Flooding
- Alkaline Flooding

Based on their investigation they concluded that steam drive has the highest recovery efficiency with oil recoveries of 400 to 800 barrels per acre-foot and 30 to 60% of the remaining oil in place. Also, they mentioned the process efficiency of the six aforementioned EOR method based on the volume or pound of material injected versus additional barrels of oil recovered. This efficiency for steam drive process reported to be between 4-6 bbl of steam per bbl of oil. They stated that the bulk of the projects have been conducted in relatively shallow (less than 2,800 feet), high permeability (500+ md), high porosity (0.25+), heavy oil (less than 20 °API) reservoirs.

Barillas et al. (2008) reviewed the aspects of the main heavy oil recovery processes (in-situ combustion, steam flooding, steam cyclic injection and SAGD) and concluded for minimizing the amount of the injected fluids, reservoir modeling and profitability analyses are required.

Ardali et al. (2012) reviewed the hybrid steam solvent heavy oil recovery processes. The authors presented the main aspects of hybrid processes such as such as Propane-SAGD, Expanding Solvent SAGD (ES-SAGD), Solvent-Aided Process (SAP), Liquid Addition to Steam to Enhance Recovery (LASER), Steam Alternating-Solvent (SAS) and VAPEX. The main conclusion which is implicitly relevant to this project made by authors of this paper (Ardali et al., 2012) is:

- The results of Solvent-Assisted SAGD tests are very encouraging but mixed. According to pilot tests, Butane and Hexane-like solvents are better options. Solvents lighter than Butane and diluents that contain heavier solvents lead to lower or no additional recovery compared to thermal-only processes.

Alvarez and Han (2013) reviewed the cyclic steam injection process. They mentioned that the Cyclic Steam Injection (CSI) was first used fortuitously in Venezuela in 1959. By that time, one of the steam injector wells began to produce, after a blowout, in much better conditions than the surrounding production wells (Trebolle et al., 1993). Alvarez and Han (2013) summarized the steps that solved or mitigated several of drawbacks of CSI during last decades. They emphasized that the method is quite effective, especially in the first few cycles providing quick payout. However, ultimate recovery by cyclic steam injection is low (10-40% of Original Oil in

Place, OOIP), compared to that of steam flooding and Steam Assisted Gravity Drainage (SAGD) which are over 50% of OOIP (Thomas, 2008; Speight, 2007; Xia and Greaves, 2006) as shown in Table 2-13.

Table 2-13: Oil recovery factor of thermal EOR methods (Alvarez and Han, 2013).

Oil Recovery Factors (successful projects)	
Thermal EOR	% of OOIP
CSI	10 - 40
Steam flooding	50 - 60
SAGD	60 - 70
In-situ Combustion*	70 - 80

*In-situ Combustion using THAI—'Toe-to-Heel Air Injection'

Based on their review, Alvarez and Han (2013) concluded:

- Cyclic Steam Injection combined with unconventional technology such as co-injection with chemical additives; horizontal drilling and hydraulic fracturing have been highly successful, improving its conventional recovery factor up to 40%.
- Cyclic Steam Injection with horizontal well has had considerable success.
- CSI with Hydraulic fracturing has shown good results for low-permeability formation.

2.6. Thermal Recovery Performed Projects or Studies

By searching in the *Open Literature*, one can find a lot of papers and documents that report some sort of field project execution or laboratory tests results on the thermal recovery methods. A few of these reports are selected and will be reviewed in the following sections.

2.6.1. The PCEJ Steam Stimulation Project

Towson and Khallad (1991) reported the results of a single well test of steam stimulation in cycling trend in the McMurray formation of the Athabasca Oil Sands Deposit in Alberta,

Canada. In addition to applying heat by injecting steam, because of very high viscosity (up to 1,000,000 cP at reservoir conditions), and the shallow formation (300 m), they used fracturing method in the wells.

Although the wells were perforated in the bottom third of the pay zone in the Lower McMurray, temperature profiles indicated heat in the shaley Upper McMurray. The fractures created by the injected steam appeared to start in the vertical plane but later may have developed a horizontal component.

It was concluded, from the SWTs (Single Well Tests) results, that bitumen production from the McMurray formation by cyclic steam stimulation is technically feasible and that a multi-well pilot is required to effectively assess the production potential of the McMurray formation.

Reservoir and fluid properties are reported as shown in Tables 2-14 and 2-15.

Table 2-14: Reservoir properties (Towson and Khallad, 1991).

RESERVOIR PROPERTIES	
NET PAY (m)	7 - 30
DEPTH (m)	300
POROSITY (%)	30
PERMEABILITY (md)	2 000 - 3 000
BITUMEN SATURATION (wt %)	11 - 16
API GRAVITY	8

Table 2-15: Reservoir fluid properties (Towson and Khallad, 1991).

RESERVOIR FLUID PROPERTIES		
API GRAVITY	@ 15.6°C	8
SPECIFIC GRAVITY	@ 15.6°C	1.107
TOTAL SULPHUR (g/kg)		50
VISCOSITY (mPa.s)	@ 20°C	350 000
DEAD OIL	@ 40°C	27 000
	@ 60°C	4 000

2.6.2. Commercial Heavy Oil Recovery by Cyclic Steam Stimulation in Kuwait

Al-Qabandi et al. (1995) reported applying cyclic steam stimulation to reduce oil viscosity in a heavy oil reservoir in Kuwait. They found that for pilot operations in eight wells in the selected area, cyclic steam injection using high initial steam rates and soak period less than 3 days was highly beneficial. Steam injection rates were in the range of 965 to 1246 bbls per day water equivalent with a well head pressure of 390 psig and temperature of 433°F. The steam slugs varied from 14729 to 27213 bbls water equivalent. Initial reservoir conditions and crude oil properties are shown in Tables 2-16 and 2-17.

Table 2-16: Initial reservoir conditions (Al-Qabandi et al. (1995).

INITIAL RESERVOIR CONDITIONS	
Sub-sea depth to the top of reservoir, ft	793
Average Gross Sand thickness, ft	134
Average Net Sand thickness, ft	68
Average Perforated intervals, ft	42
Porosity, %	31
Permeability, Darcy	3.0
Oil Saturation, %	79
Pressure, psig	204
Reservoir Temperature, °F	85

Table 2-17: Crude oil properties (Al-Qabandi et al. (1995).

CRUDE OIL PROPERTIES		
API Gravity		15.2
Sulphur Content, wt %		5.1
Nitrogen Content, wt %		0.2
Conradson Carbon, wt %		11.1
Vanadium, ppm		59.9
Nickel, ppm		10.5
Pour point,		-5.0
Viscosity, cSt	@ 85 °F	450
	@ 100 °F	260
	@ 150 °F	70
	@ 200 °F	25
Total Distillation Yield @ 695 °F		35.6

2.6.3. Steam Injection Project in Heavy-Oil Diatomite

Murer et al. (2000) reported the results of a steam injection project that was conducted in diatomite containing heavy, biodegraded oil (12°API, ~3,000 cP) in the South Belridge field, Kern County, California. After several attempt of cyclic steam injection recovery, the project was then configured for steam drive; however, the overall performance of this project has been reported poor.

2.6.4. Peace River Carmon Creek Project—Optimization of Cyclic Steam Stimulation Through Experimental Design

Koci and Mohiddin (2007) reported the optimization of cyclic steam stimulation in Peace River Carmon Creek, which is an ultra-heavy oil lease located in northwestern Alberta, Canada, approximately 700 km northwest of Edmonton. It holds nearly eight billion barrels of 7°API oil in place, spread over 370 km^2. The paper is about optimization of CSS (cyclic steam stimulation) well configuration and steaming strategy for each distinct reservoir area by deploying previously improved and history matched simulation models. A full field static model was built, comprising over 400 wells. The modeling results can be generalized as follows:

- Horizontal well near the base of the reservoir is the optimum well type for CSS at Peace River.
- Well spacing of less than 75 meters appears more attractive in the higher reservoir quality areas compared to the current assumption of 150 meters.

The CSS target is the Bluesky formation, an approximately 30 m thick semi-consolidated sand layer buried at a depth of about 600 m.

The reference case CSS well configuration and steaming strategy consists of 500 m horizontal wells drilled on 150 m spacing. There are 16 such wells drilled into a standard subsurface "pad" measuring 1300 x 1200 meters. The steam injection rate is 1,000 tons/day per well. The first cycle steam injection volume (steam slug) is 30,000 tons and the length of the first production cycle is 247 days. The steam slugs increased in subsequent cycles. The production period lengths after the first cycle are equal to 12.4 days per 1,000 tons of steam injected in that cycle. The wells are drilled 5 m above the reservoir base along their entire horizontal trajectory. The thermal

reservoir simulator STARS was used. Detailed data of formation and simulation model are available in the paper.

2.6.5. First Cyclic Steam Stimulation Pilot Test in Sudan: A Case Study in Shallow Heavy Oil Reservoir

This paper (Ruifeng et al., 2011) details the first cyclic steam stimulation (CSS) pilot test in Sudan, which was applied in the FNE shallow heavy oil reservoir. The 'B' reservoir of FNE field is a shallow, heavy oil reservoir with strong bottom water; burial depth is 520 m. Well tests have shown low oil rates under cold production averaging at 50–150 BOPD. Denser well spacing will be required if under cold production, which will be quite costly. CSS pilot tests on two wells began in 2009. Promising results have been monitored with daily well rates 3–4 times those of cold production wells with low water cut. Another six CSS wells further have come on stream since July, 2010, achieving similar positive results.

The rock and fluid reservoir properties are:

- Reservoir temperature: 46°C,
- Porosity: 26 to 34%
- 'B' reservoir is a sequence of massive and continuous sandstones inter-bedded with shales,
- Oil saturation: 61 to 86%,
- Permeability: above 3000 md,
- Average net pay: 31 m,
- Average Net to Gross: 0.8,
- Oil density: 18 °API,
- Surface viscosity: 3500 cP at 45 °C,
- GOR: 5 scf/bbl.

2.6.6. Successful Cyclic Steam Stimulation Pilot in Heavy Oilfield of Sudan

This paper (Tewari et al., 2011) illustrates the successful design, implementation, and evaluation of a cyclic steam stimulation pilot in a heavy oil field of Sudan. This field contains heavy oil in

multiple reservoirs of Bentiu formations of late Cretaceous age occurring at depths of 550–600m. Reservoirs are highly porous (~30%), permeable (1000–2000 mD), and unconsolidated in nature. Fluid properties include viscous crude of degree API 15–17 and corresponding viscosities in the range of 3700 cP and 3000 cP at reservoir conditions.

Steam quality of 75% was injected for 6–12 days and wells were subjected to soaking of 3–5 days. On production a three to fivefold improvement over primary production was realized and first cycle is sustaining more than six months. Actual results are better than predicted in simulation studies with lower steam intensity of 120 m^3 /m compared to planned 160m^3/m. The paper also discusses improvement in oil production and its variation with formation and fluid characteristics, formation thickness, depth of formations, duration of injection, and soaking periods along with response variables like oil-steam ratio and steam/water production.

2.6.7. A Preliminary Investigation on Cyclic Steam Stimulation Recovery of Nigerian Heavy Oil

This work (Ademodi et al., 2014) presents preliminary laboratory investigation on the enhanced recovery of a Nigerian heavy oil using cyclic steam stimulation (CSS) method. After two cycles of steam stimulation (1.88 wt/wt steam to oil ratio), it was observed that steam at pressure of 20 psig (126°C, 11.3 kgh^{-1}) produced 78% of original oil in place (OOIP). The recovery factor was increased to 91% following addition of alkaline solution (20ml, 0.2M NaOH). The average production rates of 0.63 liter/day and 0.83 liter/day were obtained for the system with steam injection only and the system with steam/alkaline addition, respectively. The setup for the experiment consists of steam boiler, the physical model, and a graduated container to collect the recovered oil. The density of oil was reported to be 8.6 °API.

2.6.8. The Application of Cyclic Steam Stimulation in Heavy Oil Reservoir with a High Water Cut

Al Shibli et al. (2016) reported that 'A' West field is a heavy oil field (17–25 deg API), discovered in 1972 in the South of Oman, with a 200 m thick oil column in Haradh formation.

The field development started in 1984 by cold production with vertical and horizontal wells. In 2007, the steam drive concept through 10 acre inverted 7-spot patterns was selected for the full field development. Being part of the concept, two Cyclic Steam Stimulation 'CSS' campaigns were executed between 2011 and 2014 to stimulate both the wells and the reservoir using a mobile steaming unit. Throughout the two campaigns, a number of optimizations have been implemented including: the deployment of Vacuum Insulated Tubing 'VIT', the extension of the perforated intervals, the adjustment of the injection and production cycle durations and resources management.

The deployment of the 1000 m VIT (Vacuum Insulated Tubing) during the steam injection phase confirmed the predicted oil gain, resulting from a reduction in wellbore heat losses. Along with CSS, a re-perforation campaign has been conducted on wells with low productivity index 'P' to maximize their gross off-take. After steam stimulating the re-perforated wells, it has been observed that higher oil to steam ratio 'OSR' is obtained for thicker oil column exposed to steam. In addition, for highly depleted zones in the reservoir, it has been found that producing at the maximum possible rate and right after the end of the soaking period, leads to a better OSR. CSS proved also to have improved the steam conformance within the targeted pattern.

The formation is reported to be sandstone with a high net to gross with some shale streaks. The permeability has a range of 300–1300 mD. The viscosity in 'A' West is ranging from 400 cP at the top of the reservoir to 2000 cp down at the OWC of 1005 m TVDss.

'A' West is developed by steam flood with seventeen '10 acre 7-spot' patterns and seven '3.3 acre 7-spots' patterns. The wells are drilled vertically in the reservoir section and down to the OWC with a subsurface well to well spacing of 125 m. The injectors are perforated down to a 50 m stand-off from the OWC. The producers are perforated down to 50 m above the OWC with short gaps for future possible isolation.

2.7. Optimization or Improvement of the Thermal Recovery Methods

During the last decades, several improvements on thermal recovery methods have been applied, among them hybrid steam injection is more general and used by researchers. In this method, researchers tried to get benefits of other recovery methods by adding some type of solvents to the injected steam. Ardali et al. (2012) presented a good review of this type of improvement. There

is also some improvement in devices employed in the thermal recovery process to mitigate problems such as liner expansion due to the high temperature steam injection by using 'swelled packer' (Brooks and Davis, 2010). Here, we do not consider these types of improvements; however, in the following sections, a brief review of some papers that claim improvement on a thermal recovery process is presented.

2.7.1. Optimizing Horizontal-Well Steam-Stimulation Strategy for Heavy-Oil Development

Through a 3-D reservoir simulation, Luo and Baker (2006) compared the production performance of CSS, Steam Flooding (SF), CSS followed by SF, and SAGD. They showed the importance of optimizing horizontal well steam stimulation strategy for developing heavy oil reservoirs. The authors after examining different horizontal well lay-out claimed the following general observations:

- For horizontal well application, cyclic steam stimulation followed by steam flooding is a very efficient strategy. Also, it is important to choose the proper time for changing from cyclic steam stimulation to steam flooding.
- For the SAGD process, configuration of well placement has significant impact on production performance.

2.7.2. Stochastic Optimization of Cyclic Steam Stimulation in Heavy Oil Reservoirs

Azad et al. (2013) tried to find out the optimum factors that influence the performance of a Cyclic Steam Stimulation by using numerical models. They stated that the CSS is multi-cycled steam recovery process with three stages and five operational parameters (injection rate and its duration, soak time, production rate and its duration) in each cycle. The authors proposed the use of stochastic optimization to estimate the parameters of CSS. They developed three different CSS models with three well types (vertical, horizontal and inclined wells). They used project net present value (NPV) as the objective function in the optimization process. Results showed that the NPV can be increased significantly when all the operational variables of the CSS are

optimized. This signifies the importance of simultaneous optimization of soak time, cycle length and rates. The results also showed that the vertical well model gave a higher NPV than the other two well models. The horizontal well model was found to give the lowest NPV.

2.8. Thermal Properties of Rocks and Steam

In hydrocarbon reservoir simulation modeling, usually the reservoir temperature is considered constant at datum depth, which is a correct assumption for non-thermal recovery processes. In modeling a thermal method, this assumption (constant reservoir temperature) is generally not true. Thus, having a good knowledge of thermal properties of rock is essential in this type of reservoir simulation. In the following sections, a review of these properties is briefly presented.

2.8.1. Thermal Conductivity

Thermal conductivity or the thermal conductivity coefficient of a material defines its ability to transfer heat. Somerton (1992) defined the thermal conductivity as the capacity of a material to conduct or transmit heat. This is the coefficient (λ) in Fourier's Law of heat conduction:

$$q = -\lambda \text{grad} T \quad \ldots\ldots\ldots\ldots\ldots\ldots\ldots\ldots\ldots\ldots\ldots\ldots\ldots\ldots\ldots\ldots\ldots\ldots\ldots\ldots \quad (2\text{-}22)$$

Where q = heat flux, W (watts)/m^2; λ = thermal conductivity, W/m-K; grad T = temperature gradient, K/m. The standard unit of thermal conductivity is W/m-K. Other units include cal/sec.cm.°C and Btu/hr.ft.°F. Conversion factors for this quantity are as Table 2-18 (Somerton, 1992):

Table 2-18: Conversion factors of thermal conductivity (Somerton, 1992).

Multiply	by	to convert to:
Btu/hr-ft-°F	1.73	Watts/m-K
Btu/hr-ft-°F	4.136×10^{-3}	Cal/s-cm-K
Cal/s-cm-K	4.184×10^{2}	Watts/m-K
Cal/s-cm-K	2.418×10^{2}	Btu/hr-ft-°F
Watts/m-K	2.39×10^{-3}	Cal/s-cm-K
watts/m-K	0.578	Btu/hr-ft-°F

In the hydrodynamics of flow of incompressible fluids through porous media, an analogous equation was suggested by Darcy. In the Darcy equation, the flow rate is proportional to the

pressure gradient and the coefficient proportionality is the permeability and hydrodynamic viscosity ratio (mobility), (Eppelbaum et al., 2014).

The thermal conductivity of formations is dependent on temperature, pressure, porosity, composition, and properties of pore-filling fluids and gases. Values of thermal conductivity coefficients range widely for rocks and pore-filling substances (see Table 2-19).

All pore-filling fluids have lower k values than rocks and this causes the overall thermal conductivity to decrease with increasing porosity (Poelchau et al., 1997).

Examples of the effect of porosity are presented in Figure 2-22.

Thermal conductivities of crystalline rocks decrease with increased temperature. In general, the higher the conductivity of the rock, the greater the decrease with increased temperature. Rocks containing amorphous or poorly crystallized materials, on the other hand, generally have low thermal conductivities and the conductivity may actually increase with increased temperature (Somerton, 1992).

Table 2-19: Thermal conductivities of some geological materials (Eppelbaum et al., 2014).

Thermal conductivities[a] of some geological materials (Poelchau et al. 1997)

Material	$Wm^{-1} K^{-1}$	Source
Earth's crust	2.0–2.5	Mean value, Kappelmeyer and Hänel (1974)
Rocks	1.2–5.9	Sass et al. (1971)
Sandstone	2.5	Clark (1966)
Shale	1.1–2.1	Clark (1966), Blackwell and Steele (1989)
Limestone	2.5–3	Clark (1966), Robertson (1979)
Water	0.6 at 20 °C	Birch et al. (1942)
Oil	0.15 at 20 °C	Birch et al. (1942)
Ice	2.1	Gretener (1981)
Air	0.025	CRC (1974) Handbook
Methane	0.033	CRC (1974) Handbook

[a] Please take into account that measured conductivities and some other thermal properties of rocks observed in various regions (and even within the same regions) may vary due to influence of different physical-chemical factors

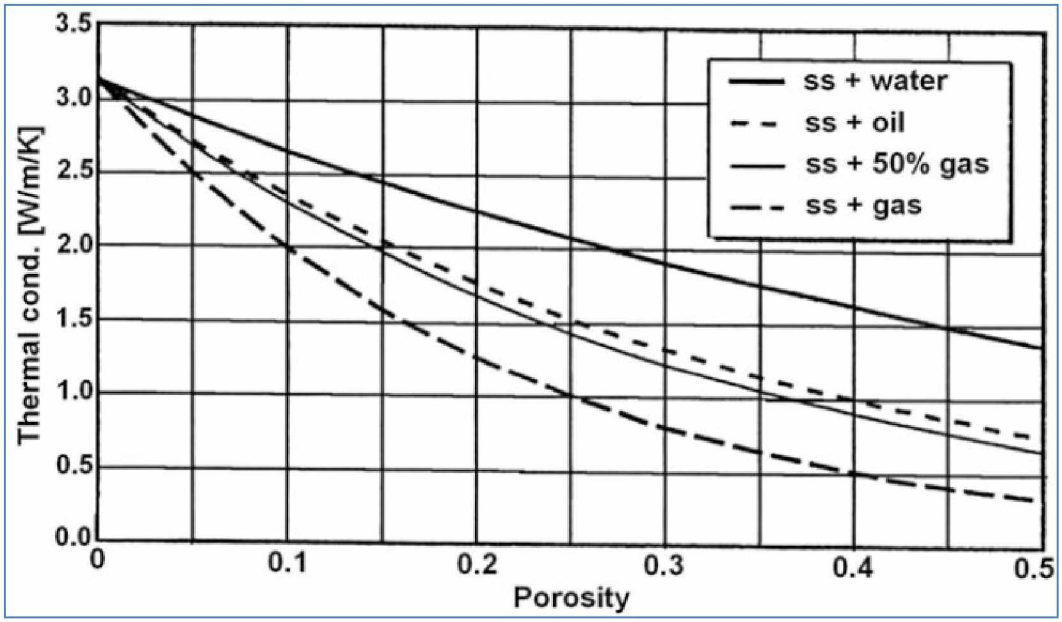

Figure 2-22: Thermal conductivity of sandstone as a function of porosity and pore fluid at ambient temperature and pressure (Poelchau et al., 1997; Eppelbaum et al., 2014).

Table 2-20 shows the effect of temperature on thermal conductivity of sedimentary rocks.

Table 2-20: Effect of temperature on thermal conductivity of sedimentary rocks (Eppelbaum et al., 2014).

Temperature effect on thermal conductivity (values are given in 10^{-3} cal/cm s °C; 1×10^{-3} cal/cm s °C = 41.86 m Wm^{-2}) of sedimentary rocks (Kappelmeyer and Hänel 1974)

Formation	ρ (g/cm^3)	0 °C	50 °C	100 °C	200 °C	300 °C	400 °C	500 °C
Dolomite	2.83	11.9	10.30	9.30	7.95			
Limestone	2.60	7.20	6.14	5.53	4.77			
Limestone, parallel	2.60	8.24	7.55	7.04	6.54			
Limestone, perpend.	2.69	6.09	5.68	5.41				
Quartz-sandstone, parallel	2.64	13.6	11.80	10.60	9.00			
Quartz-sandstone, perpend.	2.65	13.1	11.40	10.30	8.65			
Shale			2.17	2.25	2.38	2.54	2.68	2.83
Slate, parallel	2.70	6.35	6.05	5.85	5.50	5.20	4.95	4.80
Slate, perpend.	2.76	4.83	4.40	4.23	4.08			
Calcite, parallel		27.3	22.40	19.00	15.1	12.30	10.30	
Calcite, perpend.		16.3	13.50	11.80	9.70	8.40	7.40	
Halite	2.16	14.6	12.00	10.05	7.45	5.95	4.98	

The stress to which a rock is subjected has some effect on its thermal conductivity. In the case of poorly-consolidated rocks, increasing stress will substantially increase thermal conductivity. Thermal conductivities of well-consolidated and cemented rocks are only slightly affected by increased stress. Increasing pore-fluid pressure has the opposite effect, decreasing the thermal conductivity as pore-fluid pressure is increased with the external stress held constant (Somerton, 1992).

Messmer (1984) presented the following equation for calculating the thermal conductivity of sandstone in the temperature range 50-1000 °F:

$$\log \lambda = \emptyset \log \lambda_f + (1 - \emptyset) \log \lambda_s \quad \text{(2-23)}$$

Where subscripts 'f' and 's' denote 'fluid' and 'solid', respectively.

Somerton et al. (1974) presented the following equation which proved by Krupiczka (1967) for estimating the thermal conductivity of formation containing fluid:

$$\frac{\lambda}{\lambda_f} = \left(\frac{\lambda_s}{\lambda_f}\right)^{A+B\log\left(\frac{\lambda_s}{\lambda_f}\right)} \quad \text{(2-24)}$$

Where:

λ = effective thermal conductivity of system,

λ_f = thermal conductivity of fluid,

λ_s = thermal conductivity of solid,

A= 0.280 - 0.757 log ϕ,

ϕ =fractional porosity,

B= constant = - 0.057.

The factor D_{90}/D_{10} was determined as a measure of grain-size distribution, where D_{90} is the grain size for which 90 percent of the grains by weight are coarser and D_{10} is the grain size for which 10 percent of the grains by weight are coarser.

Table 2-21 gives the source and measured physical properties of the unextracted oil sands (Somerton et al., 1974).

Table 2-21: Physical properties of unconsolidated unextracted Kern River oil sands(Somerton et al., 1974).

PHYSICAL PROPERTIES OF UNEXTRACTED KERN RIVER OIL SANDS

Depth (ft)	Porosity (fraction)	Bulk Density (lb/cu ft)	Median Grain Size (in.)	Saturations		Thermal Conductivity (Btu/ft-hr-°F)
				Water	Oil	
374 to 380	0.30	128.	0.033	0.51	0.23	1.03
	0.29	132.		0.61	0.31	1.12
	0.30	132.		0.60	0.27	1.12
	0.32	123.		0.37	0.26	0.91
	0.33	122.		0.18	0.22	0.85
	0.31	125.		0.28	0.44	0.85
	0.31	129.		0.50	0.32	1.08
	0.30	125.		0.60	0.00	1.15
	0.29	132.		0.81	0.00	1.28
	0.30	121.		0.07	0.29	0.72
	0.28	134.		0.60	0.26	1.15
	0.31	118.		0.10	0.20	0.67
	0.28	116.		0.00	0.00	0.36
	0.28	135.		1.00	0.00	1.42
543 to 550	0.33	129.	0.0164	0.34	0.64	0.92
	0.33	129.		0.29	0.67	0.83
	0.33	129.		0.37	0.62	0.90
	0.35	131.		0.34	0.55	0.93
	0.33	130.		0.33	0.61	0.90
	0.33	125.		0.32	0.56	0.93
	0.30	129.		0.29	0.46	0.91
	0.30	127.		0.28	0.34	0.90
	0.35	121.		0.08	0.53	0.63
	0.31	128.		0.25	0.52	0.80
	0.31	129.		0.77	0.00	1.31
	0.31	128.		0.76	0.00	1.29
	0.33	127.		0.78	0.00	1.22
	0.31	130.		0.95	0.00	1.34
	0.32	112.		0.00	0.00	0.30
	0.31	132.		1.00	0.00	1.38
614 to 617	0.31	130.	0.0116	0.46	0.44	0.94
	0.32	129.		0.46	0.41	0.91
	0.35	125.		0.37	0.43	0.86
	0.36	127.		0.54	0.40	0.93
	0.32	126.		0.38	0.46	0.90
	0.34	127.		0.87	0.00	1.19
	0.33	117.		0.07	0.32	0.56
	0.32	121.		0.13	0.39	0.67
	0.32	117.		0.05	0.25	0.59
	0.33	124.		0.65	0.00	1.17
	0.30	127.		0.71	0.00	1.31
	0.35	126.		0.92	0.00	1.16
	0.34	122.		0.68	0.00	1.13
	0.37	103.		0.00	0.00	0.27
	0.34	129.		1.00	0.00	1.20

Somerton et al. (1974) mentioned that the effect of pressure on thermal conductivity has been found to be relatively small. They emphasized that if typical data for brine-saturated sands are used, the change in conductivity would be less than 1 percent per 1,000-psi change in pressure.

2.8.2. Heat Capacity

Heat capacity is briefly introduced in the 'Steam Properties' section; however, it is discussed in more detail in the following paragraphs.

As the name implies, heat capacity of a material is its capacity *to* store heat (Somerton, 1992). On the other hand, Eppelbaum et al. (2014) defined this parameter as the amount of energy

required to raise the temperature of a unit of the mass of a substance by 1°. The SI unit for heat capacity is Joule/kg-K but other commonly used units are cal/g-°C or Btu/lb-°F both of which have the same numerical value (Somerton, 1992).

Somerton (1992) stated that the heat capacities of dry rocks are about 25 percent of that of water.

Eppelbaum et al. (2014) proposed the following equation to calculate the heat capacity with temperature variation in a wide temperature interval.

$$c(T)=c(T_i)+\beta(T-T_i) \quad \ldots\ldots\ldots\ldots\ldots\ldots\ldots\ldots\ldots\ldots\ldots\ldots\ldots\ldots\ldots\ldots\ldots\ldots \quad (2\text{-}25)$$

Based on the experimental data of Somerton (1958), Eppelbaum et al. (2014) calculated parameters in Eq. (2-25) for several rocks. For the 70 °F (21 °C)–620 °F (327 °C) interval, they obtained the following values for sandstone c (70 °F) = 0.197 (Btu lbm^{-1} $°F^{-1}$) and $\beta = 1.24\times10^{-4}$ Btu $lbm^{-1}°F^{-2}$. The corresponding values of c (70 °F) and β are:

0.190 and 1.43×10^{-4} for shale; and 0.203 and 1.12×10^{-4} for siltstone.

From published data, Eppelbaum et al. (2014) compiled Table 2-22 data which presents the average values of specific heat capacity for certain rocks.

Table 2-22: Average values of specific heat capacity [in 10^{-3}J/(kg K)] (Eppelbaum et al., 2014)

Rock	*c*
Sand	0.96
Siltstone	0.87
Argillite, clay schist	0.86
Clay	1.10
Marl	1.55
Limestone	0.89
Chock	1.86
Granite	0.95
Granodiorite	1.02
Porpyrite	0.91
Diorite	1.00
Basalt	1.23
Diabas	0.87
Gabbro	0.98
Schist	1.10
Gneiss	1.02
Amphibolite	1.13
Gneiss-granite	1.11

Table 2-23 provides the conversion factors for heat capacity (Somerton, 1992):

Table 2-23: The conversion factors for heat capacity (Somerton, 1992).

Heat Capacity / (Specific Heat)		
Multiply	by	to convert to:
Btu/lb-°F	1.00	Cal/g-K
Btu/lb-°F	4.184×10^3	Joule/kg-K
Cal/gm-K	1.00	Btu/lb-°F
Cal/gm-K	4.184×10^3	Joule/kg-K
Joule/kg-K	2.390×10^{-4}	Btu/lb-°F
Joule/kg-K	2.390×10^{-4}	Cal/gm-K
Btu/ft^3-°F	1.602×10^{-2}	Cal/cm^3-K
Btu/ft^3-°F	6.702×10^{-2}	Joule/cm^3-K
Cal/cm^3-K	62.43	Btu/ft^3-°F
Cal/cm^3-K	4.148	Joule/cm^3-K
Joule/cm^3-K	14.92	Btu/ft^3-°F
Joule/cm^3-K	0.2411	Cal/cm^3-K

2.8.3. Thermal Diffusivity

In transient heat-transfer problems, the coefficient ***(α),*** thermal diffusivity, must be used as given in the diffusivity equation:

$$\nabla^2 q = -\alpha \frac{\partial T}{\partial t} \quad \ldots\ldots\ldots\ldots\ldots\ldots\ldots\ldots\ldots\ldots\ldots\ldots\ldots\ldots\ldots\ldots\ldots\ldots\ldots\ldots\ldots\ldots\ldots\ldots \quad (2\text{-}26)$$

Where ∇ = differential operator dependent on coordinates; q = heat flux, W/m^2; α = thermal diffusivity, m2/s; T = temperature, K; ***t*** = time, s. Thermal diffusivity is related *to* other thermal properties as:

$$\alpha = \frac{\lambda}{\rho c} \quad \ldots\ldots\ldots\ldots\ldots\ldots\ldots\ldots\ldots\ldots\ldots\ldots\ldots\ldots\ldots\ldots\ldots\ldots\ldots\ldots\ldots\ldots\ldots\ldots\ldots\ldots \quad (2\text{-}27)$$

Where α = thermal diffusivity, m^2/s; λ = thermal conductivity, W/m-K; c = heat capacity, J/kg-K; ρ = mass density, kg/m^3. Thermal diffusivity has units of cm^2/s, ft^2/s, or SI units of m^2/s. Examination of Eq. (2-27) will show that thermal diffusivity varies in a manner similar to that of thermal conductivity but amplified by the temperature behavior of heat capacity (Somerton, 1992).

From published data, Eppelbaum et al. (2014) compiled the following table (Table 2-24), which presents the average values of thermal diffusivity for some rocks.

Table 2-24: Average values of thermal diffusivity (in 10^{-7} m^2/s) (Eppelbaum et al., 2014).

Rock	*a*
Sand	9.57
Siltstone	10.28
Argillite, clay schist	9.76
Clay	7.30
Marl	7.53
Limestone	10.92
Chock	4.77
Granite	9.13
Granodiorite	5.15
Porpyrite	9.54
Diorite	6.38
Basalt	5.34
Diabas	9.93
Gabbro	9.70
Schist	9.60
Gneiss	7.98
Amphibolite	6.84
Gneiss–granite	7.24

Table 2-25 depicts the conversion factors for thermal diffusivity (Somerton, 1992).

Table 2-25: The conversion factors for thermal diffusivity (Somerton, 1992)

Thermal Diffusivity		
Multiply	by	to convert to:
ft^2/hr	0.2581	cm^2/s
ft^2/hr	2.581×10^{-5}	m^2/s
m^2/s	3.8745×10^4	ft^2/hr
cm^2/s	3.8745	ft^2/hr

Chapter 3: PVT Analysis

In hydrocarbon reservoir modeling, a reliable set of fluid properties is a basic requirement. This is especially true when encountering heavy oil. Two important characteristics distinguish heavy oil from conventional oil: high gravity and high viscosity. Because, almost all heavy oil reservoirs have a low solution gas-oil ratio (solution GOR), this high gravity and low GOR cause the mole percent of the heavy (plus) fraction of oil to be very high. Characterizing this heavy fraction is one challenge when modeling reliable experimental heavy oil data. Viscosity modeling of heavy oil has more or less the same degree of complication and significance. The viscosity of Alaska's North Slope heavy crude is expected to be higher than 100 cP at reservoir temperature (70–100°F). However, commercial PVT simulation packages (such as WINPROP of CMG) are generated for conventional oil. These two issues make it difficult to model heavy oil properties.

Before carrying out any PVT simulation, obtaining a reliable data set of reservoir fluid properties is essential. In general, one can rarely find any set of fluid properties for heavy oils. Available data are usually limited to API gravity, GOR, and dead oil viscosity. The main heavy oil reservoirs of the Alaska North Slope (ANS) are West Sak and Ugnu. Beside a brief review of ANS heavy crude properties by Olsen et al. (1992), and Attanasi and Freeman (2015) (see Table 3-1), only a few other sources of data have been found in the open literature.

Table 3-1: Fluid and Reservoir Properties of Producing Viscous Oil Pools, Alaska North Slope (Attanasi and Freeman 2015).

Pool	Unit	Depth Below Sea Level (ft)	Gravity (°API)	Viscosity (centipoise)	Net pay (ft)	Temperature (°F)	Permeability (millidarcies)	Porosity (%)	Water Saturation (%)	Gas-Oil Ratio (scf/bbl)	Original Pressure (psi)
West Sak	Kuparuk River	3500	17-21	42	7-120	75	15-2000	30	30	117-220	1000-1600
Schrader Bluff	Milne Point	4000	14-22	20-220	10-50	80	100-3000	30	40	250	1800
Orion	Prudhoe Bay	4400	15-22	7-132	60-160	87	10-1400	25-32	35	250-350	1950
Polaris	Prudhoe Bay	5000	16-24	5-120	30-105	100	10-1800	25-30	40-45	250-330	2250
Nikaitchuc-Schrader Bluff	Nikaitchuc	3760	16-19	90-188	32.5	80	300	29	26.5	80-140	1700

Data from Alaska Oil and Gas Conservation Commission (2013c, e, f, h, i). °API degrees API, °F degrees Fahrenheit, scf/bbl standard cubic feet per barrel, psi pounds per square inch. See Appendix 1 for conversion factors to SI units.

3.1. Ugnu Oil Properties

Based on the data presented by Hulm et al. (2013), the following points can be drawn:

- Average depth: 610–1524 m (2000–5000 ft) TVD,
- Gravity: 8–14 °API,
- Viscosity: 300– > 50000 cP,
- Solution GOR: 50–200 scf/STB,
- Gas: dry consisting of more than 95% methane.

Based on the data of 10 wells, Hallam et al. (1992) concluded that the gravity of the Ugnu oil varies from 7.1 to 11.5 °API. They also mentioned that based on the samples from three wells, the elemental analysis of the oil is 85.1% carbon, 10.9% hydrogen, 0.5% nitrogen, 1.8% oxygen and 1.7% sulfur. Also the same samples indicate that the oil contains 10.6% saturates, 3.0% aromatic, 30.4% resin I and 2.3% resin II, and 3.6% asphaltene.

3.2. West Sak Oil Properties

As mentioned, the West Sak reservoir is one of the major heavy oil resources in ANS. According to Hornbrook et al. (1991) the reservoir is located about 250 miles north of the Arctic Circle and to the west of the Prudhoe Bay Unit in the Kuparuk River Unit.

They summarized crude oil properties and reservoir conditions at the sampling depth of the West Sak reservoir (Table 3-2). They found composition of West Sak solution gas is composed of 98% methane.

Table 3-2: Summary of West Sak crude oil properties (Hornbrook et al., 1991)

Sampling depth, ft	4,603
Reservoir temperature, °F	80
Bubblepoint pressure, psi	1,690
Oil gravity, °API	19.2
Oil density at bubblepoint pressure, g/cm 3	0.9022
Solution GOR at bubblepoint pressure, scf/STB	210
Viscosity at bubblepoint pressure and 80°F, cp	35.4
Oil FVF, bbl/STB	1.069
Gas composition, % methane	98

3.3. ANS (Alaskan North Slope) Heavy Oil Properties

By extensive laboratory experiments, Patil et al. (2008) obtained the reservoir fluid properties of two ANS crude oils (called Crude G and Crude H). The researchers achieved this goal by performing CCE (Constant Composition Expansion) and DL (Differential Liberation) PVT measurement on ANS heavy dead oil samples recombined with pure methane (99.5% pure) to simulate live oil samples. The results are shown in Tables 3-3 through 3-5 and Figures 3-1 through 3-4.

Table 3-3: Composition (mole %) of recombined ANS crudes G and H (Patil et al., 2008)

Sammple G		Sample H	
Component	Mole %	Component	Mole %
CO2	0.00229	CO2	0.003483
N2	0.09173	N2	0.13933
C1	22.7938	C1	34.62326
C2	0.01376	C2	0.0209
C3	0.01376	C3	0.0209
C4	0.00229	C4	0.00348
C8	1.69248	C6	7.09448
C9	5.6958	C7	1.16109
C10	4.40944	C8	0.31915
C11	4.32582	C9	1.27082
C12	6.31872	C10	1.80359
C13	6.4797	C11	2.60887
C14	7.3207	C12	2.85121
C15	6.54554	C13	5.01616
C16	3.49845	C14	4.15167
C17	5.16712	C15	5.15493
C18+	25.62861	C16+	33.7566
Sp Gr C18+	1.0511	Sp Gr C16+	1.0014
MW C18+	561.28	MW C16+	531.18

Table 3-4: CCE measured data for ANS crude samples G and H (Patil et al., 2008)

CCE Data for Oil Sample G			CCE Data for Oil Sample H		
Pressure psia	Total Volume cc	Relative Volume	Pressure psia	Total volume cc	Relative Volume
1919.2	200.23	0.9783	2604.2	111.1	0.97284
1785.9	200.87	0.9814	2489.3	111.46	0.9759
1658.4	201.5	0.9845	2342.7	111.99	0.9806
1548.5	202.13	0.9876	2214.5	112.44	0.9846
1427.9	202.77	0.9907	2097.7	112.69	0.9868
1332.7	203.4	0.9938	2001.2	112.99	0.9894
1182.9	204.67	1	1890.1	113.19	0.9911
998.8	209.12	1.0217	1822.2	113.27	0.9918
769.7	215.14	1.0512	1740.3	113.31	0.9922
484	231.65	1.1318	1654	114.02	0.9984
			1596.2	114.4	1.0017
			1572	114.22	1
			1386.1	118.4	1.0368
			1009.7	124.41	1.0894
			832.6	129.29	1.1321
			635.8	139.05	1.2176

Table 3-5: DL test data for ANS crude samples G and H (Patil et al., 2008).

Differential Liberation Test Sample G at 84°F						Differential Liberation Test Sample H at 81°F					
Pressure Psia	R_s Scf/STB	B_o bbl/STB	B_t bbl/STB	Density, g/cc	μ, cP	Pressure psia	R_s Scf/STB	B_o bbl/STB	B_t bbl/STB	Density, g/cc	μ, cP
1904	123	1.098	1.098	0.9352	232.7	2510.7	194	1.065	1.065	0.942	322.3
1762	123	1.1053	1.1053	0.9345	224.2	2396.7	194	1.075	1.075	0.9405	314.2
1625	123	1.111	1.111	0.9342	221.7	2303.7	194	1.0858	1.0858	0.9398	304.9
1513	123	1.1223	1.1223	0.9339	214.9	2189.7	194	1.084	1.084	0.939	297.4
1406	123	1.1337	1.1337	0.9335	210.5	2050.7	194	1.103	1.103	0.9379	291.6
1183	123	1.1455	1.1455	0.9326	191.5	1886.6	194	1.124	1.124	0.9369	286.3
959	118	1.121	1.1335	0.9329	208.6	1709.7	194	1.143	1.143	0.9355	281.9
749	93	1.1014	1.1972	0.9375	221	1586.7	194	1.16	1.16	0.9348	274.7
462	72	1.0618	1.3435	0.9398	242	1264.7	189	1.11	1.1247	0.9357	283.9
225	37	1.032	2.0162	0.9407	267.5	1002.7	182	1.086	1.1218	0.9362	292.8
143	28	1.0188	2.7616	0.9423	299.6	836.7	159	1.065	1.156	0.937	303.2
14.7	0	1.006	23.9393	0.944	359.8	646.7	132	1.057	1.2736	0.9377	323.9
						422.7	98	1.035	1.5184	0.9382	341.6
						217.7	47	1.0334	2.73	0.9395	383.2
						14.7	0	1	36.1889	0.9429	429.23

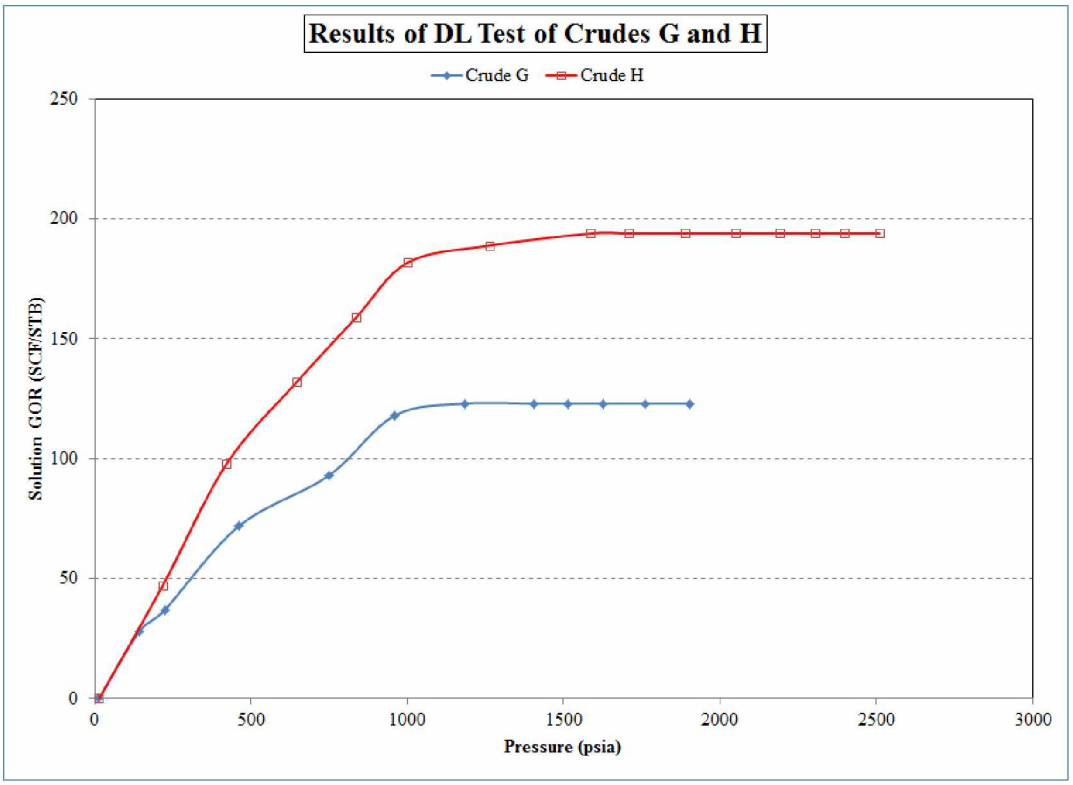

Figure 3-1: DL test results – Solution GOR (Patil et al., 2008).

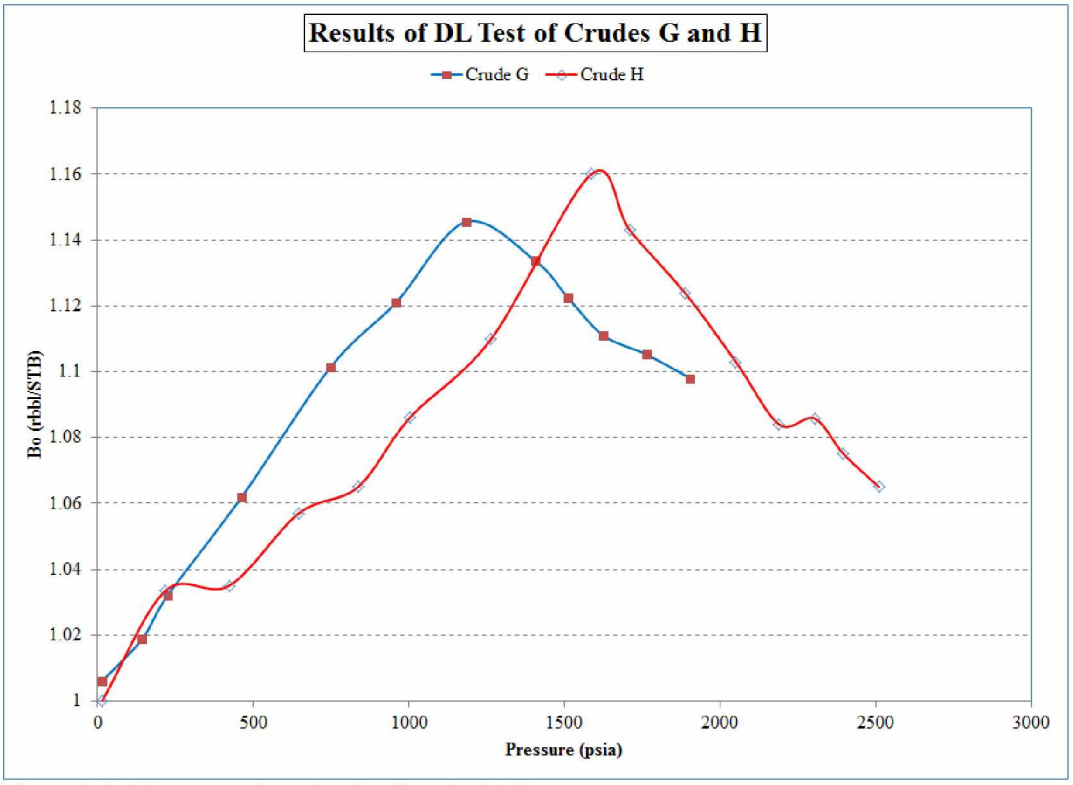

Figure 3-2: DL test results – Bo (Patil et al., 2008).

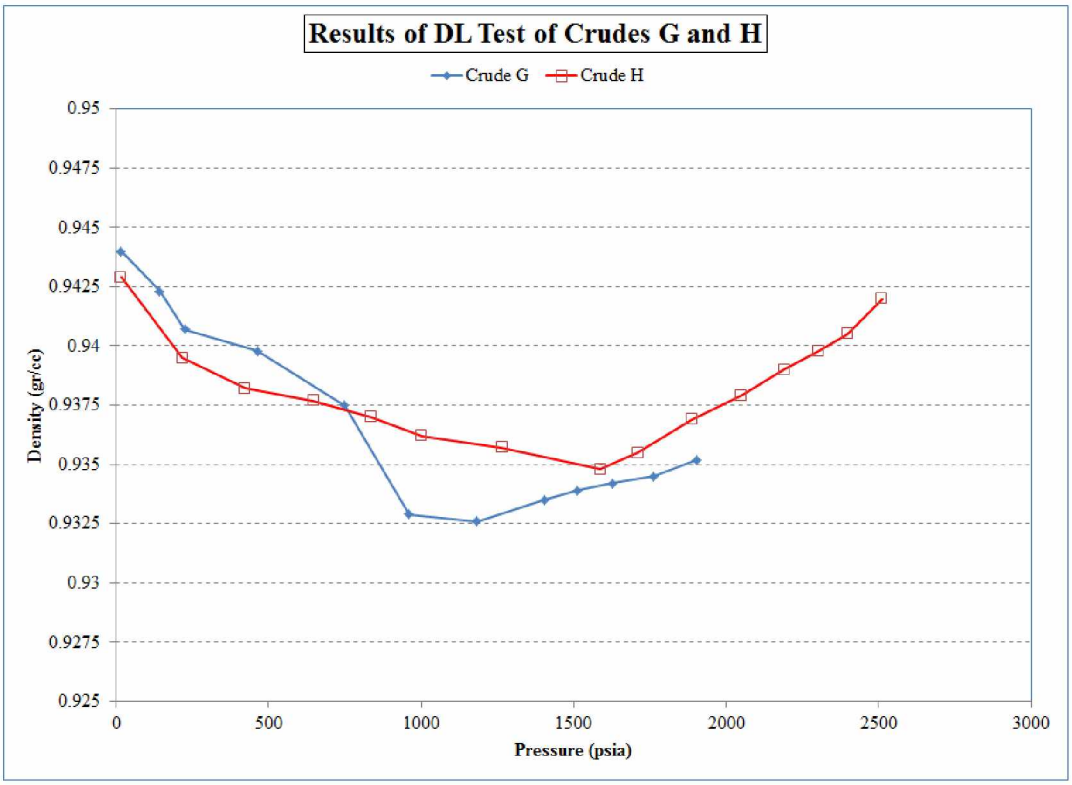

Figure 3-3: DL test results – oil density (Patil et al., 2008).

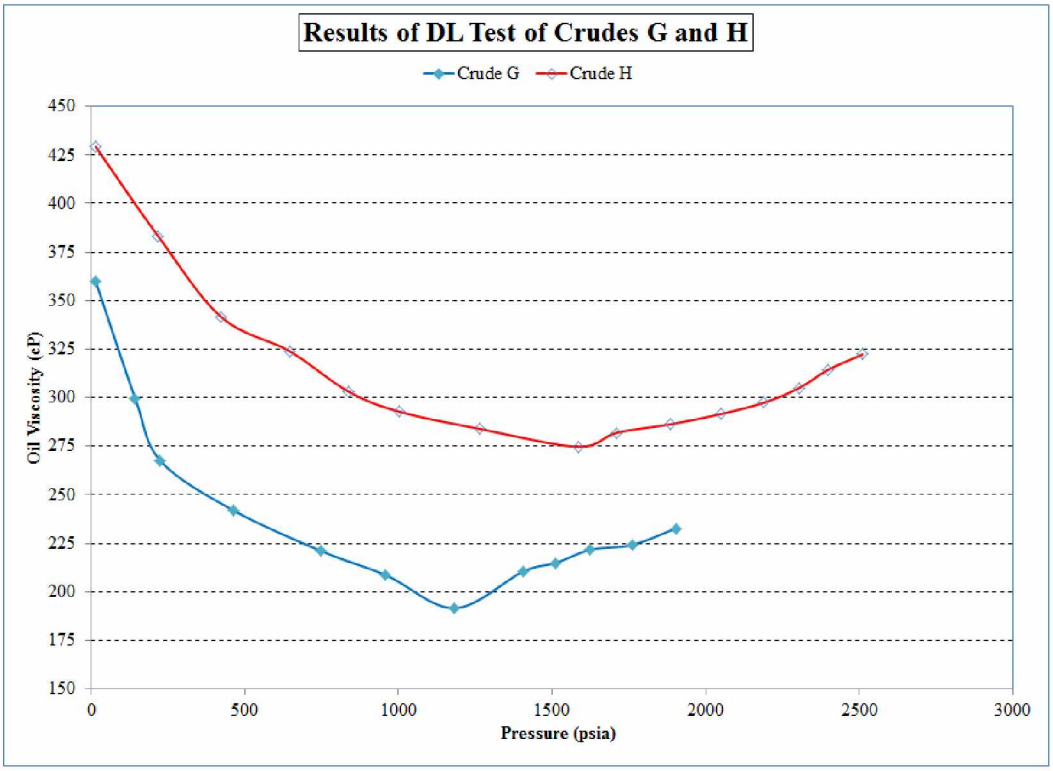

Figure 3-4: DL test results – viscosity (Patil et al., 2008).

3.4. PVT Crude Sample Selection for Simulation

Obviously, the data of crudes G and H presented by Patil et al. (2008) are more complete than the other set of data. The data of Ugnu crude (Hulm et al., 2013) are general and do not even include bubble point data. The data of West Sak crude (Hornbrook et al., 1991) are more detailed; however, they do not include any experiment data.

The data reported by Patil et al. (2008) form a complete set of data; however, the viscosity of crude(s) is in the range of 200 to 300 cP at reservoir conditions, much lower than the reported oil viscosity of the Ugnu field. But, during project execution (reservoir simulation modeling) investigating the effect of viscosity on project results is expected. Thus, for the project detailed in this thesis, built-in black oil PVT models were used in the STARS simulator. To do so, a data bank of viscosity of dead oil versus temperature and viscosity versus oil density is essential. The following tables and figure were obtained from the open technical literature.

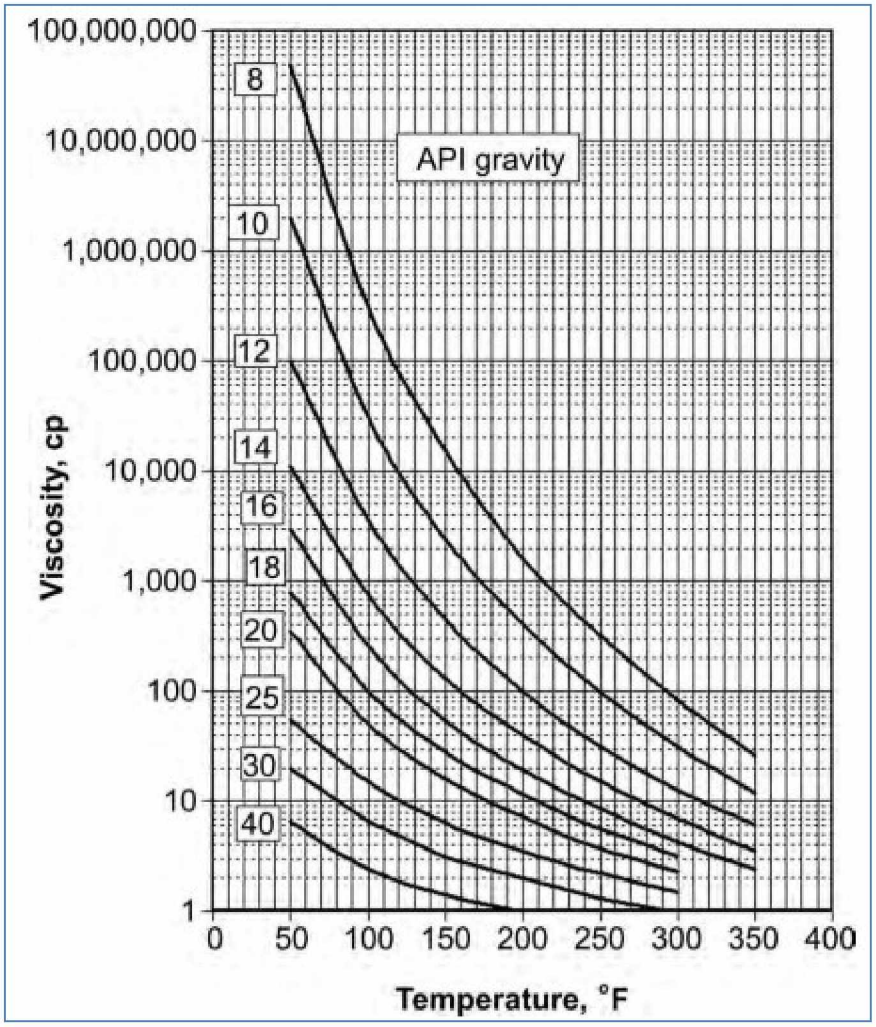

Figure 3-5: Temperature dependence of viscosity for crude oils (Jones, 2007).

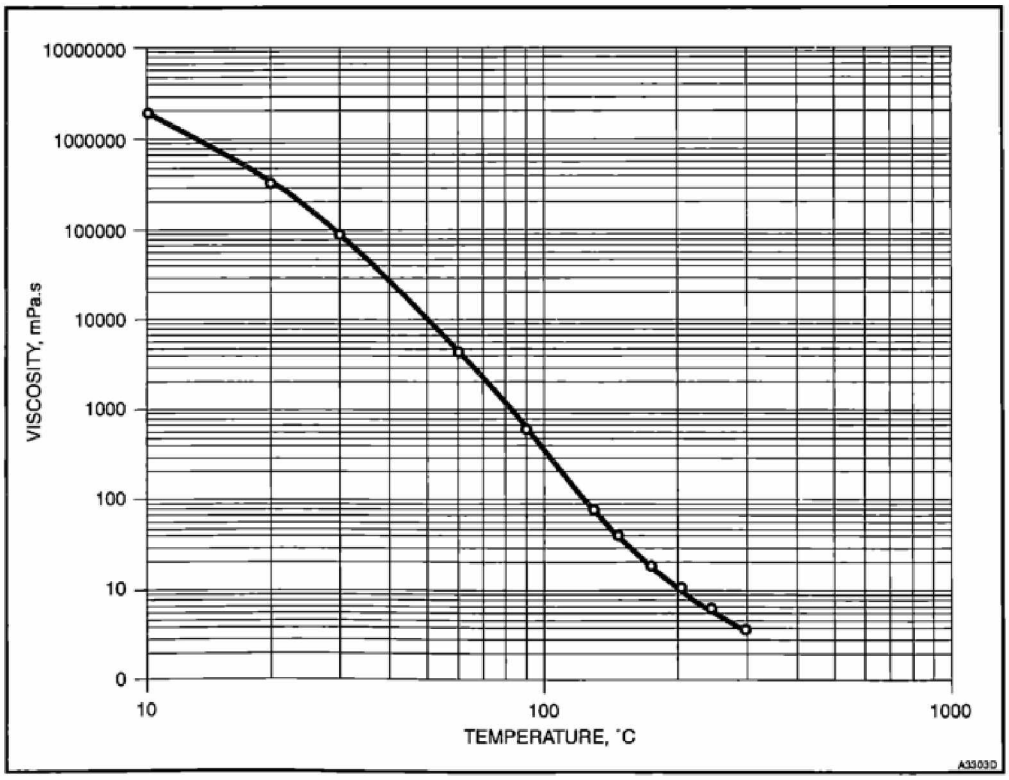

Figure 3-6: Bitumen viscosity, 8 °API (Towson and Khallad, 1991).

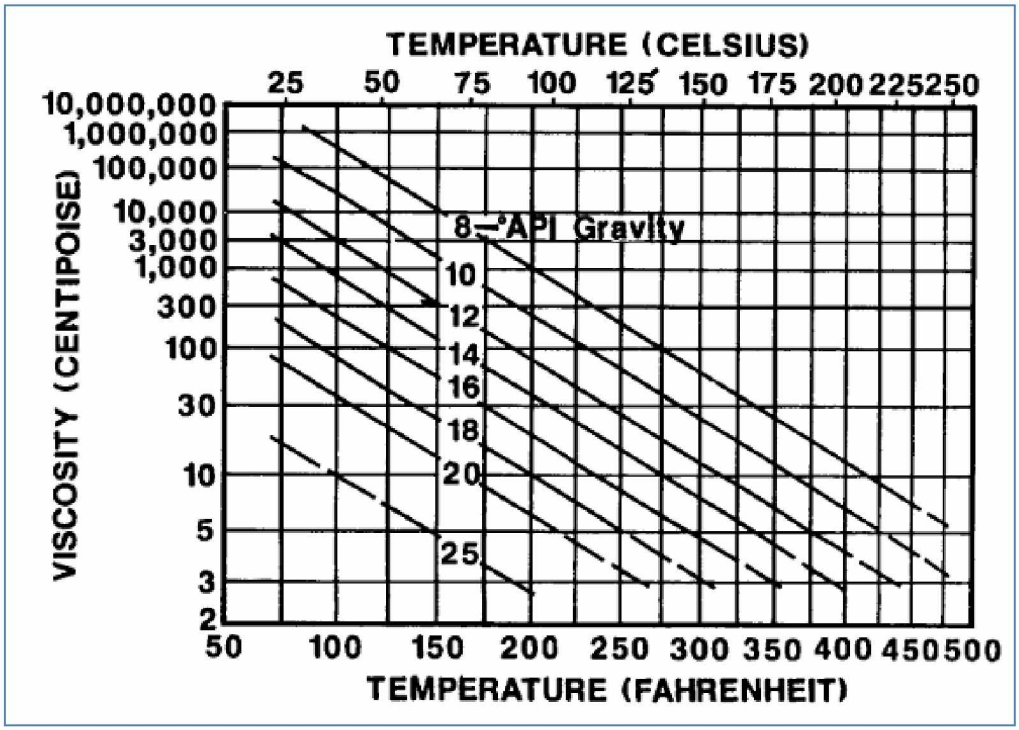

Figure 3-7: Oil viscosity as a function of temperature and gravity [from Farouq Ali and Meldau, 1983], (Carcoana, 1992).

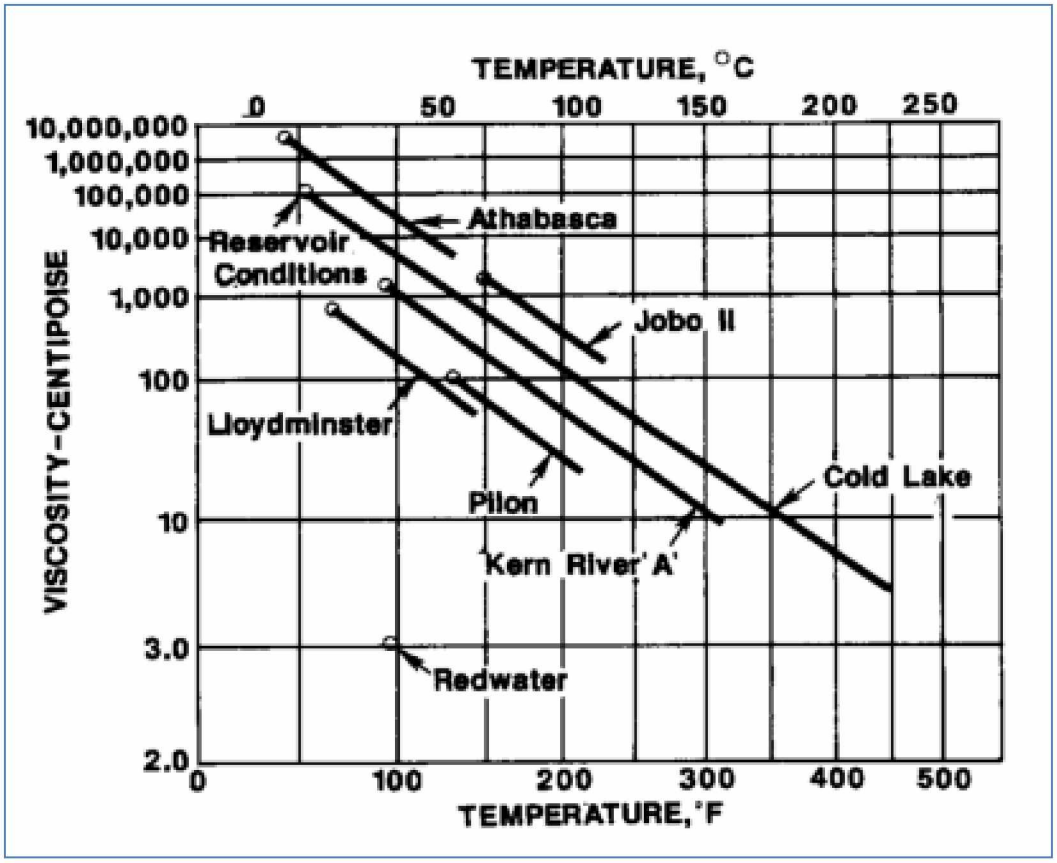

Figure 3-8: Typical heavy oil viscosity-temperature relationship [from Buckles, 1979), (Carcoana, 1992).

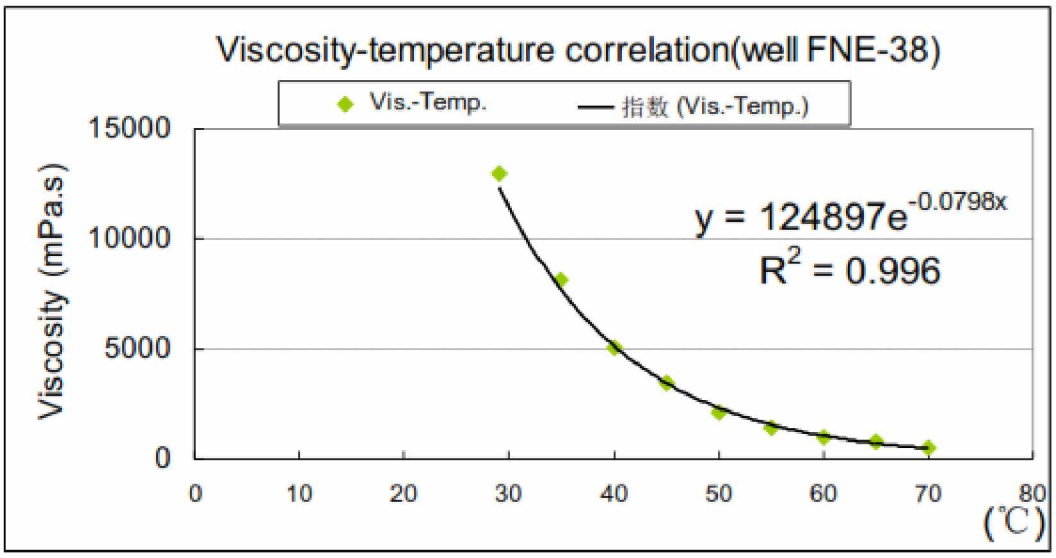

Figure 3-9: Surface heavy oil (18 °API) viscosity and temperature correlation (well FNE-38), (Ruifeng et al., 2011).

Table 3-6: Viscosity reduction with temperature – oil MW = 600, (Azad et al., 2013).

Viscosity (cP)	Temperature(°F)
6000	125
187	150
17.4	250
8.5	300
5.2	350
2.5	500

Table 3-7: Temperature-viscosity data (Luo and Baker, 2006).

Temperature and viscosity data (14 °API oil)

Temperature, °F	Viscosity, cp
75	5780
100	1380
150	187
200	47
250	17.4
300	8.5
350	5.2
500	2.5
600	2.0

Temperature and viscosity data (18 °API oil)

Temperature, °F	Viscosity, cp
75	570
100	219
150	57
200	22
250	10.5
300	5.7
350	3.4
500	1.1
600	1.0

--

The data in the preceding figures are digitized and, in conjunction with data of tables, plotted in Figure 3-10. This figure shows the general relationship between viscosity-temperature and API gravity. To find out the location of Alaskan viscous crude oil – especially the oil of Ugnu field – the range of changes of viscosity and temperature of Ugnu crude is superimposed on these plots (Figure 3-11). By careful study of Figures 3-10 and 3-11, the following points can be drawn:

- The data of Jones (2007) are classical and data of other references scattered among these sets of data.
- The available Ugnu reservoir viscosity-temperature data overlap with the viscosity-temperature data of crude with density of 10 to 16 °API, although the Ugnu density data range between 8 to 12 °API.

To show more clearly the conformance of Ugnu crude viscosity-temperature with those of data presented by Jones (2007), both sets of data are plotted in Figure 3-12. Based on these works, it seems that the viscosity-temperature changes of the Ugnu heavy oil potentially follow the same trends of data presented by Jones (2007) for crude with density of 10 to °16 API. By using Excel software, the trend lines and their equations were obtained for the viscosity-temperature curves of Jones (2007) data for oils with API degree of 10 to 16 (see Figure 3-13).

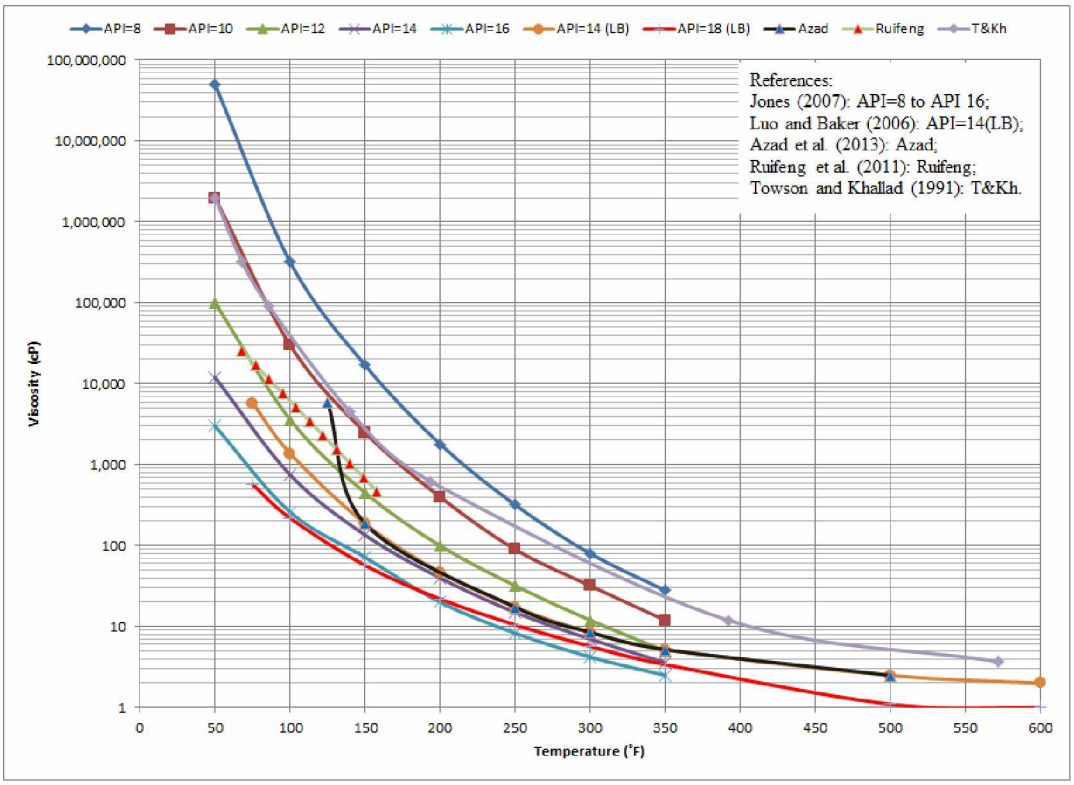

Figure 3-10: General viscosity – temperature relationship for heavy oils.

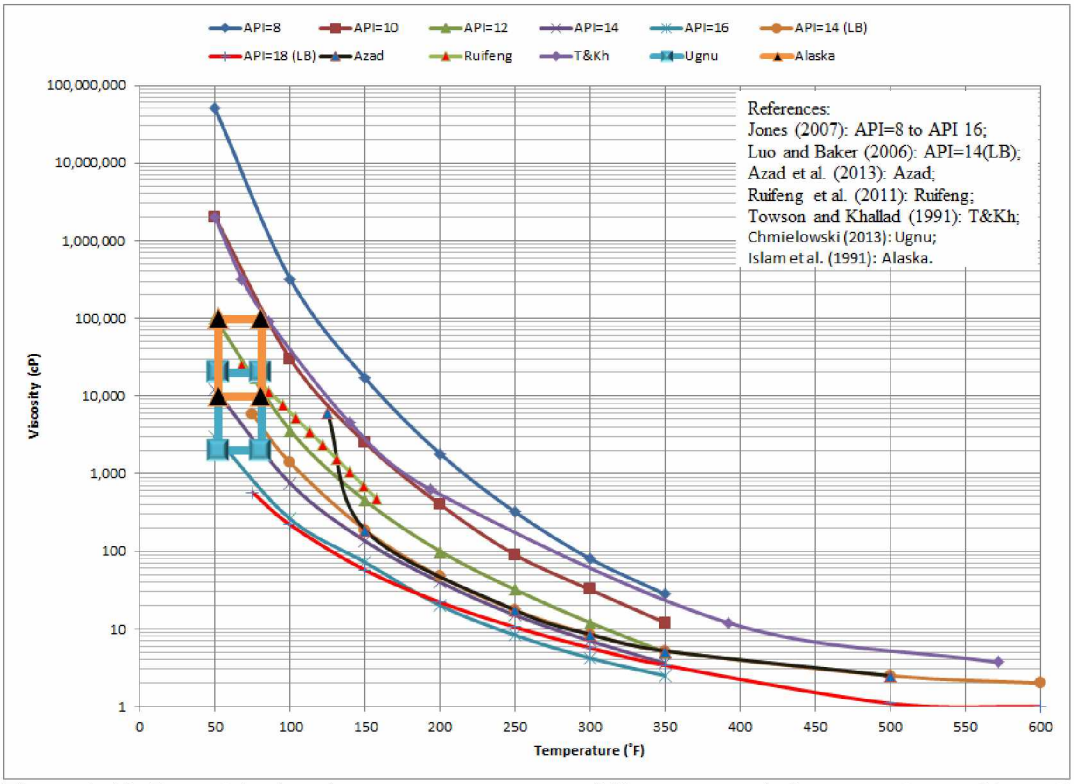

Figure 3-11: Potential viscosity-temperature range of Ugnu reservoir in comparison with available heavy crude data.

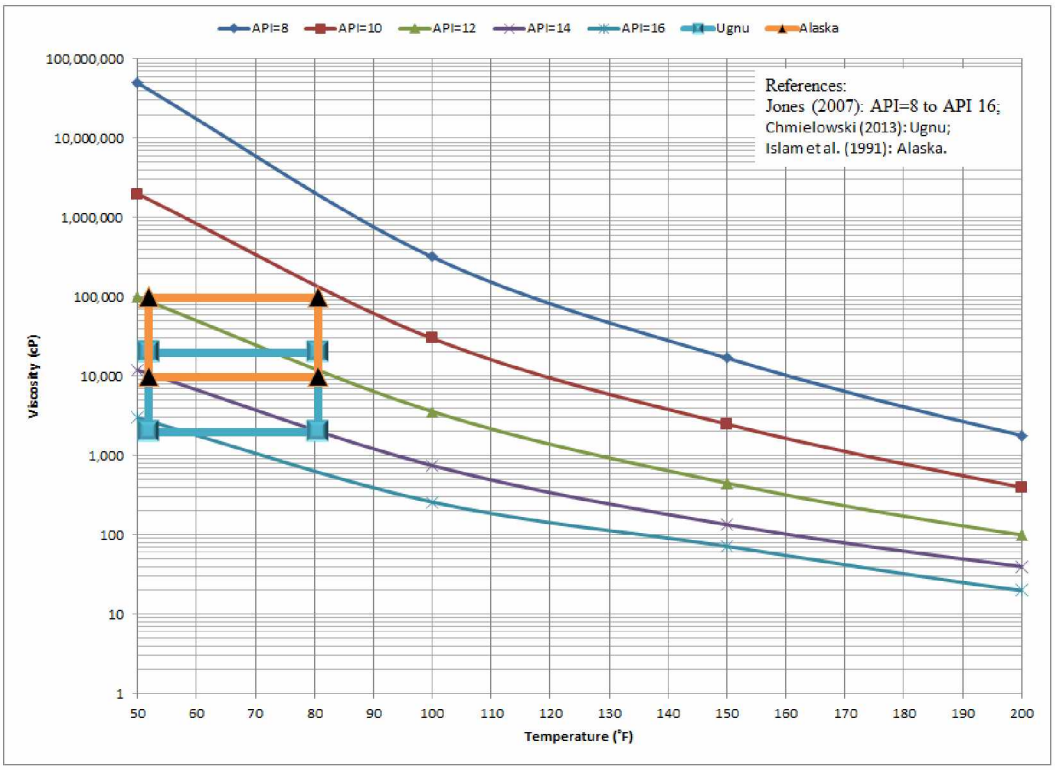

Figure 3-12: Potential viscosity-temperature range of Ugnu reservoir in comparison with Jones (2007) data.

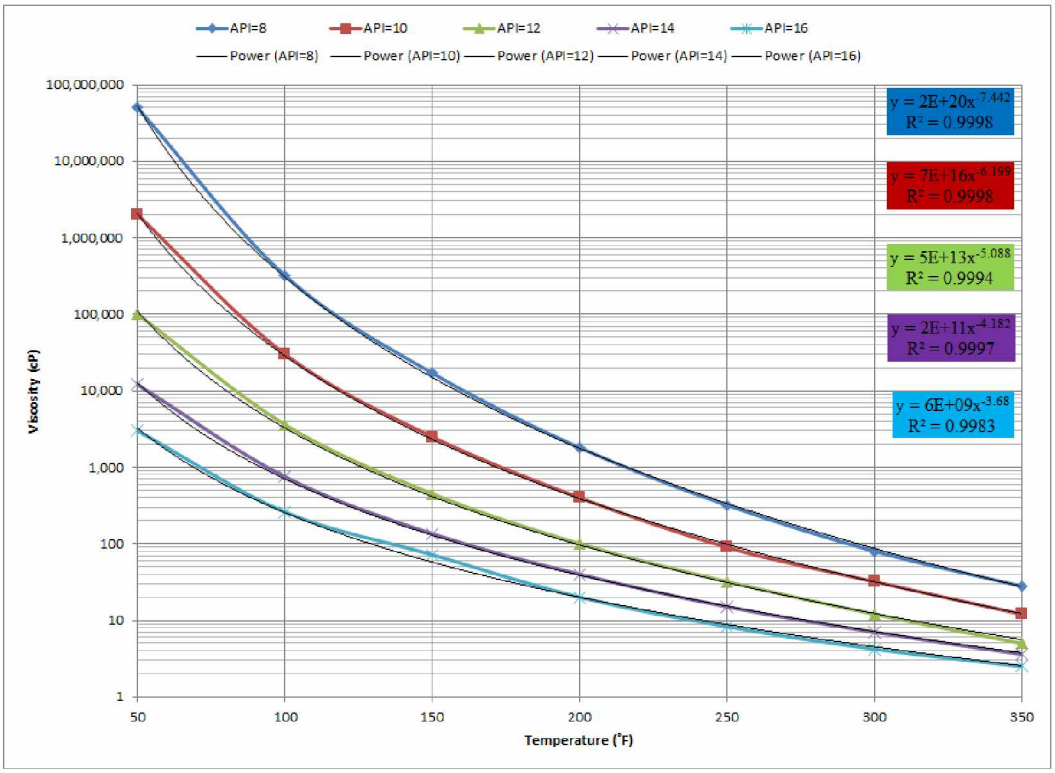

Figure 3-13: Trend lines for heavy crude data of Jones (2007) viscosity temperature data.

Based on the preceding discussion, the following equations for temperature dependency of viscosity of heavy-viscous crude oil of Ugnu reservoir were used.

$$\mu = 7 \times 10^{16} T^{-6.199} \quad \text{..... (3-1)}$$

$$\mu = 5 \times 10^{13} T^{-5.088} \quad \text{..... (3-2)}$$

$$\mu = 2 \times 10^{11} T^{-4.182} \quad \text{..... (3-3)}$$

$$\mu = 6 \times 10^{9} T^{-3.68} \quad \text{..... (3-4)}$$

Where:

μ: Viscosity, cP;

T: temperature, ˚F.

It was supposed that these equations potentially cover the Ugnu heavy-viscous crude oil in the range of 8 to 14 ˚API. Based on these equations, the viscosity temperature dependency for reservoir simulation was obtained.

Chapter 4: Geology Study

For a practical, meaningful reservoir simulation, a good geological model is essential. This means that the model can mimic actual formation properties with minimum error in comparison with the available data. These properties include but are not limited to faults, any geological barrier, porosity and its distribution, permeability and its distribution, formation heterogeneity, and relative permeability. For this project a reliable set of rock thermal properties, such as heat capacity, also is essential. In the following sections, the most reliable geological data that was gathered from the 'open literature' are presented. Data from both the Ugnu and West Sak formations are presented; however, for this thesis project, emphasis was on the Ugnu reservoir.

4.1. Regional Location and Characteristics of West Sak and Ugnu Sands

The Ugnu and West Sak sands are part of the strata called the "Shallow Sands." These strata comprise a portion of the Late Cretaceous and Early Tertiary marine and deltaic complex that developed in the Kuparuk area. The Ugnu sands are informally named for the heavy-oil/tar-bearing interval in East Ugnu Well 1 (Hallam et al., 1992).

Figure 4-1 presents a general map of Alaska's oil and gas resources. Figure 4-2 depicts the heavy oil accumulation on Alaska's North Slope.

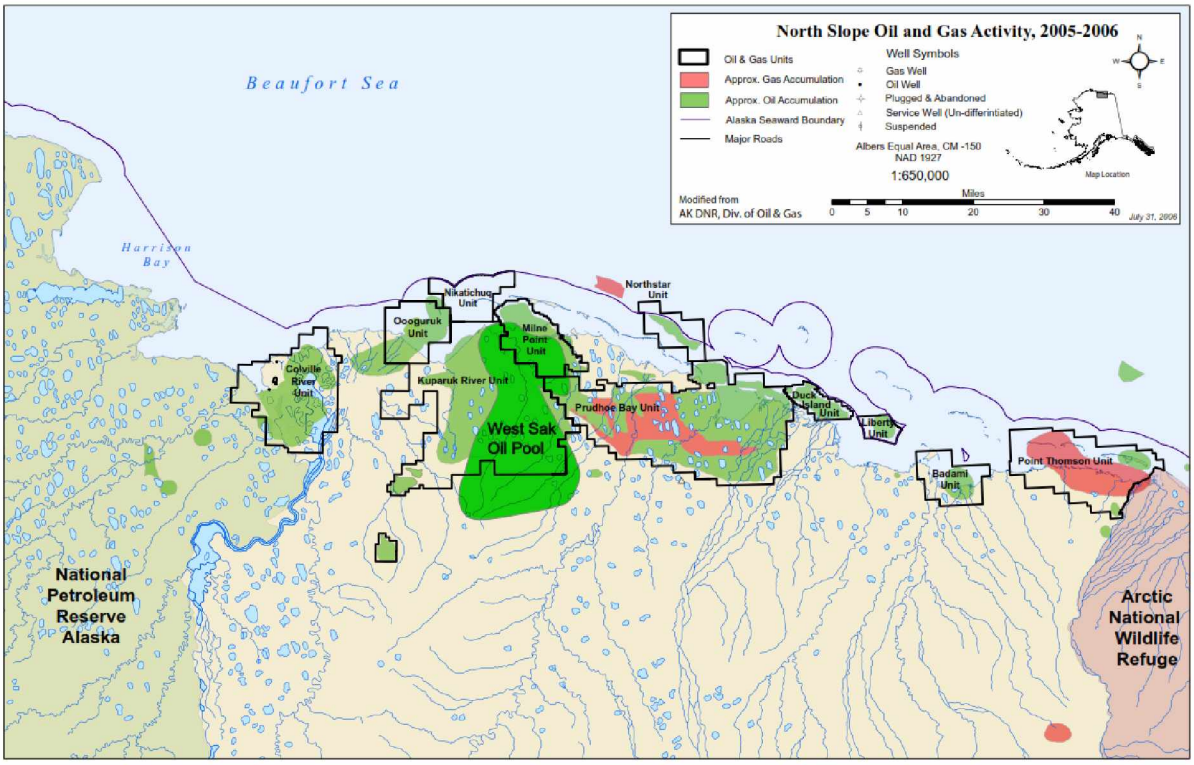

Figure 4-1: General oil and gas resources of Alaska (Alaska Division of Oil and Gas, 2016).

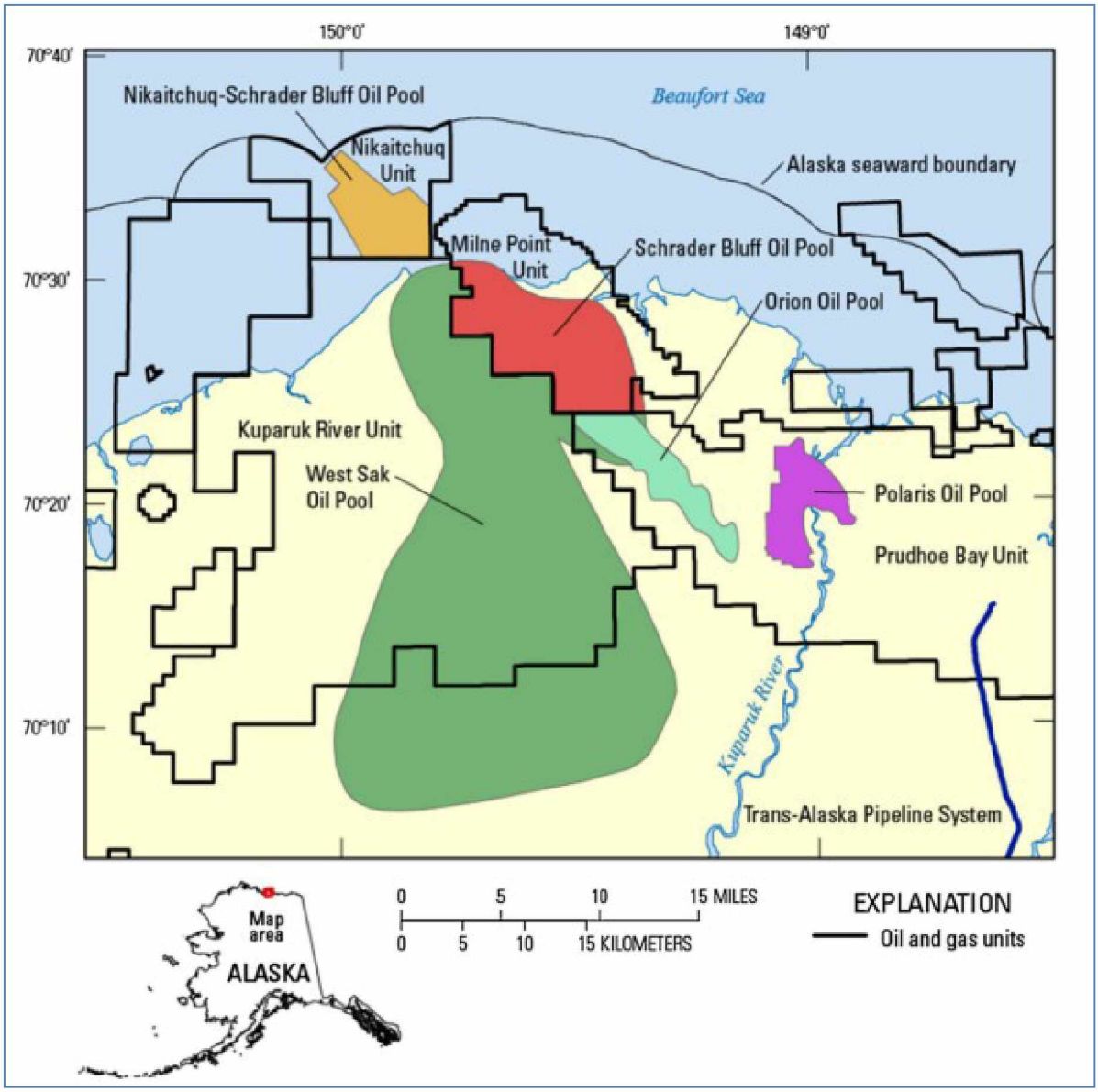

Figure 4-2 Map of the heavy oil accumulations on Alaska's North Slope showing the oil and gas units and the approximate outlines of the pools containing heavy oil (Attanasi and Freeman, 2015).

According to Attanasi and Freeman (2015), Werner (1987) presents an early discussion of the West Sak and Ugnu oil-bearing sands from a regional perspective. Werner (1987) refers to the region as the Kuparuk River Area that includes the Prudhoe Bay, Milne Point, and Kuparuk River Units. Attanasi and Freeman (2015) showed a generalized stratigraphic column representative of the Kuparuk River and Milne Point Units. It shows the Lower Ugnu stratigraphic interval overlying the West Sak interval. The West Sak and Ugnu stratigraphic intervals comprise a portion of a Late Cretaceous and Early Tertiary shallow marine deltaic complex. This sequence is part of the Brookman depositional cycle (Werner, 1987). These

stratigraphic intervals are oil bearing mainly in the Kuparuk River Unit (KRU) and Milne Point Unit (MPU); see Figure 4-2. Werner (1987) claims that the West Sak and Schrader Bluff sands lie in the same stratigraphic interval and that they are essentially equivalent. Figure 4-3 shows the composite well logs and formation for north fields provided by Werner (1987). Figure 4-4 illustrates the generalized stratigraphic column of the Kuparuk area based on Hallam et al. (1992). Also in Figure 4-5, a cross-sectional view of the Ugnu and West Sak reservoirs is presented (Islam et al., 1991).

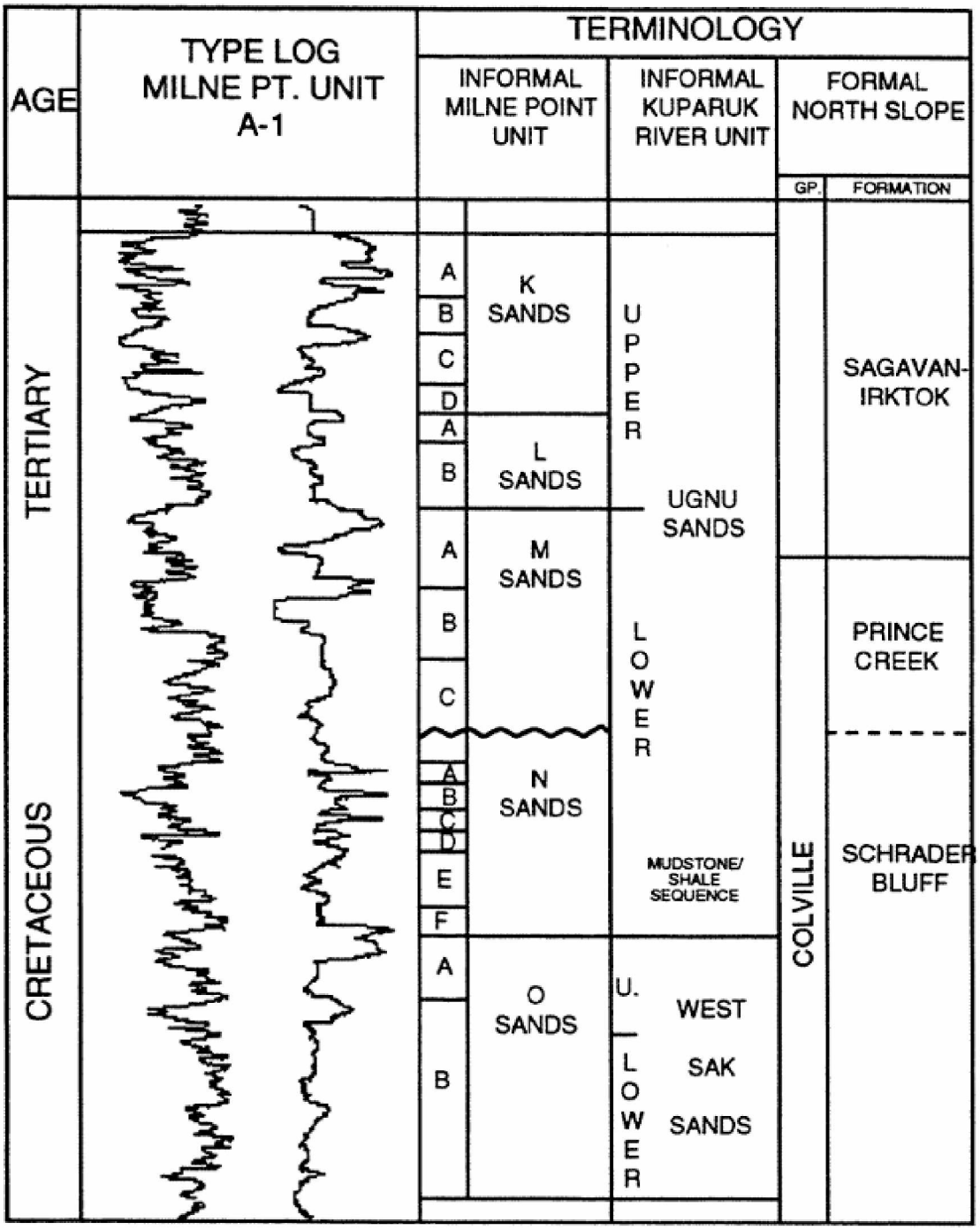

Figure 4-3: Composite well logs and formation for north fields (Werner, 1987)

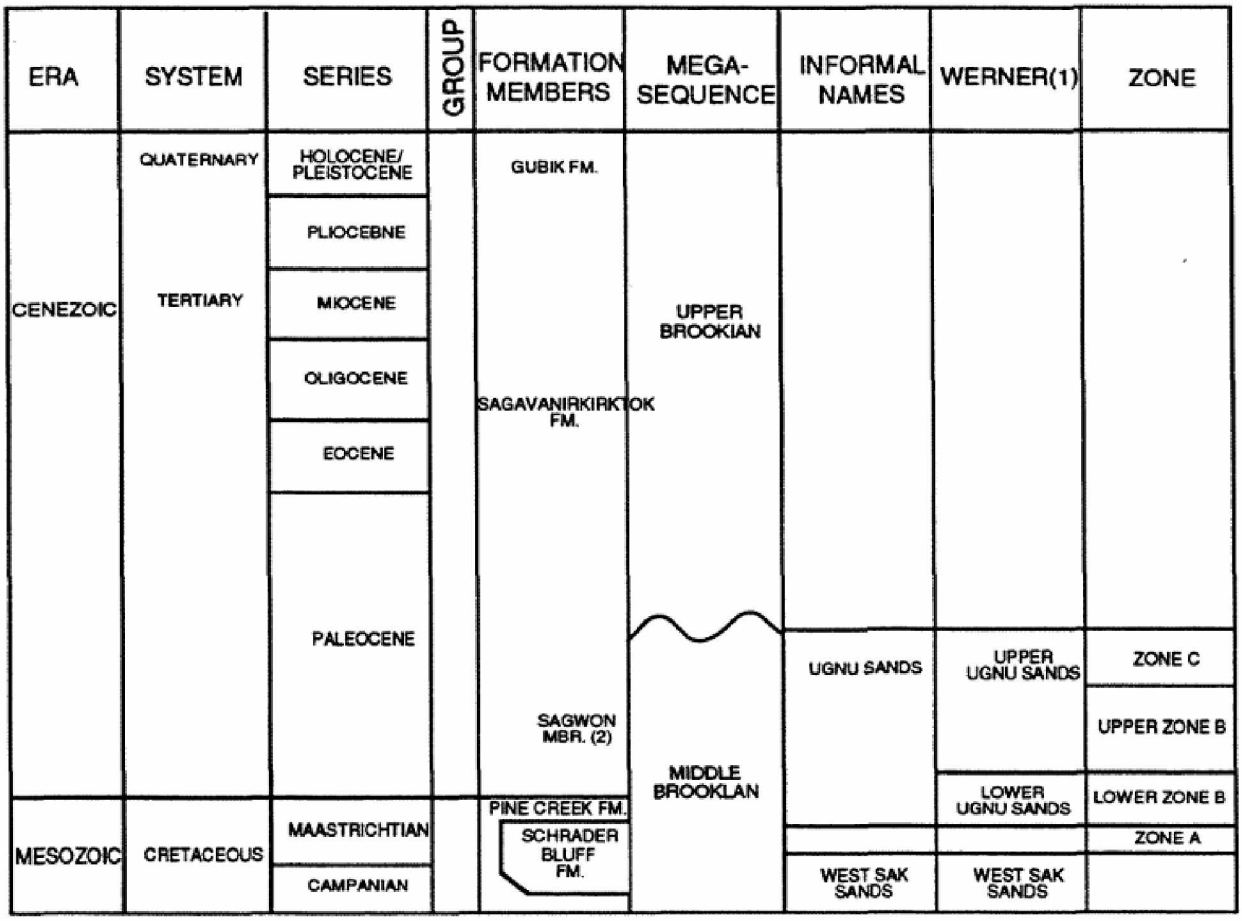

Figure 4-4: Generalized stratigraphy of the Kuparuk area (Hallam et al., 1992; Olsen et al., 1992).

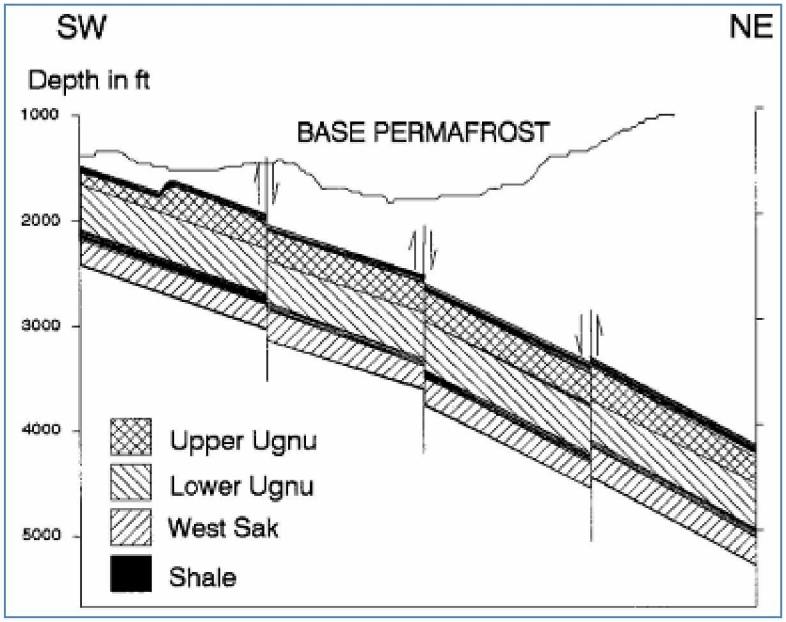

Figure 4-5: Cross-sectional view of Ugnu and West Sak reservoirs (Islam et al., 1991).

4.1.1. West Sak Accumulation

The West Sak reservoir is on the North Slope of Alaska, about 250 miles north of the Arctic Circle and to the west of the Prudhoe Bay Unit in the Kuparuk River Unit (Hornbrook et al., 1991).

Figure 4-6 shows the location of the structure on top of the West Sak stratigraphic interval. According to Werner (1987), the West Sak oil-bearing interval covers 260 square miles. The (gross) sand interval averages 300 feet, but it is thickest (450 feet) in the southwest area and thins to the northeast (200 feet). A cross section of the oil-bearing interval is presented in Figure 4-7. The sands are very fine to fine grained along with silty sandstone having interbedded siltstone and mudstone. The sands are also very friable, although calcite cemented layers occur locally (Werner, 1987). The West Sak consists of at least two sand packages, and each package consists of individual beds (Werner, 1987). According to Attanasi and Freeman (2015), API gravity values range from 14° to 24°, oil viscosity values range from 5 to 220 cP, and the gas to oil ratio values range from 80 to 350 standard cubic feet per barrel. Reservoir depth values range from 3,500 to 5,000 feet below sea level, and corresponding reservoir temperatures range from 75 to 100°F. Other reservoir properties include net pay thickness ranging from 10 to 160 feet, permeability ranging from 10 to 3,000 mD, porosity from 25 to 32%, and water saturation from 27 to 45%.

Olsen et al. (1991) pointed out that the combined thickness of the West Sak and Ugnu formations averages 1,050 ft. These two formations are oil bearing primarily in the Kuparuk River and Milne Point units, where they occur at depths ranging from 2,000 to 4,500 ft (Werner, 1987). The West Sak, at a depth of 2,000 to 4,500 ft, is fine to fine-grained sand with interbedded mudstone and claystone deposited as fluvial-deltaic sands. Its porosity averages less than 20%, and permeability is 10 to 140 mD. It contains intermediate to slightly heavy oil of 50 to 3,000 cP (14°–22.5° API gravity) at a reservoir temperature of 45°–100°F. West Sak heavy oil is believed to have the same source as that of the deeper Kuparuk, Sadlerochit, and Lisburne light oil reservoirs, but it has been biodegraded (Sharma, 1990), especially at shallower depths.

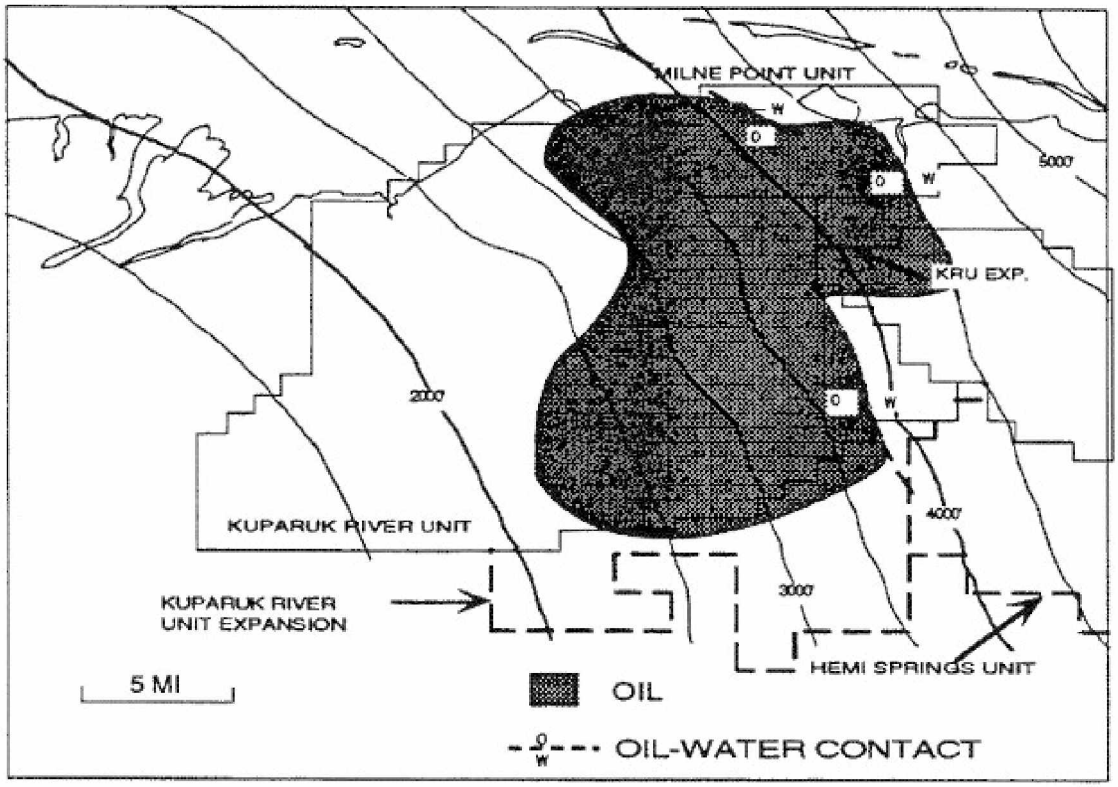

Figure 4-6: Structure on top of West Sak sands (Werner, 1987).

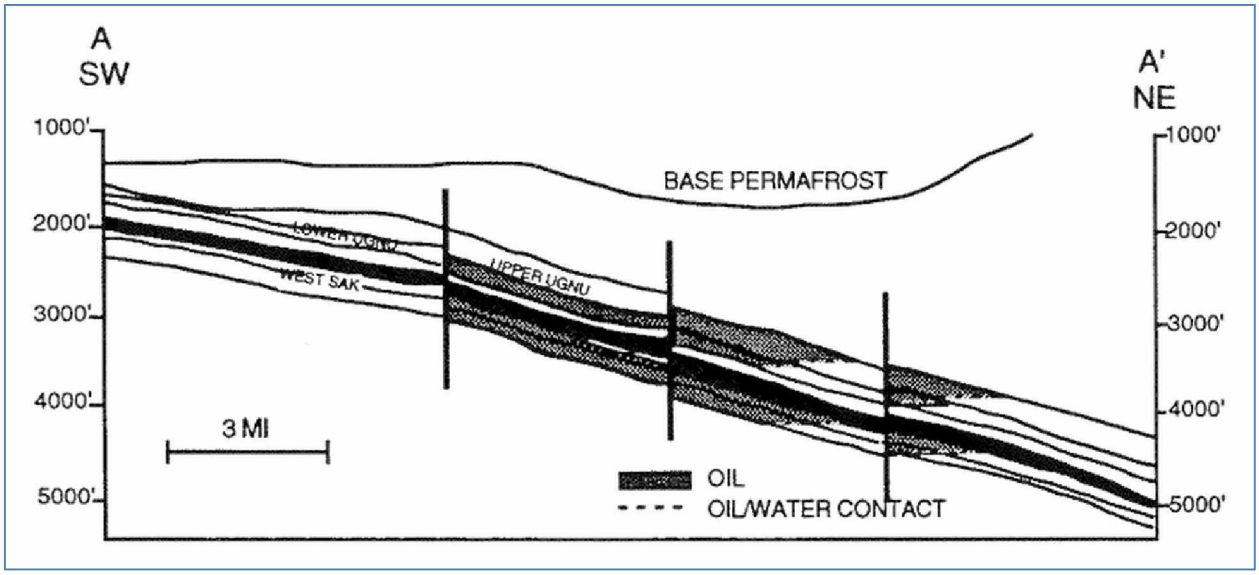

Figure 4-7: Generalized cross section of the shallow sand reservoirs of the northern Kuparuk River Unit (Werner, 1987).

4.1.2. Ugnu Accumulation

The Ugnu resource has mostly been overlooked as a development target because of high oil viscosity (Hulm et al. 2013). Hallam et al. (1992) divided the Ugnu into Zones A through C (see

Figure 4-4). Ugnu Zone B is the principal tar-bearing unit. Considered to be the delta top, Ugnu Zone-B has been divided into two subzones, Upper Zone B and Lower Zone B. Lower Zone B is composed of distributary channel sands and inter-distributary crevasse sands, as well as inter-distributary silts, mudstones, and distributary mouth bar sands. The regionally correlatable coal and the fact that Ugnu distributary channels are primarily sand-filled suggest a depositional model of a highly constructive lobate delta. The stacked channel sands are oriented in an east-west direction (Hallam et al., 1992).

The regional structure of the Ugnu dips gently from southwest to northeast at about 2°, and the thick pay intervals occur at depths from 2,200 to 3,200 ft [670 to 915 m] (Figure 4-8).
According to Hallam et al. (1992), the permafrost plays a key role in the development of the Ugnu because it influences the reservoir temperature and therefore the oil viscosity. At Kuparuk, the first 300 ft [100 m] of the permafrost consist of coarse sand, gravel, and conglomerates called "first gravels." A thick 150-ft [45-m] claystone interval caps an unconformity at about 900 ft [300 m] in the center of the Ugnu accumulation. This and other high-clay-content zones probably will provide a vertical permeability barrier to pore-pressure recharge from above or below when the permafrost melts. A series of silty-sand and silt beds exists between the first gravels and the unconformity, while sandy-silt and silty-sand intervals generally exist below the unconformity (Figure 4-9). The depth of the "ice-bearing" permafrost varies from 1200 to 1700 ft [365 to 520 m]. Within the area containing the thick Ugnu accumulation, the permafrost thickness averages about 1,650 ft [500 m]. The temperature at the base of the ice-bearing permafrost interval is about 31°F [-0.5°C]; the temperature gradient through the interval is 1.1 °F/100 ft [2°C/100 m] (Hallam, 1992).

Tables 4-1 and 4-2 summarize the reservoir data of Ugnu and West Sak, respectively.

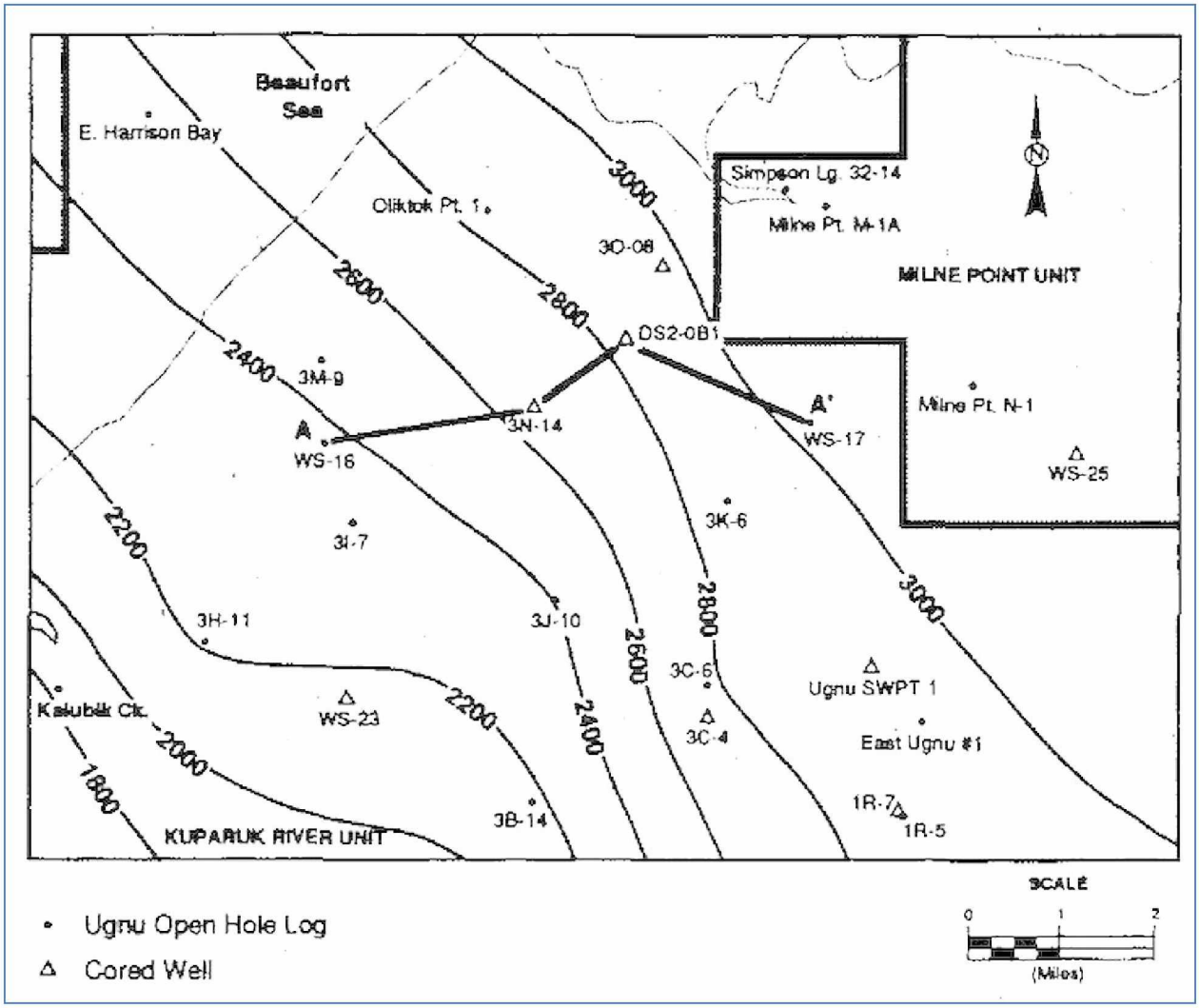

Figure 4-8: Top Ugnu zone B map (subsea depths in feet); (Hallam et al., 1992).

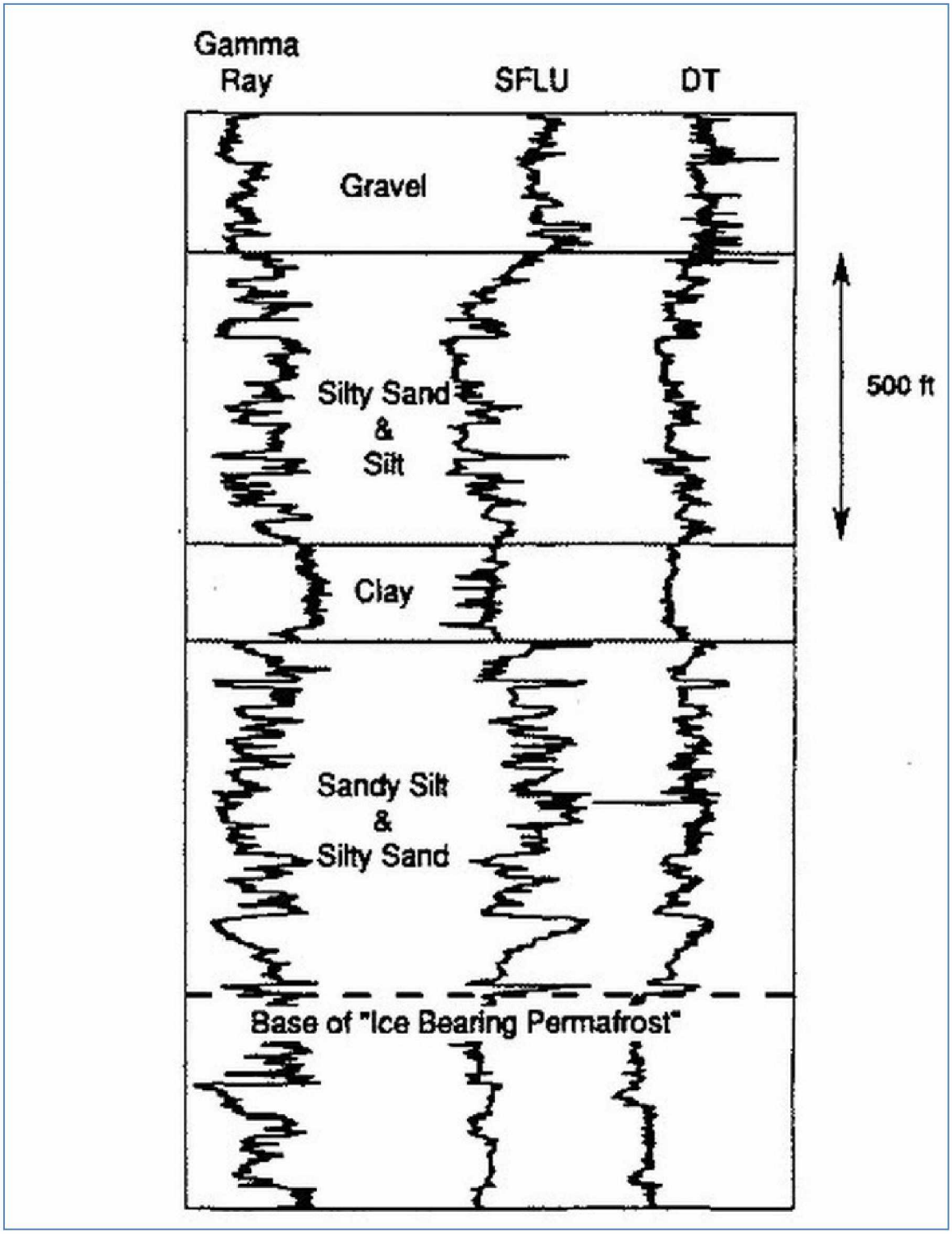

Figure 4-9: Permafrost well log (Hallam at al., 1992).

Table 4-1: Ugnu reservoir properties.

Property	Data	Reference
Top Formation (ft)	2200	Hallam et al. (1992)
	2000	Hulm et al. (2013)
Base Formation (ft)	3200	Hallam et al. (1992)
	5000	Hulm et al. (2013)
Net/Gross Ratio	0.74-0.92 (Ave=0.8)	Hallam et al. (1992)
Porosity (%)	34 to 37	Hallam et al. (1992)
	15 to 38	Hulm et al. (2013)
	30 to 35	Werner (1984) and Olsen et al. (1992)
Oil Saturation (%)	66 to 72	Hallam et al. (1992)
Air Permeability at 1000 to 2000 psi (md)	Several hundred to several thousands	Hallam et al. (1992)
Permeability (md)	0.1 to 10,000	Hulm et al. (2013)
	200 to 3000	Werner (1987) and Olsen et al. (1992)
Average porosity and permeability in best reservoir quality	35 % and 2000 mD	Hulm et al. (2013)
Reservoir temperature (˚F)	45 to 65 (2.1 ˚F/100 ft)	Hallam et al. (1992)
Reservoir Pressure (psi)	1328 at 2978 ft. (0.446 psi/ft)	Hallam et al. (1992)
Dead Oil Viscosity (cSt)	100,000 to 2,000,000	Hallam et al. (1992)
Live Oil Viscosity (cP)	300 to >50,000	Hulm et al. (2013)
API Gravity (˚)	7.1 to 11.5	Hallam et al. (1992)
	8 to 14	Hulm et al. (2013)
Rel. Perm. Of water at Sor at 230 ˚F	0.17	Hallam et al. (1992)
Initial GOR (SCF/STB)	50 – 200	Hulm et al. (2013)

Table 4-2: West Sak reservoir properties.

Property	Data	Reference
Top Formation (ft)	3000	Hornbrook (1991)
	3500	Attanasi and Freeman (2015)
Base Formation (ft)	4500	Hornbrook (1991)
	5000	Attanasi and Freeman (2015)
Net Pay (ft)	10 to 160	Attanasi and Freeman (2015)
Porosity (%)	25 to 32	Attanasi and Freeman (2015)
Water Saturation (%)	27 to 45	Attanasi and Freeman (2015)
Permeability (md)	10 to 3000	Attanasi and Freeman (2015)
Reservoir Temperature (˚F)	45 to 100	Hornbrook et al. (1991)
	75 to 100	Attanasi and Freeman (2015)
Reservoir Pressure (psi)	1000 - 1600	Attanasi and Freeman (2015)
Oil Viscosity (cP)	5 to 220	Attanasi and Freeman (2015)
API Gravity (˚)	16 to 22	Werner (1987) and Hornbrook et al. (1991)
	14 to 24	Attanasi and Freeman (2015)

Chapter 5: Relative Permeability

Relative permeability determines the proportion rate of each phase in a multi-phase flow in the porous media. It is the ratio of the effective permeability of a porous medium for a given fluid to the absolute permeability of the same porous medium. Two-phase relative permeabilities are assumed to depend on several parameters such as saturation and pore structure (Maini, 1995). Dandekar (2013) presented good discussion, explanation, and measurement methods for relative permeability. Ediriweera and Halvorsen (2105) investigated the effect of relative permeability and residual oil saturation on oil recovery. They concluded that total oil production and water breakthrough time are strongly affected by relative permeability and residual oil saturation. The impact of relative permeability is much greater than that of residual oil saturation.

Numerical simulation of reservoir processes requires relative permeability curves among other data. These curves are generally estimated from laboratory experiments involving two-phase flow in small samples of reservoir rock. Variation of both temperature and viscosity in thermal reservoir simulation further complicates the concept of relative permeability in heavy oil reservoir modeling. After measuring three series of relative permeability on heavy oil/water at ambient temperature, 122˚F, and 150˚F, and using a commercial black oil simulator, Akin et al. (1999) concluded that a single set of relative permeability curves can represent both the ambient and high temperature parts of the experiment. This suggests that relative permeability is not a function of temperature, at least for the system tested.

Nejad et al. (2011) performed a number of water/oil relative permeability measurements on core material from viscous/heavy oil fields to investigate the effect of oil viscosity on residual saturation and water relative permeability endpoint. They stated that there are two different views in the literature about the effect of oil viscosity on water/oil relative permeability. Some researchers claim that oil viscosity does not have an effect on water/oil relative permeability, while others have shown the dependency of residuals and relative permeability curves on oil viscosity. Based on the results of their experiments and on comparison with other Statoil viscous oil data (oil/water viscosity ratio was in the range of 1 to 6780), they drew several conclusions, among them the following:

- Relative permeability to water at residual oil decreases with increasing oil viscosity and increasing residual oil saturation

Ashrafi (2013) also investigated the temperature dependency of relative permeability data in heavy oil systems. Before conducting core flooding experiments, the researcher carried out some fluid behavior experiments to figure out the properties of bitumen used in the study. Experiments of core flood were conducted on glass bead packs and sand packs saturated with heavy oils with varying viscosities. Displacement experiments with water were performed at different temperatures, and an unsteady-state method of relative permeability measurement was conducted. Ashrafi concluded that the temperature dependency of relative permeabilities can be attributed to the drop in oil to water viscosity ratio by temperature. Also, he emphasized that the variations of relative permeability data with temperature were found to be related more to artifacts like viscous fingering in the experimental procedures, and to fluid viscosity changes than to fundamental flow properties.

Bennion et al. (1993) stated that examination of the data from different researchers indicates some interesting trends. In most of the studies that were conducted on synthetic or cleaned core packs using refined or synthetic oils, relative permeability was found to be generally independent of temperature, and in many cases even the residual oil saturation was found to be independent of temperature. This effect does not appear to be intuitively correct. In fact if this is true, a waterflood at 50°C in a heavy oil system should ultimately yield the same recovery as one at 340°C. But work done on preserved core samples utilizing reservoir fluids consistently indicates that irreducible water saturation increases and residual oil saturation decreases with increases in temperature.

There is very little published data regarding relative permeability measurements at elevated temperatures. Bennion et al. (1993) presented two complete water-bitumen steady state drainage and imbibition tests conducted at a temperature of 200°C at full reservoir pressure and overburden conditions utilizing composite core stacks of actual, preserved reservoir core material. Their findings are summarized in Tables 5-1 through 5-5 and Figures 5-1 and 5-2.

Table 5-1: Tests #1 and 2- core and run parameters (Bennion et al., 1993).

		Test #1	Test #2
Length (cm)		32.4	34.5
Diameter (cm)		3.81	3.81
Effective Flow Area (cm^2)		11.40	11.40
Porosity (%)		38.0	39.1
Bulk Volume (cm^2)		369.36	393.3
Pore Volume (cm^3)		140.36	140.36
Water Viscosity at 200° C (mPa.s)		0.134	0.134
Oil Viscosity at 200° C (mPa.s)		7.8	7.8
Test Temperature (° C)		200	200
Backpressure (kPag)		2000	2000
Overburden Pressure (kPag)		6200	6200
Initial Permeability to Oil	(um^2) x 10^{-3}	1544.6	1491.94
	(mD)	1565.0	1511.60
Air Permeability	(um^2) x 10^{-3}	2500.0	2701.1
	(mD)	2533 0	2736.6

Table 5-2: Test #1- water saturation increasing test results (Bennion et al., 1993).

Saturations		Permeability to Oil		Permeability to Water		Kro	Krw
S_o	S_w	(μm^2) x 10^{-3}	(mD)	(μm^2) x 10^{-3}	(mD)		
0.942	0.058	1544.6	1565.0	0.00	0.00	0.8000*	0.0000
0.911	0.089	1191.9	1207.6	1.71	1.73	0.6173	0.0009
0.819	0.181	330.7	335.1	3.65	3.70	0.1713	0.0019
0.759	0.241	221.9	224.9	5.52	5.59	0.1150	0.0029
0.695	0.305	120.3	121.9	7.98	8.08	0.0623	0.0041
0.311	0.689	0.00	0.00	120.62	122.21	0.0000	0.0625

* K_{abs} estimated to be 1930.80 x 10^{-3} (μm^2) [1956.3 mD] using the assumption that $K_o = 0.80\ K_{abs}$

Table 5-3: Test #1- water saturation decreasing test results (Bennion et al., 1993).

Saturations		Permeability to Oil		Permeability to Water		Kro	Krw
S_o	S_w	(μm^2) x 10^{-3}	(mD)	(μm^2) x 10^{-3}	(mD)		
0.311	0.689	0.00	0.00	120.62	122.21	0.0000	0.0625
0.591	0.409	232.3	235.4	15.38	15.58	0.1203	0.0079
0.667	0.333	340.8	345.3	9.87	10.00	0.1765	0.0050
0.722	0.278	477.1	483.4	5.26	5.33	0.2471	0.0027
0.794	0.206	755.8	765.8	3.31	3.35	0.3915	0.0017
0.861	0.139	1299.2	1316.3	0.00	0.00	0.6729	0.0000

Table 5-4: Test #2- water saturation increasing test results (Bennion et al., 1993).

Saturations		Permeability to Oil		Permeability to Water		Kro	Krw
S_o	S_w	$(\mu m)^2 \times 10^{-3}$	(mD)	$(\mu m)^2 \times 10^{-3}$	(mD)		
0.970	0.030	1491.94	1511.60	0.00	0.00	0.8000*	0.0000
0.904	0.096	887.71	899.40	3.65	3.70	0.476	0.00196
0.818	0.182	248.03	251.30	8.76	8.88	0.133	0.0047
0.705	0.295	91.37	92.58	15.29	15.49	0.049	0.0082
0.628	0.372	31.88	32.31	29.27	29.66	0.0171	0.0157
0.346	0.654	0.00	0.00	171.01	173.26	0.0000	0.0917

* K_{abs} estimated to be 1864.93×10^{-3} $(\mu m)^2$ [1889.5 mD] using the assumption that $k_o = 0.80\ k_{abs}$

Table 5-5: Test #2- water saturation decreasing test results (Bennion et al., 1993).

Saturations		Permeability to Oil		Permeability to Water		Kro	Krw
S_o	S_w	$(\mu m)^2 \times 10^{-3}$	(mD)	$(\mu m)^2 \times 10^{-3}$	(mD)		
0.346	0.654	0.00	0.00	171.01	173.26	0.0000	0.0917
0.569	0.431	293.11	296.18	38.60	39.11	0.125	0.0207
0.731	0.269	589.32	597.08	13.79	13.98	0.316	0.0074
0.785	0.215	876.52	888.06	9.14	9.26	0.470	0.0049
0.815	0.185	1297.99	1315.09	5.40	5.47	0.696	0.0029
0.894	0.103	1445.32	1464.36	0.00	0.00	0.775	0.0000

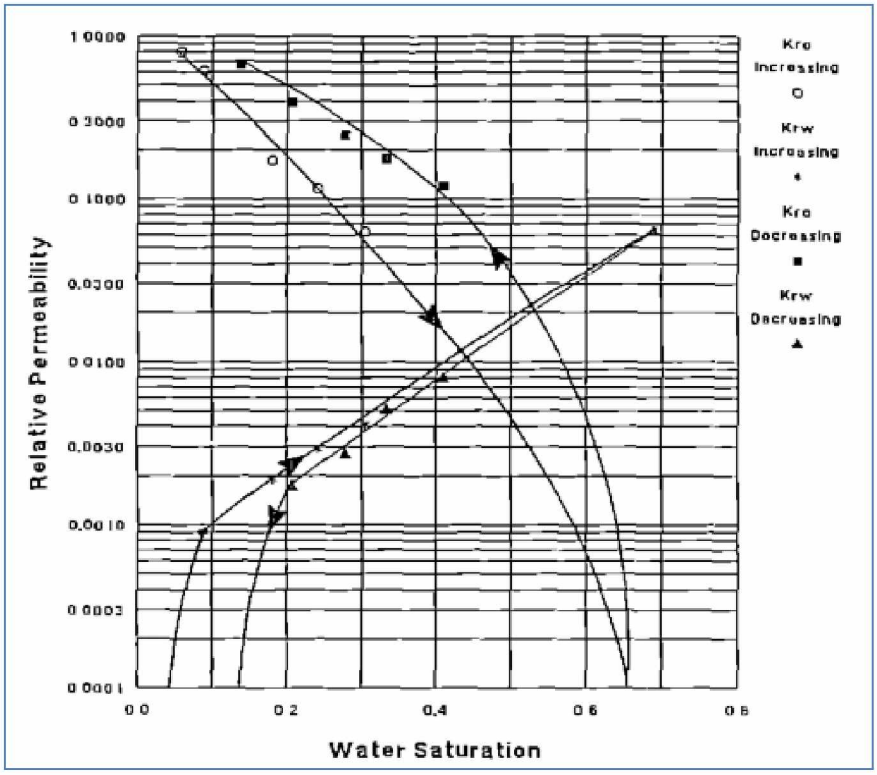

Figure 5-1: Test #1 comparison of Sw increasing and Sw decreasing relative (Bennion et al., 1993).

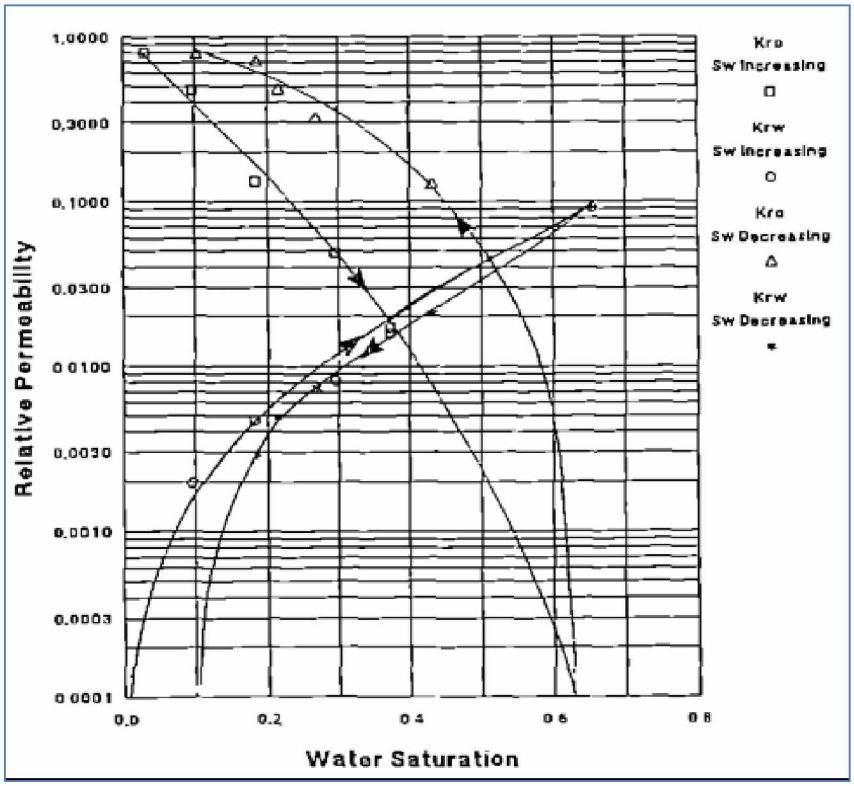

Figure 5-2: Test #2 comparison of Sw increasing and Sw decreasing relative (Bennion et al., 1993).

Bennion et al. (1993) regressed the results by using the following equation:

$$k_{ri} = k_{maxi}(S_{ei})^{E_i}_{i=0,w} \qquad \text{(5-1)}$$

Where: i = o, w (oil or water phases),

K_{ri} = calculated (regressed) oil or water relative permeability,

Ei = power law constant (regressed),

$$S_{ew} = \frac{(S_w - S_{w_{min}})}{(S_{w_{max}} - S_{w_{min}})} \qquad \text{(5-2)}$$

$$S_{eo} = 1 - S_{ew} \qquad \text{(5-3)}$$

The power law and coefficient constants are provided by the authors as follows (rewritten) in Table 5-6 and Figures 5-3 and 5-4.

Table 5-6: The regressed constant of Equation (5-1).

Test No.	Phase	Imbibition (Sw Increasing)		Drainage (Sw Decreasing)	
		k_{max}	E_i	k_{max}	E_i
1	Water	0.0625	2.81	0.0625	2.89
	Oil	0.800	5.263	0.673	3.511
2	Water	0.0917	2.53	0.0917	2.72
	Oil	0.800	4.839	0.775	2.097

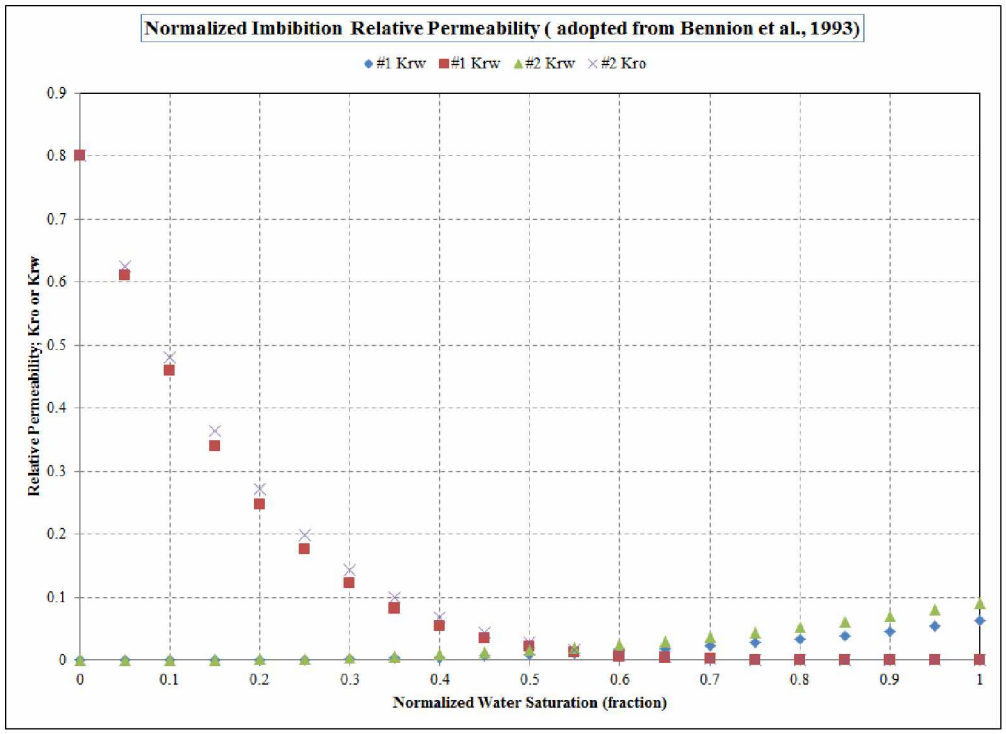

Figure 5-3: Normalized Imbibition Relative Permeability (adopted from Bennion et al., 1993).

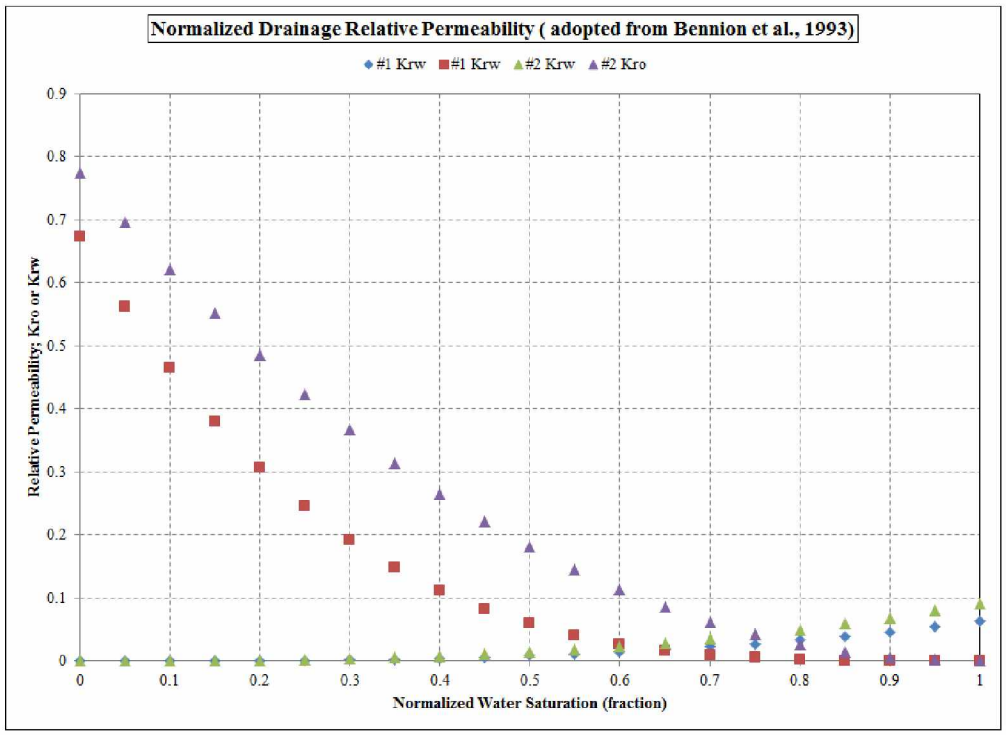

Figure 5-4: Normalized drainage relative permeability (adopted from Bennion et al., 1993).

Chapter 6: Simulation

As mentioned in the previous sections, Computer Modeling Group (CMG) hydrocarbon reservoir simulation packages were used for this project's simulation. The main modules employed were:

- Builder 2015.10,
- WINPROP 2015.10,
- STARS 2015.10,
- Results Graph 2015.10,
- Results 3D 2015.10.

To reduce the CPU time and get efficient results, the simulation started with a one-dimensional model, then was extended to three-dimensional models. In the one-dimensional model, vertical wells were considered for both injection and production; however, in light of the results from this model, horizontal wells were considered in the three-dimensional models.

Three main processes were studied by three-dimensional model. Steam Assisted Gravity Drainage (SAGD) is a continuous steam flooding that uses two types of wells: (1) an injector well and (2) a producer well, which is located in the layer below the injector's layer. Cyclic Steam Assisted Gravity Drainage (CSAGD) is a modified SAGD process. With this method, the injector well is intermittently (cyclically) opened and shut in. The third process is called Cyclic Steam Stimulation (CSS) or Cyclic Steam Injection (CSI). This process uses one well as both injector and producer. Steam is injected into the reservoir well and shut in for a predetermined time (soaking period). Then the well is opened to produce the reservoir fluid.

6.1. One-Dimensional Model

To start the simulation, a one-dimensional (1-D) model was constructed and the effect of grid dimensions on oil recovery was investigated. Table 6-1 shows the basic characteristics of the model. Figure 6-1 depicts the sketch of one dimensional model. Figure 6-2 illustrates crude oil viscosity versus temperature used in this model. Figure 6-3 depicts the results. In this figure, the effect of grid length in I-direction on the oil recovery is presented. The simulation period considered is 5 years. As is obvious from Figure 6-3, in the range of parameters used in this one-dimensional model, change in length of grid block in the fluid flow from 10 to 50 ft has negligible effect on absolute recovery.

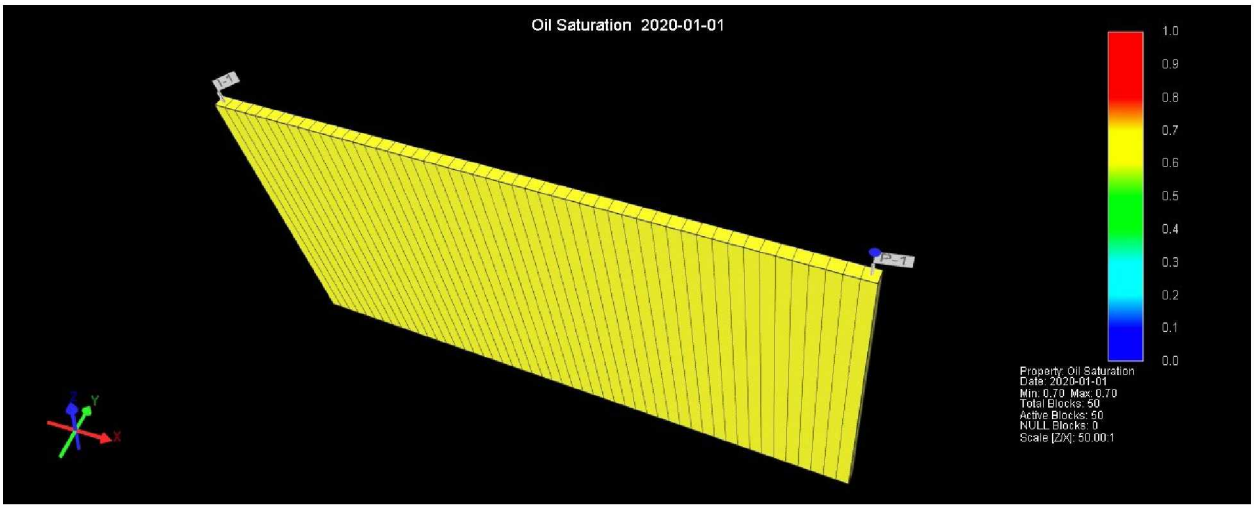

Figure 6-1: Sketch of 1-D model

Water-oil relative permeabilities used in this model are shown in Figure 6-4. These curves are based on the general common Corey's exponent equations. To investigate the effect of relative permeability, the constant parameters and exponents obtained by Bennion et al. (1993) for the imbibition process were used. With them, the relative permeabilities were generated (see Figure 6-5). The effect of this change on the oil recovery is shown in Figure 6-6.

The effect of down-hole distance between vertical injector well and vertical producer well was also investigated by fixing the grid dimensions in x, y, z direction and changing the length of the model by increasing or decreasing the number of grids in x-direction. The other properties of this model were kept the same as those of 1-D model described in the above paragraphs. The results for a period of 5-year simulation are shown in Figure 6-7. As can be seen, steam injection is more effective when the distance between injector and producer is less than 500 ft.

It is worthwhile to mention that the PVT properties of the model are generated by using the built-in black oil PVT models in the STARS simulator.

Table 6-1: General characteristics of one-dimensional model.

Number of Grid	Grid Dimension (ft)			top (ft)	Datum Pres. (psi)	Porosity (fraction)	Permeability (md)			Steam quality	Steam temp. (°F)
	I	J	K				I	J	K		
50*1*1	5	10	10	2000	1000	0.3	500	500	10	0.8	500

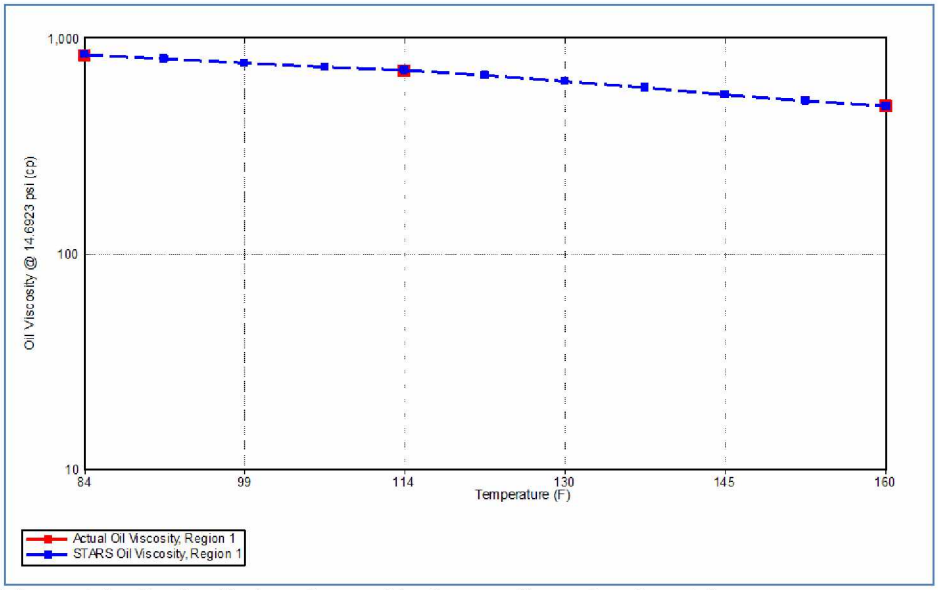

Figure 6-2: Crude oil viscosity used in the one-dimensional model.

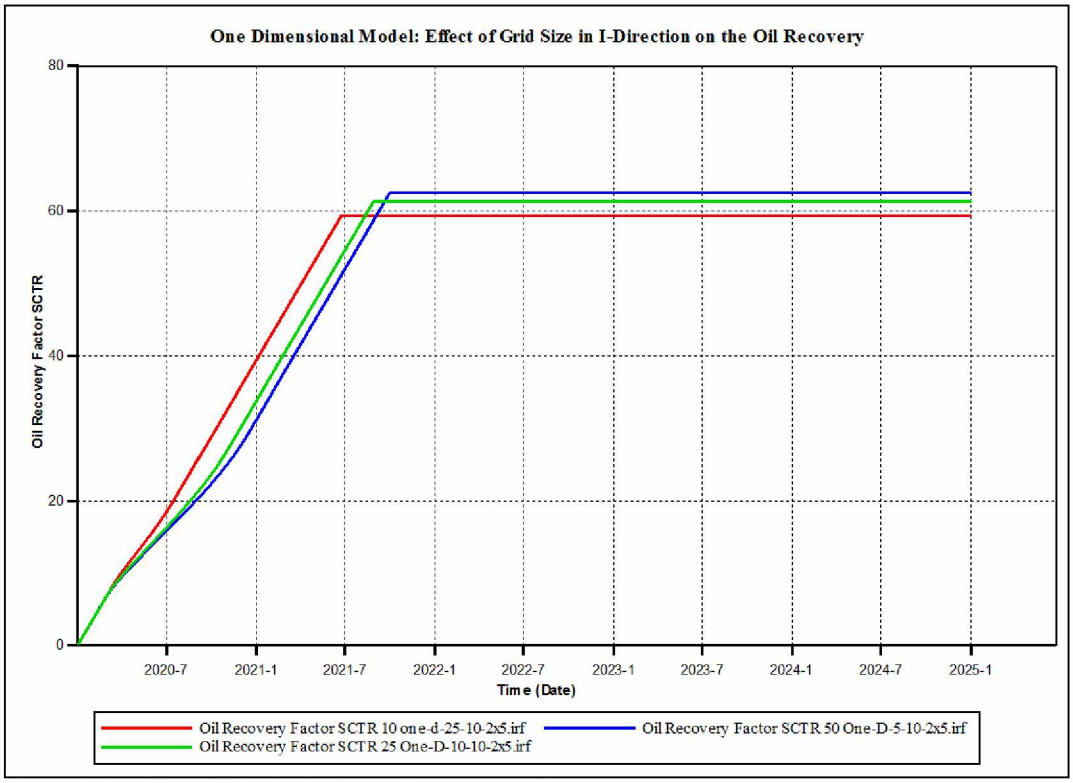

Figure 6-3: Effect of block size in x-direction on oil recovery.

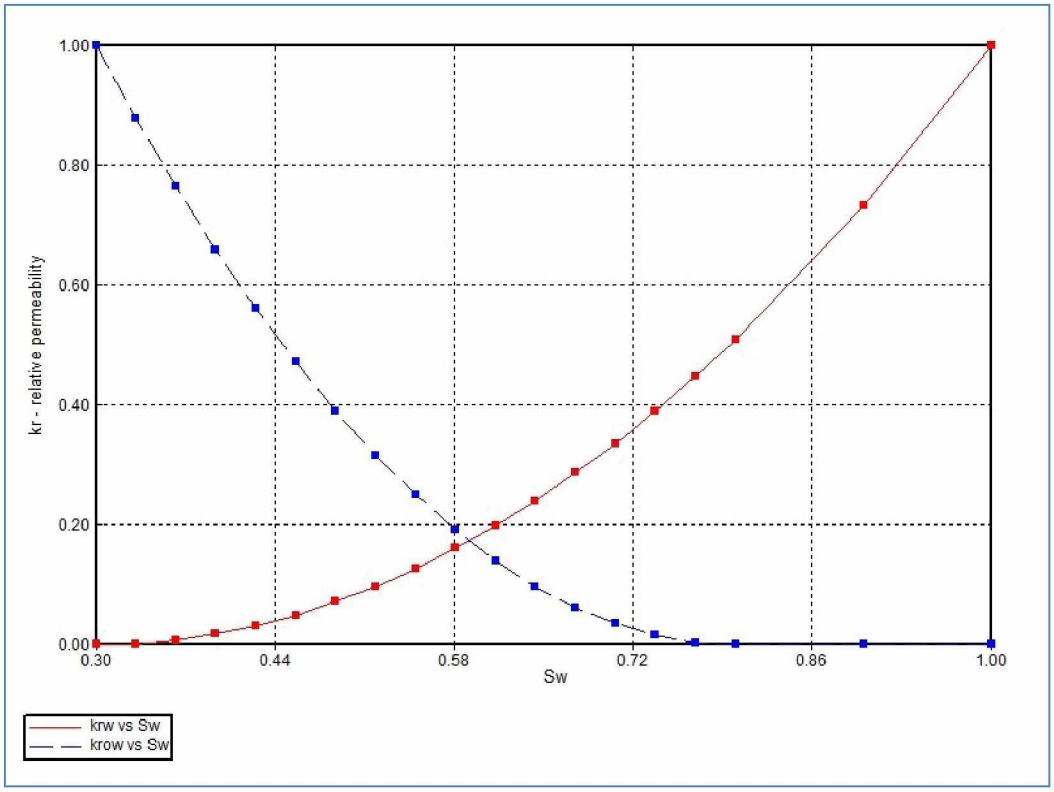

Figure 6-4: Water-oil relative permeabilities used in one-dimensional model.

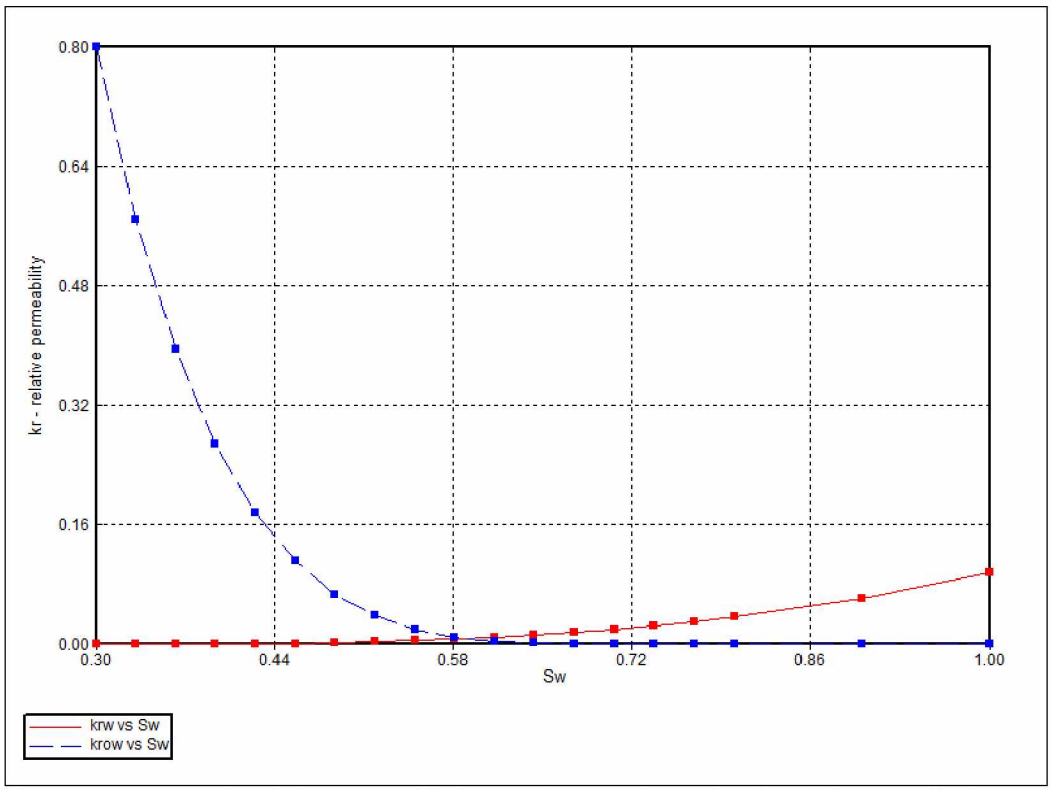

Figure 6-5: Water-oil relative permeabilities used in one-dimensional model by employing Bennion et al. (1993) parameters.

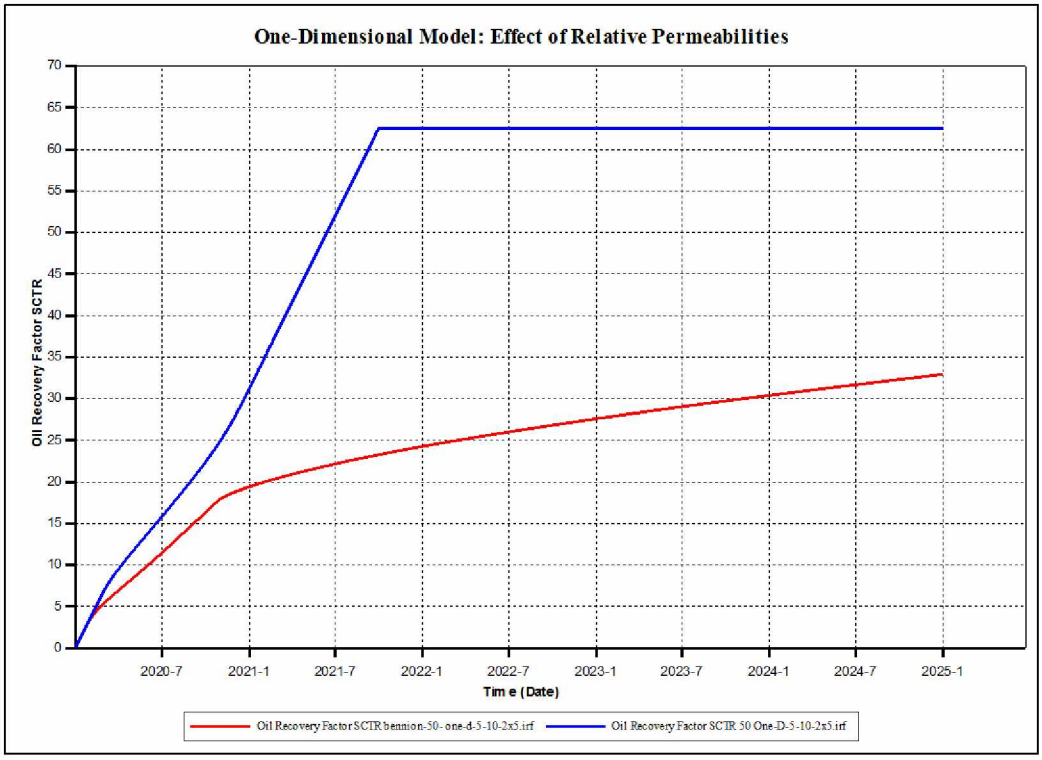

Figure 6-6: Effect of changing relative permeabilities on oil recovery, one-dimensional model.

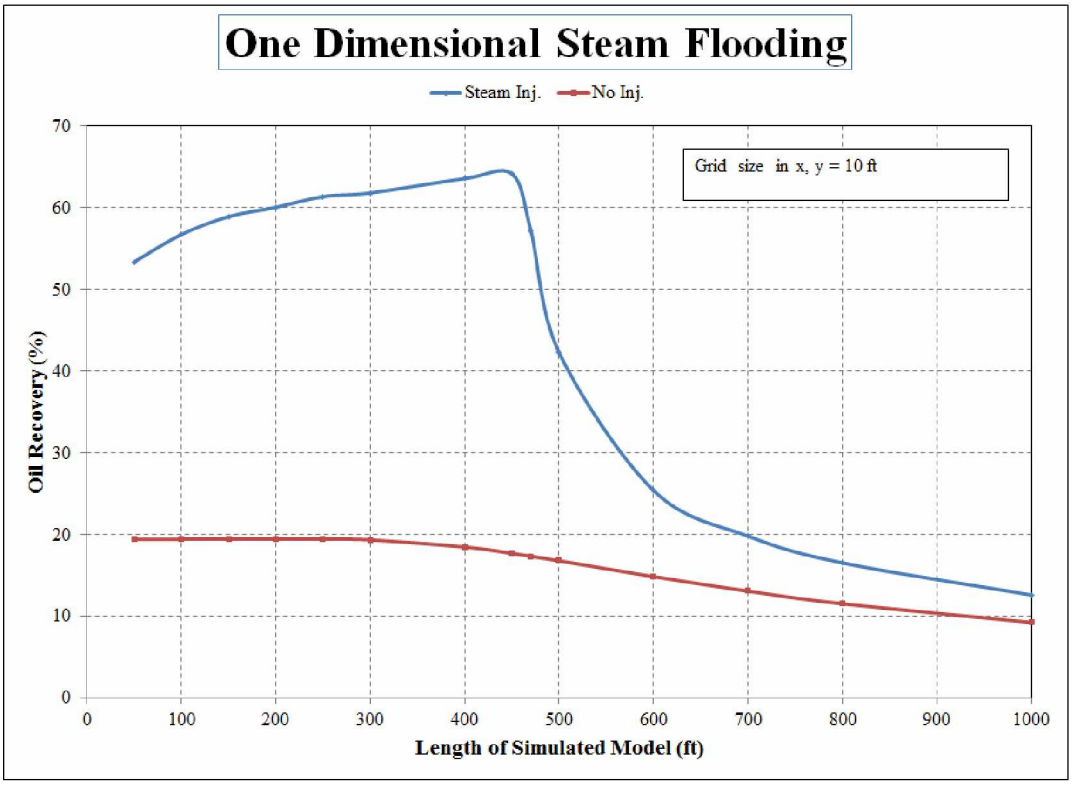

Figure 6-7: Effect of distance between injector and producer vertical wells, one-dimensional model, steam injection and natural depletion (No Inj.).

6.2. Three-Dimensional Model

Based on the available data, partly presented in the previous sections, the following points were considered for the base case of the 3-D model.

* Reservoir Temperature = 55˚F,
* Dead oil viscosity = 300,000 cP,
* Live oil viscosity = 30,000, cP,
* Dead oil density = 11 ˚API,
* GOR = 100 SCF/STB,
* Horizontal wells for injector and producer based on the Steam Stimulation Gravity Drainage (SAGD) model.

A schematic of layers in conjunction with a few rock properties was considered (see Table 6-2). The schematic of the generated model by Builder is shown in Figure 6-8. For the base model, the injector and producer were assumed to be drilled in the middle of layers 9 and 13 (Ugnu Lower B), respectively. Lateral length of both wells was about 800 ft in a reservoir with both length and width equal to 1250 ft.

Table 6-2: Simulator schematic layers.

Model's layer Number	Formation	Schematic	Top formation (ft)	grid thickness (ft)	porosity (fraction)	Permeability (md)			Water Sat. (%)
						I	J	K	
1	Sagvanirtktok-Sandstone		1800	200	0.1	10	10	1	100
2				5	0.001	0.01	0.01	0.001	100
3				190	0.1	10	10	1	100
4	Shale			5	0.001	0.01	0.01	0.001	100
5	Ugnu C			45	0.3	500	500	50	0.3
6	Shale			5	0.001	0.01	0.01	0.001	0.3
7	Ugnu Upper Zone B			45	0.3	500	500	50	0.3
8	Shale			5	0.001	0.01	0.01	0.001	0.3
9	Ugnu Lower Zone B			10	0.3	500	500	50	0.3
10				10					
11				10					
12				10					
13				10					

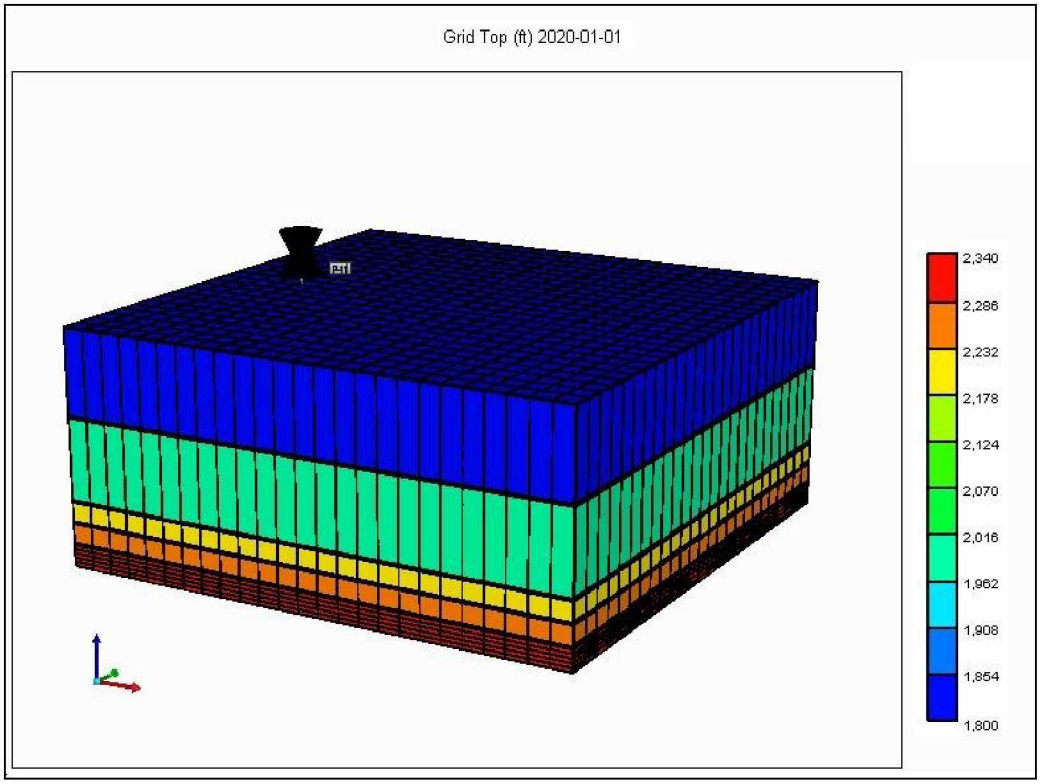

Figure 6-8: Schematic of 3-D model.

As oil viscosity has a major role in the performance of a heavy crude oil, two models were constructed: reservoir oil with medium viscosity and reservoir oil with high viscosity. The live oil viscosities of these two models are shown in Figures 6-9 and 6-10. The live oil viscosity of medium viscosity crude is about 1,000 cP and that of the high viscosity crude is 30,000 cP at reservoir pressure. The reason of why the viscosity-curve flattens in Figures 6-9 and 6-10 can be justified by considering the temperature of measured viscosity (55 F), low GOR and high gravity of crude which cause the viscosity change above the bubble point pressure to be low.

In Figure 6-11, medium-viscosity and high-viscosity oil reservoirs' natural depletion performances are compared. Figure 6-12 depicts the effect of steam injection on the high-viscosity oil reservoir production. Injection of steam has a great positive effect on the high-viscosity oil reservoir.

In the following sections, the results of studies of the effect of different parameters on oil recovery and Steam Oil Ratio (SOR) are presented.

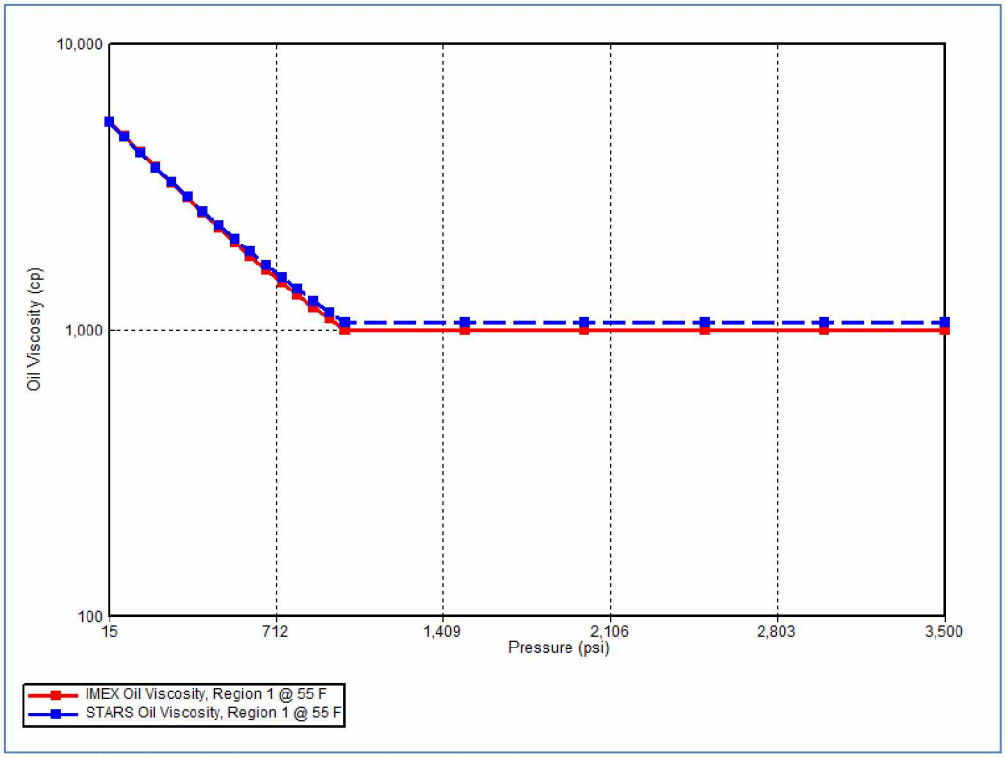

Figure 6-9: Live oil viscosity of medium-viscosity oil.

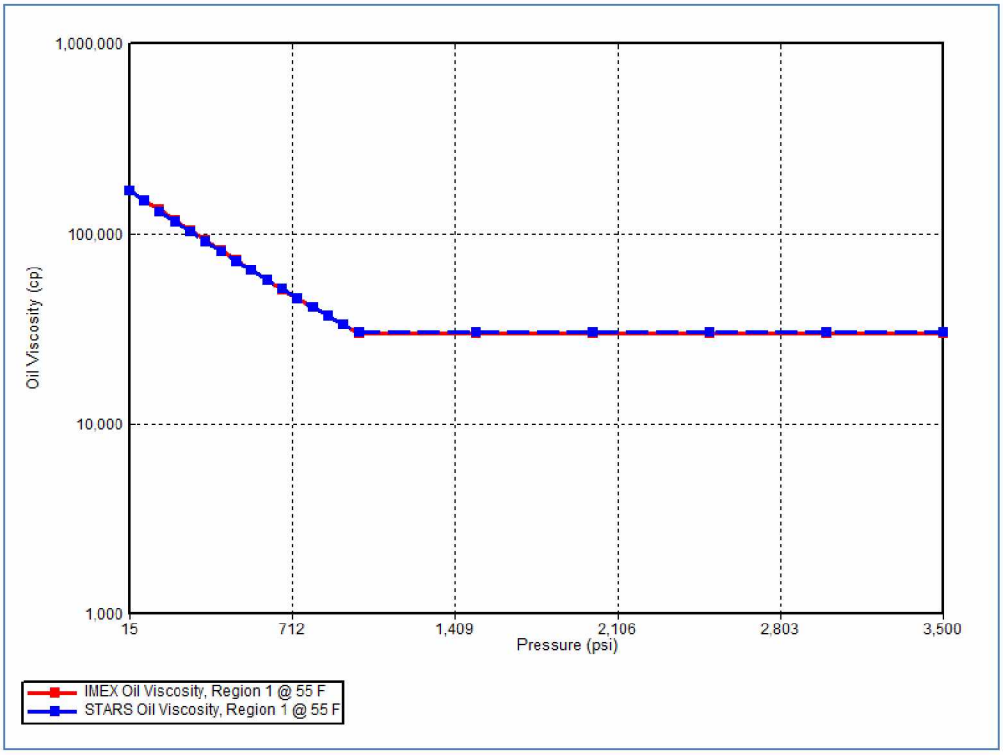

Figure 6-10: Live oil viscosity of high-viscosity oil.

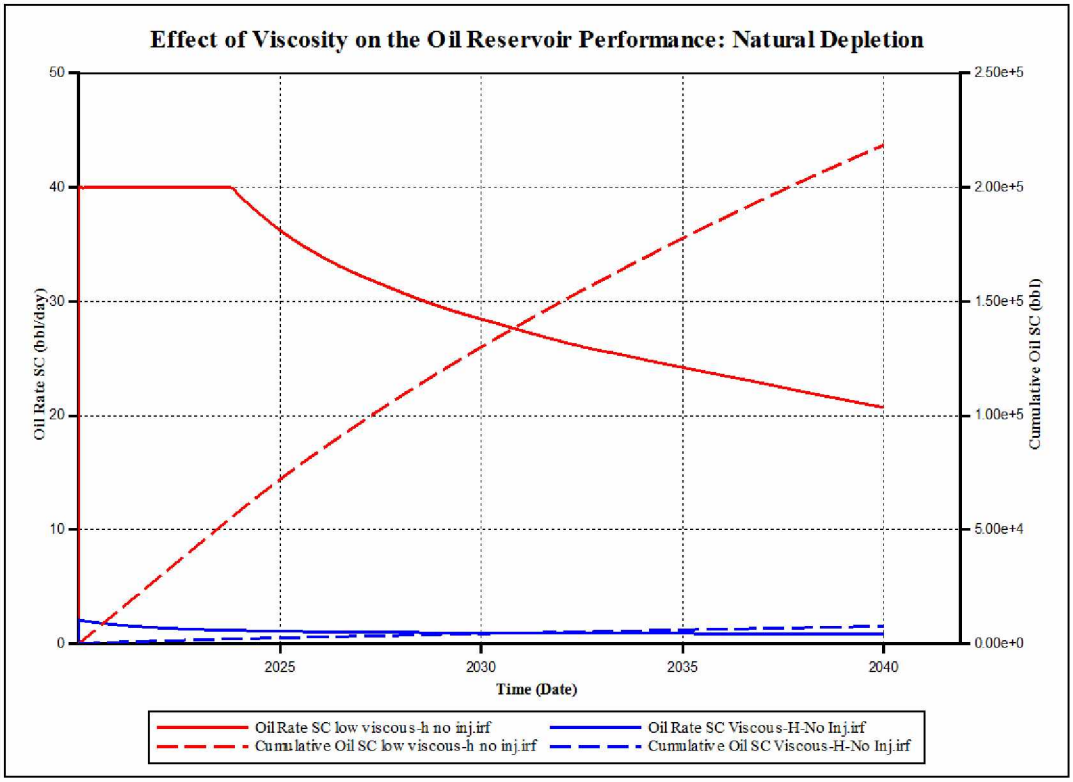

Figure 6-11: Comparison of medium-viscosity and high-viscosity oil reservoir performance in the case of natural depletion.

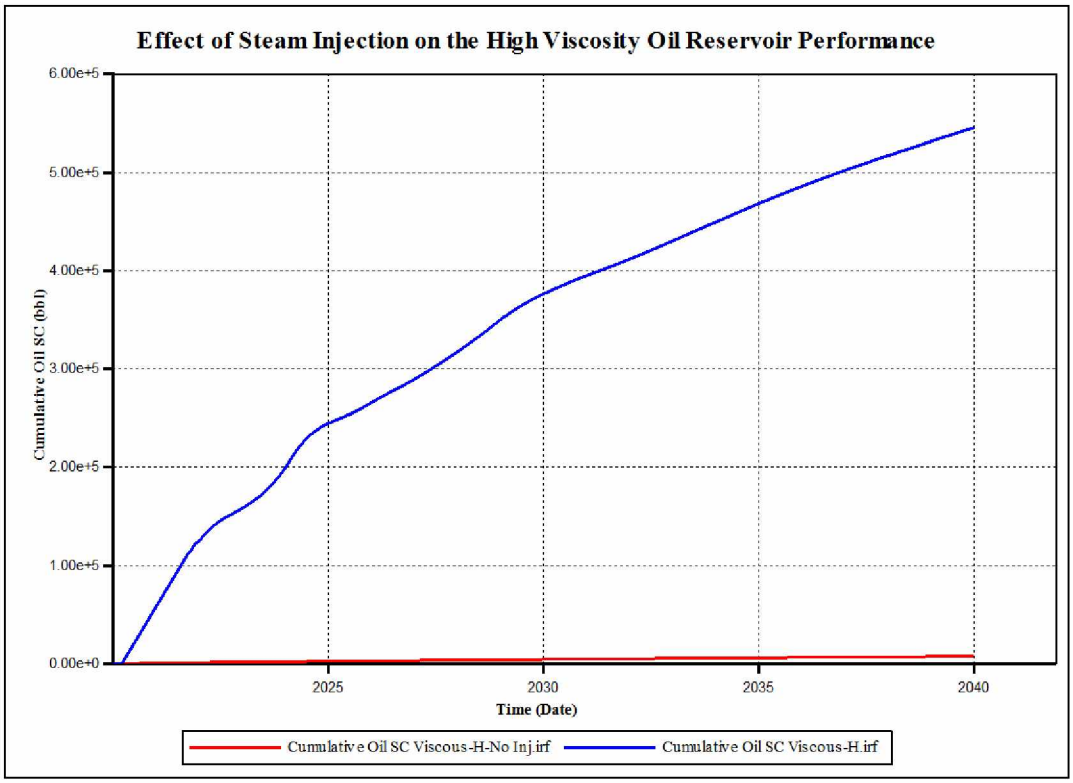

Figure 6-12 Effect of steam injection on high-viscosity oil reservoir production.

6.2.1. Steam-Nitrogen Injection

As mentioned, based on the available data, the inventors claimed that they invented a system that can be installed in the down-hole wells. By using a type of monopropellant chemical and a special catalyst, the system can produce steam and nitrogen. No other data were received. No information is available about the amount of steam and/or nitrogen or the system's effluent temperature. In the literature survey chapter, Section 2.2.2., exothermic reactions of a few monopropellants are presented and discussed. Among them, it seems that the following equation shows the final result of a series of reactions (Zumdahl and Zumdahl, 2007).

$$N_2H_4(l) + O_2(g) \longrightarrow N_2(g) + 2H_2O(g) \qquad \Delta H^\circ = -622 \text{ kJ}$$

Therefore, it is assumed that the proposed system can produce steam and nitrogen gas at different steam-to-nitrogen ratio and different effluent temperature.

To simulate reservoir, the 3-D model discussed in the previous section with high viscosity oil properties and average thermal rock properties is employed. By conducting several runs, the following constraints were selected for injector and producer. The criterion for selection of these constraints was producer well rate. The selected constraints should cause a constant producer well rate at least for a few months.

- Injector well:

Maximum Bottom Hole Pressure (BHP) = 2000 psi,

Maximum surface total phase rate = 2000 bbl/day.

- Producer well:

Minimum Bottom Hole Pressure (BHP) = 28 psi,

Maximum surface oil rate = 200 bbl/day.

The model is run for several different surface-volume percent of steam and nitrogen (Table 6-3). In Figure 6-13, the oil recovery for these scenarios is illustrated. Obviously, with increase of the volume ratio of nitrogen, the oil recovery decreases.

Table 6-3: Scenarios' composition of injected fluid in case of nitrogen injection.

Run name	Surface Volume (%)		Water Volume	Nitrogen Volume
	Water	Nitrogen	(bbl/day)	(ft3/day)
100S-0N2	100	0	2000	0
95S-5N2	95	5	1900	561.5
90S-10N2	90	10	1800	1123
80S-20N2	80	20	1600	2246
70S-30N2	70	30	1400	3369
60S-40N2	60	40	1200	4492
50S-50N2	50	50	1000	5615

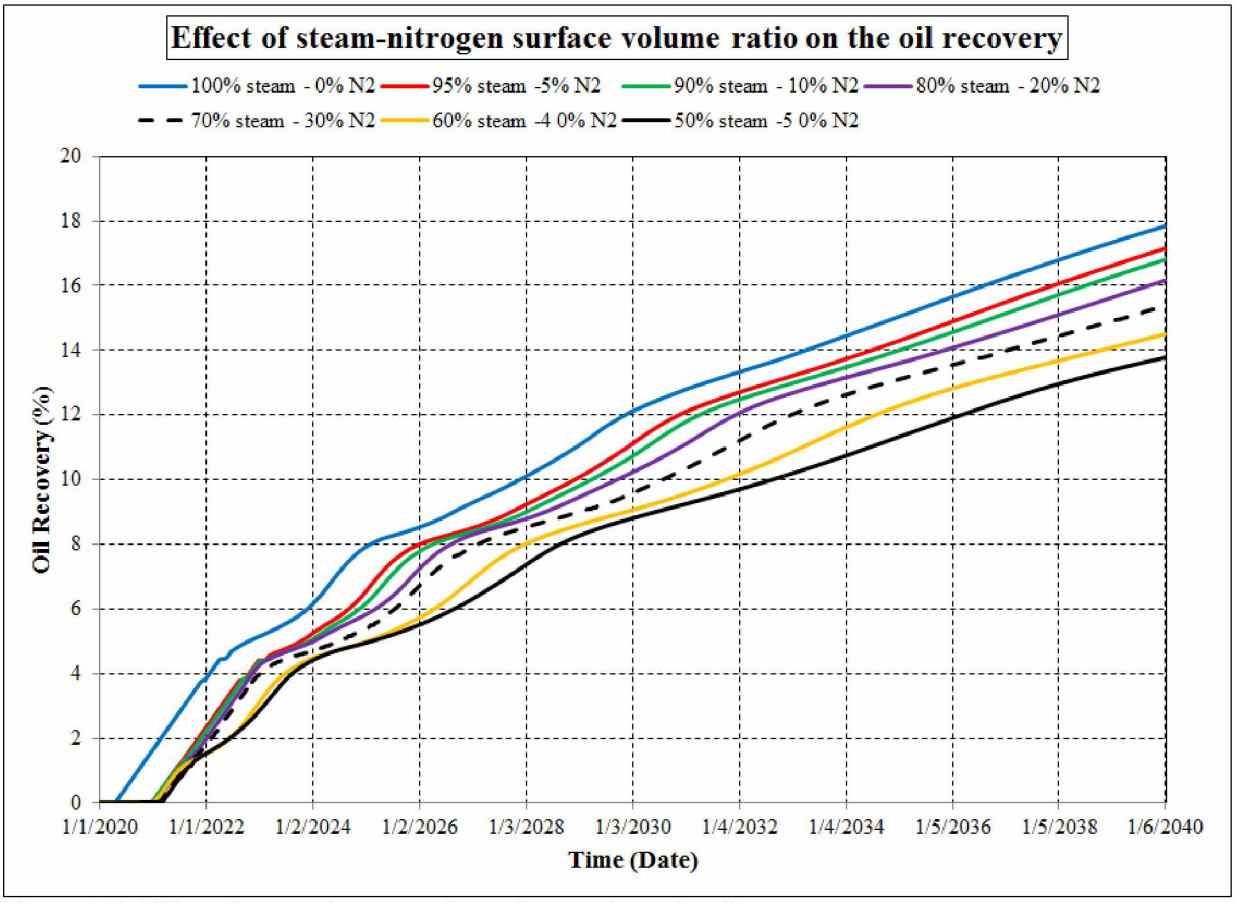

Figure 6-13: Effect of steam-nitrogen surface volume ratio on the oil recovery.

To investigate the reasons for this reduction in oil recovery, a scenario with the same conditions as the '50S-50N2' (1000 bbl/day water and 5615 ft^3/day) case is defined and run, but with different injection fluid and injection rate. In this scenario, the maximum surface water rate considered to be 1000 bbl/day but no nitrogen injection. The oil recovery is compared with

those of scenarios '50S-50N2' and '100S-0N2' (2000 bbl/day water with no nitrogen); see Figure 6-14.

Results show that addition of nitrogen to injection fluid not only has no positive effect on the oil recovery (at the conditions of constructed models), it also reduces the oil recovery. The oil recovery of the case of steam injection just 1000 bbl/day equivalent of water is less than the case when the injection rate of steam is 2000 bbl/day of equivalent water and it is reasonable; however, addition of nitrogen in the case of injection 1000 bbl/day (water equivalent) steam and 5615 ft^3/day nitrogen decreases the oil recovery which shows the negative effect of nitrogen on the oil recovery.

In order to evaluate the effect of nitrogen on heat transfer in the reservoir, especially in the vertical direction, temperature at the end of the simulation period is considered. Temperatures of all 13 vertical layers at the middle of lateral reservoir length were recorded for the above-mentioned three scenarios. For layer numbers refer to Table 6-2. Figures 6-15 and 6-16 show these temperature variations versus layer number and depth. Depths are the middle of the corresponding layer. The results show that the addition of nitrogen gas into the injected steam stream has negligible effect on the vertical temperature profile in the reservoir; however, this additional nitrogen gas reduce the oil recovery of the steam injection process, at the same other conditions. Note that vertical temperature profile depends on the rock thermal conductivity of reservoir rock and overburden layers and thickness of these layers. In this case, addition of nitrogen gas to the injected steam stream has little effect on the thermal conductivity of reservoir rock and no effect on that of over burden layers. For this reason, the vertical temperature profile does not significantly change.

It is worthwhile to mention that effect of addition of nitrogen is studied by a model with areal dimension of 1250 ft × 1250 ft (see Figure 6-8)

Based on the results, the simulation was continued just with steam injection.

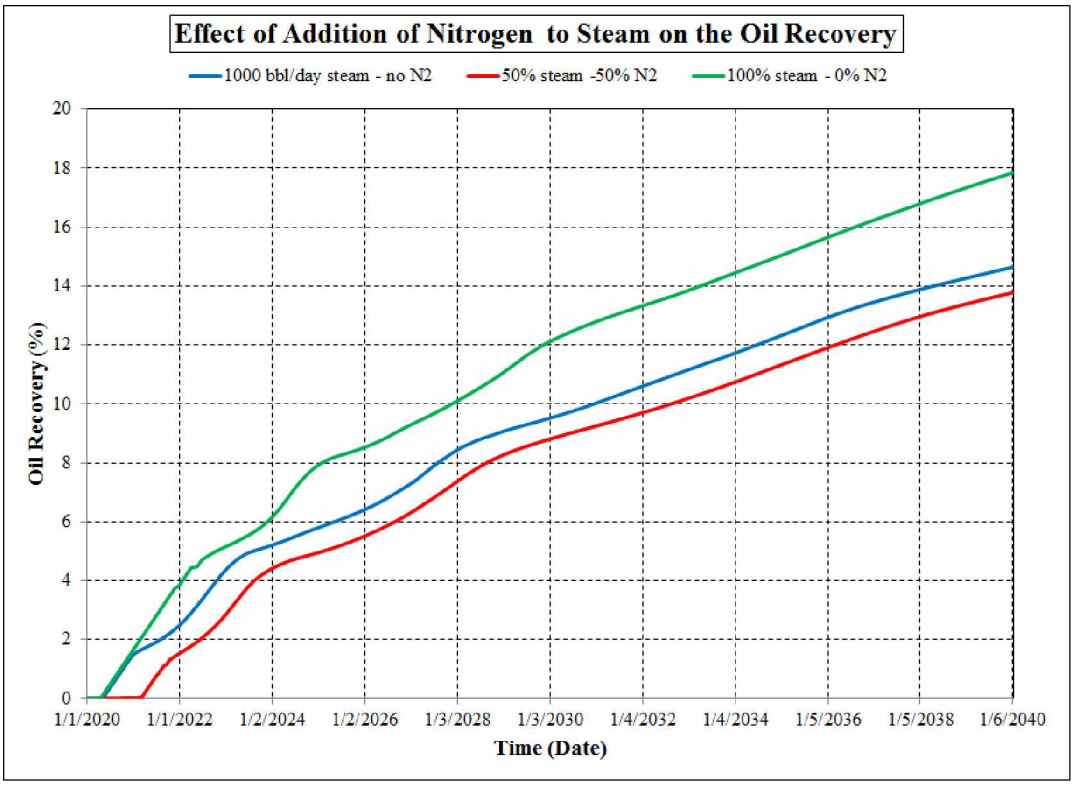

Figure 6-14: Effect of nitrogen injection on oil recovery.

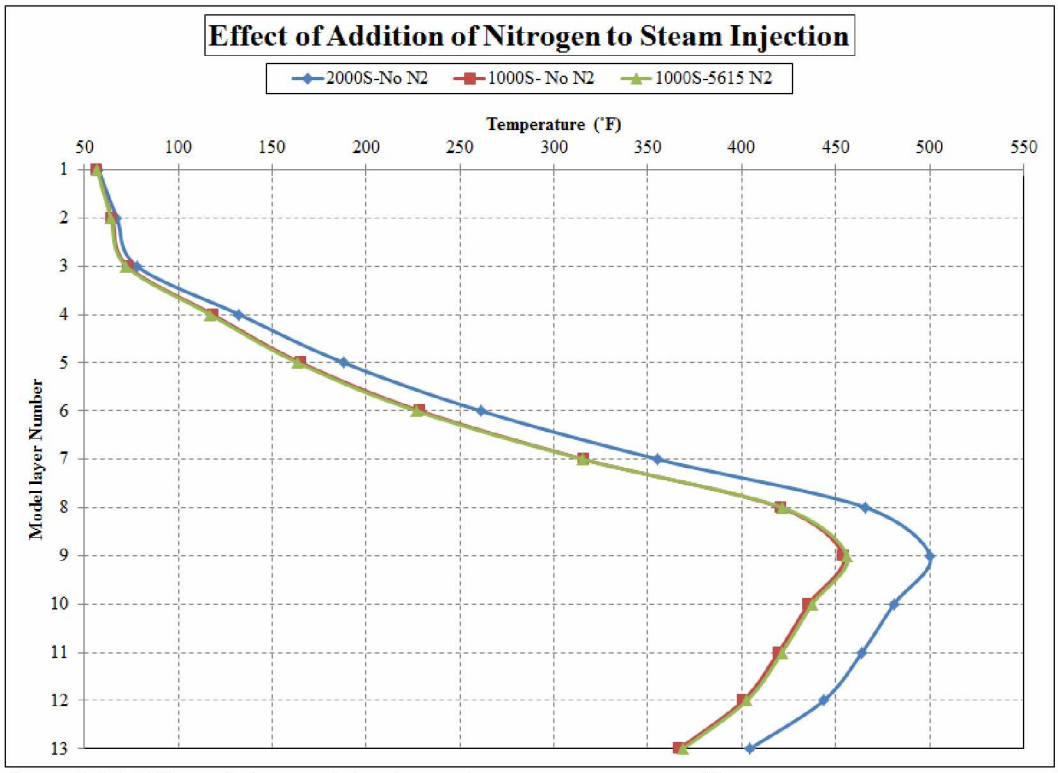

Figure 6-15: Effect of nitrogen injection on layer temperature profile.

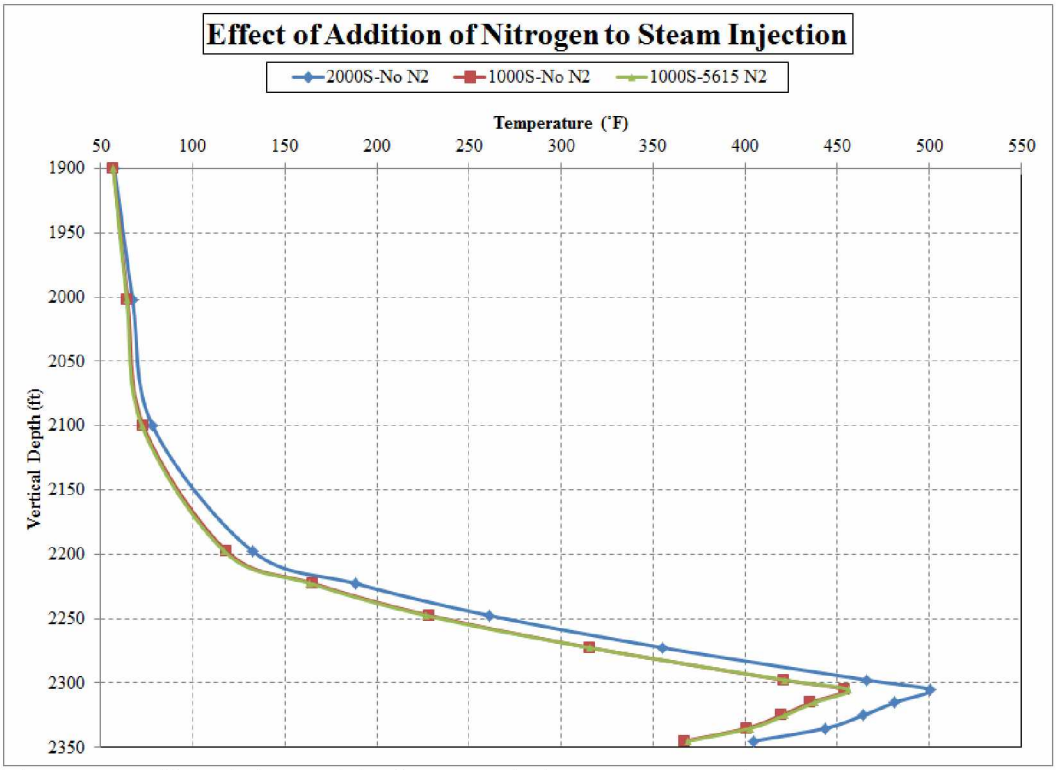

Figure 6-16: Effect of nitrogen injection on vertical temperature profile.

6.2.2. Reservoir Width Selection

Areal temperature distributions in the injector and producer layers in the model described in Section 6-2 show that one injection and one producer horizontal wells cannot cover the entire reservoir model (see Figures 6-17 and 6-18 for model of 2000 bbl/day water equivalent steam injection, no nitrogen injection). So, a decision was made to reduce the width (y-axis or J-grid) of the reservoir model. The horizontal length of each well was set as before: 800 ft in a reservoir with lateral length of 1250 ft. The wells drilled in the same vertical layer as the previous model: layers 9 and 13 for injectors and producers, respectively. The number of considered-J-grids were odd numbers (3, 5, 7, 9, 11, 13 and 25), and the wells were drilled in the middle of the reservoir width (J-grids 2, 3, 4, 6, 7, and 13), for the different scenarios. All other properties of the models were the same. Figure 6-19 depicts oil recovery versus time for all scenarios. Figure 6-20 is another way to present the effect of reservoir width on oil recovery for a 20-year simulation period. In addition to oil recovery, vertical temperature profile is important in this project; and at the end of the simulation period, the temperature profiles for three cases (reservoir width of 150

ft, 250 ft, and 1250 ft) at the middle of the reservoir length were extracted. Figure 6-21 illustrates the STARS' schematic of reservoir models with width of 150, 250 and 1250 ft. It means that the temperatures extracted at length of about 625 ft for different layer (depth). Figure 6-22 depicts the vertical temperature profile for these three cases that led to selection of the model with 150 ft width for further investigation.

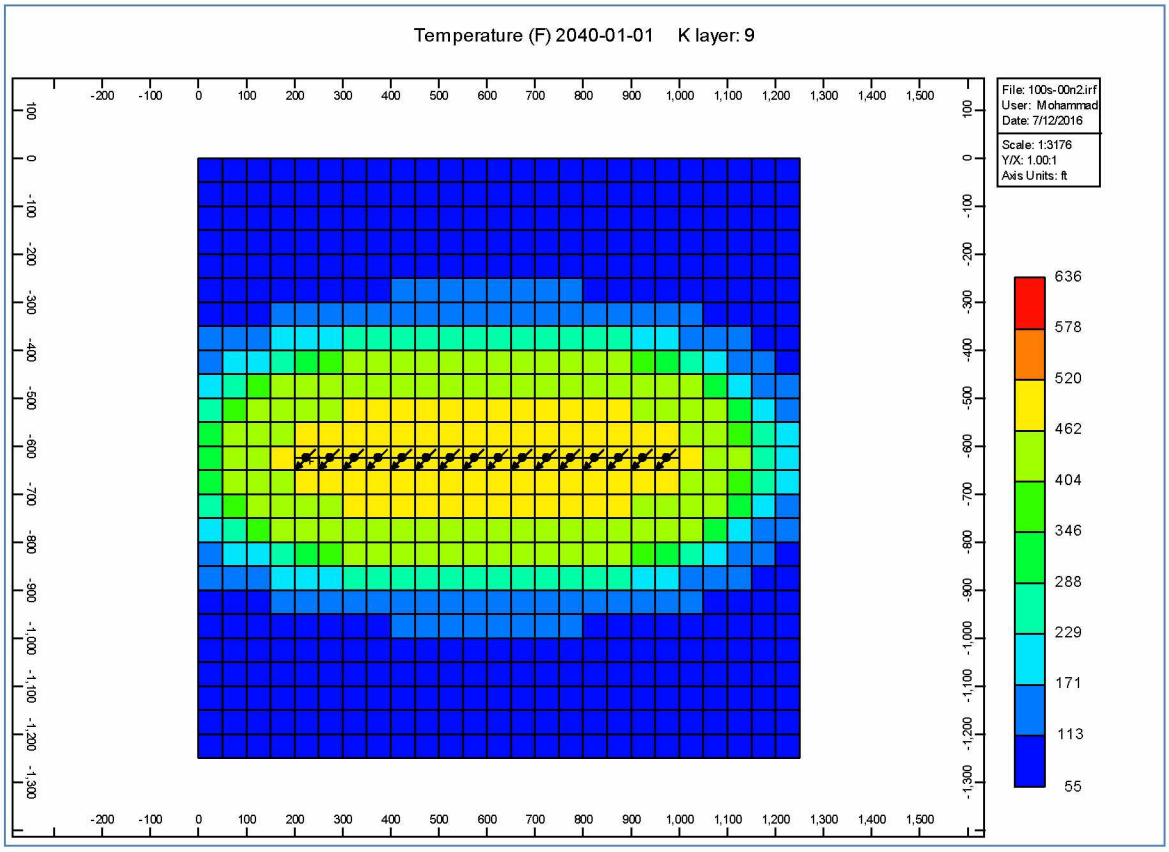

Figure 6-17: Temperature (˚F) distribution of injector-well layer at the end of simulation period.

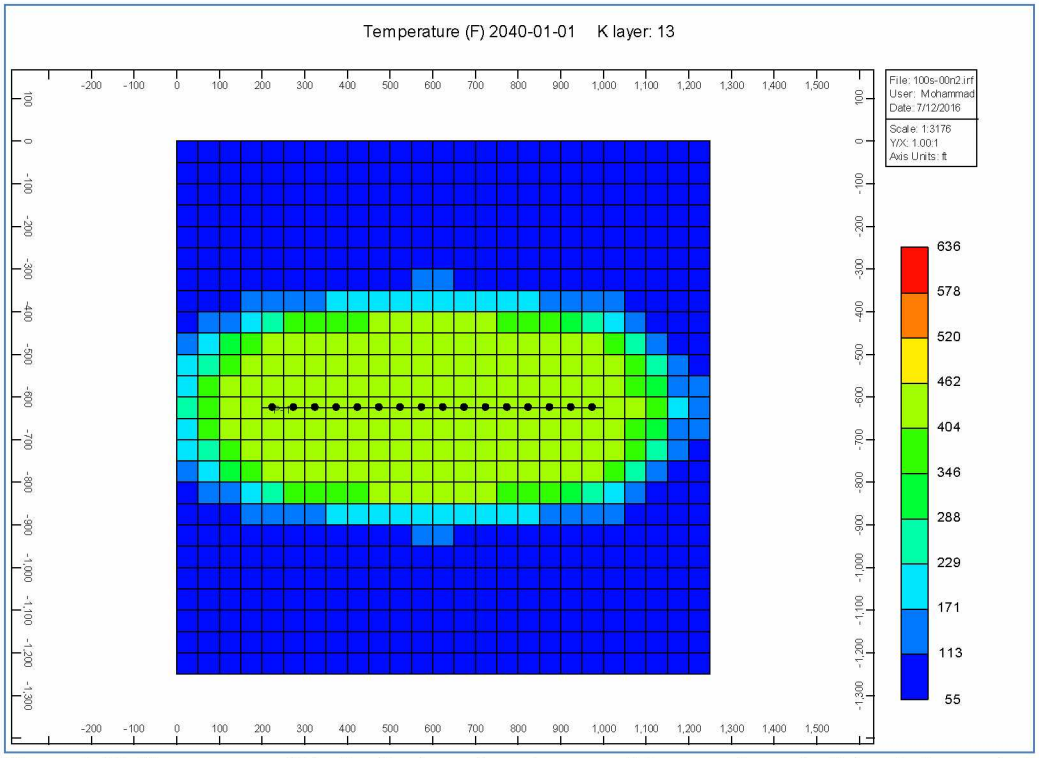

Figure 6-18: Temperature (˚F) distribution of producer-well layer at the end of simulation period.

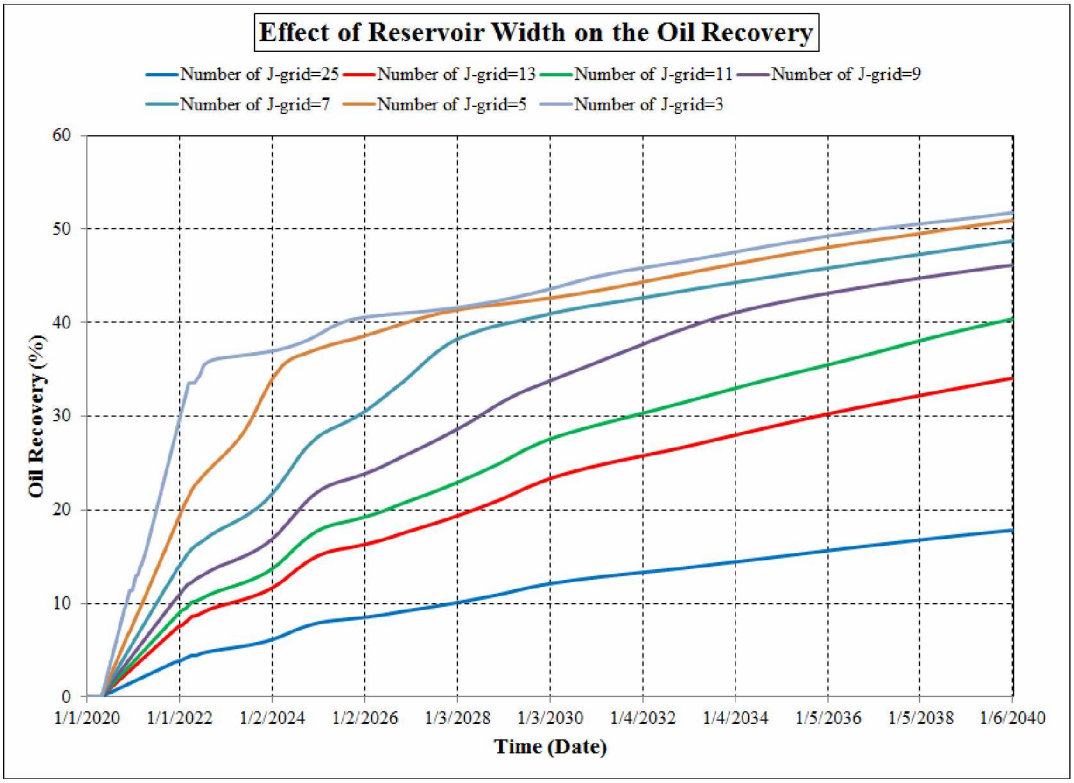

Figure 6-19: Effect of reservoir width on the oil recovery.

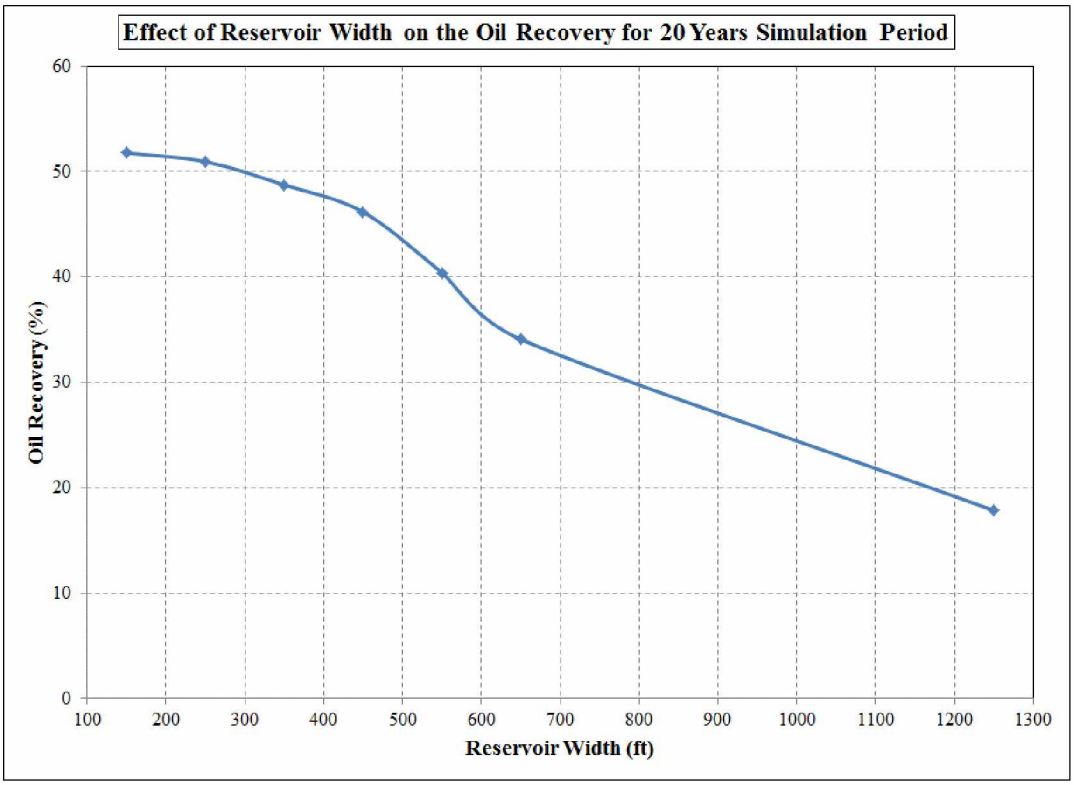

Figure 6-20: Effect of reservoir width on the oil recovery for 20-year simulation period.

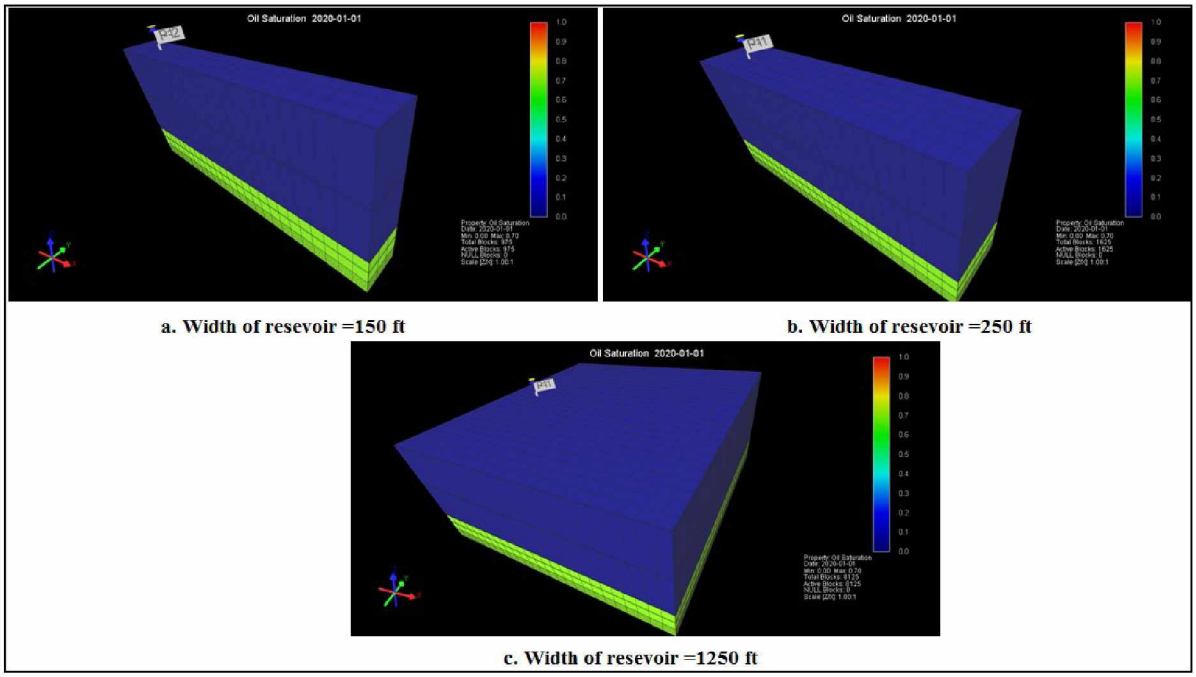

Figure 6-21: STARS' schematic of reservoir models with width of 150, 250 and 1250 ft.

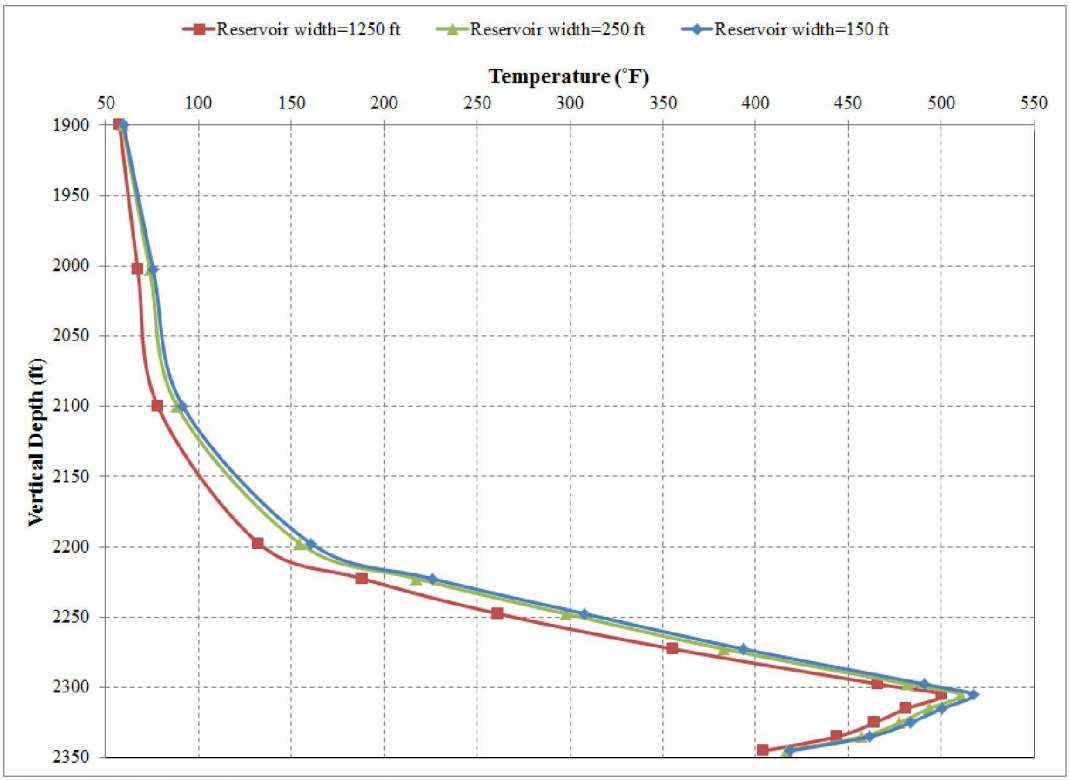

Figure 6.22: Effect of reservoir width on the vertical temperature profile.

6.2.3. Effect of Rock Thermal Properties

One factor that potentially affects the results of a thermal simulation is the thermal properties of formation rock. Based on the available data (see Literature Survey section), a range of rock thermal properties was selected. The minimum, average, and maximum of each property were used to test their effect on simulation results. The vertical temperature profile was used for comparison. The schematic 3-D model used for this and the other sensitivity analysis is shown in Figure 6-23. This model is selected based on the results of previous section (Reservoir Width Selection).

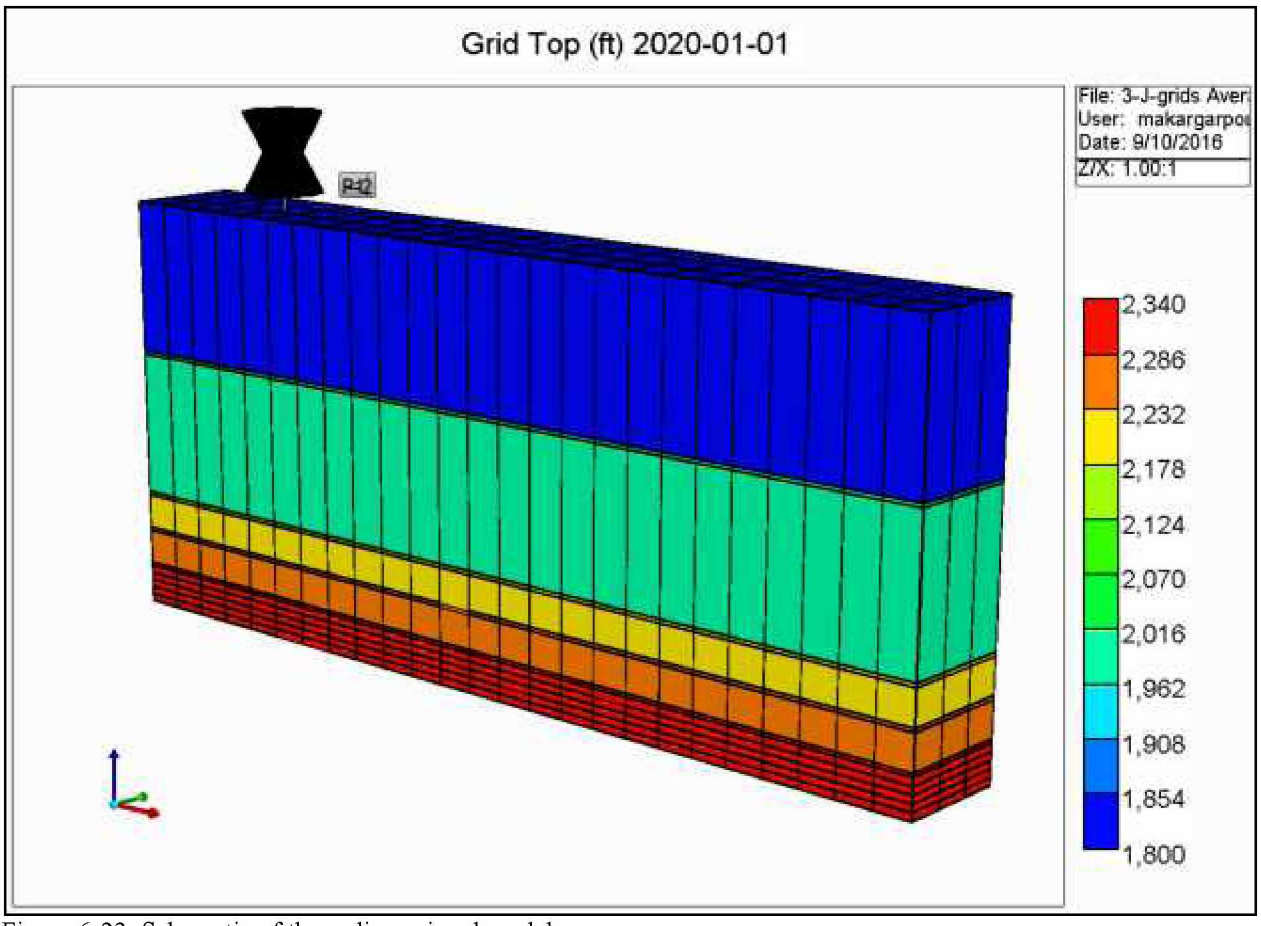

Figure 6-23: Schematic of three-dimensional model.

Three scenarios with different thermal rock properties (as shown in Table 6-4) were defined and run. The other model properties were the same in all three scenarios. The results are shown in Figures 6-24 through 6-26. Based on these results, the effect of this property variation is negligible. So, it was decided to use the average value of thermal properties for the remaining simulations.

Table 6-4: Rock thermal properties used in models.

	Rock Volumetric Heat Capacity						Thermal conductivity					
	J/(m^3 ˚C)			Btu/(ft^3 ˚F)			J/(m day ˚C)			Btu/(ft day ˚F)		
	Min.	Ave.	Max.	Min.	Ave.	Max.	Min.	Ave.	Max.	Min.	Ave.	Max.
Formation Rock	2.01E+06	2.35E+06	2.68E+06	30	35	40	2.2E+05	2.5E+05	2.8E+05	35	40	45
Overburden	2.01E+06	2.35E+06	2.68E+06	30	35	40	1.2E+05	1.5E+05	1.9E+05	20	24.1	30
Underburden	2.01E+06	2.35E+06	2.68E+06	30	35	40	1.2E+05	1.5E+05	1.9E+05	20	24.1	30

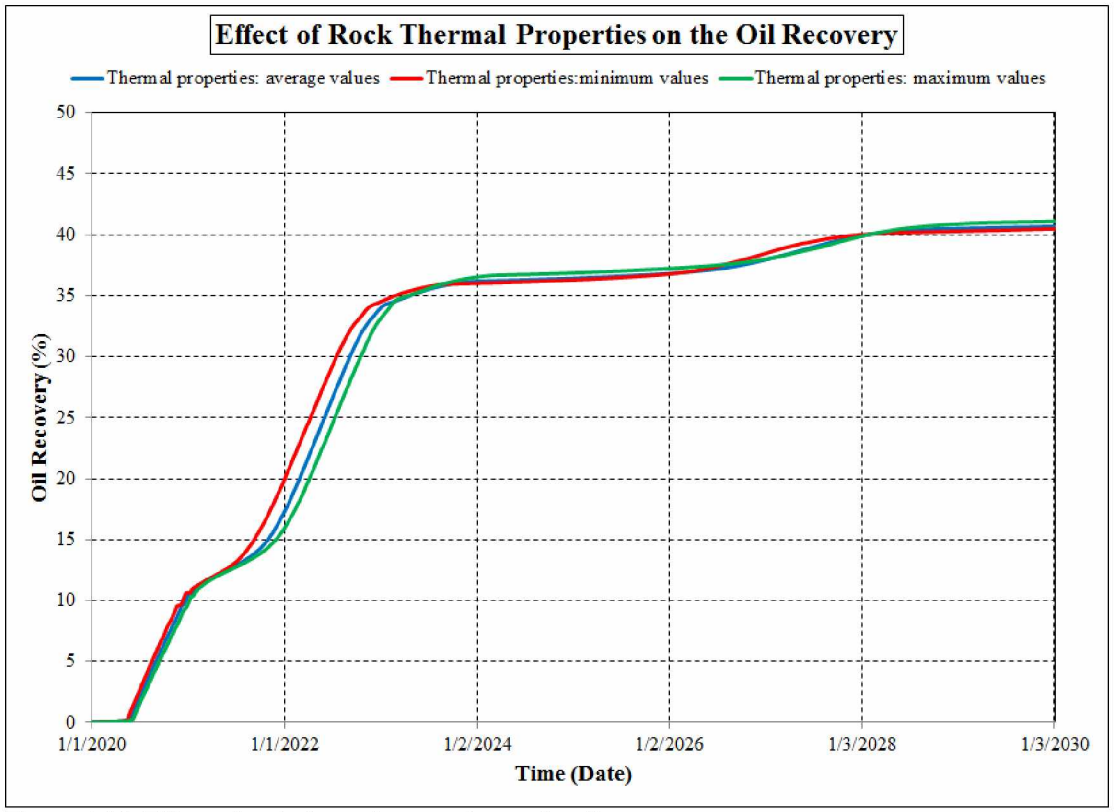

Figure 6-24: Effect of rock thermal properties on the oil recovery.

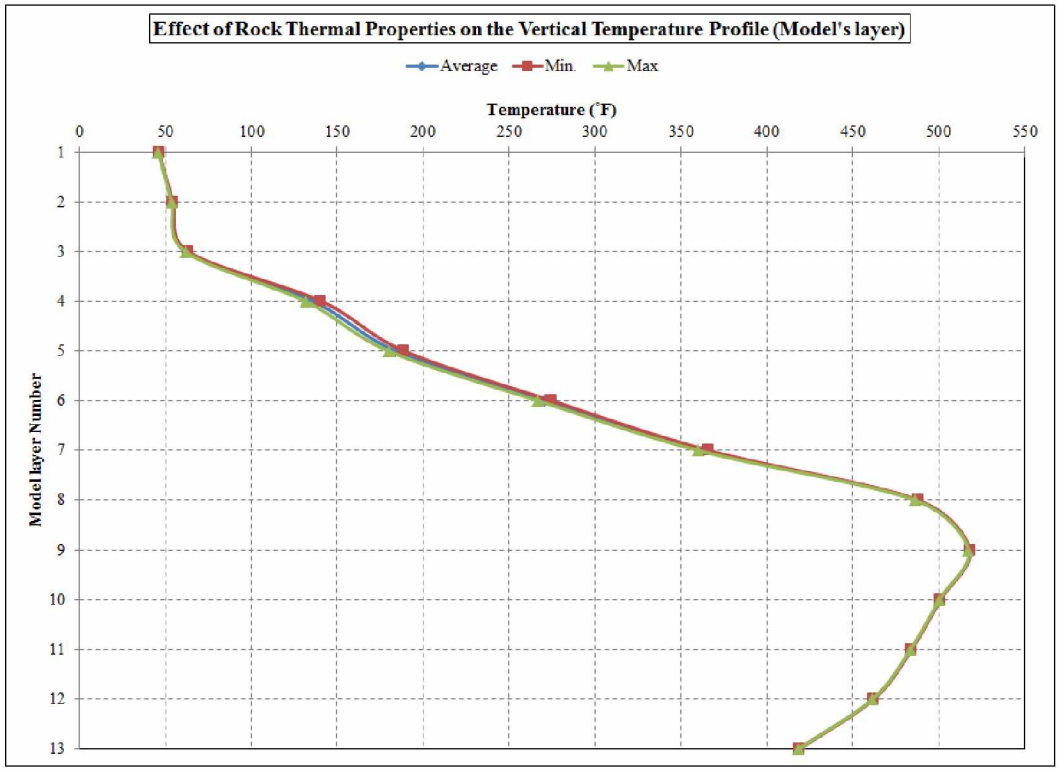

Figure 6-25: Effect of rock thermal properties on the vertical temperature profile (model's layer).

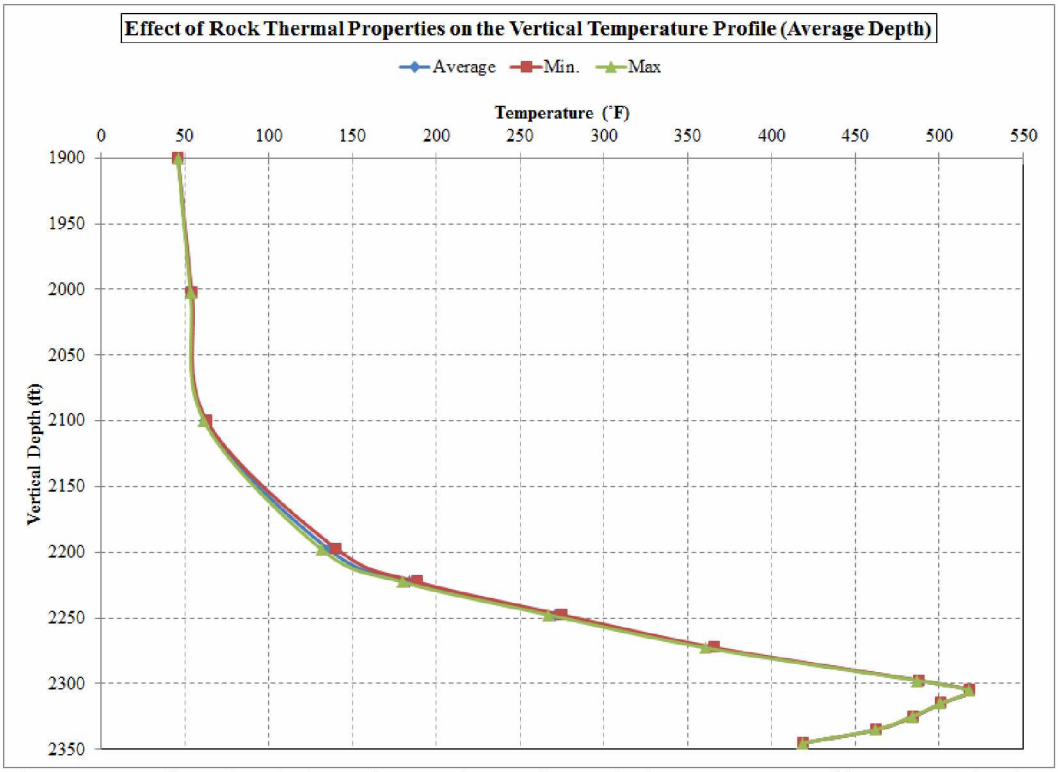

Figure 6-26: Effect of rock thermal properties on the vertical temperature profile (average depth).

6.2.4. Optimization of Grid Block Size

As mentioned in the previous section, a width of 150 ft was selected for the reservoir model. This model is the same as the model described in Table 6-2. The number of model areal grids considered was 25 and 3 in x and y direction, respectively. Grid size has a great effect on results of the simulation model. To find optimum grid size for further steps of simulation, five different models (with different grid sizes) were constructed with the same reservoir width and length: [10 ft × 10 ft], [12.5 ft × 12.5 ft], [20 ft × 20 ft], [25 ft × 25 ft] and [50 ft × 50 ft]. The number of layers and their thicknesses were the same for all of these models.

The effect of these variations in grid block size on oil recovery is shown in Figure 6-27. Based on the results, it was decided to use grid size 25 ft × 25 ft in subsequent models; however, as shown in the next sections, in some cases, models with grid size of 10 ft × 10 ft were used.

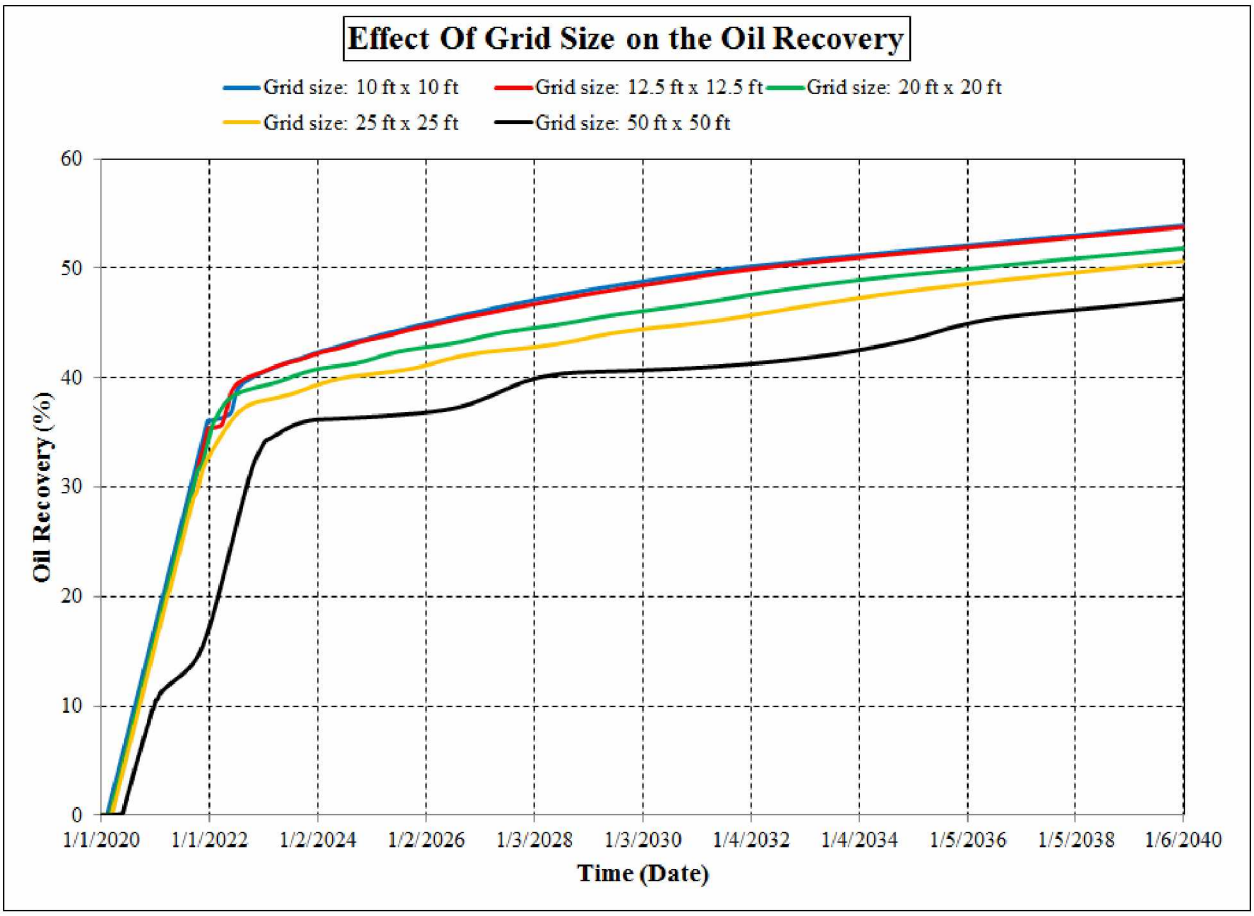

Figure 6-27: Effect of grid block size on oil recovery.

6.2.5. Effect of Well Constraints

The well constraints, in conjunction with other parameters, have significant effect on the simulation results. By using a 1250 ft (length) × 150 ft (width) with the properties of Table 6-2, the effect of different well constraints is investigated.

6.2.5.1. Effect BHP of Producer Well

Flowing Bottom Hole Pressure (BHP) is one parameter which is operationally used to control the producer well flow rate (by applying a back pressure with adjusting the well head flowing pressure). This parameter controls the well rate as well flow rate and is directly proportional to well draw down (P_r-P_{wf}), where P_r and P_{wf} are average (boundary) reservoir pressure and BHP, respectively. To study the effect of this parameter, different models are constructed and run using BHP equal to 28, 100, 200, 300, 400 and 500 psi. The results are shown in the Figure 6-28.

As it is seen in the modeling results, it seems that BHP's variation has no considerable effect on the oil recovery. This is not in agreement of what is common for conventional reservoirs with low viscosity and can be attributed to two features of this type of simulation (steam injection):

* Under natural depletion conditions, producer cannot flow or its rate is negligible,
* The flooding pressure (BHP of injector well) is high enough; so, we can have any BHP of producer well, at least up to 500 psi.

Based on the results it is decided to continue simulation campaign with BHP of producer well equal to 200 psi.

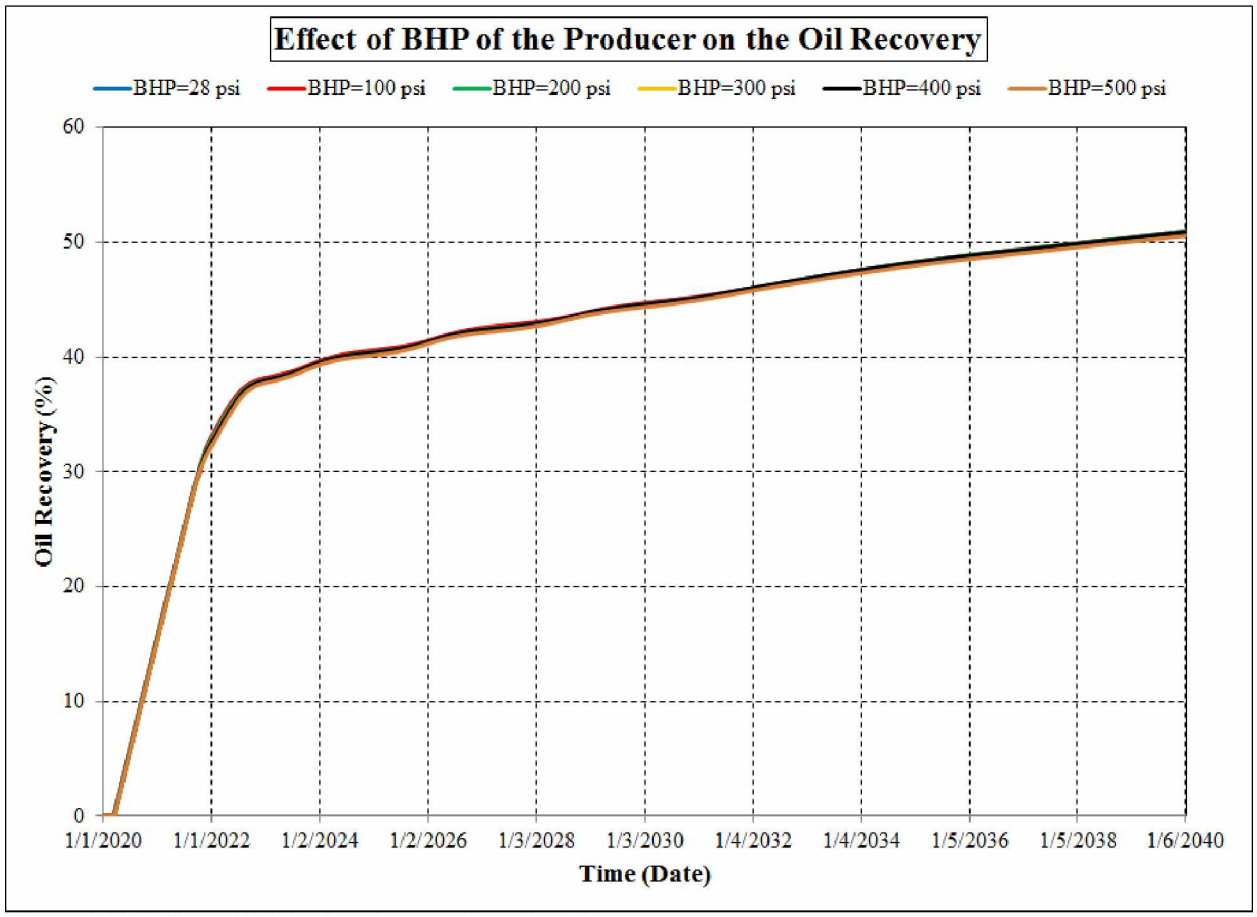

Figure 6-28: Effect of BHP of producer well on the oil recovery.

6.2.5.2. Effect of Injector and Producer Wells Rates

To investigate the effect of injector and producer wells' rate, several models were constructed and run. The models were based on the properties introduced in Table 6-2 and horizontal grid size of '25 ft × 25 ft'. Since the Steam Oil Ratio (SOR) in conjunction with oil recovery have great effect on the economy of a steam injection project, these two parameters (SOR and oil recovery) were obtained from simulation results and are shown in Figure 6-29. The x-axis depicts the injector well rate and each curve is for one producer well rate. The oil recovery and SOR are computed at the end of the simulation period (20 years).

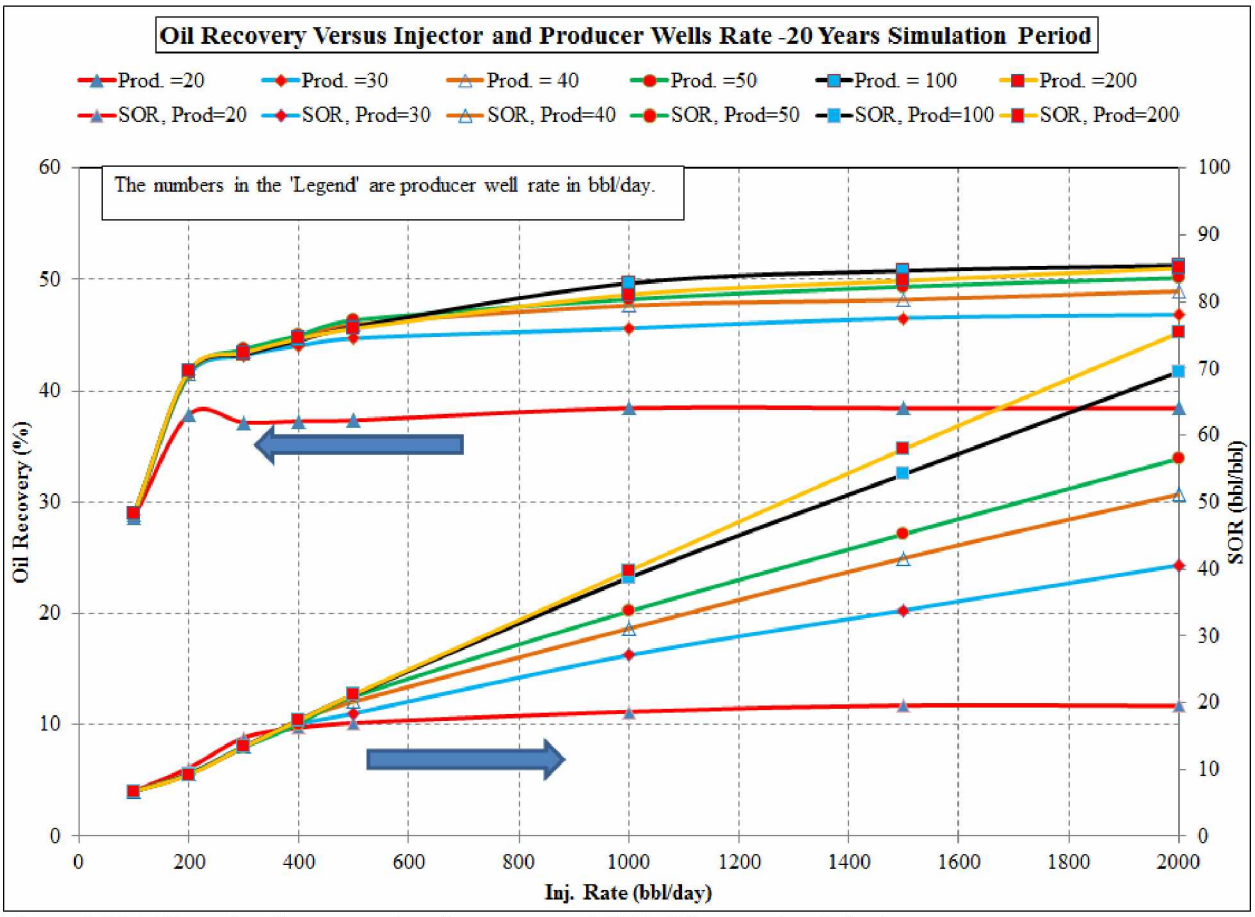

Figure 6-29: Effect of wells rate on the oil recovery and SOR (20 years simulation).

The SOR even at production rate of 200 bbl/day is high. An -SOR of about 7 bbl/bbl can result in an economic project (Hammershaimb et al., 1983); this means that the SOR's of 20 – 75 are uneconomical. The recovery at an oil production rate of 100 bbl/day is a little higher than that of 200 bbl/day. Figure 6- 30 shows the oil recovery at an oil production rate of 100 and 200 bbl/day. As it is obvious from this figure, at the early year of simulation, the recovery of the

scenario with an oil production of 200 bbl/day is greater than that of scenario with an oil production rate of 100 bbl/day. At later times, the oil production rate decline in the case of 200 bbl/day will be much higher than that of the case of 100 bbl/day. This difference in oil production decline rates results in compensating the early years difference in cumulative oil recovery. So, the cases were again run for a 10-year simulation period. The results for this simulation period are shown in Figure 6-31. From this figure, one can conclude that the optimal range of steam injection can be in the range of 300 to 500 bbl/day (equivalent water) and the range of oil production is about 50 to 200 STB/day.

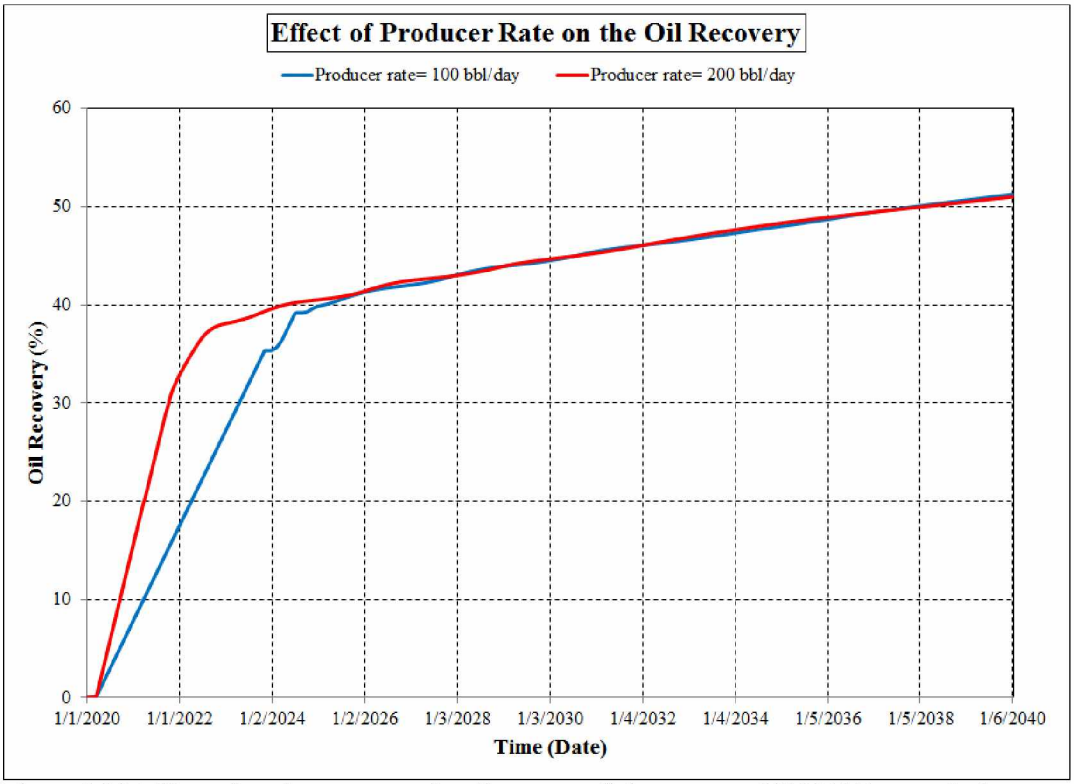

Figure 6-30: Effect of producer rate on the oil recovery (injector rate= 2000 bbl/day; equivalent water).

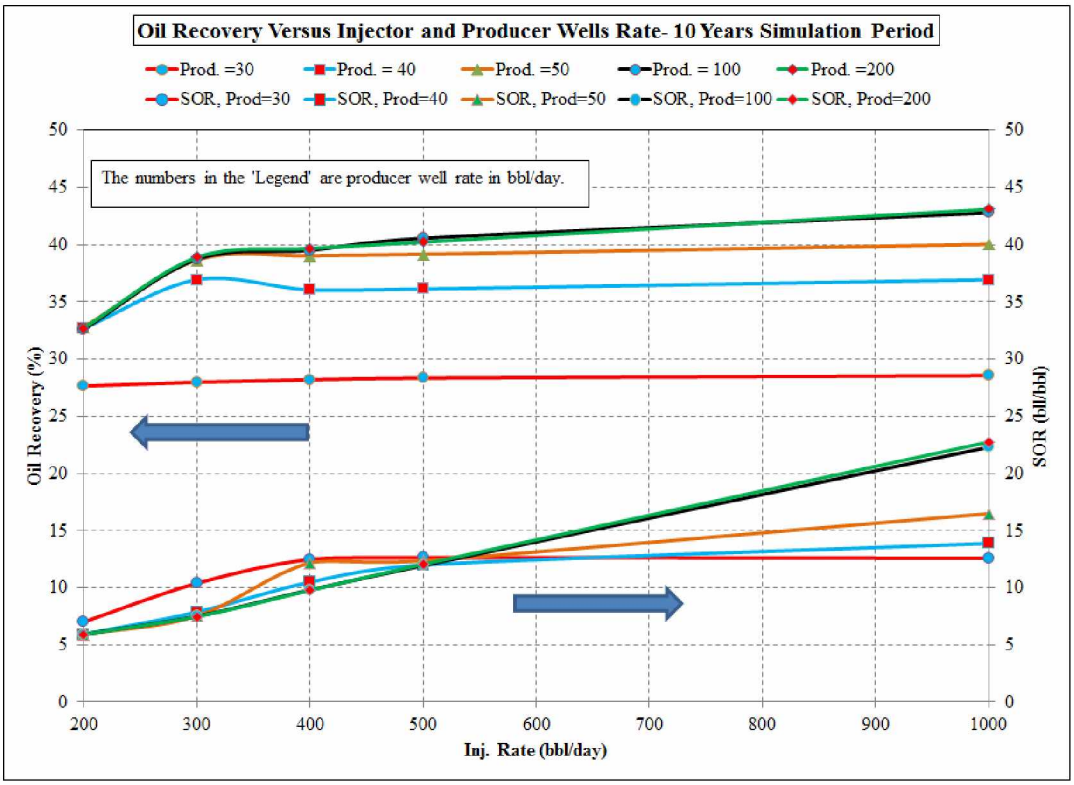

Figure 6-31: Effect of wells rate on the oil recovery and SOR (10 years simulation).

6.2.5.3. Effect of BHP of Injector Well:

Based on the results of previous sections, the main driving force in this viscous oil model is the steam injection; so, it is valuable to study the effect of injection pressure on the reservoir performance. Based on the results of previous studies on the wells constraints, the following constraints are selected as optimum ones:

- Injector well: maximum surface total phase rate of steam = 500 bbl/day (equivalent water),
- Producer: minimum BHP = 200 psi, maximum Stock Tank Oil (STO) rate = 200 bbl/day.

By fixing these constraints, the effect of BHP of injector well in the range of 1100 to 2500 psi is studied. Note: the reservoir pressure is set equal to 1000 psi. The results (oil recovery and SOR) are shown in Figures 6-32 and 6-33.

- As it can be seen; in this model and with its constraints, increasing the BHP of injector above 2000 psi has negligible effect on the oil recovery and/or SOR.
- Results show that at BHP of injector well of about 2000 psi maximizes the oil recovery.

Based on the results, it is decided to continue simulation by setting the BHP of injector well to 2000 psi.

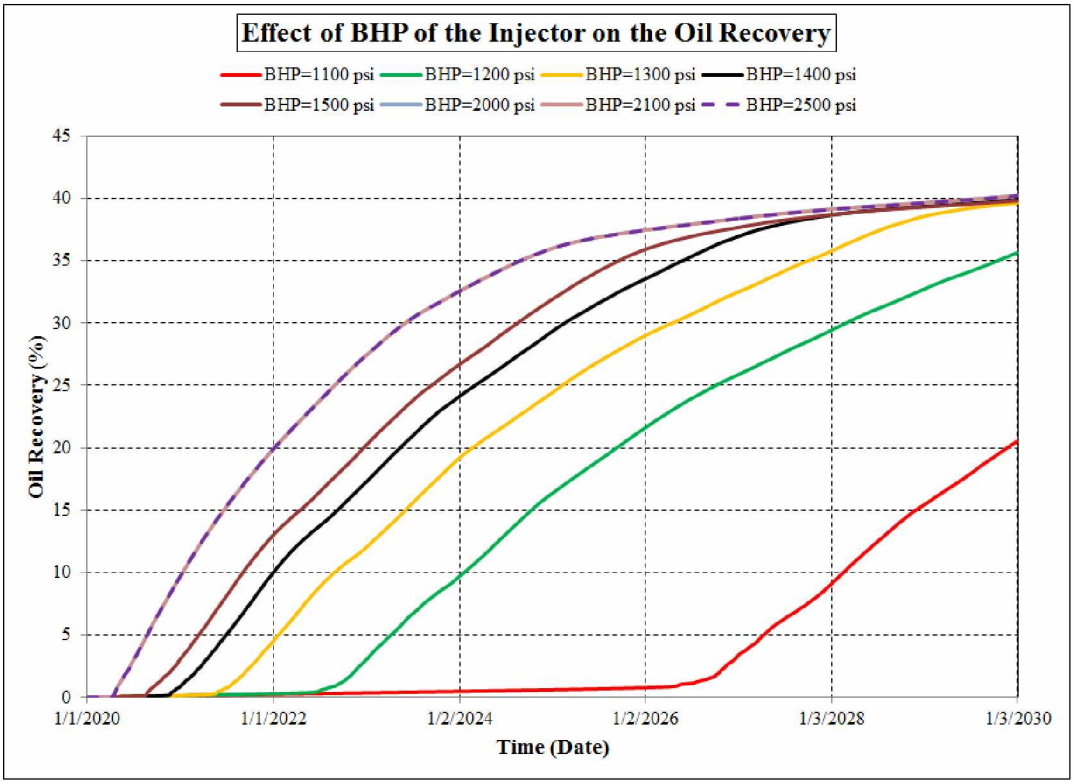

Figure 6-32: Effect of Injector's Bottom Hole Pressure (BHP) on the oil recovery.

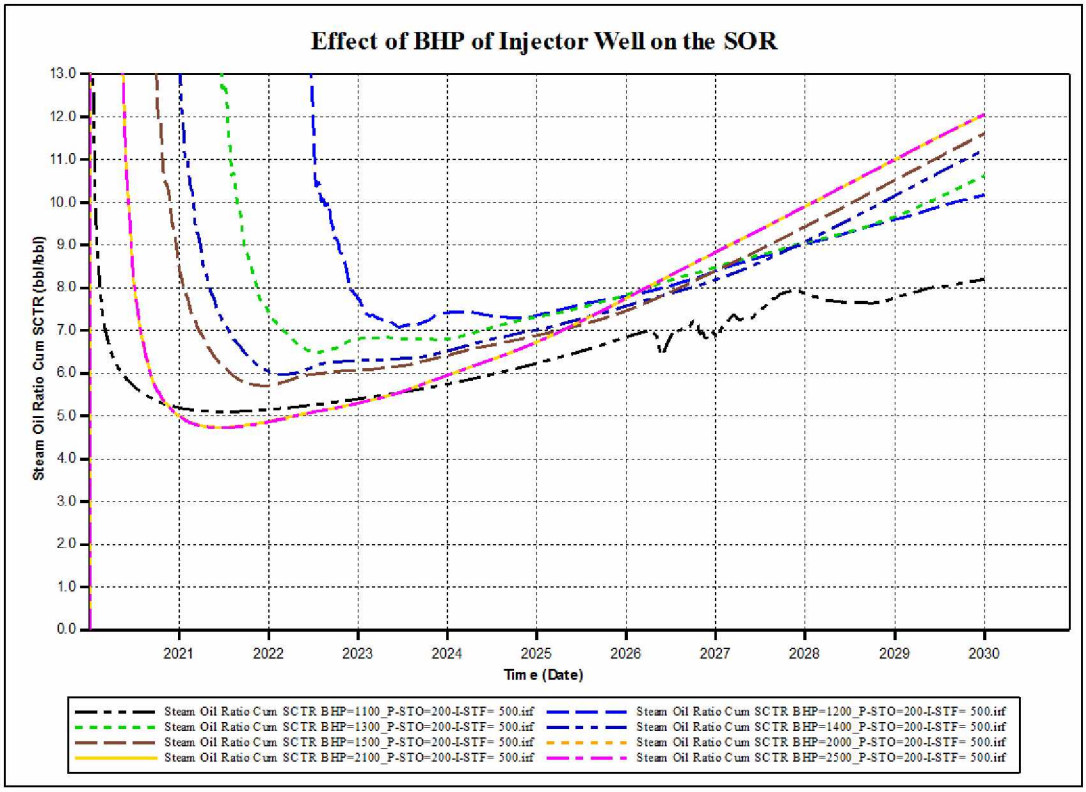

Figure 6-33: Effect of Injector's Bottom Hole Pressure (BHP) on the Steam Oil Ratio (SOR).

6.2.6. Effect of K_v to K_H Ratio

The permeability heterogeneity [which is usually shown by the ratio of vertical permeability (K_v) to horizontal permeability (K_H)] has a great impact on the horizontal well performance. To study the effect of K_v to K_H ratio, based on the results of previous studies on the wells constraints, the following constraints are selected as optimum ones:

- Injector: maximum surface total phase rate = 500 bbl/day, max BHP = 2000 psi,
- Producer: minimum BHP = 200 psi, maximum STO = 200 bbl/day.

Different models with K_v/K_H ratios of 0.1, 0.5, 0.9 and 1.0 are run. The K_v/K_H ratios are randomly are selected. The results are illustrated in Figures 6-34 and 6-35. In a heterogeneous reservoir, horizontal well productivity increases with increasing the K_v/K_H ratio. By increasing the K_v/K_H ratio and at constant K_H, K_V increases. This means more oil will flow from top layer toward lateral of horizontal well. The results are different from expectation: by increasing the K_v/K_H the oil recovery decreases. To understand and explain this contradiction, two other simulation activities have been carried out.

First, it was checked that the results are inherent to steam flooding and not a malfunction of the model. To carry out this study, two natural depletion scenarios are run with K_v/K_H = 0.1, and 0.5. The results are shown in Figure 6-36, which are in agreement with experience, by increasing K_v/K_H the oil recovery increases.

Secondly, several other runs (extended cases) are conducted to justify the effect of K_v/K_H in SAGD process. In these cases, in addition to other scenarios, very low K_v/K_H (hypothetical) scenarios are also run (K_v/K_H = 0.001 and 0.01).

Based on the results, following explanation can be made:

Having good sweep efficiency is very important in steam injection. In steam injection process, by decreasing the K_v/K_H, the sweep efficiency increases and subsequently the oil recovery also increases in a long term production. However, it is time dependent: at early time, oil recovery increases with increasing the Kv/K_H. In Figure 6-37, the oil recovery curves are crossing each other. This crossing shows that at low Kv/K_H and at early times of simulation (steam injection), the oil production is low; however at later times, more volume of the reservoir is swept by steam and the oil production and consequently the recovery is increased. It means that for final decision a detailed economic analysis is required, which is beyond of scope of this project. But the value Kv/K_H equal to 0.1 is used for further simulation.

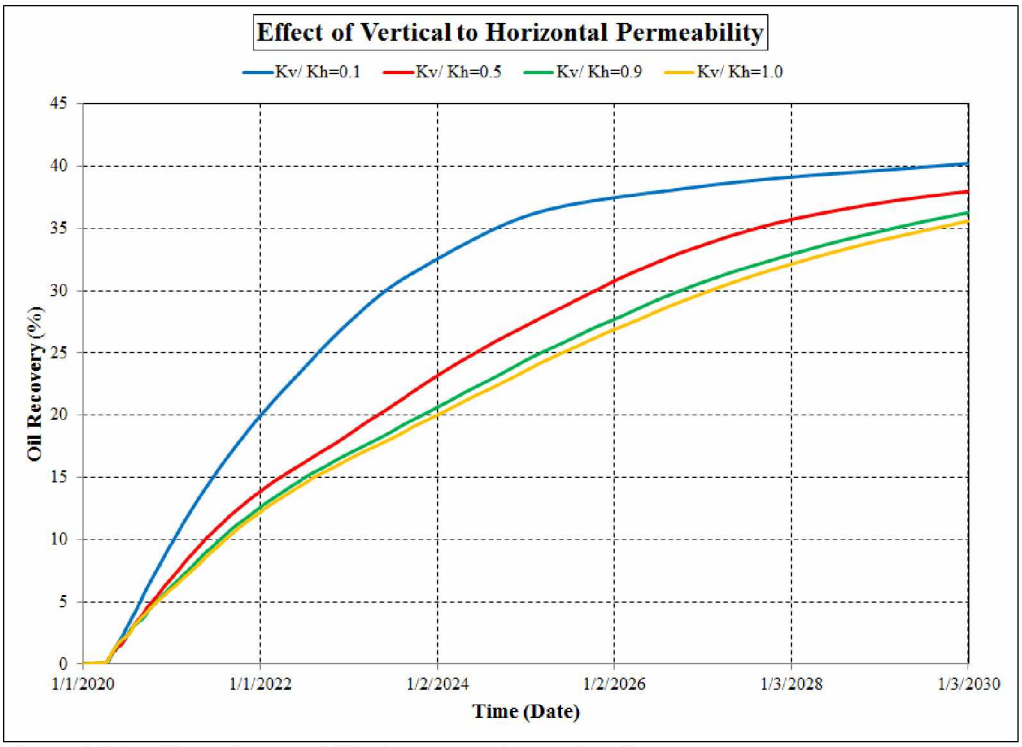

Figure 6-34: Effect of permeability heterogeneity on the oil recovery.

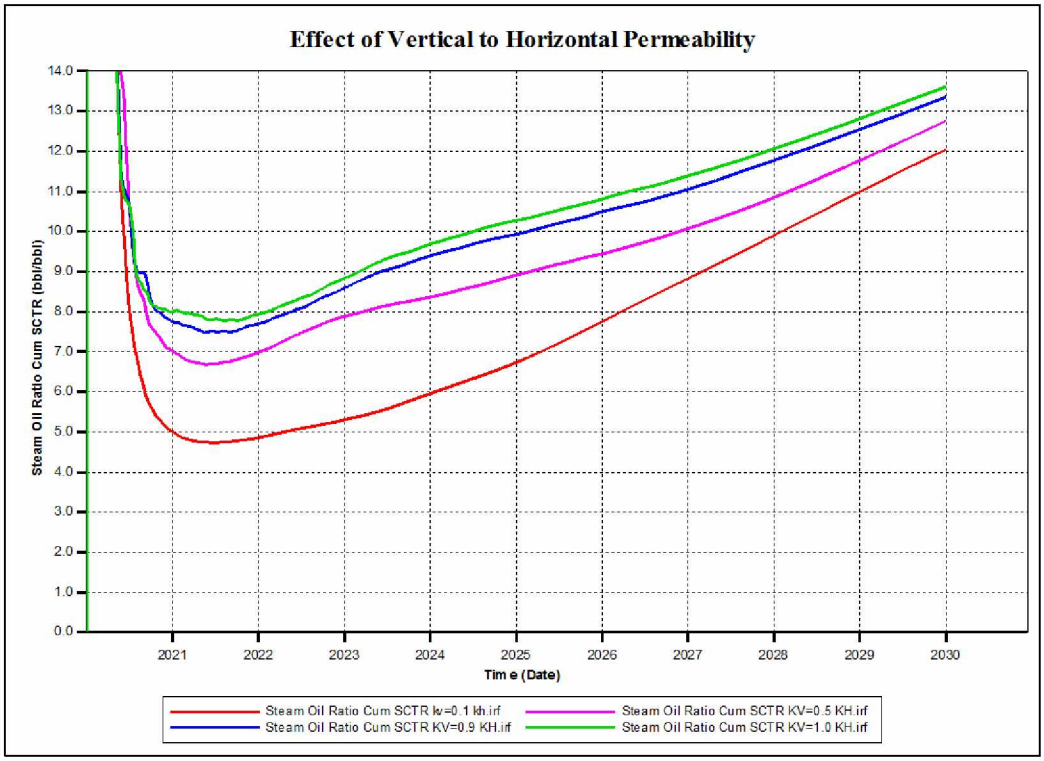

Figure 6-35: Effect of permeability heterogeneity on the SOR.

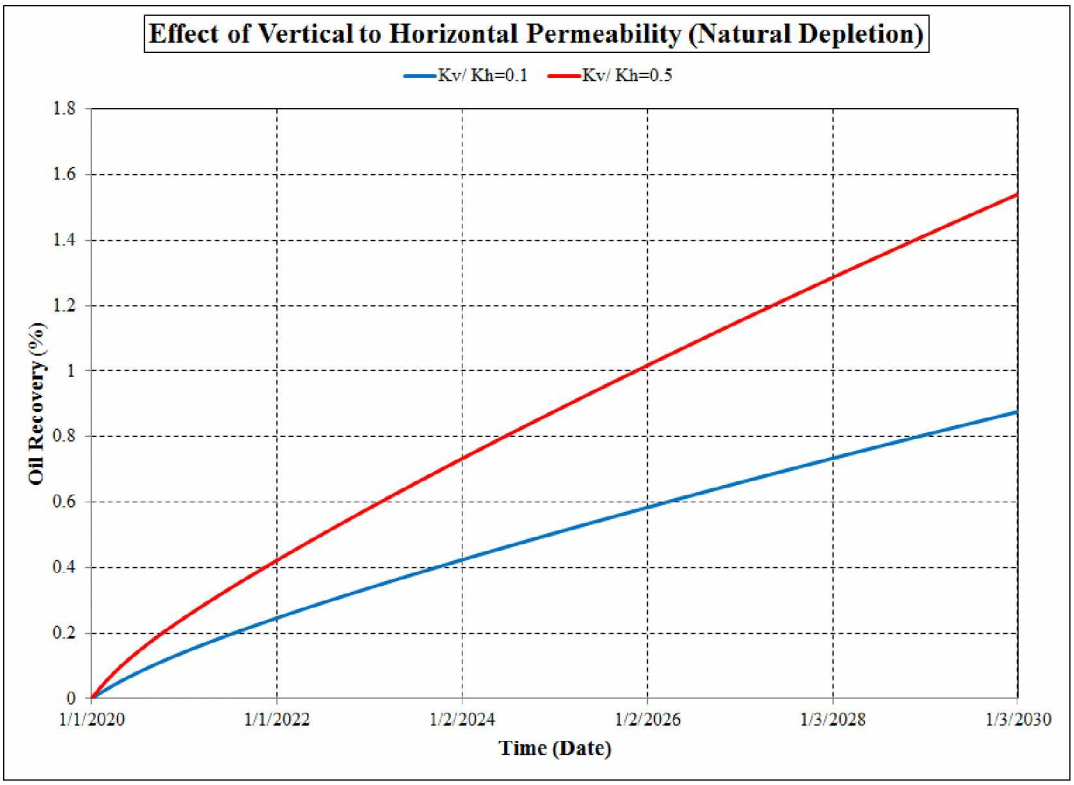

Figure 6-36: Effect of permeability heterogeneity: natural depletion.

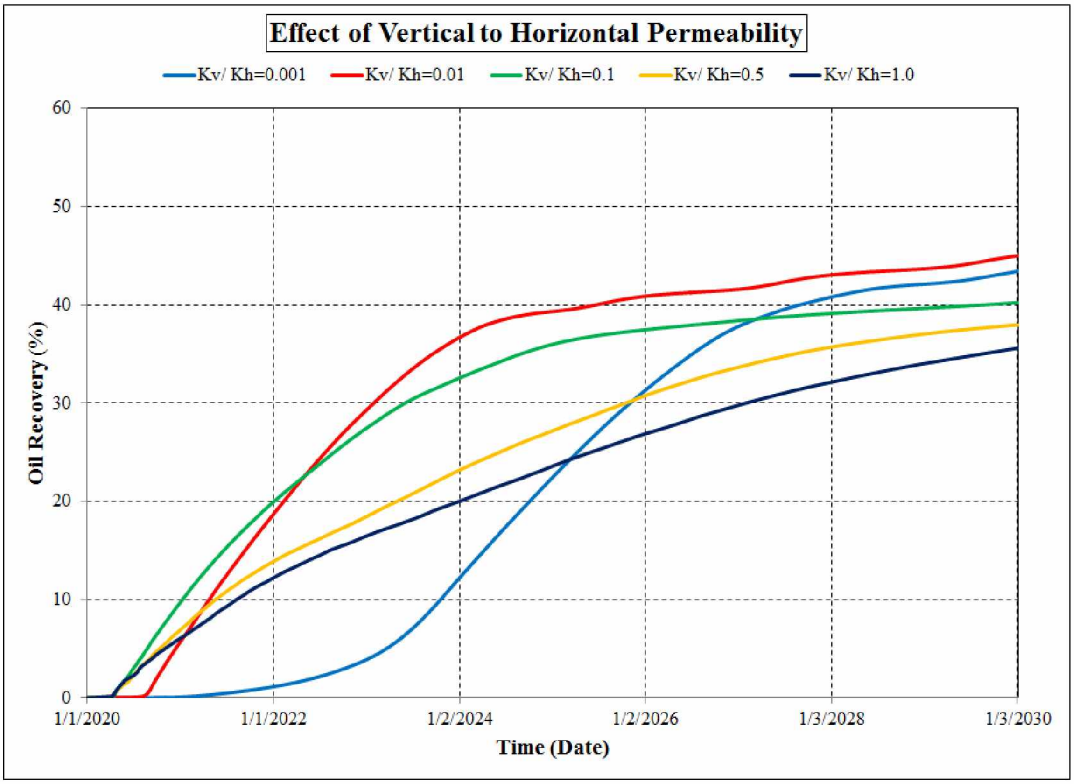

Figure 6-37: Effect of permeability heterogeneity on the oil recovery (extended cases).

6.2.7. Effect of Absolute Permeability

As mentioned before, the Ugnu reservoir permeability is reported to be as high as 3000 mD (see Table 4-1); however, the average permeability is much lower than this value. To investigate the effect of this parameter on reservoir performance, a series of models were constructed and run. The same fine grid (25 ft × 25 ft) model with selected optimum well constraints (as follow) was used:

- Injector: max. surface total phase rate = 500 bbl/day, max BHP = 2000 psi,
- Producer: minimum BHP = 200 psi, maximum STO = 200 bbl/day.

Absolute permeability was set to 500, 600, 1000, and 1500 md for different models. The results are illustrated in Figures 6-38 and 6-39.

The results reveal that the permeability variation in the range of 500 to 1500 md has negligible effect on the oil recovery and SOR.

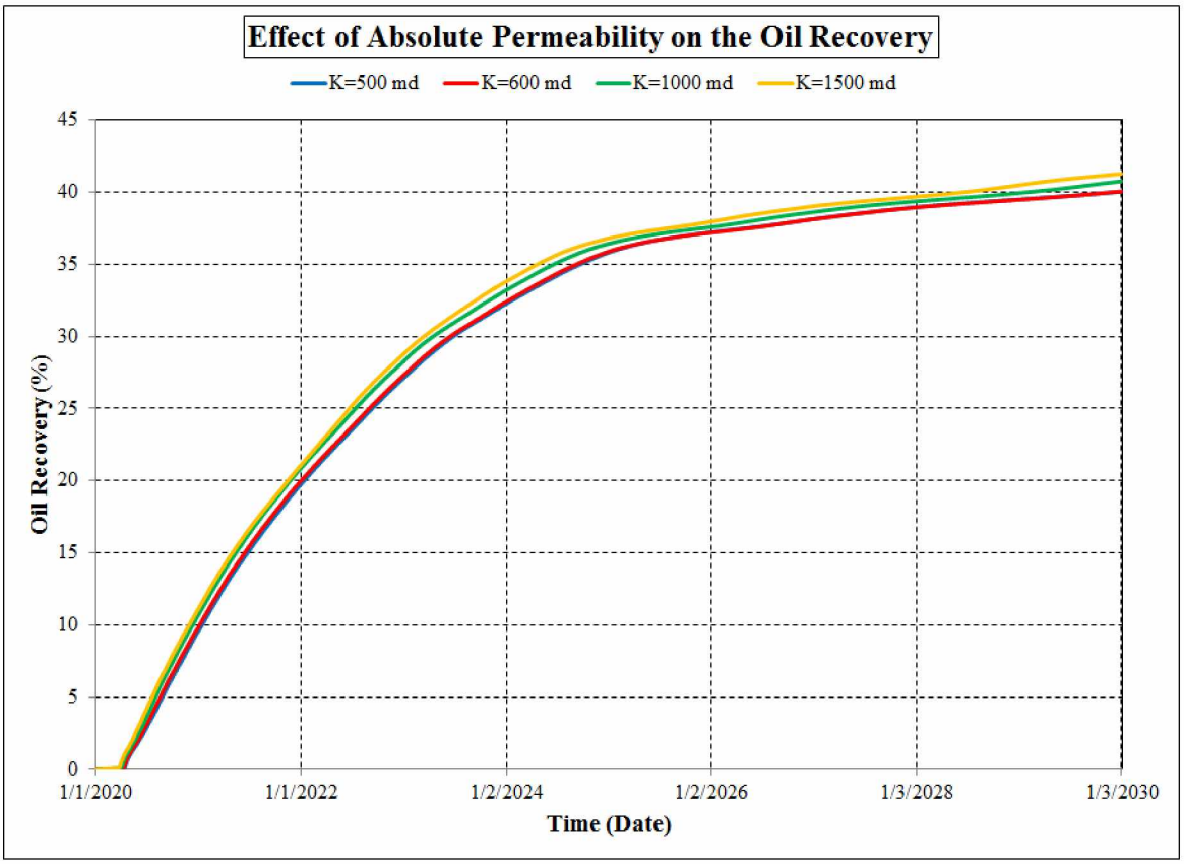

Figure 6-38: Effect of absolute permeability on the oil recovery.

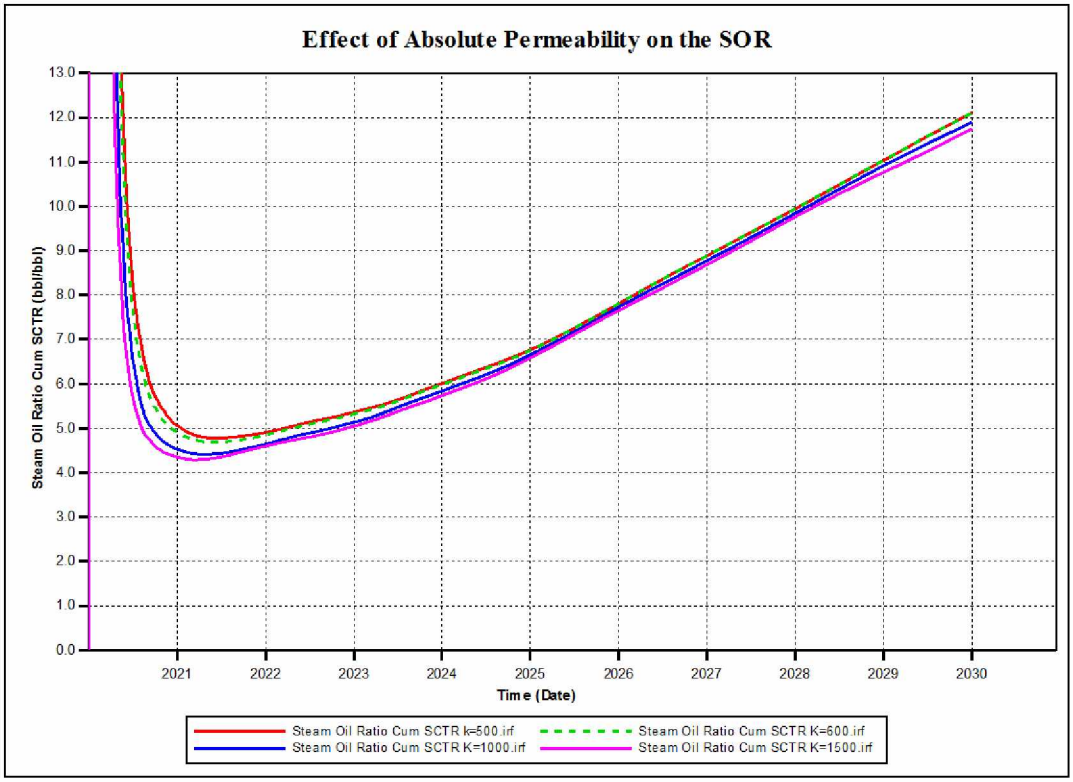

Figure 6-39: Effect of absolute permeability on the SOR.

6.2.8. Effect of Layer's Wells Location

As mentioned in previous sections, injector and producer wells are assumed to be drilled in the layers number 9 and 13, respectively (see Table 6-2). To study the effect of vertical distance between the horizontal wells in a SAGD process, in addition to the base case model (Injector layer's number = 9), two other scenarios are defined and run: injector's layer number = 10 and injector's layer number = 11. The other models' properties are set to be the same.

- Injector: max. surface total phase rate = 500 bbl/day, max BHP = 2000 psi,
- Producer: minimum BHP = 200 psi, maximum STO = 200 bbl/day.

The results are shown in Figures 6-40 and 6-41. The peaks appears in the curve of steam oil ratio (inj=layer 11, Prod=layer 13) in Figure 6-41 (green color curve) seems to be due to closeness of injection and production layers which makes an instability in flow. The results reveal that by decreasing the vertical distance between the injector and producer wells, the oil recovery decreases and the SOR increases. This can be attributed to volumetric sweep efficiency. By decreasing the vertical distance between wells, the sweep efficiency decreases and consequently

causes a decrease in oil recovery. More details will be discussed on this concept (the effect of vertical distance between injector and producer wells on the oil recovery) in Section 6.2.16, to find out the optimum vertical distance between the wells.

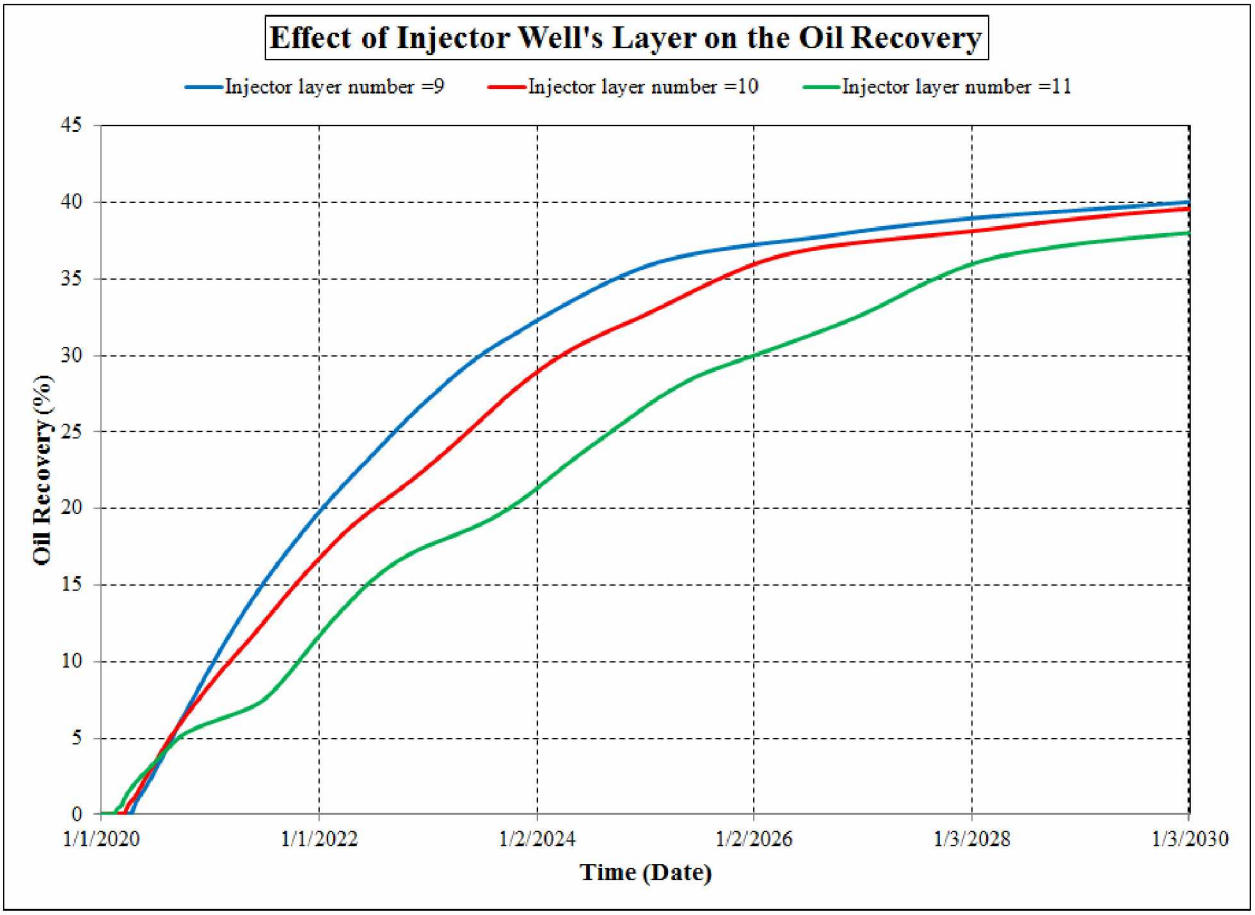

Figure 6-40: Effect of injector well's location on the oil recovery.

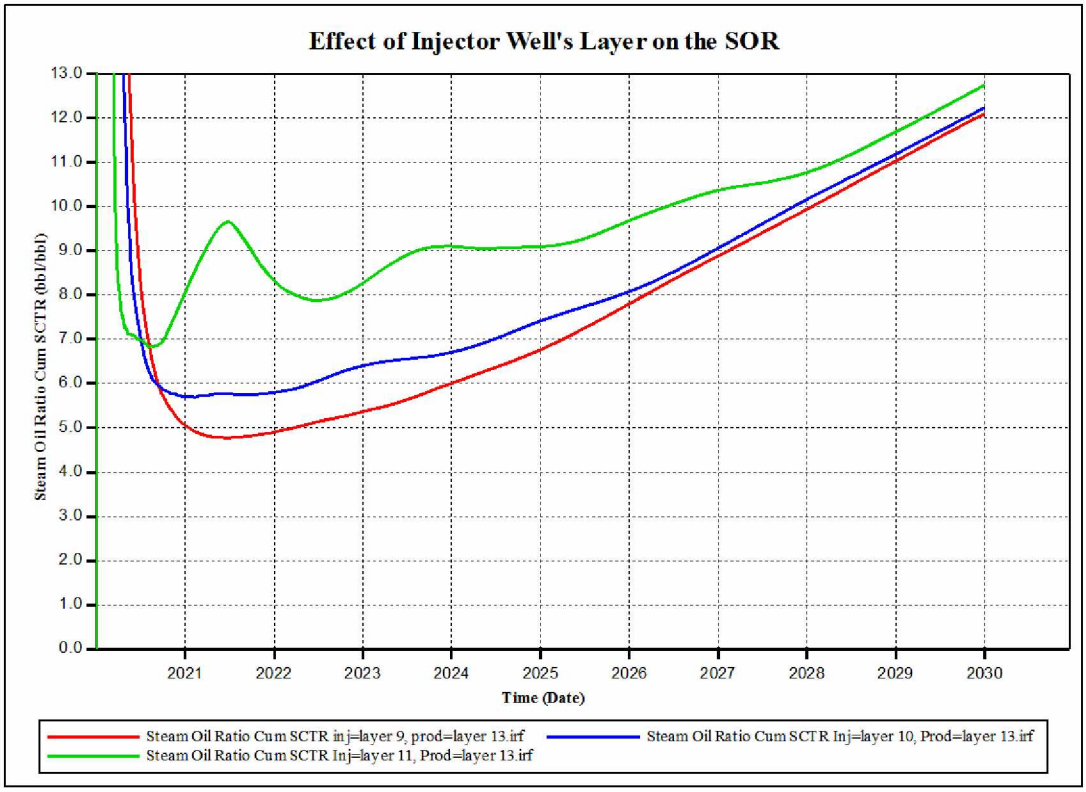

Figure 6-41: Effect of injector well's location on the SOR.

6.2.9. Effect of Producer's Length Opening

As mentioned, in addition to the oil recovery and SOR (Steam Oil Ratio) what is important in this project is temperature profiles, especially down-hole producer wellbore temperature. If the entire length of producer well is opened to flow, it is logical to assume that the producer well bore temperature would be very high. It is envisaged that if just a few feet of lateral producer well is opened to flow, the produced fluid will be cooled down in lateral tubing when produced fluids flow from opening (toe of the well) to the heel of well. To study this hypothesis, several models are constructed and run. In all cases the length of reservoir is 1250 ft and the producer well length is considered to be 800 ft drilled in the middle of the reservoir. The following cases are defined:

- Base case: the entire producer well length opens to flow (800 ft),
- 1-first-P-50ft: two first grids of producer open to flow (50 ft),
- Middle-P-50ft: two middle grids of producer open to flow (50 ft),

- 3-last-P-50ft: grids number 35 and 36 of producer open to flow (50 ft),
- 2-last-P-50ft: grids number 37 and 38 of producer open to flow (50 ft),
- Last-P-50ft: last two grids (number 39 and 40) of producer open to flow (50 ft).

For schematic of lateral producer wells the reader is referred to Figure 6-42.

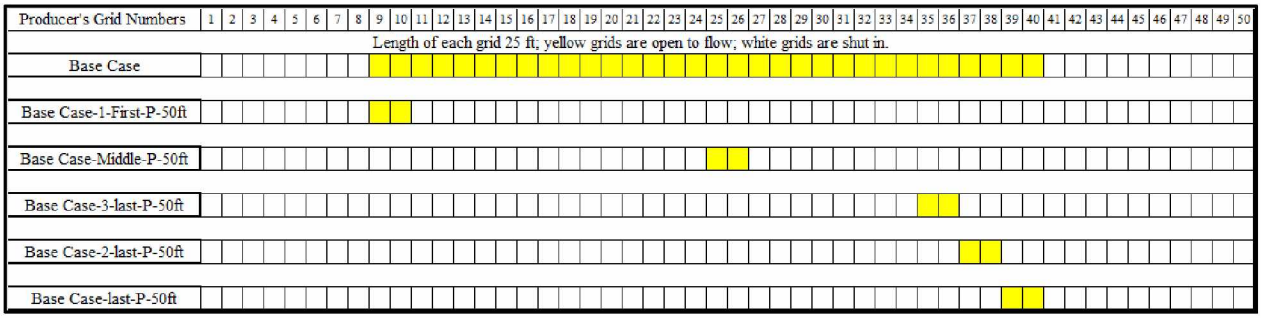

Figure 6-42: Schematic of lateral producer well for scenarios of 'effect of producer's length opening' study.

The effect of these variations on the oil recovery and SOR are shown in Figures 6-43 and 6-44. Also, in Figure 6-45 the lateral temperature profiles of producer well's layer for different scenarios are depicted. This figure shows that the minimum producer well bore temperature can be obtained when just last 50 ft of lateral length of the well is perforated.

The temperature profiles shown in Figure 6-45 are the grid block temperatures. However, in reality, the lateral length of well is completed with appropriate size and type of liner and the predetermined length of it is opened to flow by applying the optimum system, for example perforation. The CMG reservoir simulation package has this facility to install casing and tubing in the simulated model. This type of well is called 'flexwell'. The method of pressure drop and heat transfer calculation in 'flexwell', in the STARS User's Guide (CMG, 2015), it is emphasized: 'Friction pressure drop is calculated in each string. First a flow regime is determined from gas and liquid velocities then the appropriate friction pressure drop is computed. An overall heat transfer coefficient is calculated for the radial heat flow. Heat resistance is added up from all participating pieces of the wellbore. If wall, insulation and/or cement thickness are specified as zero then only fluid resistance will participate in the calculation. Fluid resistance is evaluated from dimensionless parameters such as Nusselt number'.

Therefore, models are reconstructed by using 'flexwell' for producer. Figure 6-46 compares the oil recovery of models with regular producer and 'flexwell' producer. When full length of producer well is opened to flow, there isn't any appreciable difference between the results; however, when just 50 ft of toe of lateral well is opened to flow, the model with 'flexwell' shows a little higher oil recovery. A comparison of producer's lateral temperature profile between two models (using 'flexwell' versus regular well) is presented in Figure 6-47. Again the temperature profile is the same in scenario of 'full length opening' of the producer well in both cases. In the scenario of 'last 50 ft opening' of the producer well, the temperature of regular well is higher than the case of using 'flexwell'. In the case of using 'flexwell', the lateral length of the producer well is covered by cemented tubing; however, in the case of using regular well, the lateral length of producer is left opened. In other words, in regular well the well has open-hole completion but in the 'flexwell', the well is cased and perforated. This difference affects the amount of heat transfer and consequently the well temperature.

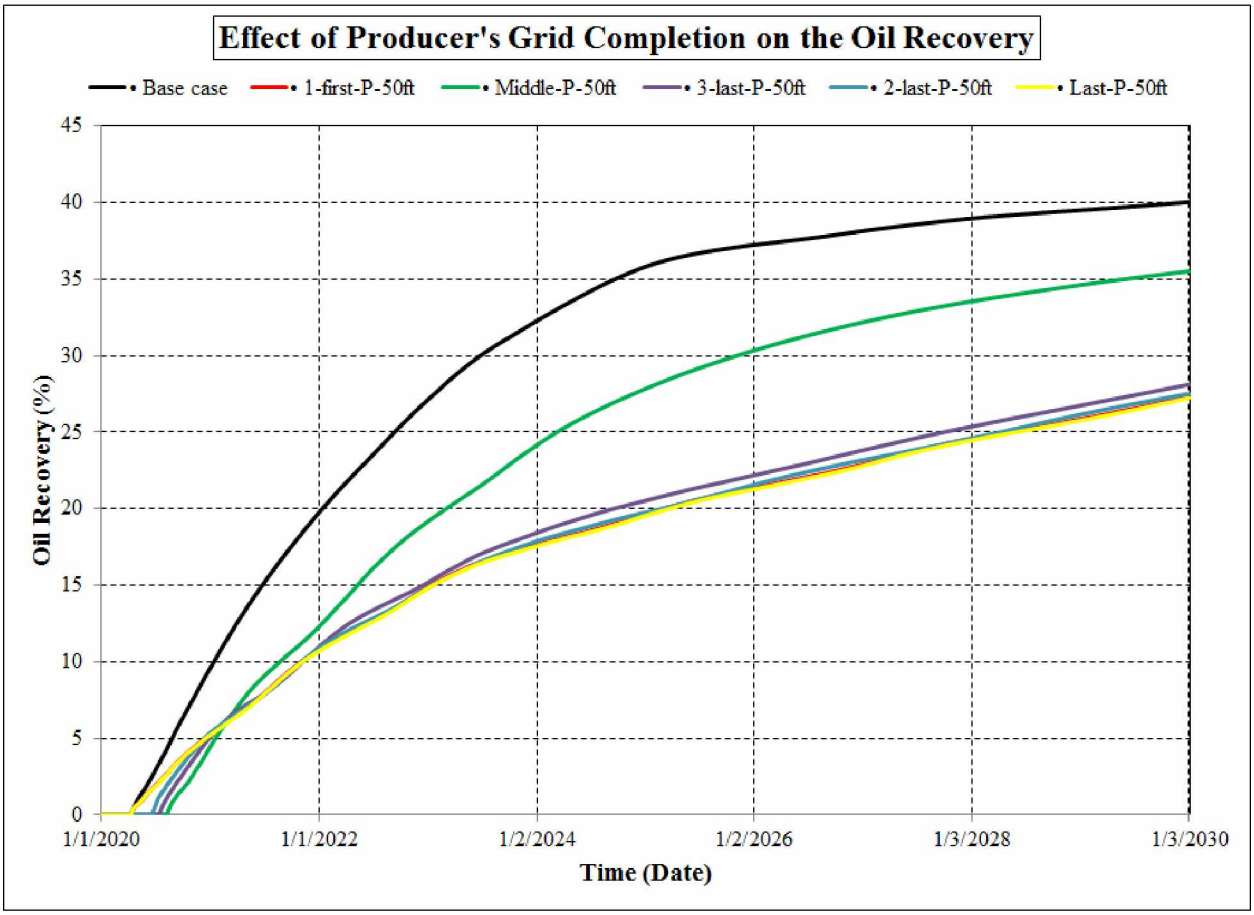

Figure 6-43: Effect of producer's grid completion on the oil recovery.

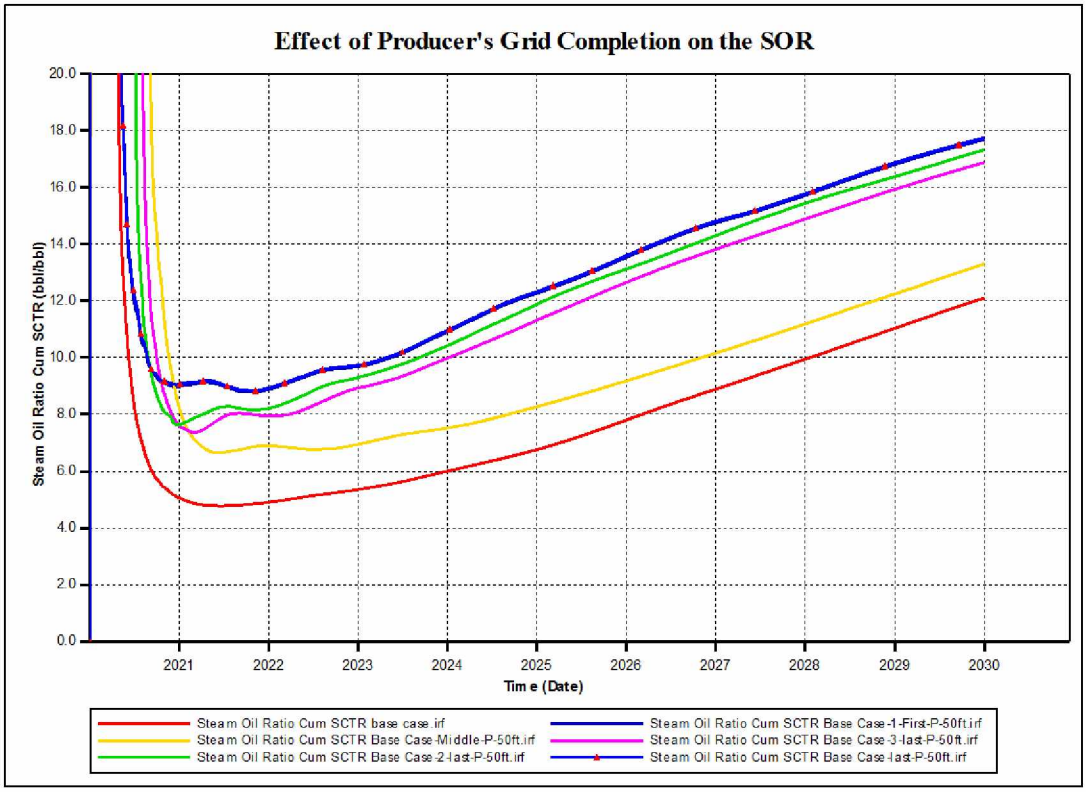

Figure 6-44: Effect of producer's grid completion on the SOR.

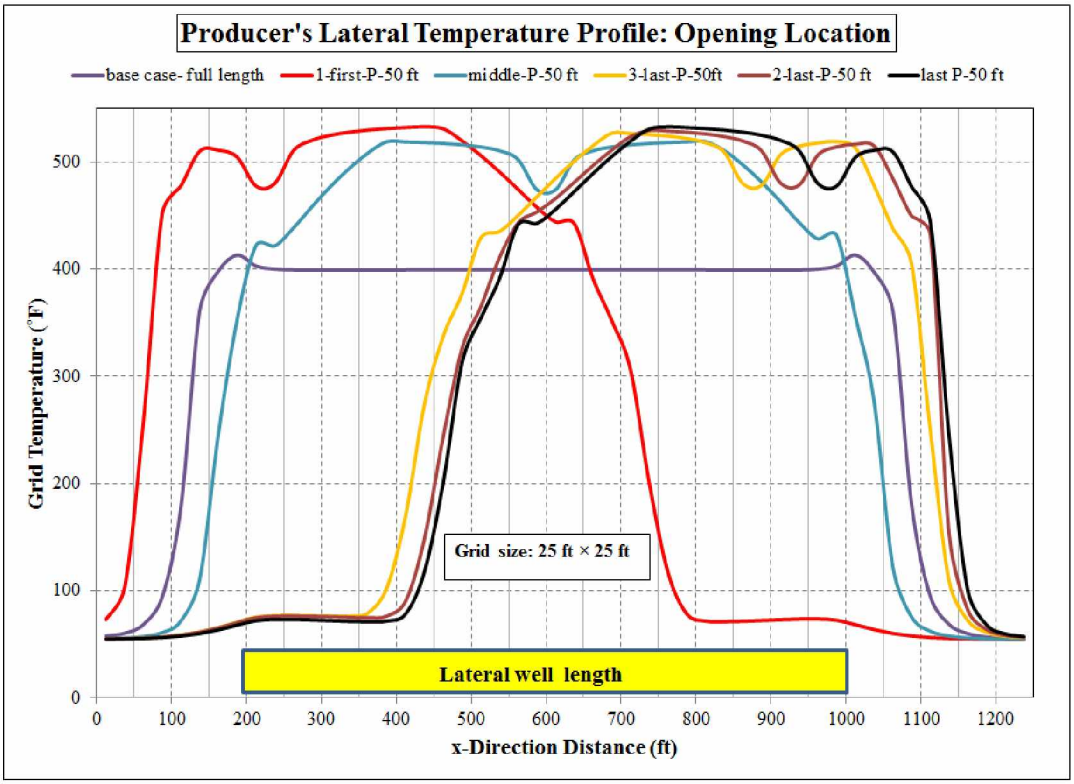

Figure 6-45: Lateral producer well's temperature profile.

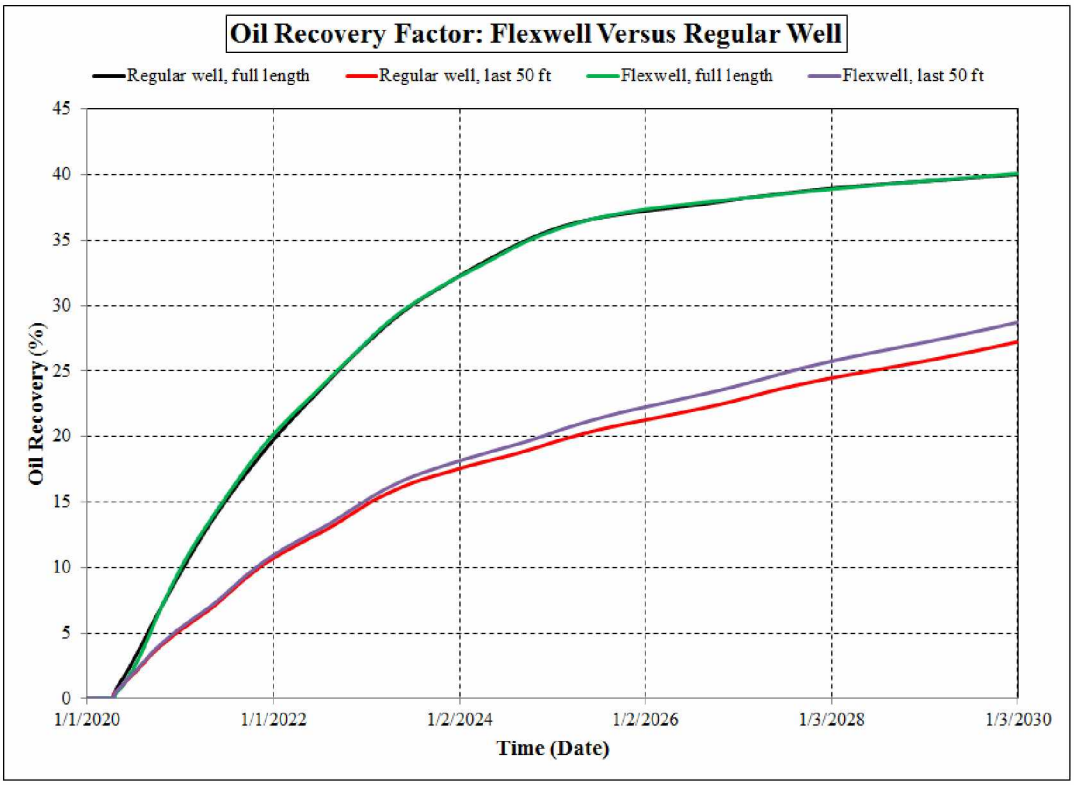

Figure 6-46: Effect of using 'flexwell' on the oil recovery.

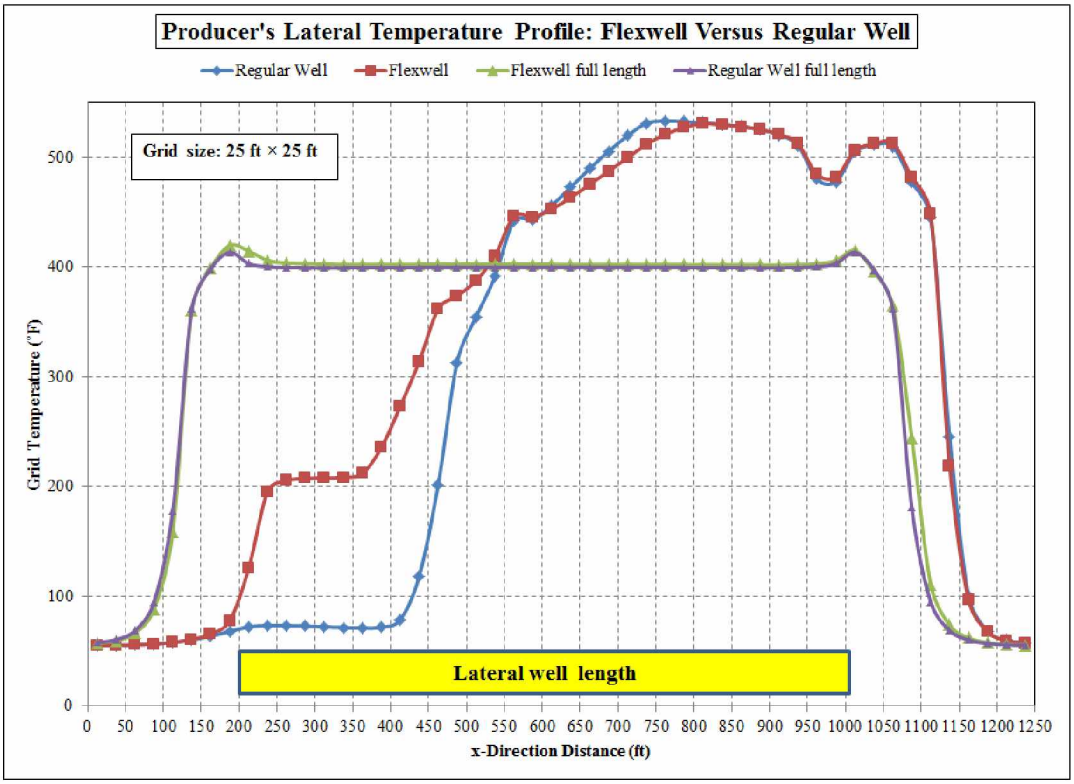

Figure 6-47: Effect of 'flexwell' on the lateral temperature profile.

6.2.10. Effect of Steam Properties

The amount of transferred heat to the reservoir is controlled by the rate of steam injection and its properties (temperature and quality). As the steam generators are designed for steam quality equal to 0.8, this steam quality is used to study the effect of the steam properties on the reservoir performance. The main properties of the models are those mentioned in Table 6-2. A 'flexwell' producer with last 50 ft opening is used in the models. The mass rate of steam is fixed to 500 bbl/day (equivalent water) with BHP of 2000 psi. The scenarios with steam temperature equal to 300, 400, 500, 600 and 700 °F are run. The oil recovery and SOR results are shown in Figures 6-48 and 6-49, respectively.

As it is seen, the steam temperature has a little effect on the oil recovery; however, the oil recovery in cases of steam temperature equal to 500 and 600 F is higher than other cases. By referring to thermodynamic properties of water, the obtained results appear reasonable. A magnified portion of thermodynamic properties of water is depicted in Figure 6-51. For better demonstration, temperature lines of 400, 500, 600, and 700°F are colored. The producer's lateral temperature profile is shown in Figure 6-50. Here again, effect of steam temperature on the producer temperature, especially, well bore temperature is negligible. Therefore, for subsequent simulation models, steam with temperature of 600°F and quality of 0.8 is used; unless stated otherwise.

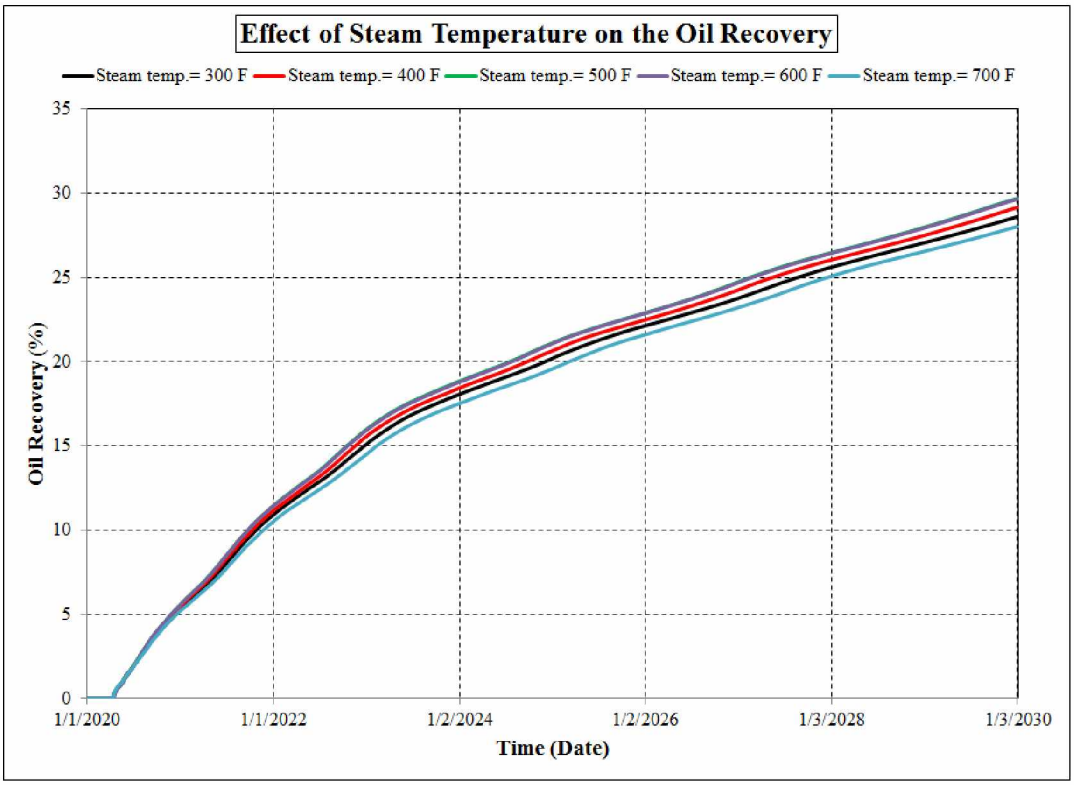

Figure 6-48: Effect of steam temperature on the oil recovery.

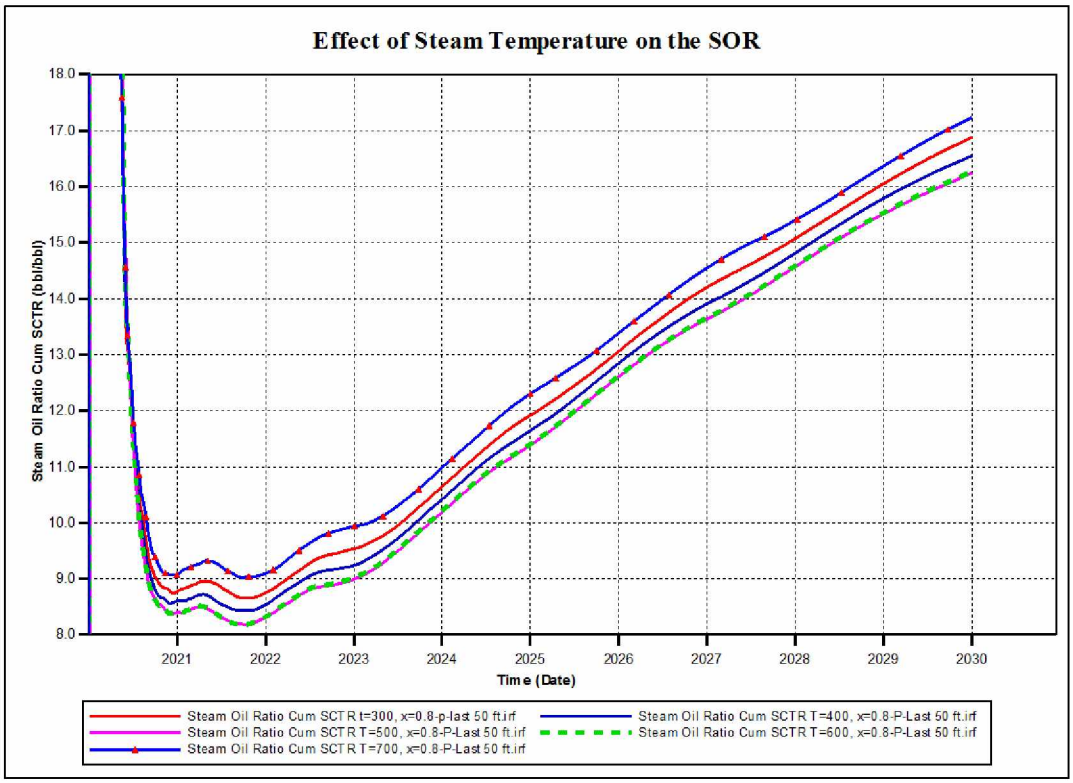

Figure 6-49: Effect of steam temperature on the SOR.

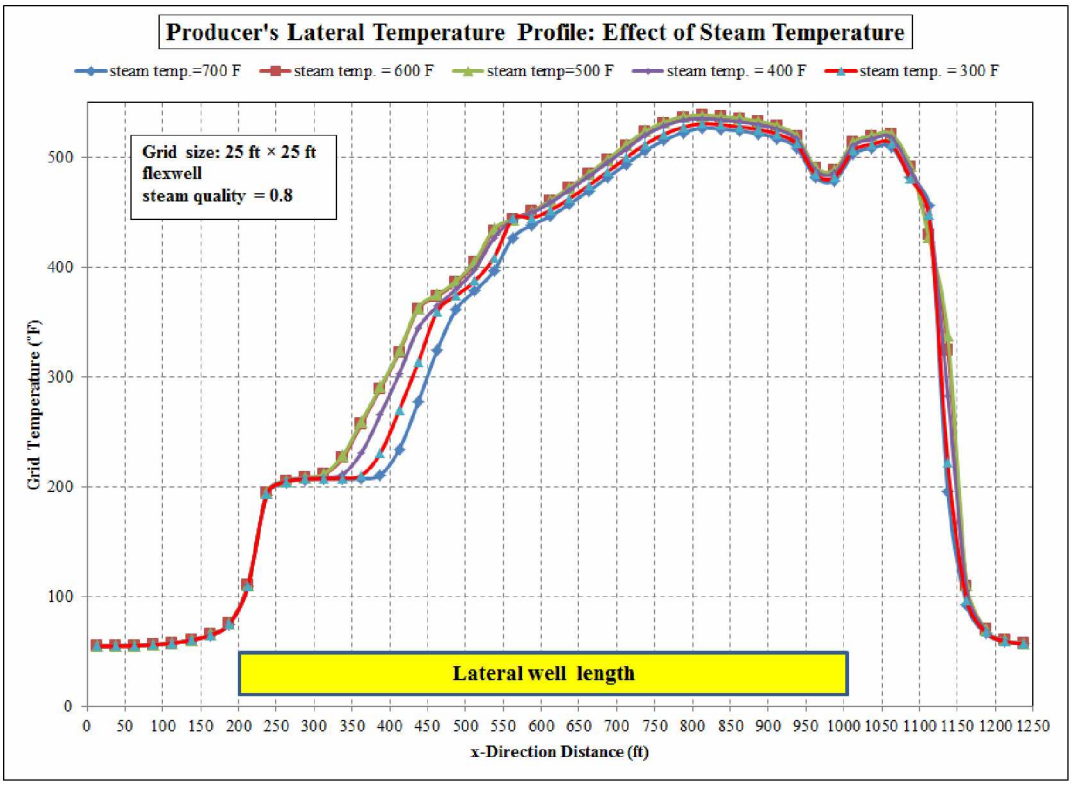

Figure 6-50: Effect of steam temperature on the producer lateral temperature profile.

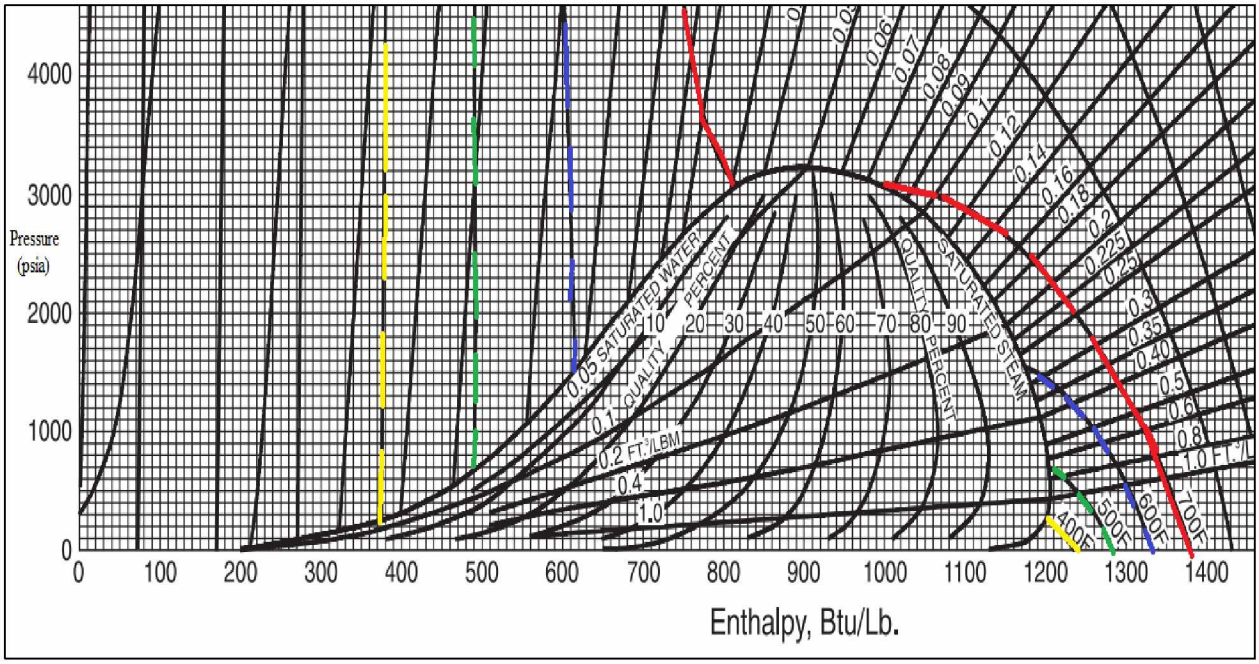

Figure 6-51: Magnified portion of thermodynamic properties of water (original Figure from GPSA, 2004)

6.2.11. Effect of Injector's Well Length Opening

Based on the previous simulation results, it is decided to continue with the producer to be perforated at the last 50 ft out of 800 ft lateral length of the well. Up to this point, it is considered that the entire of 800 ft of lateral length of injector well to be opened to flow. In this section, the effect of opening length of injector well is studied. The well constraints are set as follow:

- Injector: max of BHP = 2000 psi, max well rate = 500 bbl/day (equivalent water),
- Producer: min of BHP = 200 psi, max well rate = 200 STB oil/day.

The lateral well length opens to flow as follow:

- ✓ Producer: last 50 ft out of 800 ft.
- ✓ Injector: 1^{st}, 2^{nd}, 3^{th}, 4^{th}, 5^{th}, 6^{th}, 7^{th}, 8^{th} 50 ft from toe, first 50 ft from heel, 50 of middle of the well length and entire 2^{nd} half of well length.

The results are shown in Figure 6-52. For simplicity, curves of two cases (cases that first and 8^{th} 50 ft from the toe of injector is opened to flow) are deleted. The oil recovery factors for these cases are zero for 10 years simulation. For these cases the injector well is supposed to be perforated in the grids of 'first half' of well length. Based on the results, it is decided to continue the simulation with entire (800 ft) lateral length of injector well to be perforated. This case maximizes the oil recovery for a 10-year simulation period.

In Figure 6-52, similar to Figure 6-37, the oil recovery curves are crossing each other. The explanation is the same as what provided for Figure 6-37. This behavior can also be explained by considering the sweep efficiency of steam injection.

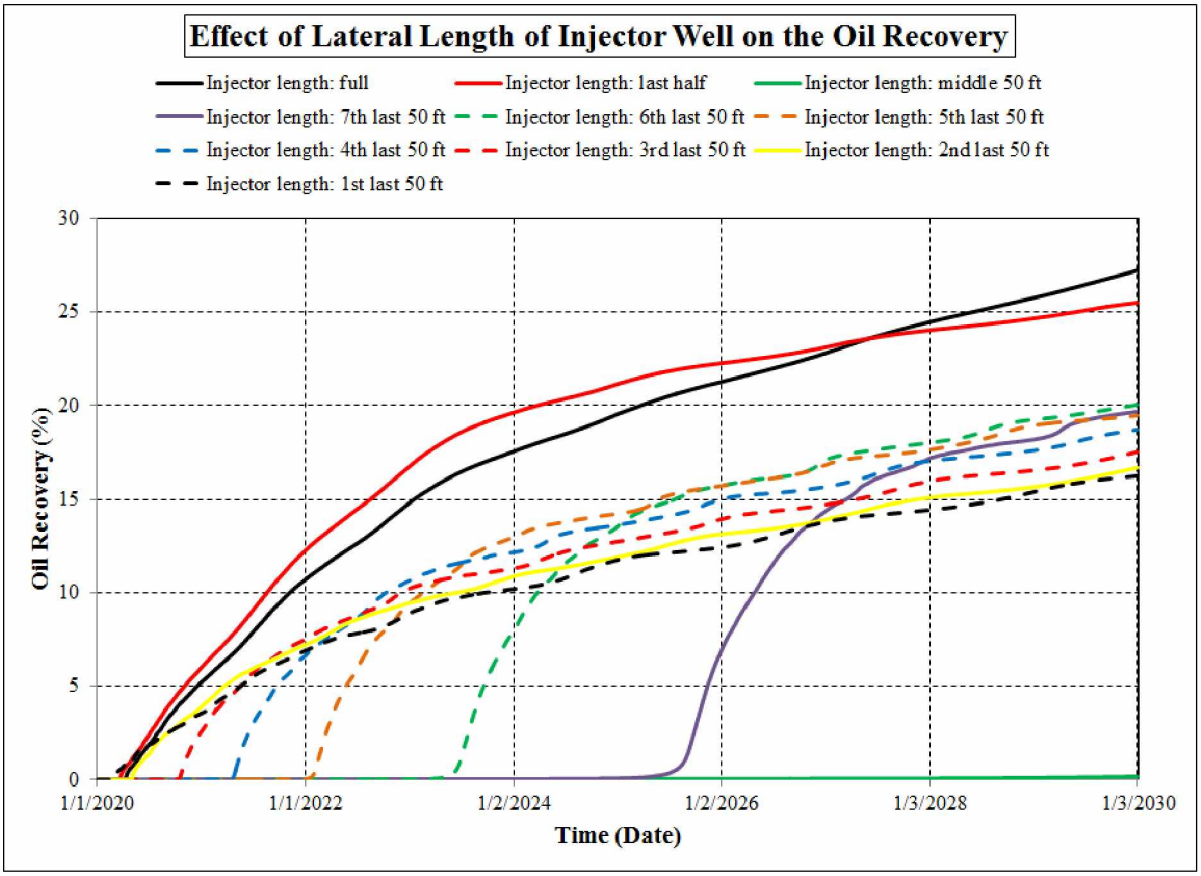

Figure 6-52: Effect of injector's lateral well length opening on the oil recovery.

6.2.12. Effect of Direction of Flow in Injector Well

In all models, it is assumed that the heel and toe of both injector and producer well would be drilled in the same areal grids (but in different layers). To study the effect of location of heel and toe of wells, two models were constructed:

In one case, the regular wells' direction is considered. In this case, the injector and producer wells are drilled in the same direction and the well-heads of the wells are located on the same location. This case is here called 'co-current' drilled-direction case. In the other case, the injector and the producer wells are drilled in opposite direction and the well-heads of wells are located on some distance to each other. This second case is here named 'counter-current' drilled-direction. The STARS' schematics of these two models are shown in Figures 6-53 and 6-54.

With these two models, four scenarios are defined and run:

- ✓ Co-current 50 ft: just 50 ft out of 800 ft of producer well is opened to flow,
- ✓ Co-current full length: entire 800 ft of producer well is opened to flow,
- ✓ Counter-current 50 ft: just 50 ft out of 800 ft of producer well is opened to flow,
- ✓ Counter-current full length: entire 800 ft of producer well is opened to flow,

The summary of results is shown in the Table 6-5. The results do not show any significant difference. The results can be justified by saying that the sweep efficiency is the same for both cases.

Table 6-5: Brief results of 'co-current' versus 'counter-current' well model.

Injection well length= 800 ft in the Middle		
Production well length= 800 ft in the Middle		
SimulationModel	Well-bore temp.	Oil Recovery
Model	(°F)	(%)
Co-current 50 ft	180.8	35.12
Co-current full	413.6	43.55
Counter-current 50 ft	179.8	35.12
Counter-current full	413.6	43.72

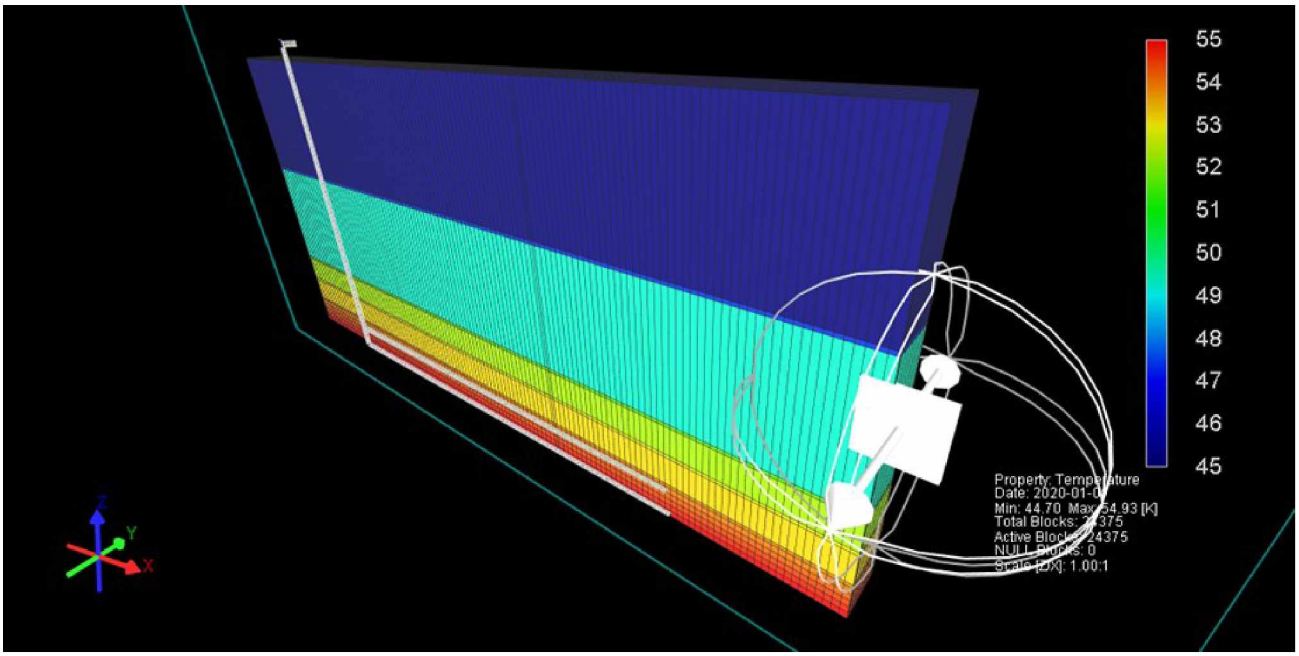

Figure 6-53: STARS' schematic of 'co-current' well model.

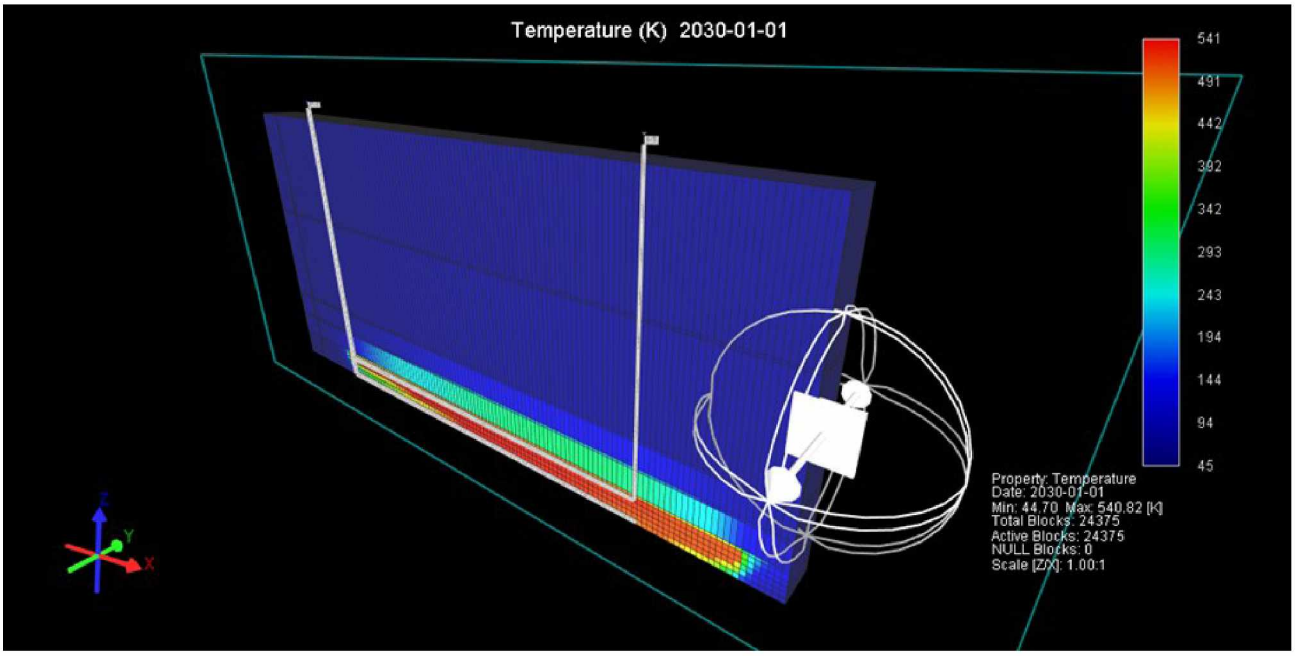

Figure 6-54: STARS' schematic of 'counter-current' well model.

6.2.13. Effect of Injector and Producer Well Lateral Length

The lateral length of both the injector and the producer wells is considered to be 800 ft out of 1250 ft reservoir length. To study the effect of lateral length of producer and injector wells, 6 (six) different sets of simulation models were constructed and run:

1. Lateral producer well length= 1250 ft, lateral injector well length= 200, 400, 600, 800, 1000 and 1250 ft.
2. Lateral producer well length= 1000 ft, lateral injector well length= 200, 400, 600, 800, 1000 and 1250 ft.
3. Lateral producer well length= 800 ft, lateral injector well length= 200, 400, 600, 800, 1000 and 1250 ft.
4. Lateral producer well length= 600 ft, lateral injector well length= 200, 400, 600, 800, 1000 and 1250 ft.

In the above model the producer is drilled from the first block; however, in the following set of models, the producers are drilled in the middle of the reservoir:

5. Lateral producer well length= 800 ft, lateral injector well length= 200, 400, 600, 800, 1000 and 1250 ft.
6. Lateral producer well length= 600 ft, lateral injector well length= 200, 400, 600, 800, 1000 and 1250 ft.

Schematic of two of these sets of models are shown in Figure 6-55. The yellow color indicates the length which is opened to flow and the red color indicates the interval is drilled but is not perforated. The remaining is rock formation.

Based on the well bore temperature and the oil recovery results presented in Table 6-6, the model with producer well length of 800 ft drilled in the middle of the reservoir was selected. The selected model produces more oil (higher oil recovery) and has lower producer well-bore temperature.

In the above models, steam injection rate was set to 500 bbl/day equivalent water. The effect of varying the injection rate was studied by using the selected model.

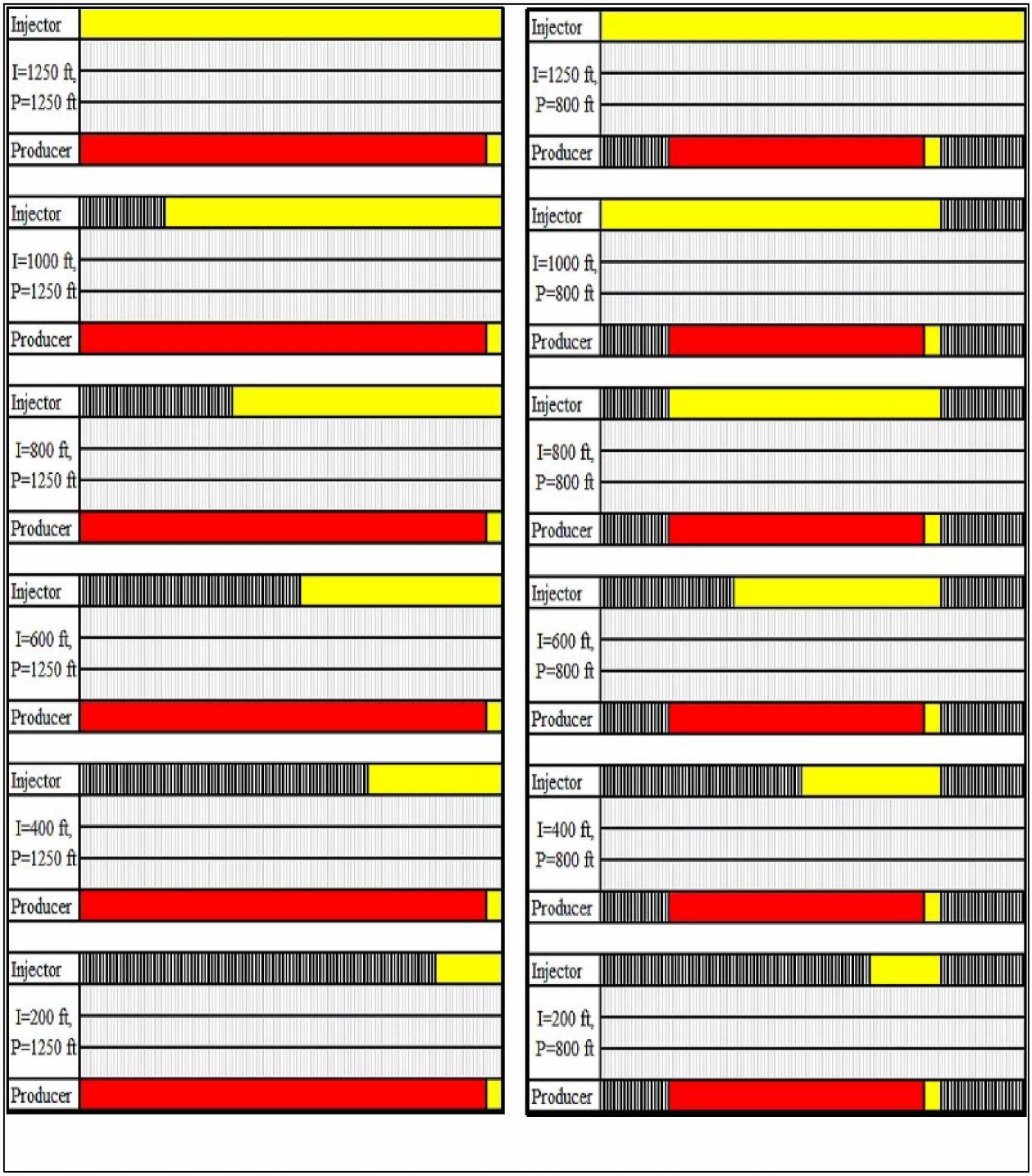

Figure 6-55: Lateral length of injector and producer wells: thickness of each layer = 10 ft.

Table 6-6: Effect of lateral length of injector and producer wells.

Production well length= 800 ft in the Middle		
Inj. Length	Well-bore temp.	Oil Recovery
(ft)	(F)	(%)
200	135.1	22.50
400	136.1	28.08
600	136.1	33.14
800	180.8	35.12
1000	169.8	34.92
1250	145.8	34.95

Production well length= 600 ft (from first block)		
Inj. Length	Well-bore temp.	Oil Recovery
(ft)	(F)	(%)
200	187.7	22.47
400	192.1	27.97
600	491.1	31.88
800	385.4	36.35
1000	344.2	41.59
1250	329.1	44.05

Production well length= 1000 ft (from first block)		
Inj. Length	Well-bore temp.	Oil Recovery
(ft)	(F)	(%)
200	225.185	22.50
400	225.4	28.09
600	226.289	33.19
800	226.1	35.09
1000	231.912	34.92
1250	231.9	34.98

Production well length= 600 ft in the Middle		
Inj. Length	Well-bore temp.	Oil Recovery
(ft)	(F)	(%)
200	196	22.47
400	164.3	28.03
600	358.9	32.97
800	338.1	34.92
1000	300.1	35.34
1250	274.6	38.44

Production well length= 800 ft (from first block)		
Inj. Length	Well-bore temp.	Oil Recovery
(ft)	(F)	(%)
200	187	22.44
400	188.3	28.08
600	188.1	33.11
800	235.2	35.03
1000	195.4	37.46
1250	195.3	42.40

Production well length= 1250 ft (from first block)		
Inj. Length	Well-bore temp.	Oil Recovery
(ft)	(F)	(%)
200	228.3	13.85
400	228.4	19.93
600	227.1	25.60
800	225.4	28.81
1000	226.3	28.95
1250	232.9	28.75

6.2.14. Effect of Injection Rate

In Section 6.2.5.2, the results of study of the effect of injector and producer wells rates on the oil recovery and SOR are presented. In that section a 25 ft × 25 ft model was used for that study. In this section based on the results of previous section, a finer grid model (10 ft × 10 ft) is used to investigate the effect of injection rate on the oil recovery and producer well bore temperature.

Among the models which used in the previous section (section 6.2.13.), the following two models are used to study the effect of injection rate:

- Lateral injector well length= 1250 ft,
- Lateral injector well length= 800 ft,

In both models the lateral producer well length is set to 800 ft and is in the middle of the reservoir. The reservoir length is the same as previous models (1250 ft). The results, oil recovery and well bore temperature, are shown in Figures 6-56 and 6-57. The sudden increase in well bore temperature in Figure 6-57 can be interpreted as propagation of heat waves in the reservoir. By decreasing the lateral length of injector well, the heat waves propagate faster in reservoir. The same phenomenon is encountered and discussed in section 6.2.18. There is a negligible difference between the two models; so, the second model (800 ft lateral length for both injector and producer) is preferred. Shorter lateral length of a horizontal well means lower cost of

drilling. The effect of the injector rate on the well bore temperature after one year is shown in Figure 6-58.

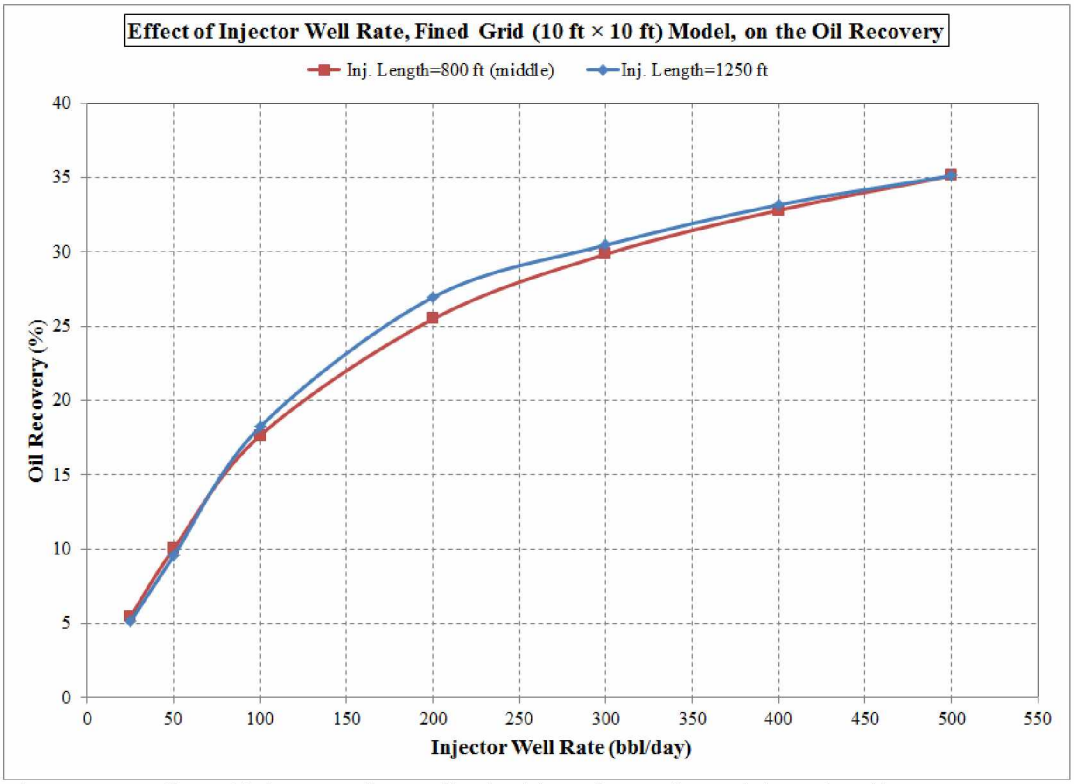

Figure 6-56: Effect of injector well rate [fined grid (10 ft × 10 ft) model] on the oil recovery.

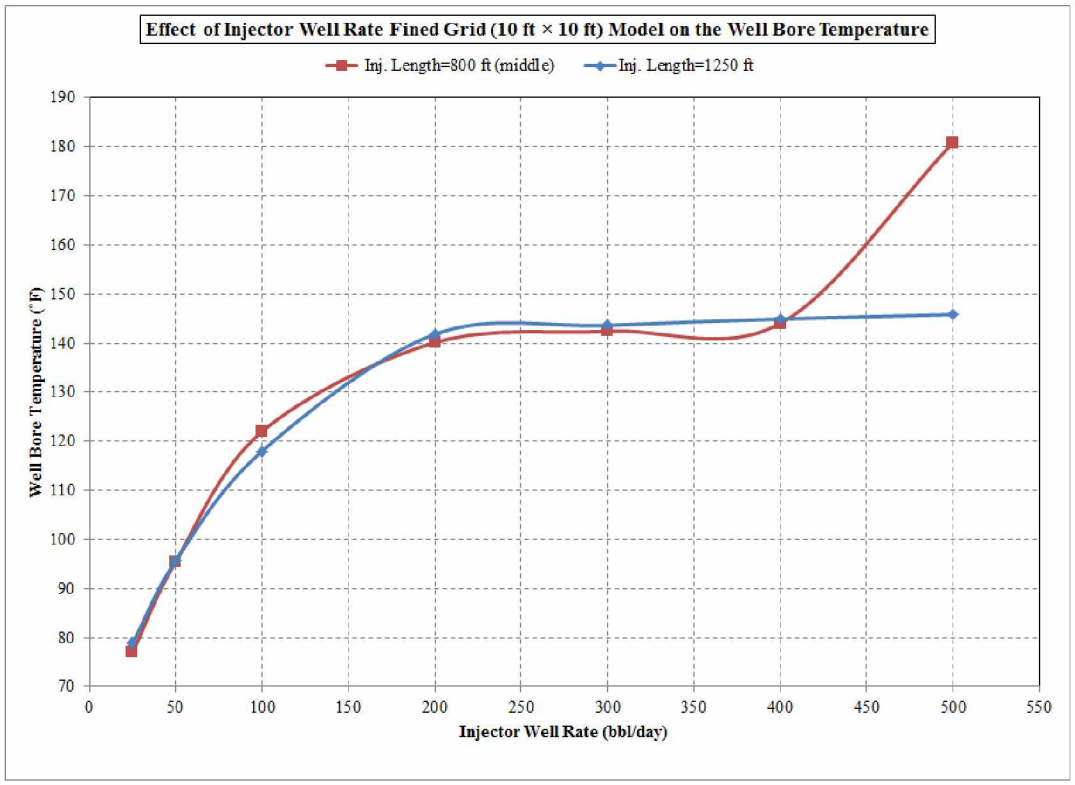

Figure 6-57: Effect of injector well rate [fined grid (10 ft × 10 ft) model] on the well bore temperature.

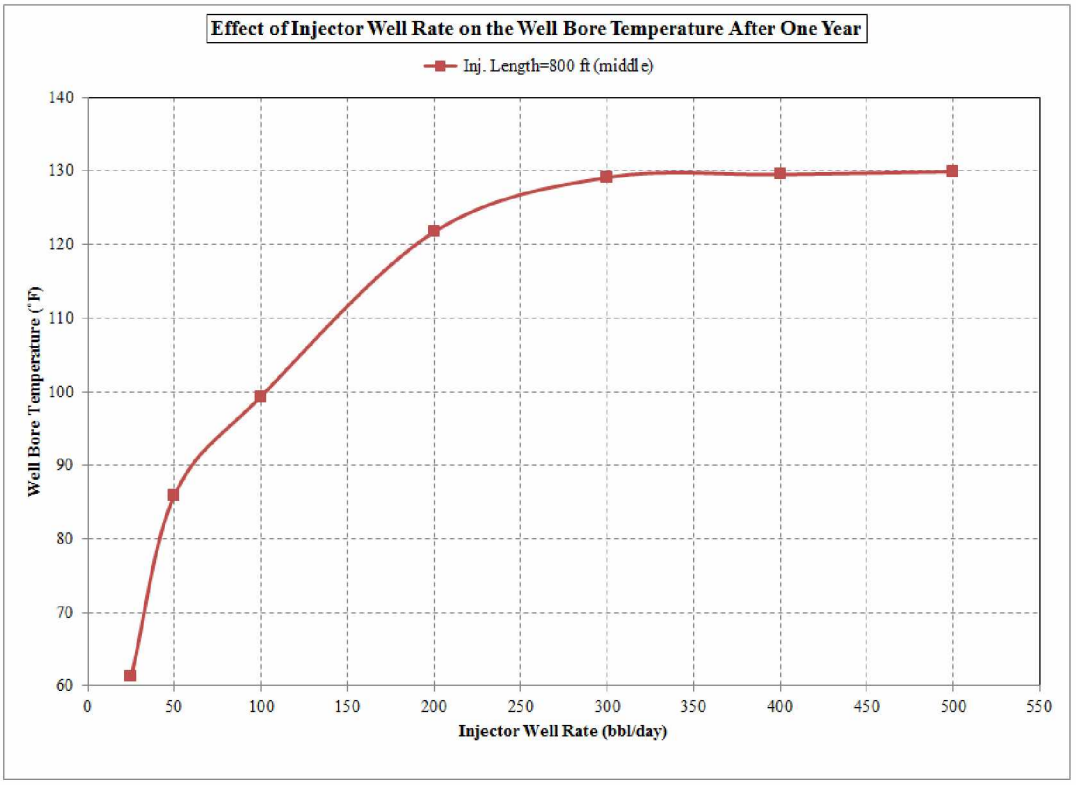

Figure 6-58: Effect of injector well rate on the well bore temperature after one year.

6.2.15. Well Bore Temperature versus Time

The selected model (800 ft injector and producer wells lengths in the middle of reservoir) was used to generate the variation of producer well bore temperature versus time. To better show this variation, the model was run for 30 years. The result is shown in Figure 6-59. Slope variation of curve in different periods of time shows the effect of different 'heat wave' propagation in the reservoir. In the first year of simulation, the slope of increasing temperature is very steep, and after that it flattens out. From Year 8, the temperature starts to increase sharply up to Year 20; after that the slope decreases.

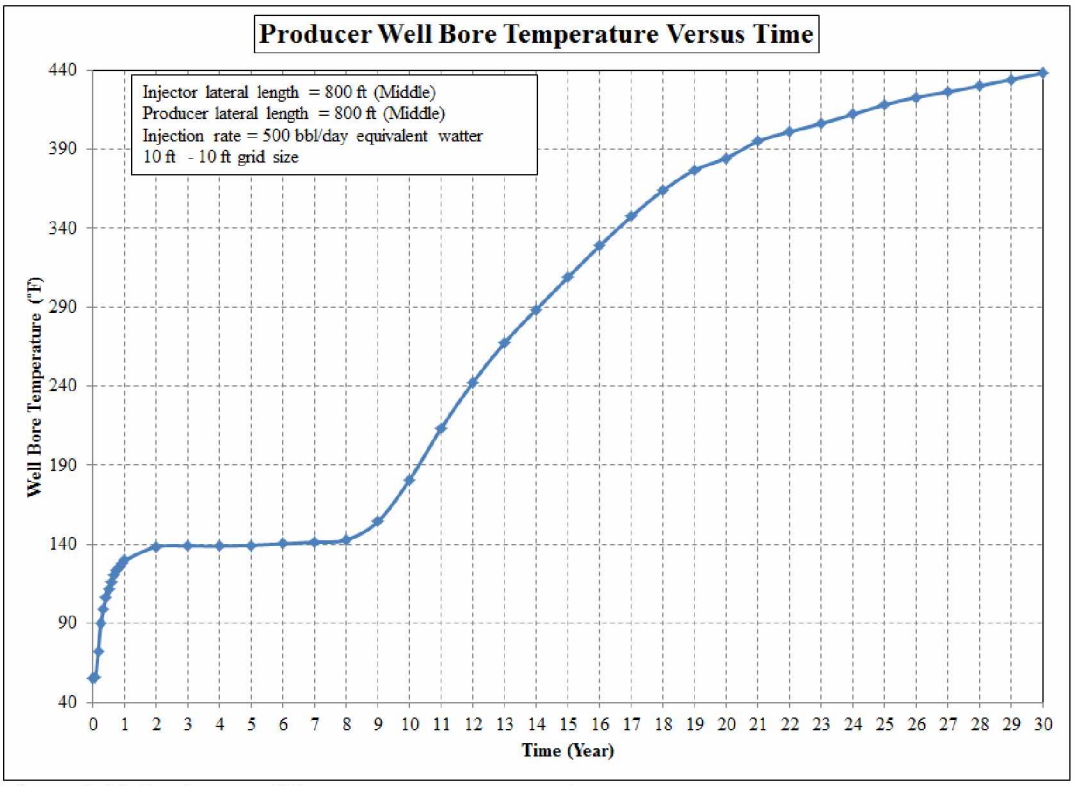

Figure 6-59: Producer well bore temperature versus time.

6.2.16. Effect of Reservoir Thickness

In all the above models, the thickness of the reservoir is considered to be 50 ft. In Section 6.2.8, the effect of changing the vertical thickness between lateral sections of the injector and producer wells layers is studied and the results are presented (for a reservoir thickness of 50 ft and model's

layer thickness of 10 ft). In that section, it is concluded that by increasing the vertical distance between injector and producer model's layers, the oil recovery increases at constant reservoir thickness. In this section, the same model is used; however, the thickness of reservoir is varied. The same areal grid size (10 ft × 10 ft) and same model's layer thickness (10 ft) are used. For clarification, the reservoirs with thickness of 50, 60, 80 and 100 ft are represented by 5, 6, 8 and 10 vertical layers, respectively. In all models, the injector well and producer well are drilled in the first (top most) and last (bottom most) layers, respectively. The oil recovery results are shown in Figure 6-60. The results show an increase in oil recovery by increasing the reservoir thickness for 10 years simulation. However, by increasing the thickness of reservoir the payoff time increases. It means that in a real case, the vertical distance between laterals of the injector and vertical wells should be optimized by considering both oil recovery and the payoff time.

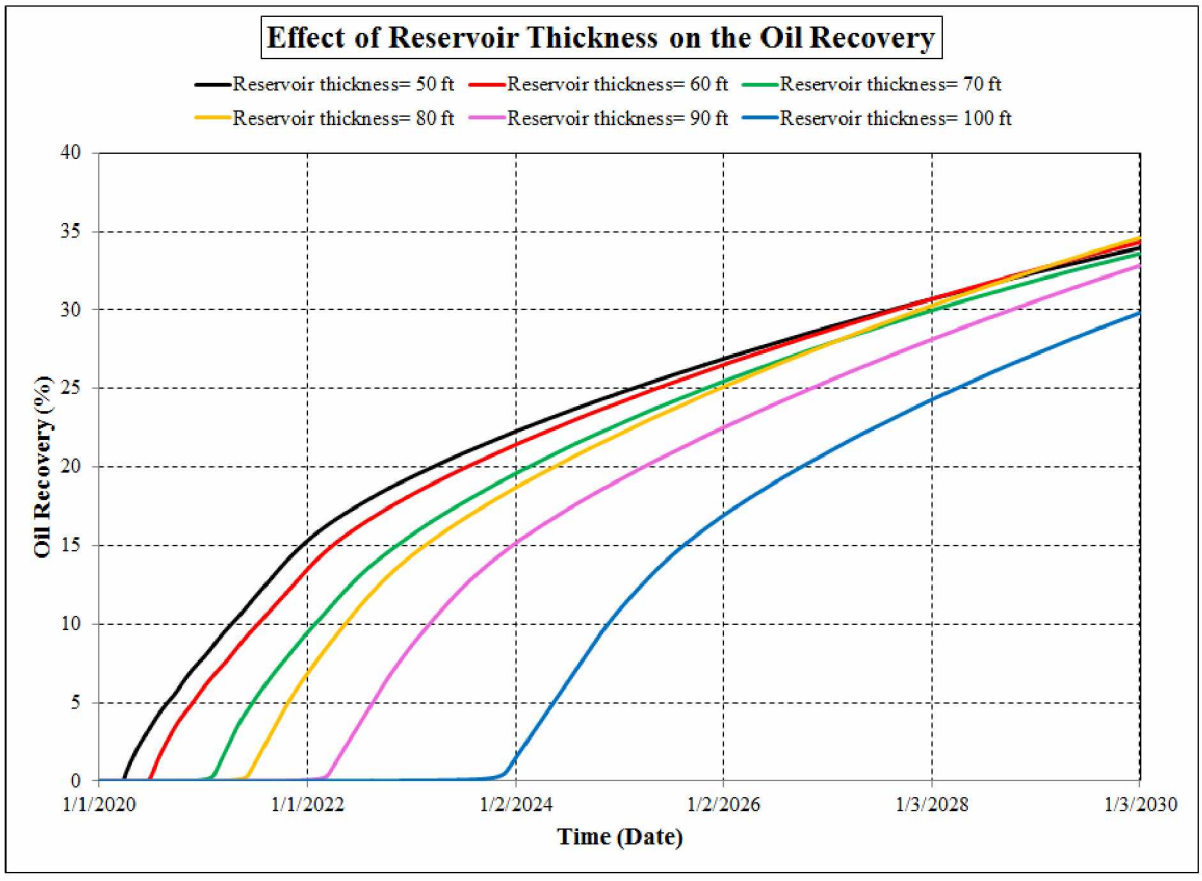

Figure 6-60: Effect of reservoir thickness on the oil recovery.

6.2.17. Effect of Sagavanirktok Sand Formation

The Sagavanirktok sand formation, with varying thickness, separates the Ugnu viscous oil reservoir and the permafrost layer (refer to Figures 4-3 and 4-4). This means that this formation (Sagavanirktok) can act as a 'heat barrier' between the Ugnu reservoir and the permafrost. This sand layer helps dissipate steam injection heat in the oil reservoir before it reaches the permafrost layer. To study the effect of Sagavanirktok sand thickness on the vertical temperature profile, a model with 53-layer was constructed with 10 ft - 10 ft grid size. The model has 99,375 grids (125×15×53). The injector and producer wells were drilled in layers 49 and 53, respectively. The well constraints in this series of models were set as follows:

Injector:

- maximum BHP = 2000 psi,
- maximum steam injection rate = 500 bbl/day equivalent water,
- steam temperature = 500°F
- steam quality = 0.8

Producer:

- minimum BHP = 200 psi,
- maximum surface rate = 200 bbl/day.

The thickness of Sagavanirktok formation is considerably variable, see Figure 2-4. No quantitative values are available. For this reason, various thicknesses for Sagavanirktok sand above the Ugnu reservoir were considered: 500, 400, 300, 220, 200, 180, 140, 130, 120, 110 and 110 ft. The temperature profile of the first layer (adjacent to base of permafrost) at the end of simulation period (10^{th} year) is shown in Figures 6-61. To show better view of temperature variation, the temperature profiles for cases of Sagavanirktok thickness equal to 180, 200, 220, 300, and 500 ft are redrawn and shown in Figure 6-62. To verify the 'bell type' shape of lateral temperature profile of layer adjacent to the permafrost, the lateral temperature profile of a few layers in the case of Sagavanirktok formation thickness equal to 500 ft is shown in Figure 6-63.

With the same layers in all models, the oil recovery for all cases, as expected, is the same. Results show that when the thickness of Sagavanirktok is equal to or greater than 300 ft, the lateral temperature profile of layer adjacent to the permafrost remains constant at its initial condition and this ensures no risk of damaging the permafrost by heat transfer through the subsurface layers when applying steam injection in the Ugnu heavy oil reservoir. Based on the results, steam injection is suggested when the thickness of the Sagavanirktok sand formation is equal to or higher than 300 ft.

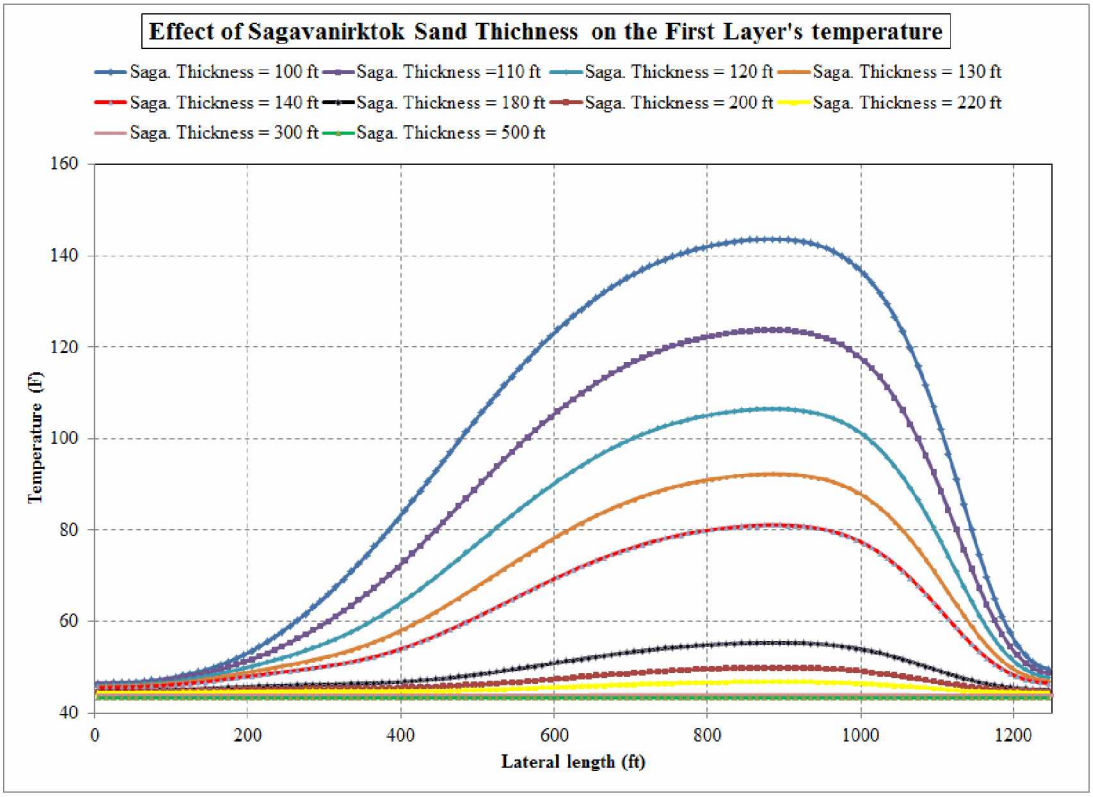

Figure 6-61: Effect of Sagavanirktok formation on the lateral temperature profile of first layer adjacent to permafrost.

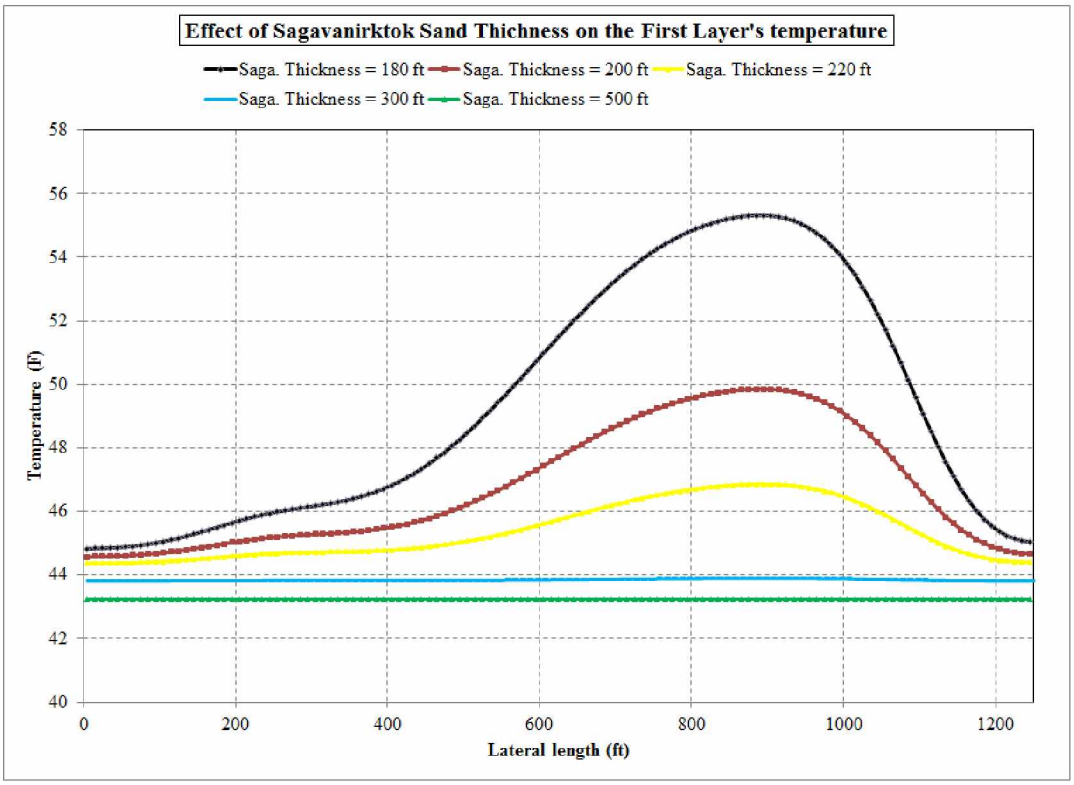

Figure 6-62: Magnified the vertical axis of Figure 6-61.

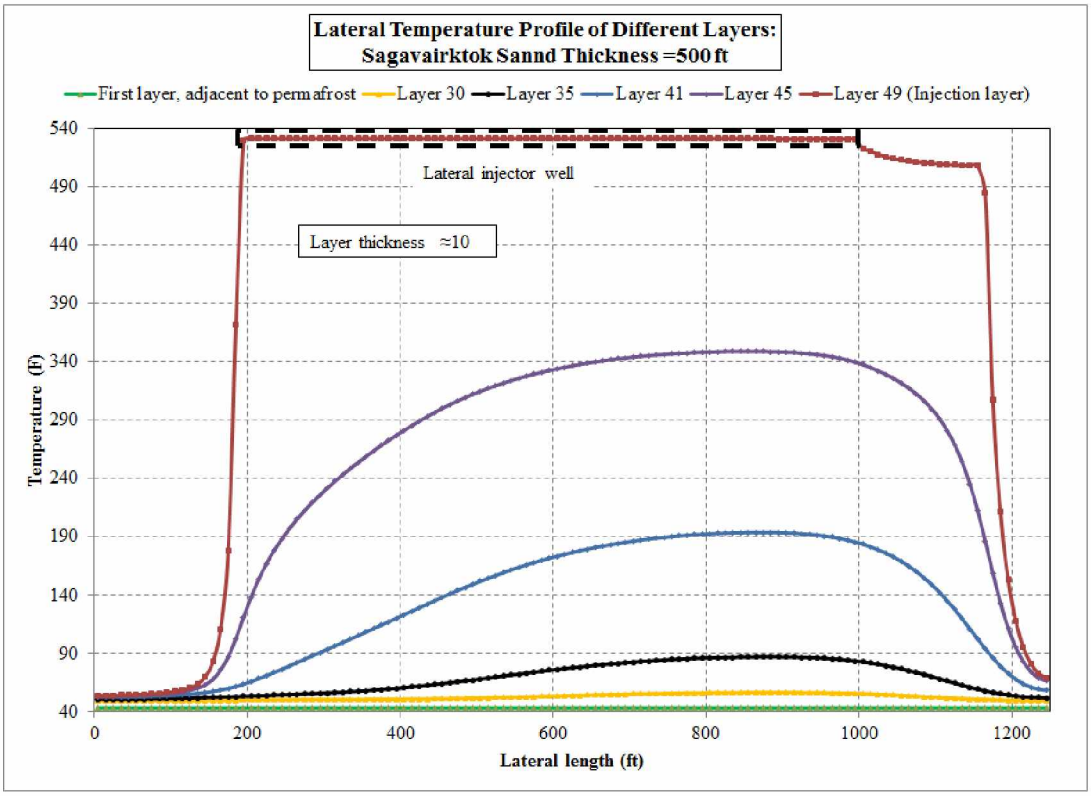

Figure 6-63: Lateral temperature profile of different layer, Sagavanirktok formation thickness = 500 ft.

6.2.18. Final SAGD Model and Results

Based on the results of the sensitivity analyses, a model with following properties was constructed and used for the SAGD process study:

- Reservoir length and width = 1250 ft and 150 ft, respectively,
- Number of layers = 13 layers (as shown in Table 6-2),
- Areal grid block size = 10 ft × 10 ft,
- Maximum BHP of injector well = 2000 psi
- Maximum steam injection = (three cases are considered) 300, 400, and 500 surface bbl/day (equivalent water),
- No nitrogen injection,
- Minimum BHP of producer well = 200 psi,
- Maximum surface oil rate of producer = 200 bbl/day,
- Steam quality = 0.8,
- Steam temperature = 500°F,
- Injector well length = 800 ft in the middle of reservoir (entire length opens to flow),
- Producer well length = 800 ft in the middle of reservoir (last 50 ft of lateral length opens to flow).

For the selected SAGD model, Figures 6-64 through 6-66 show the oil recovery, SOR, and well bore temperature, respectively. The producer well bore temperature is as high as about 140°F, even at the end of the first year of simulation. The temperature profile flattens in the period of 2 to 13 years for different cases, then again starts to increase. This behavior is interpreted as propagation of heat waves in the reservoir. To verify this hypothesis, the lateral temperature profile of the layer above (adjacent to) the producer layer is obtained. The results are shown in Figure 6-67. This figure shows that the temperature of adjacent layer of the lateral of producer well is constant for an interval part of lateral of the well and by increasing the time of simulation (steam injection), this constant-temperature interval gradually decreases and finally vanishes at about 7^{th} to 8^{th} year of simulation.

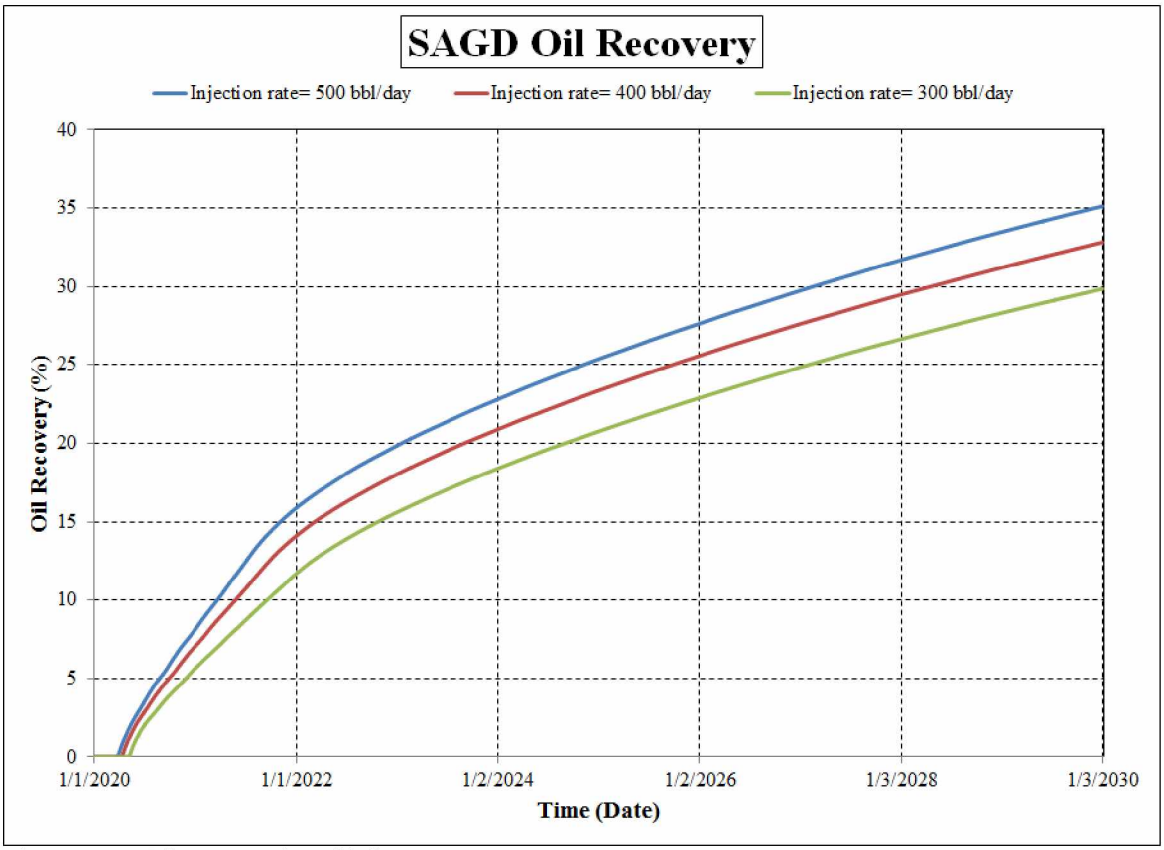

Figure 6-64: Oil recovery in a SAGD process.

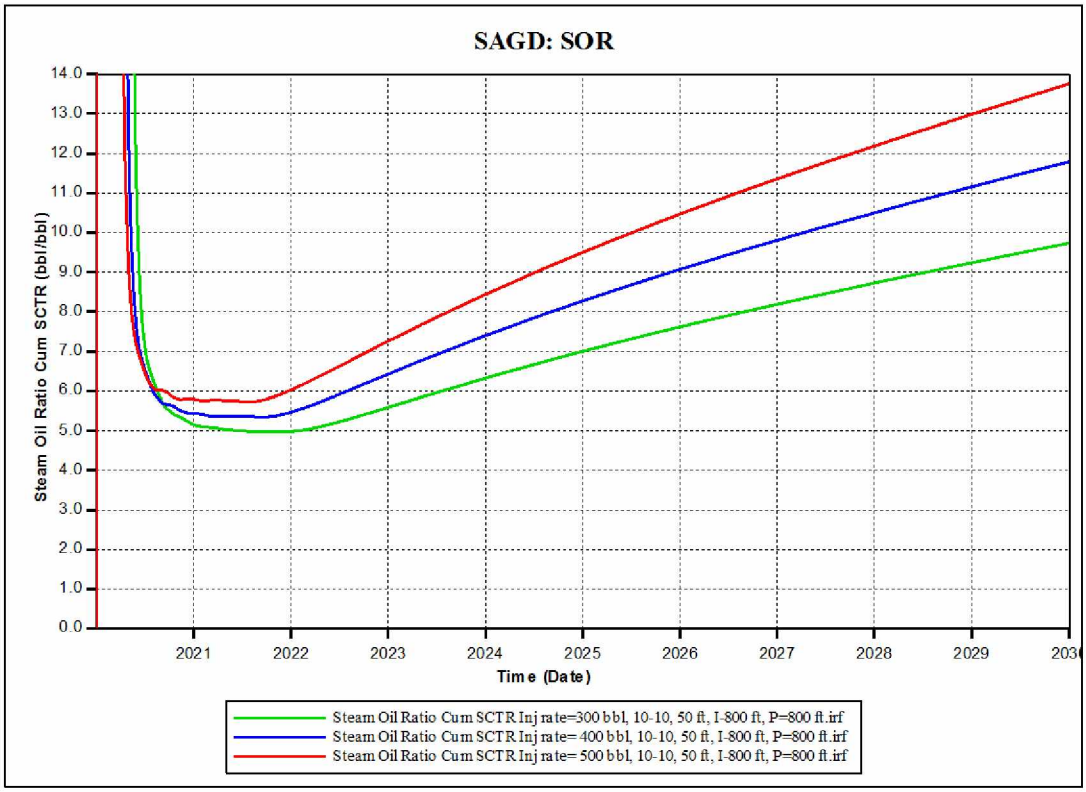

Figure 6-65: Steam Oil Ratio (SOR) in a SAGD process.

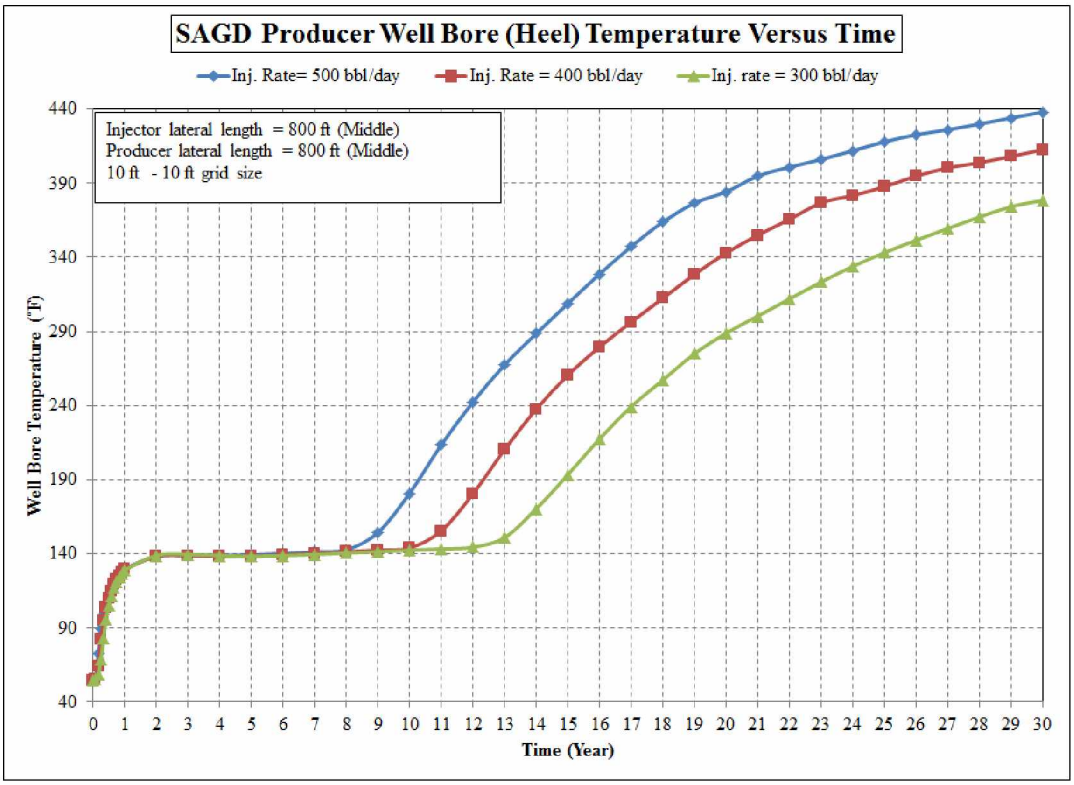

Figure 6-66: SAGD process: producer well bore temperature versus time.

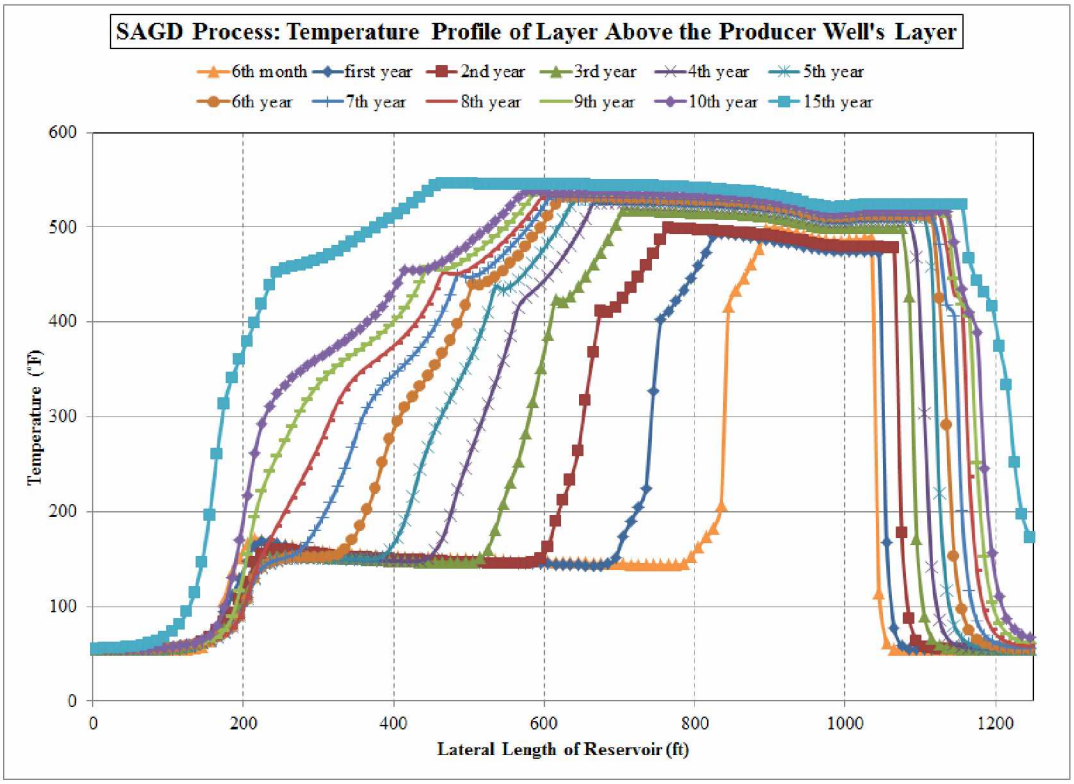

Figure 6-67: SAGD process: temperature profile of layer above the producer well's layer.

6.2.19. Cyclic Steam Assisted Gravity Drainage (CSAGD) Process

In addition to the SAGD process, a Cyclic SAGD process was also examined. In this type of steam injection process, the same model as that described in previous section (for the SAGD process) was employed. The injector and producer wells were drilled in the same layers and the same grids as those in the SAGD process. The lengths of wells considered to be opened to flow are the same as those with the SAGD model, entire length of injector and the last 50-ft of producer open to flow.

In this process the producer well is left 'open' for the entire simulation period; however, the injector well is opened for one month and shut in for different periods of time: 4 scenarios are modeled:

- Injector one month open, 4 months shut in (5-month cycle),
- Injector one month open, 5 months shut in (6-month cycle),
- Injector one month open, 6 months shut in (7-month cycle),
- Injector one month open, 8 months shut in (9-month cycle).

Oil recovery and SOR results are shown in Figures 6-68 and 6-69, respectively. Producer well bore (heel) temperature versus time for these scenarios is shown in Figure 6-70.

Another set of models was constructed and run to study the effect of steam injection rate variation (200, 300, 400, and 500 bbl/day equivalent water) at constant period of injection and shut in time (1 and 4 months, respectively) of the injector well. The results (oil recovery and producer well bore temperature) are shown in Figures 6-71 and 6-72, respectively.

From the temperature graphs the following points can be concluded:

- The well bore temperature is not low enough to use CSAGD process for heavy oil reservoirs located beneath the permafrost.
- In some cases the amount of steam injected is more than the requirement; for this reason, the average wellbore temperature increases versus time. To better illustrate this phenomenon, in Figure 6-72 a portion of each curve is cut and trend line is drawn through it (see Figure 6-73). The slope of these trend lines confirms the conclusion made in this 'bullet'.

- In some cases the amount of steam injected is less than the requirement; for this reason, the average wellbore temperature decreases versus time (see Figures 6-72 and 6-73).
- From the results, one can conclude that there is an optimum injection cycle that stabilizes the producer well bore temperature. For constraints and properties used in the models, the optimum injection cycle is a cycle period around 1-month injection and 4-months shut in for steam injection rate of 400 bbl/day (water equivalent).

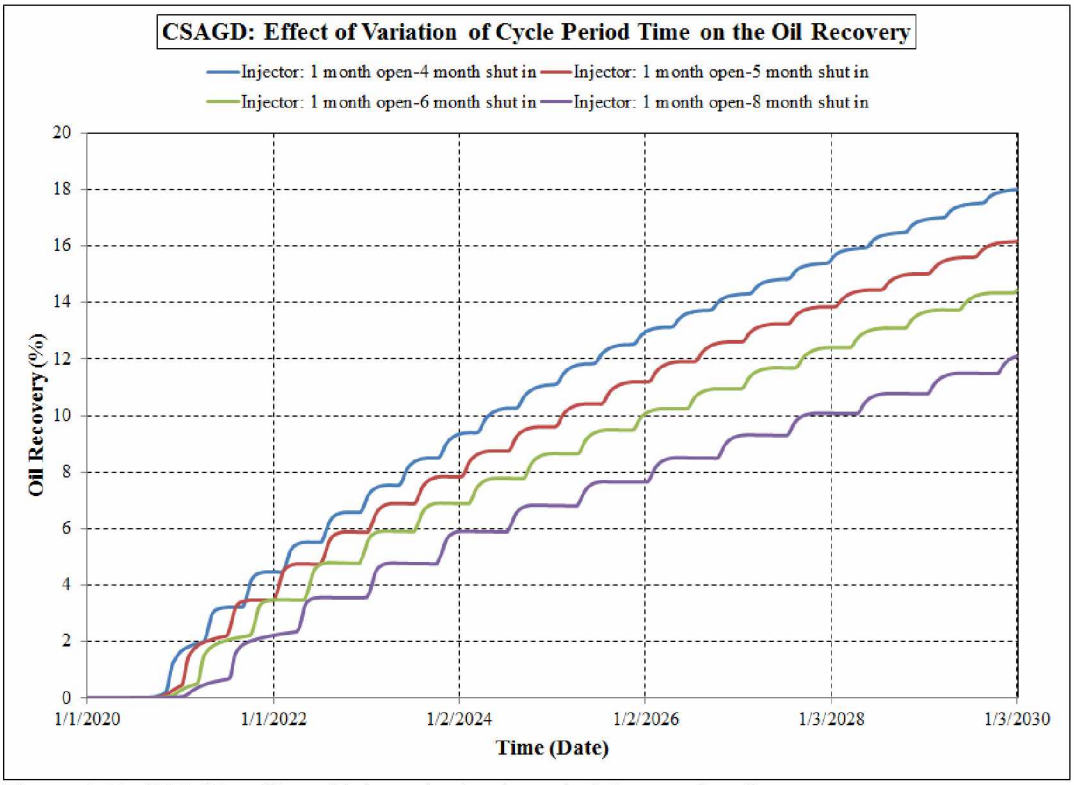

Figure 6-68: CSAGD: effect of injector's shut in period time on the oil recovery.

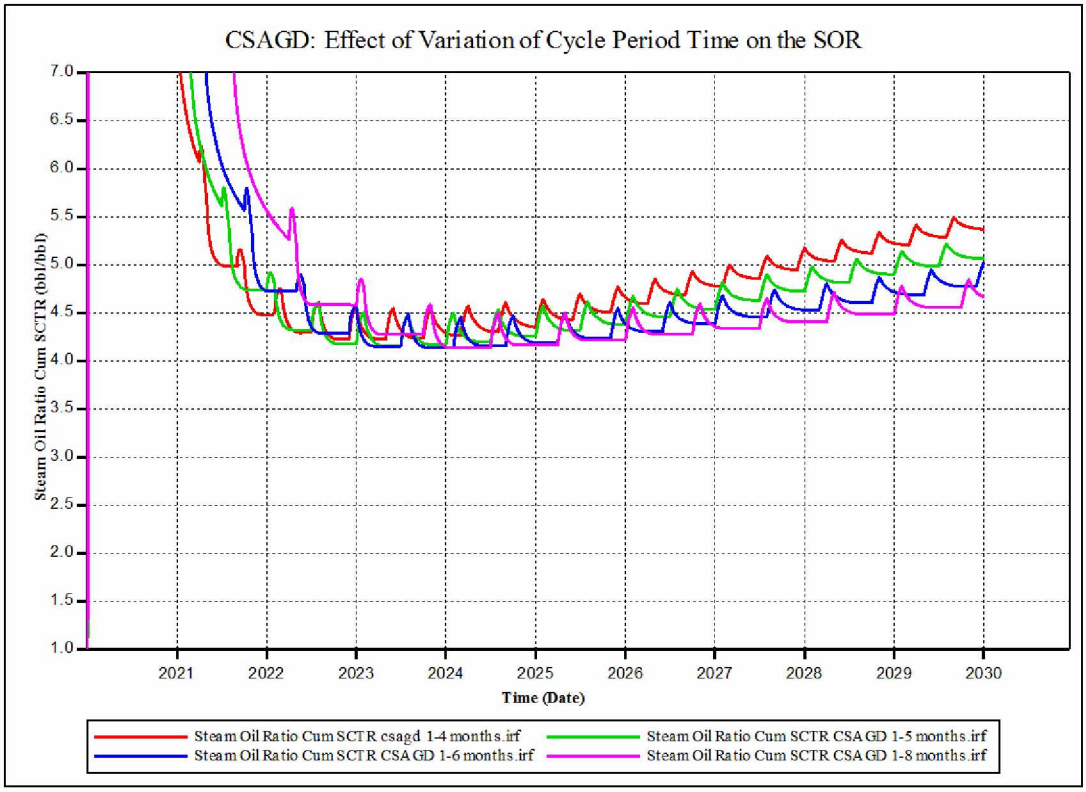

Figure 6-69: CSAGD: effect of injector's shut in period time on the SOR.

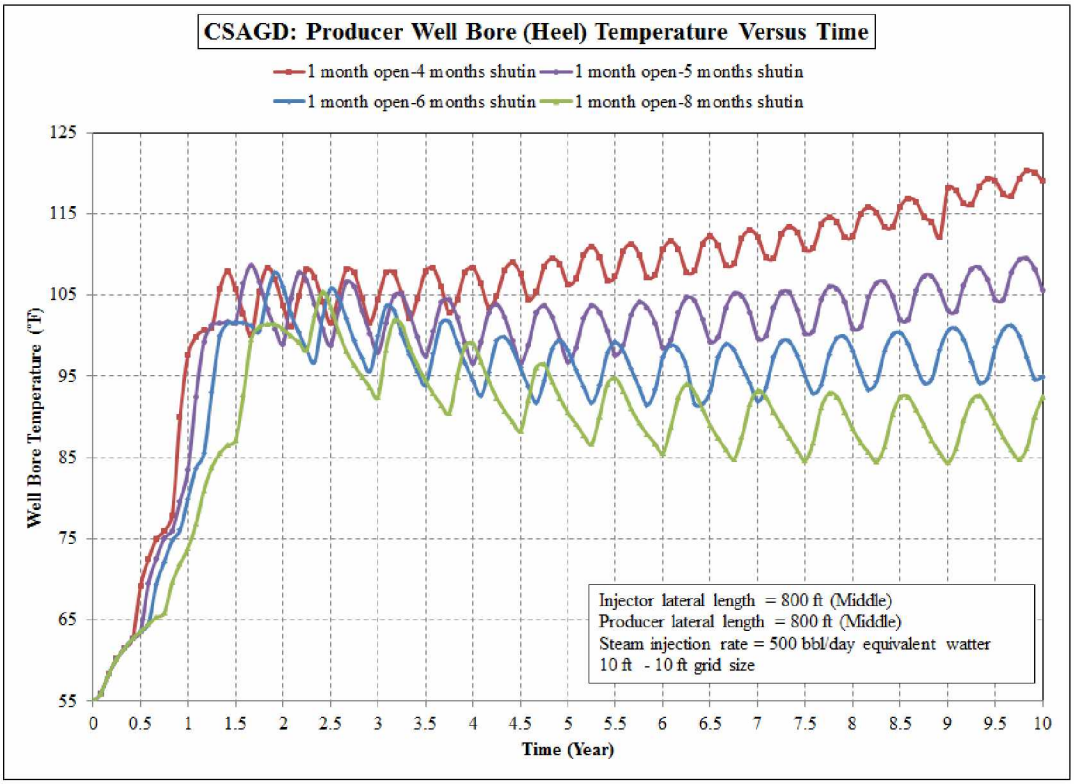

Figure 6-70: CSAGD: producer well bore temperature versus time for different injection cycle period times.

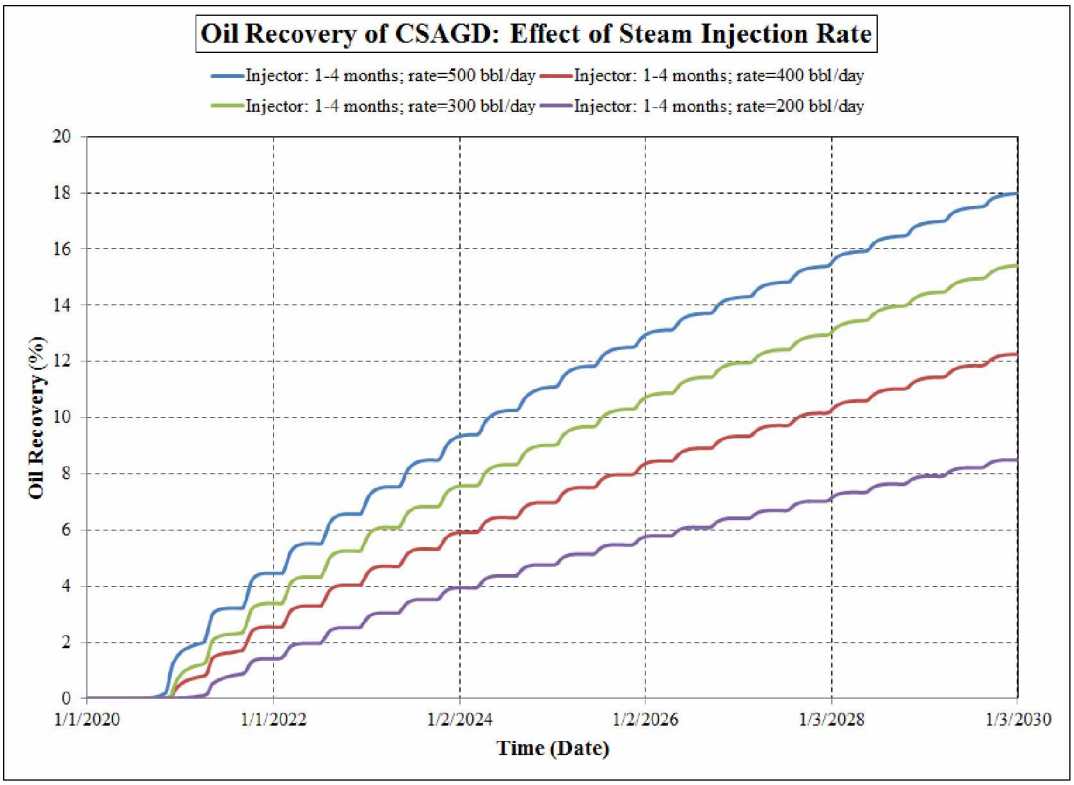

Figure 6-71: CSAGD: effect of injector's steam rate on the oil recovery.

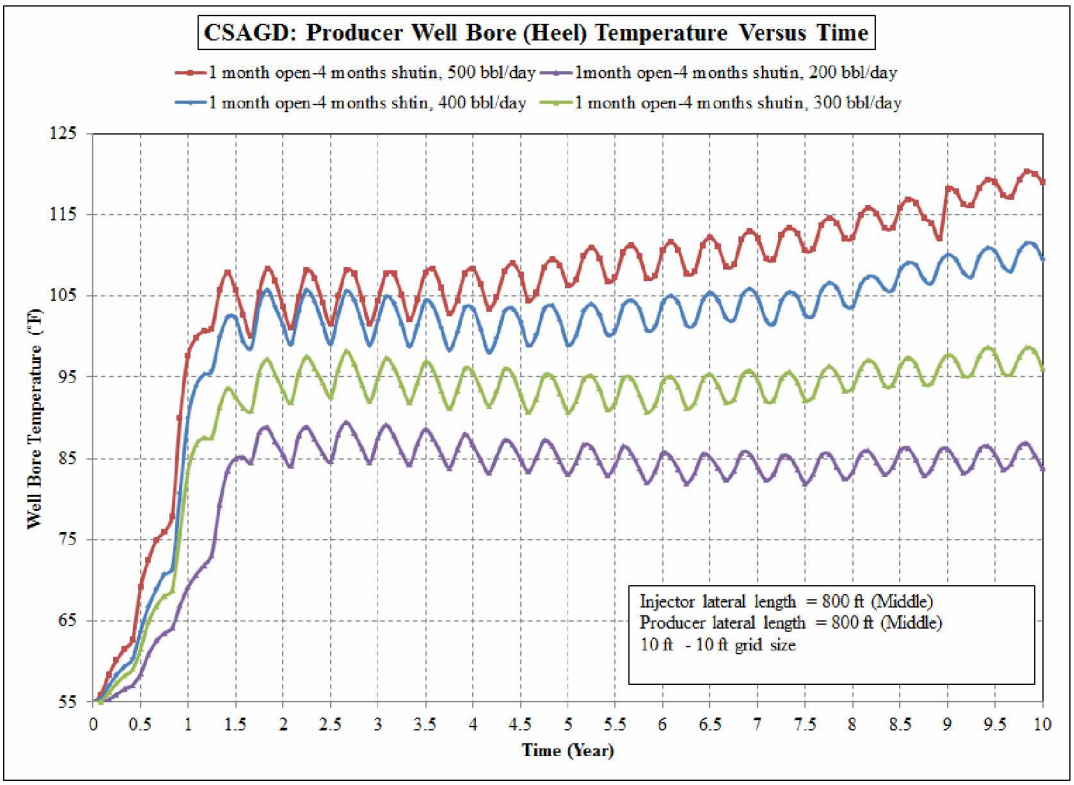

Figure 6-72: CSAGD: producer well bore temperature versus time for different injection rate.

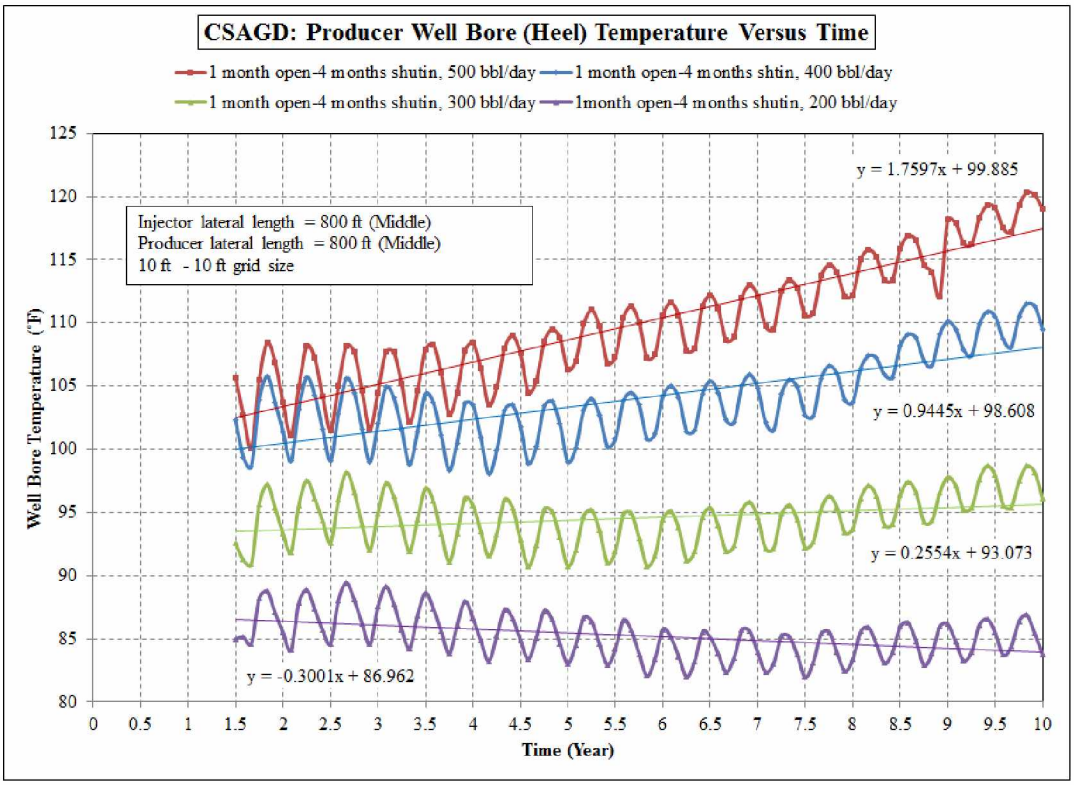

Figure 6-73: CSAGD: producer well bore temperature versus time for different injection rate (trended lines).

6.2.20. Cyclic Steam Stimulation (CSS) Process

In Cyclic Steam Stimulation (CSS), one well is used for injecting steam and for producing the reservoir fluid. For this reason and for economic considerations, in some cases this method is more popular than others. This method is also called Cyclic Steam Injection (CSI) or 'huff and puff.' In this method, there are three periods in each cycle: steam injection, shut in or 'soaking,' and production.

To study the effect of Cyclic Steam Stimulation (CSS), the same model of SAGD was employed; however, a horizontal well drilled in the middle of the reservoir was used as both the injector and producer. The reservoir section of the model had five layers, each 10 ft thick. The well was drilled in the middle layer. In Table 6-2, the middle layer of the simulated reservoir section is layer #11.

Two cases were simulated: (1) the entire lateral length of the well is opened to flow, and (2) the last 50 ft of toe is opened to flow. In the first case, oil recovery was high; however, the producer

well bore temperature was also very high (in the range of 400°F to 500°F). So, the other model was employed: the lateral length of the well was 800 ft, but the last 50 ft of well was open to flow.

In the latter case, with the last 50 ft of toe opened to flow, different scenarios were run:

- 1 month injection, and subsequent month production (1-1month); no shut-in (soaking) period,
- 1 month injection, one month shut in, and one month production (1-2 months),
- 1 month injection, two months shut in, and one month production (1-3 months),
- 1 month injection, three months shut in, and one month production (1-4 months).

Figures 6-74 and 6-75 present the oil recovery and SOR results. In this set of scenarios, the 1-3 month case had the maximum oil recovery. It can be said that by increasing the shut in period, the sweep efficiency of injected steam increases and this increases the oil recovery. However, by increasing the shut in time, the heat loss also increases which means the reservoir's oil receive less heat and this decreases the oil recovery. It seems the 1-3 month case optimizes these two effects: the sweep efficiency of steam and heat loss.

Figure 6-76 shows producer wellbore temperature versus time for the different scenarios.

The 'one month injection, subsequent month production' scenario had the most stable low temperature profile; however, its recovery was low.

In all scenarios, temperature was higher than desired.

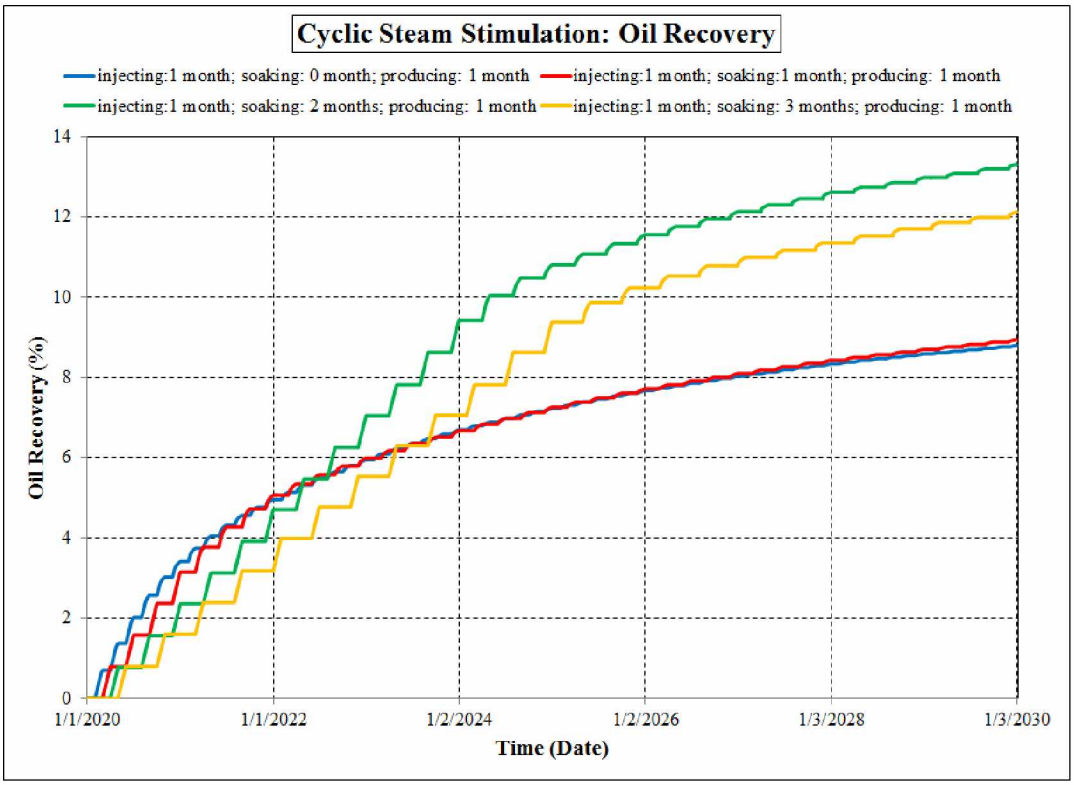

Figure 6-74: Cyclic Steam Stimulation (CSS): oil recovery.

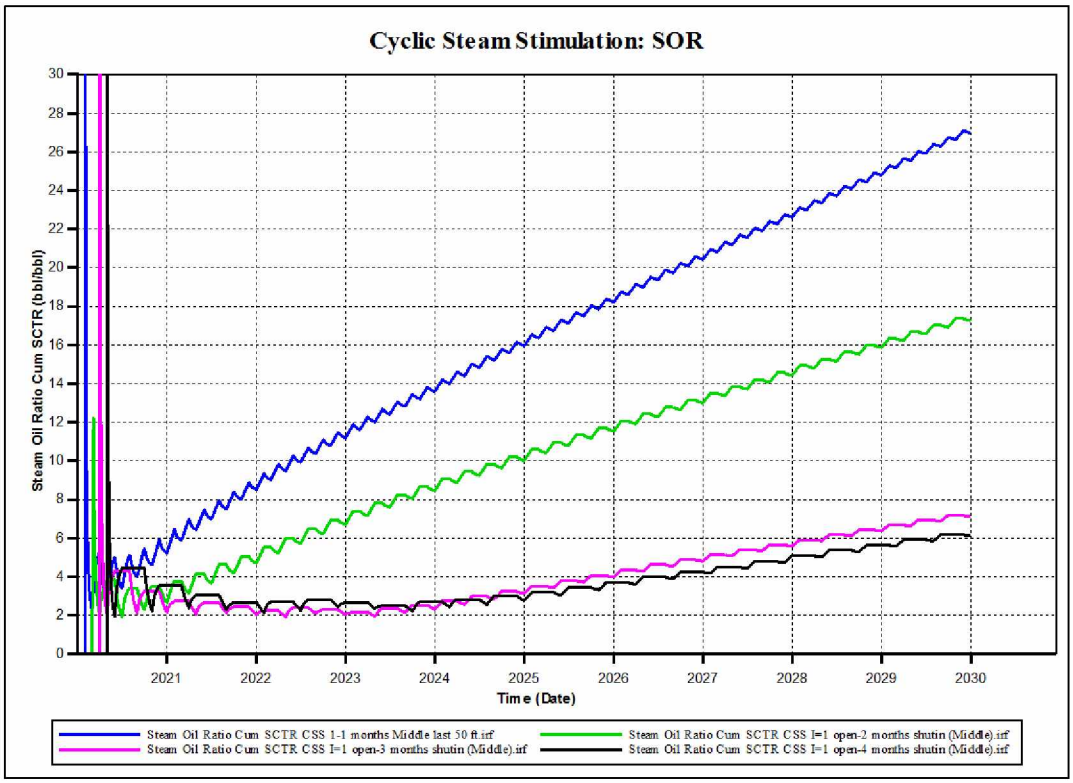

Figure 6-75: Cyclic Steam Stimulation (CSS): SOR.

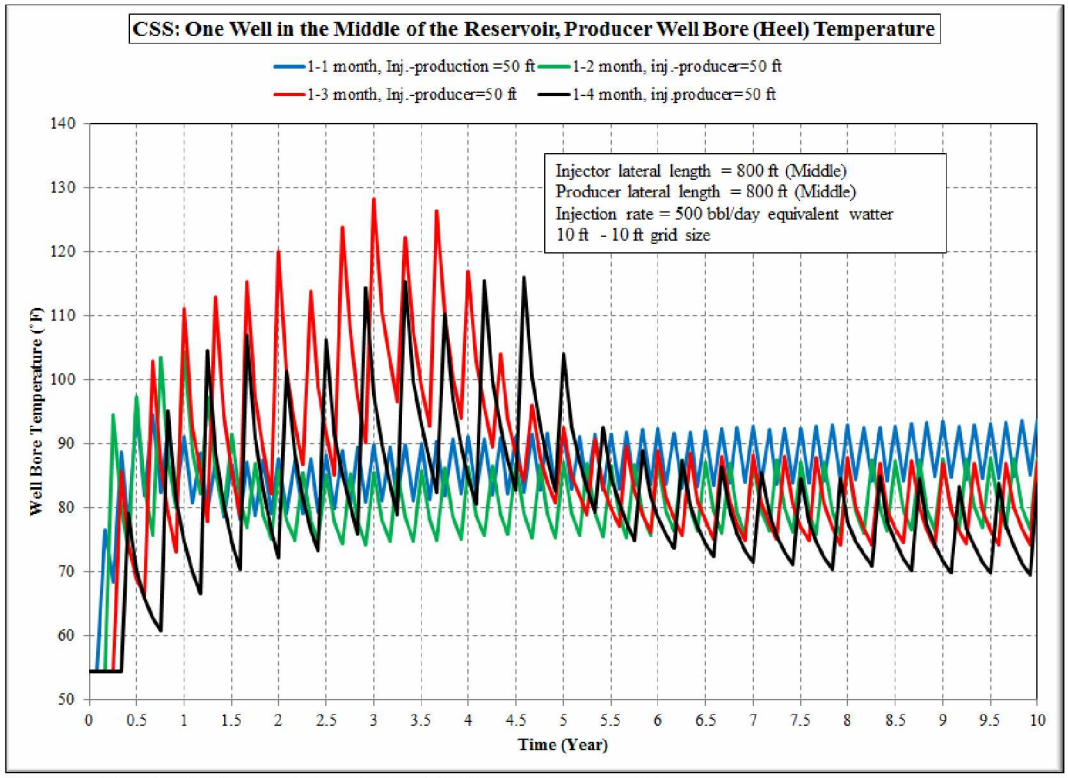

Figure 6-76: Cyclic Steam Stimulation (CSS): producer well bore temperature.

Chapter 7: Discussion

The development of heavy oil reservoirs in Alaska and other arctic regions is a challenging issue. Thermal oil recovery for developing the heavy oil reservoirs is a mature method; however, this method is not easily applicable to Alaskan heavy oil reservoirs because of the presence of a relatively thick permafrost layer. Injection of any hot fluid or producing hot reservoir fluid would have the potential to jeopardize the permafrost.

Applying any thermal method to heavy oil reservoirs which underlie the permafrost can melt this ice bearing layer. Damaging the permafrost can happen in three different locations:

7.1 In the injection well: as the permafrost is a near-surface phenomenon, all injector wells are drilled through the permafrost. By transferring the hot fluid from the surface to down-hole in the injector well, some of heat is transferred from the injected fluid to the permafrost layer. This situation not only causes some heat loss from the injected fluid but also would potentially melt the permafrost interval that is in contact with the casing.

7.2 In the production well: the same phenomenon as in the injection well can happen. Some of heat of the warm reservoir fluid is transferred to the permafrost via the casing and again permafrost starts to melt.

In both types of the wells, the main mechanism of heat transfer is convection. Of course, conduction heat transfer also occurs via the casing, cement and even in the permafrost layer.

7.3 In the reservoir: some of the heat which is transferred to the reservoir rock through the injection of hot fluids or in-situ heat generation would potentially be lost to adjacent layers. This happens by heat conduction. Part of this type of heat loss can potentially reach the permafrost layer and cause the permafrost to melt. This type of damage can be very harmful because of the extent of the affected area and also because it cannot be easily monitored.

The main objective of this thesis was to examine the feasibility of using a new method of down-hole heat generation to develop the heavy oil reservoirs of the Alaskan North Slope. The inventor of this new technology has claimed that the products of the catalytic chemical decomposition will be steam and nitrogen. The results of this thesis can also be applied to any down-hole steam generation technology.

By using down-hole heat generation, the risk of heating the permafrost via the casing of injection well will be eliminated. To address two other potential sources of damage of permafrost, the following criteria were set:

- Monitoring the well-bore (down-hole) temperature of the producer well,
- Monitoring the temperature of the closest layer to the permafrost which can implicitly be considered as the base of permafrost.

Applying a down-hole steam injection for developing the heavy oil reservoir(s) of Alaska is considered to be feasible if the temperatures of both these two points at the end of simulation period stay as close as to their static temperature as possible. It ensures no heat transfer to permafrost either in production well by convection or in the reservoir by conduction.

In regard to the type of hot fluid injected into the reservoir, the main difference between the new down-hole heat generation technology and conventional down-hole steam injection is the simultaneous injection of steam and nitrogen. To address the effect of the addition of nitrogen to the injected steam, several scenarios were defined and run, with different proportions of steam-nitrogen mixture considered.

Two main heavy oil resources are available in Alaska: West Sak viscous oil reservoir with oil viscosity less than 300 cP (see Table 4-2) and Ugnu heavy oil reservoir with live oil viscosity even more than 50,000 cP (see Table 4-1). As the West Sak reservoir is under development using different Enhanced Oil Recovery (EOR) methods, the Ugnu oil reservoir is considered a target for studying the feasibility of using down-hole heat generation.

7.1 Vertical versus Horizontal Wells

The drilling and completion of a vertical well is cheaper than that of a horizontal well. For this reason, vertical wells are favored in any development plan. In the project detailed by this thesis, the performance of vertical wells was studied by use of a 1-D flow reservoir simulation model. Here, the oil recoveries of a two-well (one injector and one producer) model under natural depletion and steam injection are compared. Results showed steam injection to be more effective if the down-hole distance between injector and producer is less than 500 ft (see Figure 6-7). This means that to develop a giant heavy oil reservoir such as Ugnu, a great number of vertical wells

would be necessary. So, it seems that the use of vertical wells is not economical. For this reason, horizontal wells were considered for further simulation studies.

7.2 The Temperature of the Closest Layer to the Permafrost

The Sagavanirktok sand formation lies between Ugnu reservoir and permafrost. The Sagavanirktok formation varies in thickness and can potentially act as a heat barrier during application of any type of steam injection on the Ugnu heavy oil reservoir. To effectively prevent heat transfer, the heat barrier thickness should be greater than some value. A 53-layer 3-D reservoir simulation model was used to estimate the minimum Sagavanirktok thickness needed to ensure that no heat reaches the permafrost when steam injection is applied on the Ugnu formation. In the range of reservoir rock and fluid properties used in the simulation model, this minimum thickness was estimated to be around 300 ft.

No direct data about the Sagavanirktok formation's range of thickness variation where it overlies Ugnu reservoir are available. But based on the data of Figure 2-4, the minimum thickness of Sagavanirktok in this area seems to be more than 300 ft. So, with application of the steam injection method on Ugnu reservoir, no substantial heat should reach the permafrost by transfer through the Sagavanirktok sand formation.

7.3 Producer Well-Bore Temperature

3-D simulation flow models with one horizontal injector well and one horizontal producer well were used to investigate the effect of steam injection in a heavy oil reservoir with PVT properties similar to that of Ugnu reservoir. After running the following sensitivity analysis on the simulation model, an optimal model was selected to study Steam Assisted Gravity Drainage (SAGD), Cyclic SAGD, and Cyclic Steam Stimulation (CSS) methods.

- Rock Thermal Properties
- Optimization of grid block size
- Effect of BHP of producer well
- Effect of BHP of injector well
- Effect of wells rate

- Effect of K_V to K_H Ratio
- Effect of absolute permeability
- Effect of vertical distance between horizontal leg of injector and producer wells
- Effect of producer's length opening
- Effect of Steam Properties
- Effect of injector and producer wells lateral length
- Effect of direction of flow in injector and production wells (counter current versus co-current flow).

In the SAGD process, the producer well-bore temperature increases above 140°F until about the end of the second year of simulation, flattens in the period of 2 to 13 years for different cases, then again starts to increase (see Figure 6-66). This phenomenon can be attributed to the rate of propagation of heat waves in the reservoir. The rate of heat wave propagation depends on the rate of steam injection. By increasing the steam injection rate, the flattened portion of the temperature profile is shortened (see Figure 6-66).

In the literature, nothing can be found about CSAGD. This term is used here for a special case of the SAGD process. In the SAGD method, both horizontal injector and producer wells are continuously opened. However, to decrease the well-bore temperature of the producer as much as possible, the injector well has been opened and shut in cyclic periods; however, the production well is continuously opened. This particular method of SAGD is called Cyclic SAGD (CSAGD). The well-bore temperature of the producer in CSAGD is less than that of CSAGD but more than the desired static reservoir temperature. In CSAGD, in some cases studied the amount of steam injected was more than the requirement, and for this reason the average wellbore temperature increases versus time. In other cases, the amount of steam injected was less than the requirement and the average wellbore temperature decreases versus time (see Figures 6-72 and 6-73). So, it can be concluded that there is an optimal injection cycle that stabilizes the producer well-bore temperature. For the constraints and properties used in the models for this project the optimal injection cycle period was approximately 1-month injection and 4-month shut-in for steam injection rate of 400 bbl/day (water equivalent).

In Cyclic Steam Stimulation (CSS), the same well that is used for injecting steam is used to produce the reservoir fluid. Figure 6-74 presents the oil recovery for the CSS method. From the results, it can be judged that by increasing the shut-in period, the sweep efficiency of injected steam increases and that this increases the oil recovery. However, by increasing the shut-in time, heat loss also increases, which means the reservoir's oil receives less heat and oil recovery decreases. In the range of the simulation model constraints and rock and fluid properties, oil recovery is maximized in a '1 month injection, 2 months shut in, 1 month production' scenario. In all CSS method scenarios, temperature was higher than desired.

It is worth mentioning that the 10-year simulation period oil recoveries for SAGD, CSAGD, and CSS cases were approximately 35%, 18%, and 12%, respectively.

7.4 Adding of Nitrogen to Injected Steam

As mentioned, the products of the discussed new down-hole heat generation technology are steam and nitrogen. One reservoir simulation model was constructed to study the effect of adding nitrogen to the injected steam. The results showed negative effect on oil recovery and negligible effect on the temperature profile. This negative effect can be related to the decrease in sweep efficiency of steam due to the presence of non-condensable nitrogen gas. Nitrogen gas can block some of the reservoir pores and prevent the availability of these pores to the injected steam.

7.5 Cooling the Producer Well String

This study revealed that although one can reduce the well-bore temperature of the producer by considering some provisions (such as perforating a short interval of the toe of a long horizontal producer well or optimizing the injection steam rate), the producer's well-bore temperature remains much higher than desired/allowed. This means that no steam injection method can be applied to heavy oil reservoirs without a method for cooling the producer well string.

The suggested schematic for cooling the producer well-string is shown in Figure 7-1. In this system, two concentric tubings are hung in a casing. The warm produced fluids are lifted to the surface through the inner tubing. Cold water (with predetermined temperature and rate) is injected in the annulus and will be produced via the outer tubing. A detailed economic analysis

should be used to select the optimal production method, using the actual data and available services for a real case.

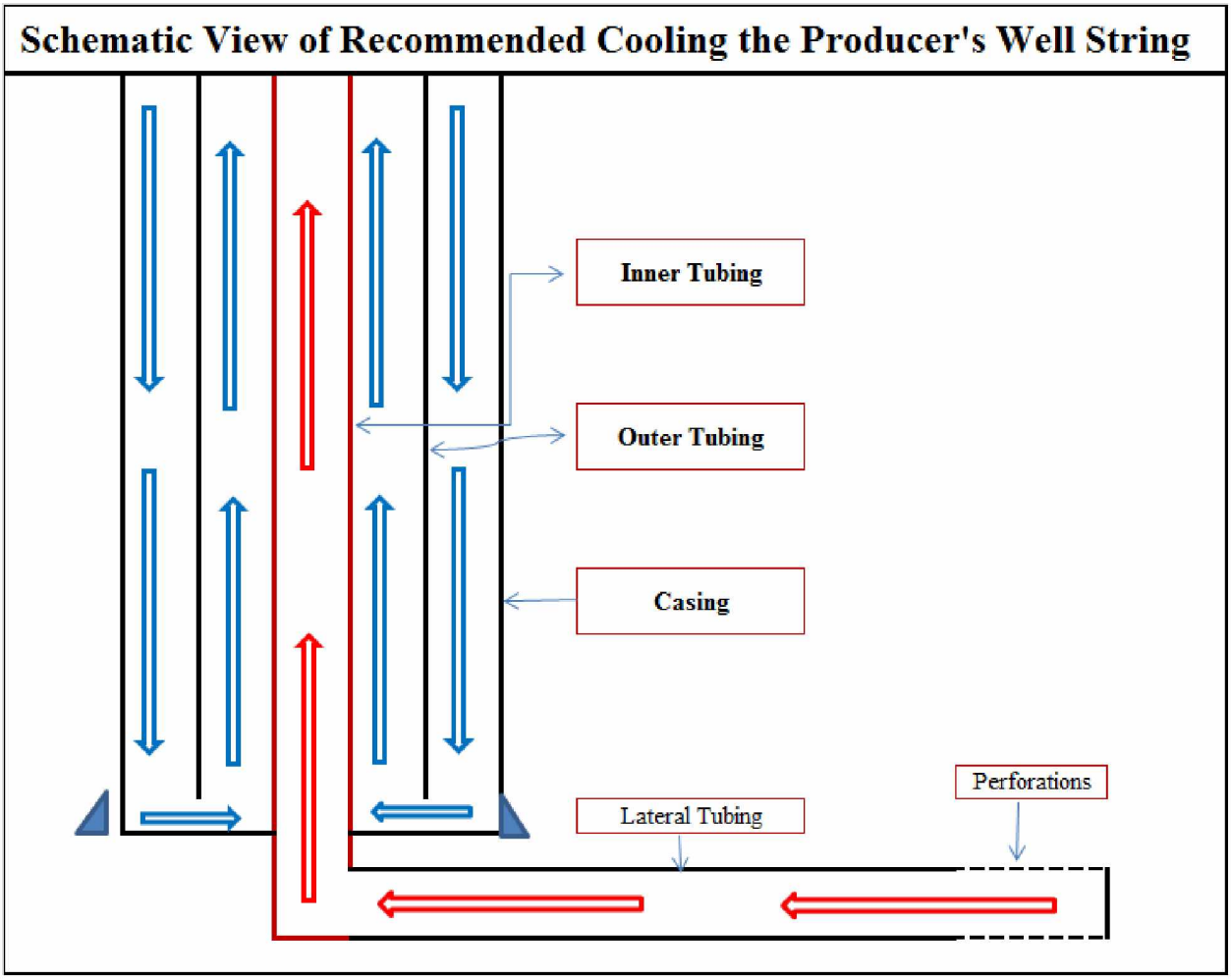

Figure 7-1: Schematic view of recommended producer well string cooling.

Chapter 8: Conclusions and Recommendations

Different simulation models are constructed to study different steam injection methods and different scenarios are run to investigate the effect of different parameters. Based on the results and the criterion considered for well bore temperature (near to its static reservoir temperature), it seems that applying steam injection in a heavy oil reservoir beneath the permafrost is not directly feasible. However, from the results of simulations and discussions, the following points can be drawn:

1. The steam injection is more effective; when the down-hole distance between injector and producer is less than 500 ft. So, it seems, using vertical wells for applying any steam injection method on the heavy oil Ugnu reservoir is not economical.
2. Use of the horizontal well for both injector and producer wells, for SAGD, CSAGD or/and CSS methods is recommended.
3. In a drainage area with a length of 1250 ft, drilling the injector and producer horizontal wells with lateral length of about 800 ft in the middle of reservoir can be recommended.
4. For Steam Assisted Gravity Drainage (SAGD) and Cyclic Steam Assisted Gravity Drainage (CSAGD), it is recommended to leave the entire length of the injector well open to flow; however, leave just the last 50 ft of lateral length (at the toe of the well) of the producer well open to flow.
5. For Cyclic Steam Stimulation (CSS), it is suggested to leave the last 50 ft of lateral well open to flow.
6. Based on the simulation results, application of any steam injection recovery method (SAGD, CSAGD or CSS) for Ugnu reservoir is only recommended when the thickness of the Sagavanirktok sand formation is at least 300 ft. This ensures no risk of vertical heat transfer from the heated oil-bearing layer to the permafrost via conduction process in the bulk of formations.
7. In applying Cyclic SAGD process, there is an optimum cycle time period and optimum rate of steam injection for each reservoir's conditions that should be estimated, to avoid over-heating or under-heating the reservoir.

8. The addition of nitrogen to injected steam, by any means, would reduce the oil recovery with negligible effect on the temperature profile.
9. In applying CSS process, for maximum oil recovery there is an optimum cycle time period that should be estimated. In the studied model, the optimum cycle time period is 1 month injection, two months shut in, and one month production.

References

Ademodi, B.; Alade, O.S.; Abolarin, S.O. and Adelakun, S.O., 2014. A Preliminary Investigation on Cyclic Steam Stimulation Recovery of Nigerian Heavy Oil, SPE paper 172362, the SPE Nigeria Annual International Conference and Exhibition, Lagos, Nigeria, 05–07 August 2014.

Akin, S.; Castanier, L.M. and Brigham, W.E., 1999. Effect of Temperature on Heavy Oil/Water Relative Permeabilities, SPE paper 54120, the 1999 SPE International Thermal Operations and Heavy Oil Symposium, Bakersfield, CA, 17-19 March 1999.

Alaska Division of Oil and Gas, (2016). North Slope Oil and Gas Activity, 2005-2006. Alaska Division of Oil and Gas, Alaska Department of Administration, Retrieved May 23, 2016, from: http://doa.alaska.gov/ogc/annual/current/18_Oil_Pools/Kuparuk%20River%20-%20Oil/Kuparuk%20River,%20West%20Sak%20Oil/1_Oil_1.htm.

Al-Qabandi, S., AI-Shatti, Y. and Gopalakrishnan, P., 1995. Commercial Heavy Oil recovery by Cyclic Steam Stimulation in Kuwait, SPE paper 30288, International Heavy Oil Symposium, Calgary, Alber1a, Canada, 19-21 June 1995.

Al Shibli, A., Al Hinai, S., Belghache, A., and Al Habsi, S., 2016. The Application of Cyclic Steam Stimulation in Heavy Oil Reservoir with a High Water Cut, SPE Paper 179809-MS, SPE EOR Conference at Oil and Gas West Asia, Muscat, Oman, 21–23 March 2016.

Alvarez, J. and Han, S., 2013. Current Overview of Cyclic Steam Injection Process, Journal of Petroleum Science Research, Volume 2 Issue 3, July 2013.

Amri, R., Gibbon, D. and Rezoug, T., 2012. The design, development and test of one newton hydrogen peroxide monopropellant thruster. Aerospace Science and Technology 25 (2013) 266–272. Doi:10.1016/j.ast.2012.02.002.

Ardali, M.; Barrufet, M.A.; Mamora, D.D. and F.Qiu, F., 2012. A Critical Review of Hybrid Steam-Solvent Processes to Recover Heavy Oil, SPE paper 159257, the SPE Annual Technical Conference and Exhibition, San Antonio, Texas, USA, 8-10 October 2012.

Ashrafi, M., 2013. Experimental Investigation of Temperature Dependency of Relative Permeability Data in Heavy Oil Systems with Applications to Thermal Recovery, Thesis for the degree of Philosophiae Doctor, Norwegian University of Science and Technology (NTNU), Trondheim, May 2013.

Attanasi, E.D. and Freeman, P.A., 2015, Evaluation of Development Options for Alaska North Slope Viscous and Heavy Oil. Natural Resources Research, Vol. 24, No. 1, March 2015 (c 2014), DOI: 10.1007/s11053-014-9240-1.

Azad, M.S.; Alnuaim, S. and Abeeb A. Awotunde, A.A. 2013. Stochastic Optimization of Cyclic Steam Stimulation in Heavy Oil Reservoirs, SPE paper 167378, the SPE Kuwait Oil and Gas Show and Conference, Kuwait, 7-10 October 2013.

Babadagli, T., 2012. Specialized Short Course on EOR/IOR Technologies. Training course presented at Kish Island of Iran, 21-25 April 2012.

Bansal, R.K., 2005. A Text Book of Fluid Mechanics and Hydraulic Machines, ninth edition. Laxmi Publication (P) LTD, New Delhi, India.

Barillas, J.L.M.; Dutra, T. V., Jr. and Mata, W., 2008. Improved Oil Recovery Process for Heavy Oil: a Review, Brazilian Journal of Petroleum and Gas. v. 2, n. 1, pp. 45-54.

Bayless, J.H. and Williams, R.E., 1989. Recovery of Viscous Oil From Geological Reservoirs Using Hydrogen Peroxide. United States Patent, Patent Number: 4,867,238.

Bennion, G.B.; Sarioglu, G.; Chan, M.; Hirata, T.; Courtnage, D. and Wansleeben, J., 1993. Steady State Bitumen -Water Relative Permeability Measurements at Elevated Temperatures in Unconsolidated Porous Media, Petroleum Society of CIM, paper no. CIM 93-25, the CIM 1993 Annual Technical Conference in Calgary, May 9-12, 1993.

Bera, A. and Babadagli, T., 2015. Status of electromagnetic heating for enhanced heavy oil/bitumen recovery and future prospects: A review. Applied Energy, volume 151, 1 August 2015, pp. 206–226, 0306-2619/ 2015 Elsevier Ltd. http://dx.doi.org/10.1016/j.apenergy.2015.04.031.

Birch, F.; Schairer, J.F. and Spicer, H.C. (eds), 1942. Handbook of physical constants, Geological Society of America. Special papers, No. 36.

Blackwell, D.D. and Steele, J.L., 1989. Thermal conductivity of sedimentary rocks: measurement and significance. Naeser, N.D., McCulloch, T.H. (eds), Thermal history of sedimentary basins, Springer, New York, pp 5–96.

Bleakley, W. B., 1965. Finding Enthalpy and Specific Volume from Charts, Part 5, Oil and Gas Journal, February 15, 1965, p. 121.

British Petroleum (BP) 2010. Heavy Oil vs. Light Oil. Juneau, February 2010. http://www.legis.state.ak.us/basis/get_documents.asp?session=26&docid=5177.

Bridger, G.W. and Woodward C., 1975. Formulation, and Operation of Methanation Catalysts, Chapter 4 of Book 'Methanation of Synthesis Gas', Editor(s): Seglin, L., Volume 146, American Chemical Society, 1975.

Brooks, R.T. and Davis, T.W. 2010. Optimizing Steam Injection in Heavy Oil Reservoirs, SPE paper 104520, the Abu Dhabi International Petroleum Exhibition & Conference, Abu Dhabi, UAE, 1–4 November 2010.

Buckles, R. S., 1979. Steam Stimulation Heavy Oil Recovery at Cold Lake Alberta, SPE paper 7994-MS, the 49th California Regional Meeting, Ventura, California, April 18-20, 1979.

Burns, J., 1969. A Review of Steam Soak Operations in California, Journal of Petroleum Technology, January 1969, pp. 25-34.

Carcoana, A., 1992. Applied Enhanced Oil Recovery, Prentice-Hall Inc., New Jersey, USA.

Carrizales, M.A.; Lake, L.W. and Johns, R.T., 2008. Production Improvement of Heavy-Oil Recovery by Using electromagnetic Heating, SPE No. 115723, Annual Technical Conference and Exhibition held in Denver, Colorado, USA, 21–24 September 2008.

Chmielowski, J. (2013), BP Alaska Heavy Oil Production from the Ugnu Fluvial-Deltaic Reservoir. Pacific Section AAPG, SEG and SEPM Joint Technical Conference, Monterey, California, April 19-25, 2013.

Chopra, S.; Lines, L.; Schmitt, D.R. and Batzle, M., 2010. Heavy Oils: Reservoir Characterization and Production Monitoring. Society of Exploration Geophysicists, Tulsa, OK U.S.A., Chapter 1.

Clark, S.P. Jr., (Ed.), 1966. Handbook of physical constants (revised edition), Geological Society of America. Memoir 97, Washington, DC.

CMG, 2015. STARS User's Guide - Advanced Processes & Thermal Reservoir Simulator, Version 2015, pp. 1167-1168.

Collett, T.S.; Kvenvolden, K.A. and Magoon, L.B., 1990. Characterization of hydrocarbon gas within the stratigraphic interval of gas-hydrate stability on the North Slope of Alaska, U.S.A., Applied Geochemistry, Vol. 5, pp. 279-287, 1990.

CRC Handbook on Chemistry and Physics, 1974. 55th Ed., CRC Press, Florida.

Dandekar, A., 2013. Petroleum Reservoir Rock and Fluid Properties, second edition, CRC Press, Taylor & Francis Group, Boca Raton, FL., USA.

Delshad, M., 2011. Fundamentals of Enhanced Oil Recovery, training and consulting MAT Group, June 2011.

Davison, R.J., 1995. Electromagnetic Stimulation of Lloydminster Heavy Oil Reservoirs: Field Test Results, The Journal of Canadian Petroleum Technology, April 1995, volume 34, No. 4, pp. 14-24.

Dickson, J.L; Leahy-Dios, A. and Wylie, Ph. L., 2010. Development of Improved Hydrocarbon Recovery Screening Methodologies, SPE paper 129768, SPE Improved Oil Recovery Symposium held in Tulsa, Oklahoma, USA, 24–28 April 2010.

Donaldson, E.C.; Chilingarian, G.V. and Yen, T.F., 1989. Enhanced Oil Recovery, II: Processes and Operations, Elsevier Science Publishers B. V., New York, USA.

Ediriweera, M.P. and Halvorsen, B.M., 2015. A Study of the Effect of Relative Permeability and Residual Oil Saturation on Oil Recovery, the 56th SIMS, October 07-09, 2015, Linkoping, Sweden. DOI: http://dx.doi.org/10.3384/ecp15119339.

Eppelbaum, L.; Kutasov, I. and Pilchin, A., 2014. Applied Geothermics, Lecture Notes in Earth System Sciences, Springer-Verlag Berlin Heidelberg, 2014.

Er-rbib, H. and Bouallou, Ch., 2013. Modelling and Simulation of Methanation Catalytic Reactor for Renewable Electricity Storage, Chemical Engineering Transactions, 35, 541-546. DOI:10.3303/CET1335090.

eSteam™, 2016. Downhole Steam Generator, Frequently Asked Questions, www.esteamoil.com/wp-content/uploads/eSteamΓäó-FAQ-Overview-WEBSITE.

Farouq Ali, S.M., 1970. Oil Recovery by Steam Injection, Bradford, PA: Producers.

Farouq Ali, S.M., and R. F. Meldau, R.F., 1983. Steam Flooding, Chapter VII in *Improved Oil Recovery* (Oklahoma City, OK: Interstate Oil Compact Commission, March 1983), pp. 314, 324, 339.

Farouq Ali, S.M., Jones, J.A., and Meldau, R.F. (1997). Practical Heavy Oil Recovery.

Fox, R. L. and Stosur, J.J., 1981. US. Department of Energy R&D on Downhole Steam Generator for the Recovery of Heavy Oil, Enhanced Oil Recovery (Edited by E. John Fayers), Proceedings of the third European Symposium on Enhanced Oil Recovery, Bournemouth, U.K., September 21-23,1981, Elsevier Scientific Publishing Company, 1981, pp. 543-547.

Gates, C. F, and Ramey, H. J., JR., 1964. Better Technology Opens Way for More Thermal Projects, Oil and Gas Journal (July 13, 1964).

GPSA, 2004. Engineering Data Book, FPS Version, Volumes I & II, twelfth edition, Gas Processors Suppliers Association.

Gretener, P.E., 1981. Geothermics: using temperature in hydrocarbon exploration, AAPG, Short Course Notes, 17.

Hallam, R.J.; Plekenbrock, E.J.; Abou-Sayed A.S.; A.M Garon, A.M.; Putnam, T.W.; Weggeland, M.E. and Webb, K.J., 1992. Resource Description and Development Potential of the Ugnu Reservoir, North Slope, Alaska, SPE Formation Evaluation, September 1992, pp 211-218.

Hascakir B.; Babadagli T. and Akin. S., 2008. Experimental and numerical modeling of heavy-oil recovery by electrical heating. SPE/PS/CHOA 117669-PS2008-340, SPE international thermal operations and heavy oil symposium, Calgary, Alberta, Canada, 20–23 October 2008.

Hammershaimb, E.C.; Kuuskraa, V.A. and Stosur, G., 1983. Recovery Efficiency of Enhanced Oil Recovery Methods: A Review of Significant Field Tests, SPE paper 12114, The 581h Annual Technical Conference and Exhibition, San Francisco, CA, October 5-8, 1983.

Hornbrook, M.W.; Dehghani, K.; Qadeer, S.; Ostermann, R.D. and Ogbe, D.O., 1991. Effects of CO2 Addition to Steam on Recovery of West Sak Crude Oil. SPE Reservoir Engineering, August 1991, pp. 278-286.

Hulm, E., Bernaski, G., Kostic, B., Lowe, S., and Matson, M. (2013), Integrated Reservoir Description of the Ugnu Heavy-oil Accumulation, North Slope, Alaska. Heavy-oil and oil-sand petroleum systems in Alberta and beyond: AAPG Studies in Geology 64, p. 481–508, DOI: 10.1306/13371589St643558.

Islam, M.R.; Wadadar, S.S. and Bansal, A., 1991. Enhanced Oil Recovery of Ugnu Tar Sands of Alaska Using Electromagnetic Heating With Horizontal Wells, SPE paper 22177, the International Arctic Technology Conference, Anchorage, Alaska, May 29-31, 1991.

Isaev P.P., Tsigankova E.V., 2011. Electrical Bottom Hole Heating System (EBHHS), Siberian Federal University, УДК 622.323, http://conf.sfu-kras.ru/sites/mn2011/thesis/s2/s2_14.pdf.

Jamaluddin, A.K.M.; Mehta, S.A. and Moore, R.G., 1998. Down-hole Heating Device to Remediate Near- Wellbore Formation Damage Related to Clay Swelling and Fluid Blocking, Paper 98-73, the 49th Annual Technical Meeting of The Petroleum Society of CIM in Calgary, Alberta, Canada, June 8-10,1998.

Jones, J., 2007. Thermal Recovery by Steam Injection, Petroleum Engineering handbook, Edited by L.W. Lake, Volume V, Reservoir Engineering and Petrophysics, Edited by E.D. Holstein, Society of Petroleum Engineers, Richardson, TX., USA, 2007, Chapter 15.

Kappelmeyer, O. and Hänel, R., 1974. Geothermics with special reference to application, Gebruder Borntrargen, Berlin, Stuttgart.

Keenan, J. and F. Keyes, F. 1967. Thermodynamic Properties of Steam, John Wiley & Sons, New York.

Kim, E.S., 1987. Reservoir Simulation of in situ Electromagnetic Heating of Heavy Oils, PhD dissertation, Texas A & M U., College Station, Texas.

Koci, P.F. and Mohiddin, J.G., 2007. Peace River Carmon Creek Project—Optimization of Cyclic Steam Stimulation Through Experimental Design, SPE paper 109826, SPE Annual Technical Conference and Exhibition held in Anaheim, California, U.S.A., 11–14 November 2007.

Krupiczka, R., 1967. Analysis of Thermal Conductivity in Granular Materials, intl. Che. Eng. (1967) Vol. 7, No.1, 122.

Law, D.H.-S., 2011. A New Heavy Oil Recovery Technology to Maximize Performance and Minimize Environmental Impact. Society of Petroleum Engineers, Distinguished Lecturer Program.

Lauwerier, H. A., 1955. The Transport of Heat in an Oil Layer Caused by the Injection of Hot Fluid, Applied Science Research, No.5, Sec. A (1955), p. 145.

Luo, S. and Baker, A., 2006. Optimizing Horizontal-Well Steam-Stimulation Strategy for Heavy-Oil Development, SPE paper 104520, the 2006 SPE Eastern Regional Meeting, Canton, Ohio, U.S.A., 11–13 October 2006.

Madaoui, K., 2005. Reservoir Engineering Courses: Enhanced Oil Recovery Processes, Training course held by TOTAL Company, 4-7 of July 2005, Tehran, Iran.

Maini, B.B., 1995. Is it Futile to Measure Relative Permeability for Heavy Oil Reservoirs?, Petroleum Society of CIM, paper 95-97, the 46th Annual Technical Meeting of The Petroleum Society of CIM, Banff, Alberta, Canada, May 14 - 17, 1995.

Makled, A. E. and Belal, H., 2009. Modeling of Hydrazine Decomposition for Monopropellant Thrusters. 13th International Conference on AEROSPACE SCIENCES & AVIATION TECHNOLOGY ASAT- 13, May 26 – 28, 2009, Military Technical College, Kobry Elkobbah, Cairo, Egypt.

Marx, J. W. and Langenheim, R H., 1959. Reservoir Heating by Hot Fluid Injection, Petroleum Transactions (AIME), 216 (1959), p. 312.

McGuire, P. L., Redman, R. S., Jhaveri, B. S., Yancey, K.E. and Ning, S.X., 2005. Viscosity reduction WAG—an effective EOR process for North Slope viscous oils. Paper SPE 93914 presented at SPE Western Regional Meeting. Irvine, CA, 30 March–1 April 2005.

Messmer, J.H., 1984. The Effective Thermal Conductivity of Quartz Sands and Sandstones, SPE paper 13011.

Meyer, R.F., Emil D. Attanasi, E.D., and Freeman, P.A., (2007). Heavy Oil and Natural Bitumen Resources in Geological Basins of the World. U.S. Geological Survey Open-File Report 2007-1084.

Mohsin Rehman, M. and Meribout, M., 2012. Conventional versus electrical enhanced oil recovery: a review, Journal of Petroleum Exploration Production Technology, December 2012, Volume 2, Issue 4, pp 157–167. DOI 10.1007/s13202-012-0034-x.

Muraza, O. and Galadima, A., 2015. Aquathermolysis of heavy oil: A review and perspective on catalyst development, Fuel, Volume 157, 1 October 2015, pp. 219–231, 0016-2361/ 2015 Elsevier Ltd. http://dx.doi.org/10.1016/j.fuel.2015.04.065.

Murer, A.S.; McClennen, K.L.; Ellison, T.K.; D.C. Larson, D.C.; Timmer, R.S.; Thomsen, M.A. and Wolcott, K.D., 2000. Steam Injection Project in Heavy-Oil Diatomite, SPE Reservoir Eval. & Eng. 3 (1), February 2000.

National Geography, 2016: http://education.nationalgeographic.org/encyclopedia/permafrost/

Nejad, K.S.; Berg, E.A. and Jon Knut Ringen, J.K., 2011. Effect of Oil Viscosity on Water/Oil Relative Permeability, SCA2011-12, the International Symposium of the Society of Core Analysts, Austin, Texas, USA 18-21 September, 2011.

Ning, S. X., and McGuire P. L., 2004. Improved oil recovery in under-saturated reservoirs using the US-WAG process. Paper SPE 89353 presented at 2004 SPE/DOE Fourteenth Symposium on Improved Oil Recovery. Tulsa, OK, 17–21 April 2004.

Ning, S.X., Jhaveri, B.S., Jia, N., Chambers, B. and Gao, J., 2011. Viscosity reduction EOR with CO2 and enriched CO2 to improve recovery of Alaska North Slope viscous oils, Paper SPE 144358-MS presented at SPE Western North American Regional Meeting. Anchorage, AK, 7–11 May 2011.

Offeringa J., Barthel R. and Weijdema J., The Interplay Between Research and Field Operations in The Development of Thermal Recovery methods. The third European Symposium on Enhanced Oil Recovery, Edited by Fayers, F.J., Bournemouth, U.K., September 21-23, 1981, pp. 527-541.

Okassa, F.; Godi, A.; De Simoni, M.; Matteo, M. and Misenta, M., 2010. A nonconventional EOR technology using RF/MW heating coupled with a new patented well/reservoir interface,

SPE paper 134324, SPE annual technical conference and exhibition, Florence, Italy, 22–23 September 2010.

Olsen, D.K.; Taylor, E. C. and Mahmood, S. M., 1992. Feasibility Study of Heavy Oil Recovery - Production, Marketing, Transportation, and Refining Constraints to Increasing Heavy Oil Production in Alaska. NIPER-610, Distribution Category UC- 122, Rev. December 1992.

Pacheco, E. F. and Farouq Ali, S.M., 1972. Well-Bore Heat Losses and Pressure Drop in Steam Injection, *Journal of Petroleum Technology* (February 1972).

Patil, S.; Dandekar, A. and Khataniar, S., 2008. Phase Behavior, Solid Organic Precipitation, and Mobility Characterization Studies in Support of Enhanced Heavy Oil Recovery on the Alaska North Slope. United States Department of Energy, National Energy Technology Laboratory, December 2008.

Paul Chen, J. and Lim, L.L., 2002. Key factors in chemical reduction by hydrazine for recovery of precious metals, Chemosphere 49 (2002) 363–370, Pergamon.

Poelchau, H.S.; Baker, D.R.; Hantschel, T.h.; Horsfield, B. and Wygrala, B., 1997. Basin simulation and the design of the conceptual basin model, Welte, D.H.; Horsfield, B. and Baker, D.R. (eds), Petroleum and basin evaluation. Springer, Berlin, pp 36–41.

Pospisil, G. (2011). Heavy oil vs Light Oil, presentation, Alaska Oil and Gas Assoc., Anchorage, AK, January 6, 2011.

Prats, M., 1982. *Thermal Recovery,* SPE Monograph Series, New York, Dallas: American Institute of Mining, Metallurgical and Petroleum Engineers, 1982.

Precision Combustion, Inc., 2015. Downhole Steam Generator, http://www.precision-combustion.com/cdownhole.html.

Ramey, H. J., JR., 1962. Well-bore Heat Transmission, *Petroleum Transactions* (AIME, 1962), pp. 225, 427.

Ramey, H. J. JR., 1965. How to Calculate Heat Transmission in Hot Fluid Injection, in Fundamentals of Thermal Oil Recovery (Dallas, TX: Petroleum Engineer, 1965), p.165.

Ramey, H. J., JR., 1967. A Current Review of Oil Recovery by Steam Injection. WPC 12247, 7th World Petroleum Congress, 2-9 April 1967, Mexico City, Mexico

Rhoades, C.A. and Meeks, T., 1983. Steam Injection Method and Apparatus for Recovery of Oil, United States Patent, 4,372,386.

Ried, T.B. (1996). Feasibility Study of Heavy Oil Recovery in the United States. BDM-Oklahoma, Inc. Bartlesville, Oklahoma, NIPER/BDM-0225, March 1996.

R.I.I. North America, 2016. Downhole Steam Generation, The holy grail for heavy oil recovery technology, http://www.riina.ca/technology.html.

Ritchey, H.W., 1956. Radiation heating. USA Patent Application, USA Patent Application, Serial No. 2,757,738, filed on 20 September, 1948; 1956.

Robertson, E.C., 1979, Thermal conductivity of rocks, U.S. Geological Survey open file report, 79–356.

Rubinstein, L.I., 1959. The Total Heat Losses in Injection of a Hot Liquid into a Stratum, Neft I Gas, Moscova Vol. 2 (1959), p. 41.

Ruifeng, W.; Xianghong, W.; Xintao, Y.; Li, W.; Xinzheng, Z. and Xiaoling, Y., 2011. First Cyclic Steam Stimulation Pilot Test in Sudan: A Case Study in Shallow Heavy Oil Reservoir, SPE paper 144819, the SPE Enhanced Oil Recovery Conference, Kuala Lumpur, Malaysia, 19–21 July 2011.

Sahni, A.; Kumar, M.; Knapp, R.B. and Livermore, L., 2000. Electromagnetic Heating Methods for Heavy Oil Reservoirs, Paper SPE 62550, SPE/AAPG Western Regional Meeting, Long Beach, California, 19-23 June, 2000.

Sass, J.H.; Lachenbruch, A.H.; Munroe, R.J.; Greene, G.W. and Moses, T.H. Jr., 1971. Heat flow in the western United States, J. Geophys. Res. 76:6376–6413.

Sengupta, D.; Mazumder, S.; Cole J.V. and Lowry, S., 2004. Controlling Non-Catalytic Decomposition of High Concentration Hydrogen Peroxide, CFD Research Corporation,215 Wynn Drive, Huntsville, AL, 35805.

Sharma, G. D., 1990. Development of Effective Gas Solvents including Carbon Dioxide for the Improved Recovery of West Sak Oil, Final Report, DO~61114-2, University of Alaska, Fairbanks, June 1990.

Sierra, R.; Tripathy, B.; Bridges, J.E. and Farouq Ali, S.M., 2001. Promising progress in field application of reservoir electrical heating methods. SPE 69709, SPE symposium on international thermal operations and heavy oil margarita, Venezuela, 12-14 March 2001.

Somerton, W.H., 1958. Some thermal characteristics of porous rocks. Trans AIME, 213:375–378.

Somerton, W.H.; Keese, J.A. and S. L. Chu, S.L., 1974. Thermal Behavior of Unconsolidated Oil Sands, SPE paper 4506, Society of Petroleum Engineers Journal, October 1974, pp. 513-521.

Somerton, W.H., 1992. Thermal Properties and Temperature-Related Behavior of Rock/Fluid Systems, Elsevier Science Publishing Company Inc., New York, USA.

Speight, J. G., 2007. The Chemistry and Technology of Petroleum, CRC Press/Taylor & Francis, 4th Edition, Volume 114, Chapter 6.

Taber, J.J.; Martin, F.D. and R.S. Seright, R.S., 1997a. 2: Introduction to Screening Criteria and Enhanced Recovery Field Projects, SPE Reservoir Engineering, August 1997, pp. 189-198.

Taber, J.J.; Martin, F.D. and R.S. Seright, R.S., 1997b. EOR Screening criteria Revisited- Part 2: Applications and Impact of Oil Prices, SPE Reservoir Engineering, August 1997, pp. 199-205.

Targac, G.W, Redman, R.S., Davis, E.R, Rennie, S.B., McKeever, S.O, Chambers, B.C., 2005. Unlocking the Value in West Sak Heavy oil, SPE paper 97856, presented at SPE International Thermal Operations and Heavy Oil Symposium, Calgary, Canada,1-3 November (2005).

Tewari, R.D.; Abdalla, F.; Lutfi, H.G.; Keqiang, Y.; Faroug, A.; Bakri, H. and Guocheng, L., 2011. Successful Cyclic Steam Stimulation Pilot in Heavy Oilfield of Sudan, SPE paper 144638, the SPE Enhanced Oil Recovery Conference, Kuala Lumpur, Malaysia, 19–21 July 2011.

Thomas, S., 2008. Enhanced Oil Recovery – An Overview, Oil & Gas Science and Technology – Rev. IFP, Vol. 63. No. 1, pp. 9-19.

Total, 2006. Extra-Heavy Oil and Bitumen Reserves for the Future, Exploration and Production, Total World Side.

Towson, D. and Khallad, A., 1991. The PCEJ Steam Stimulation Project, CIM/AOSTRA 1991, Technical Conference in Banff, April 21-24, 1991.

Trebolle, R. L.; Chalot, J. P. and Colmenares, R., (1993). The Orinoco Heavy-Oil Belt Pilot Projects and Development Strategy, SPE paper 25798, SPE International Thermal Operations Symposium, Bakersfield, California, 8-10 February 1993.

Van Lookeren, J., 1982. A Further Analysis of the Steam Stimulation of Heavy-Oil Wells and Reservoirs, SPE paper 11216, 57th Annual Fall Technical Conference and Exhibition of the Society of Petroleum Engineers of AIME, New Orleans, LA, Sept. 26-29, 1982.

Ventura, M. and Wernimont, E., 2001. Advancements in high concentration hydrogen peroxide catalyst beds, AIAA-01-3250, Utah, 2001.

Vermeulen, F. and McGee, B., 2000. In situ electromagnetic heating for hydrocarbon recovery and environmental remediation, Journal of Canadian Petroleum Technology, Volume 39, No. 8, August 2000.

Wang, W. and Gong, J., 2011. Methanation of carbon dioxide: an overview, Front. Chem. Sci. Eng. 2011, 5(1): 2–10. DOI 10.1007/s11705-010-0528-3.

Wen, Sh.; Zhao, Y.; Liu, Y. and Hu, Sh., 2007. A Study on Catalytic Aquathermolysis of Heavy Crude Oil During Steam Stimulation, SPE Paper 106180, SPE International Symposium on Oilfield Chemistry, Houston, Texas, U.S.A., 28 February–2 March 2007.

Werner, M. R., 1987. Tertiary and Upper Cretaceous Heavy-Oil Sands, Kuparuk River Unit Area, Alaskan North Slope. Exploration for Heavy Crude Oil and Natural Bitumen. AAPG Studies in Geology No. 25, October/November 1987, pp. 537-547.

White, P. D. and Moss, J. T., 1983. Thermal Recovery Methods, Penn Well, Tulsa, Oklahoma, Chapter 6.

Willman, B. T.; Valleroy, V. V.; Runberg, G.W., Cornelius, A.J., and Powers, L.W., 1961. Laboratory Studies of Oil Recovery by Steam Injection, Petroleum Transactions (AIME), 222 (1961), p. 681.

Xia, T. X. and Greaves, M., 2006. In Situ Upgrading of Athabasca Tar Sand Bitumen Using THAI, Chemical Engineering Research and Design, Volume 84, Issue 9, September 2006, page 856-864.

Zumdahl, S.S. and Zumdahl, S.A., 2007. Chemistry, Seventh Edition, Houghton Mifflin Company, Boston, MA., USA.